AFOSR 66-1856

AD 639647

University of Utah

Department of Chemical Engineering

CLEARINGHOUSE
FOR FEDERAL SCIENTIFIC AND
TECHNICAL INFORMATION

Hardcopy	Microfiche		
$ 7.25	$ 2.00	427 pp	as

1 ARCHIVE COPY

DDC
SEP 20 1966
C

Salt Lake City, Utah

Distribution of this
document is unlimited

DISCLAIMER NOTICE

THIS DOCUMENT IS BEST QUALITY PRACTICABLE. THE COPY FURNISHED TO DTIC CONTAINED A SIGNIFICANT NUMBER OF PAGES WHICH DO NOT REPRODUCE LEGIBLY.

TECHNICAL REPORT

IGNITION OF AMMONIUM PERCHLORATE-BASED PROPELLANTS BY CONVECTIVE HEATING

UNDER GRANT AF AFOSR 40-63 AND 64

August 1, 1966

Report prepared by: John A. Keller

Report approved by: Norman W. Ryan
Norman W. Ryan
Principal Investigator

Alva D. Baer
Alva D. Baer
Principal Investigator

PREFACE

This report is taken from the thesis of J. A. Keller (Ph.D., University of Utah, 1965). The work was performed under sponsorship of the Air Force Office of Scientific Research, Grant AF-AFOSR 40-63 and 64. It was presented at the AIAA Third Aerospace Sciences Meeting in New York City, January, 1965.

ABSTRACT

A study was made of the ignition of ammonium perchlorate-based propellants by convective heat fluxes of 20 to 160 cal/(cm)^2(sec) in a shock-tube apparatus. The results of this research showed that ammonium-perchlorate propellants ignite by a thermal process in which the slow step in the sequence of events which lead to steady deflagration of the propellant is raising the surface to its ignition temperature. The results also suggest that the key chemical process in ignition is the thermal decomposition of ammonium perchlorate; reactions involving fuel ingredients become important immediately following that reaction.

For ignition studies described in this thesis, the driven section of the shock tube was modified to accommodate a test section. The propellant sample was mounted in the wall of the constant-area flow channel in the test section where it was subjected to forced-convection heating as shock-heated gases were passed through the channel.

The test variables in this study were:

1. Heat Flux. The heat flux at the propellant surface was varied by altering either the initial shock tube conditions or the gas velocity through the constant-area flow channel of the test section.

2. Gas Velocity. The velocity of the test gas through the flow channel was varied over the range of 50 to 800 m/(sec), corresponding to Mach numbers of 0.07 to 1.0, respectively.

3. Gas Temperature. The temperature of the test gas was varied over the range of 1000 to 2600°K.

4. Test Pressure. Propellant ignition was studied at pressures in the range of 14 to 25 atmospheres.

Propellant compositions were varied for determining the effect of propellant ingredients on ignition characteristics. Some of the compositional factors studied were:

1. Percentage of Ammonium Perchlorate in the Propellant.

2 Particle Size of the Ammonium Perchlorate.

3. Catalysts. Materials which were known to modify the ballistic properties of propellants or to catalyze the decomposition of ammonium perchlorate were added to propellant compositions.

4. Fuels. Most of the propellants studied contained a binder-fuel of polybutadiene-acrylic acid copolymer with an epoxy curing agent, in others the rubbery binder-fuel was replaced with carbon black or paraformaldehyde.

It was concluded from the experimental results of this study that ammonium-perchlorate propellants ignite by a simple thermal ignition process. The time for ignition to occur in convective heating experiments, provided the propellant has a smooth surface or gas velocity across the surface is high, is a function only of the initial, uniform propellant temperature, externally applied surface heat flux, the thermophysical properties of the propellant, and the kinetics of

the key ignition reaction as predicted by thermal ignition theory. Data obtained at high-convective heat fluxes for the conditions described above or at low-radiant heat fluxes could be correlated by a simple ignition time-heat flux relationship as suggested by thermal ignition theory.

Propellant samples with surface irregularities were found to ignite in shorter times at low gas velocities than samples with smooth surfaces for equivalent heat fluxes at the propellant surface. It is postulated, as suggested by the experimental data on ignition, that the improved ignitability of propellants with rough surfaces is produced by supplementary, secondary ignition reactions among propellant decomposition products that are generated at the surface by two-dimensional heating of surface irregularities. The net effect of these secondary reactions on the ignition process is to augment the externally applied heat flux at the propellant surface to bring the propellant surface more quickly to its ignition temperature. At high gas velocities, greater than about 400 m/(sec), or for propellant samples with smooth surfaces, these secondary reaction processes are not important.

TABLE OF CONTENTS

		Page
ABSTRACT		iii
LIST OF FIGURES		xi
LIST OF TABLES		xviii
Chapter		
I	INTRODUCTION	1
II	IGNITION THEORY	7
	DISCUSSION OF TERMINOLOGY	11
	Ignition Time	12
	Ignition Temperature	15
	Mean Surface Heat Flux	18
	THERMAL IGNITION	20
	Thermal Ignition with Bulk-Phase Reactions	20
	Thermal Ignition with Surface Reactions	25
	Thermal Ignition with Surface Heating from Secondary Ignition Reactions	30
	Thermal Ignition Theory and Composite Propellants	32
III	EARLIER WORK ON PROPELLANT IGNITION	35
	IGNITION BY CONVECTIVE HEAT FLUXES	35
	IGNITION BY RADIANT HEAT FLUXES	42
IV	SHOCK-TUBE APPARATUS	51
	HEAT TRANSFER TO WALL OF TEST SECTION	54
	HEAT TRANSFER TO PROPELLANTS	59
V	IGNITION OF F-PROPELLANT	63
	TEST VARIABLES FOR IGNITION OF F-PROPELLANT IN THE SHOCK TUBE	65
	NATURE OF EXPERIMENTAL DATA	67

Chapter Page

IGNITION IN NITROGEN. 71
Description of Experimental Results. 71
Ignition at Low Gas Velocities. 71
Ignition at Intermediate Gas Velocities 74
Ignition at High Gas Velocities and the Ignition Paradox 75
Effect of Test Variables on Ignition 79
Discussion of Results with Respect to Ignition Theory. 82
Simple Thermal Ignition of F-Propellant 82
Thermal Ignition of F-Propellant with Secondary Ignition Reactions 86

IGNITION IN ARGON 105

IGNITION IN AIR 111

HIGH-SPEED MOTION PICTURE STUDIES OF F-PROPELLANT IGNITION 113

SUMMARY 120

VI IGNITION OF OTHER CAST PROPELLANTS 125

IGNITION OF PROPELLANTS CONTAINING COPPER CHROMITE 125
Ignition of Modified F-Propellant. 125
Effect of Particle-Size Distribution and Loading of Ammonium Perchlorate 131
Effect of Ammonium-Perchlorate Particle Size 136
Ignition of Propellants S and U in Nitrogen . . . 136
Summary of Ignition Results on Propellants S and U in Nitrogen. 144
Ignition of U-Propellant in Argon and Oxygen. . . 148

IGNITION OF PROPELLANTS CONTAINING IRON OXIDE 154
Ignition of J-Propellant in Nitrogen 154
Effect of Ammonium-Perchlorate Particle Size, Catalyst Concentration, and Cure Time 158
Ignition of Propellant AD in Argon 165
Ignition of Propellants AD and AE in Oxygen. 168

APPARENT ROLE OF CATALYSTS IN THE IGNITION PROCESS. . . 170
Effect of Catalysts on the Thermal Decomposition of Ammonium Perchlorate 172

Chapter | Page

Ignition of Propellants Containing Different Catalysts 175
Discussion of Results from Catalyst Study. . . . 182

VII SPECIAL STUDIES ON PROPELLANT IGNITION 192

IGNITION OF PROPELLANTS WITH POLYMER-RICH SURFACES. 192

IGNITION OF PROPELLANTS WITH SALTED, POLYMER-RICH SURFACES 204

IGNITION OF PRESSED PROPELLANTS 209
Pressed Propellants of Ammonium Perchlorate and Copper Chromite 209
Pressed Propellants with Carbon Black Fuel . . . 210
Ignition of Propellant CB 210
Ignition of Propellant E. 216
Pressed Propellants Containing Paraformaldehyde Fuel (Propellant D) 218

IGNITION OF EXTENDED-PHASE PROPELLANTS. 220

VIII CONCLUSIONS. 227

IX RECOMMENDATIONS FOR FURTHER RESEARCH 234

LIST OF REFERENCES. 237

Appendix

A DESCRIPTION OF SHOCK-TUBE APPARATUS. 246

B EXPERIMENTAL PROCEDURE 256

C STUDIES FOR CHARACTERIZING SHOCK TUBE AND TEST SECTION 260

D PROCEDURES USED FOR DETERMINING THERMOPHYSICAL PROPERTIES OF PROPELLANTS AND PROPELLANT INGREDIENTS 297

E CALCULATIONS FOR IGNITION TEMPERATURE AND HEAT FLUX. . 302

F PROPELLANT SAMPLES 307

G CALIBRATION OF FLOW-CONTROL ORIFICES 314

H HEAT FLUX GAUGES 316

Appendix		Page
I	ANALYSIS OF DATA FROM HEAT FLUX GAUGE MEASUREMENTS. . .	326
J	EFFECTIVE TEST TIME IN THE SHOCK-TUBE APPARATUS	346
K	TABLES OF DATA.	348
L	TABLE OF NOMENCLATURE	404

LIST OF FIGURES

Figure		Page
1	Idealized Surface-Temperature History for a Semi-Infinite Slab of Propellant Undergoing Simple Thermal Ignition.	14
2	Idealized Surface-Temperature History for a Semi-Infinite Slab of Propellant Undergoing Thermal Ignition with Part of the Heat Flux at the Surface Supplied by Secondary Ignition Reactions. .	17
3	Surface-Temperature History for a Propellant Undergoing Thermal Ignition Illustrating the Effect of Secondary Ignition Reactions on the Ignition Process	31
4	Ignition Data for Propellants F and G for Low Radiant Heat Fluxes at Atmospheric Pressure	48
5	Cutaway Sketch of Driven End of Shock Tube Showing Position of the Test Section	52
6	Sketch of Test Section	53
7	Range of Test Conditions for Heat Transfer Study . . .	56
8	Photomicrographs of a Freshly Cut Surface of F-Propellant.	64
9	Oscilloscope Records of Pressure Pickup and Photocell Signals for Ignition Runs on F-Propellant at Various Test Conditions.	69
10	Ignition Data for F-Propellant in Nitrogen at Low Gas Velocities for Pressures of 14 to 25 Atmospheres	73
11	Ignition Data for F-Propellant in Nitrogen at Intermediate Gas Velocities for Pressures of 20 to 25 Atmospheres	74
12	Ignition Data for F-Propellant Obtained by Different Methods	78
13	Effect of Gas Velocity on Ignition Time of F-Propellant for Different Values of Externally Applied Heat Flux in Nitrogen.	81

Figure		Page
14	Ignition Data for F-Propellant in Nitrogen at a Test-Gas Velocity of Mach 0.13 for Pressures of 14 to 25 Atmospheres	95
15	Range of Experimental Variables for Data Presented in Figures 11 and 12.	96
16	Ignition Data for F-Propellant in Nitrogen at a Test-Gas Velocity of Mach 0.09 for Pressures of 20 to 25 Atmospheres	102
17	Ignition Data for F-Propellant in Nitrogen at a Test-Gas Velocity of Mach 0.07 for Pressures of 14 to 25 Atmospheres	103
18	Variation of Surface Heat Flux with Gas Temperature for Ignition of F-Propellant at Pressures of 20 to 25 Atmospheres in Nitrogen and Argon at a Test-Gas Velocity of Mach 0.13.	106
19	Variation of Surface Heat Flux with Gas Temperature for Ignition of F-Propellant at Pressures of 20 to 25 Atmospheres in Nitrogen at Mach 0.28 and in Argon at Mach 0.27	108
20	Ignition Data for F-Propellant (Batch F-32) in Argon for Pressures of 20 to 25 Atmospheres	109
21	Ignition Data for F-Propellant in Air for a Test-Gas Velocity of Mach 0.13 for Pressures of 14 to 25 Atmospheres.	112
22	Photographs of F-Propellant Ignition in Air at a Test-Gas Velocity of Mach 0.13	116
23	Photographs of F-Propellant Ignition in Air at a Test-Gas Velocity of Mach 0.28.	117
24	Photographs of F-Propellant Ignition in Air at a Test-Gas Velocity of Mach 1.0	118
25	Photomicrographs of the Surface on a Sample of F-Propellant Recovered from an Ignition Test in Nitrogen at a Test-Gas Velocity of Mach 1.0 . . .	121
26	Ignition Data for Modified F-Propellant in Nitrogen at Intermediate and High Gas Velocities for Pressures of 14 to 25 Atmospheres	128

Figure		Page
27	Ignition Data for Modified F-Propellant in Nitrogen at Low Gas Velocities for Pressures of 14 to 25 Atmospheres	129
28	Comparison of Ignition Results in Nitrogen for Regular and Modified F-Propellant	130
29	Ignition Data for O-Propellant in Nitrogen for Pressures of 20 to 25 Atmospheres	132
30	Ignition Data for P-Propellant in Nitrogen for Pressures of 20 to 25 Atmospheres	133
31	A Comparison of Ignition Results in Nitrogen for Propellants F, O, and P	134
32	Ignition Data for S-Propellant in Nitrogen for Pressures of 20 to 25 Atmospheres	137
33	Photomicrographs of Surfaces on Samples of Propellant U-5	139
34	Ignition Data for U-Propellant in Nitrogen for Pressures of 20 to 25 Atmospheres	140
35	Approximate Test Time in Shock-Tube Apparatus for Various Flow-Control Orifices Compared with the Heat Flux-Ignition Time Relationship for Simple Thermal Ignition of F-Propellant	142
36	A Comparison of Ignition Results for Propellants F, P, S, and U.	145
37	Ignition Data for U-Propellant in Argon at Test-Gas Velocities of Mach 0.13 and 0.27 for Pressures of 20 to 25 Atmospheres	149
38	Ignition Data for U-Propellant in Oxygen at Test-Gas Velocities of Mach 0.28 and 1.0 for Pressures of 20 to 25 Atmospheres	150
39	Ignition Data for J-Propellant in Nitrogen for Pressures of 14 to 25 Atmospheres	156
40	Ignition Data for Propellants with Different Concentrations of Iron Oxide and Different Cure Times for Ignition in Nitrogen at a Test-Gas Velocity of Mach 0.13 and Pressures of 20 to 25 Atmospheres.	160

Figure		Page
41	Ignition Data for Propellants with Different Concentrations of Iron Oxide for Ignition in Nitrogen at Intermediate and High Gas Velocities and Pressures of 20 to 25 Atmospheres .	162
42	Ignition Data for Propellants Containing 2.0 Per Cent Iron Oxide, but Different Particle Sizes of Ammonium Perchlorate, for Ignition in Nitrogen at a Test-Gas Velocity of Mach 0.13 . . .	163
43	Ignition Data for Propellants Containing 2.0 Per Cent Iron Oxide, but Different Particle Sizes of Ammonium Perchlorate, for Ignition in Nitrogen at a Test-Gas Velocity of Mach 0.28 . . .	164
44	Ignition Data for Propellant AD in Argon at a Test-Gas Velocity of Mach 0.13 for Pressures of 18 to 25 Atmospheres	166
45	Ignition Data for Propellants AD and AE in Oxygen at a Pressure of 20 Atmospheres.	169
46	Compositions of Propellants Tested in Catalyst Study.	176
47	A Comparison of Ignition Data for Propellants with Different Catalysts	178
48	Oscillographs for Ignition Runs on Propellant AD Showing Different Kinds of Ignition Characteristics.	189
49	Ignition Data for Samples of Propellants F, P, and U with Polymer-Rich Surfaces at a Test-Gas Velocity of Mach 0.13.	194
50	Effect of Ammonium-Perchlorate Particle Size on Ignition Time for Propellants with Polymer-Rich Surfaces at a Test-Gas Velocity of Mach 0.13 in Nitrogen	199
51	Effect of Ammonium-Perchlorate Particle Size on Ignition Time for Propellants with Polymer-Rich Surfaces at a Test-Gas Velocity of Mach 0.28 in Nitrogen	201
52	Effect of Polymer-Film Thickness and Test-Gas Velocity on Ignition Time for Samples of S-Propellant with Polymer-Rich Surfaces in Nitrogen.	203

Figure		Page
53	Photomicrographs of Surfaces on Samples of U-Propellant Prepared by Different Methods.	205
54	The Effect of Surface Conditions on Ignition Time for U-Propellant in Nitrogen at a Test-Gas Velocity of 0.13.	206
55	The Effect of Surface Conditions on Ignition Time for U-Propellant in Nitrogen at a Test-Gas Velocity of 0.28.	207
56	Ignition Data for Pressed Propellant CB (with Carbon Black Fuel) at Low-Radiant and High-Convective Heat Fluxes.	212
57	Ignition Data for Pressed Propellant CB in Nitrogen at Test-Gas Velocities of Mach 0.13 and Mach 0.28	215
58	Ignition Data for Pressed-Oxidant Propellant E . . .	217
59	Ignition Data for Pressed Propellant D (with Paraformaldehyde Fuel) in Nitrogen.	219
60	Photomicrographs (5X) of Surfaces on Extended-Phase Propellants	221
61	Ignition Data for Simple Thermal Ignition of Propellants F, G, and CB Plotted in Dimensionless Form as Suggested by Thermal Ignition Theory	230
62	x,t Diagram of Wave Pattern in Shock Tube for Operation with "Matched" Interface.	247
63	Pressurization System for Shock Tube	250
64	Wiring Diagram for Shock-Tube Instruments.	253
65	Attenuation of Incident Shock Wave in Air, Nitrogen, or Argon.	263
66	Photograph of Heat Flux Gauges	265
67	Oscillograph for Heat Transfer Run Showing the Initial Heating and Pressure Transients in the Test Section.	273
68	Oscillograph for Heat Transfer Run No. 35-31-2 . . .	275
69	Oscillograph for Heat Transfer Run No. 35-31-7 . . .	275

Figure		Page
70	Initial, Instantaneous Temperature Rise Behind Reflected Shock Wave at the Test-Section Wall for Air.	278
71	Initial, Instantaneous Temperature Rise Behind Reflected Shock Wave at the Test-Section Wall for Argon	279
72	Heat Transfer Coefficients at the Test-Section Wall for High-Temperature Air, Correlated in Terms of Mass Flow Rate Through Flow Channel and Gas Film Temperature	284
73	Heat Transfer Coefficients at the Test-Section Wall for High-Temperature Air, Correlated in Terms of Mass Flow Rate Through the Flow Channel and Gas Stagnation Temperature.	286
74	Heat Transfer Coefficients at the Test-Section Wall for High-Temperature Argon as a Function of Mass Flow Rate Through the Flow Channel.	295
75	Photograph of Sample Holders Filled with Propellant.	309
76	Ignition Data for F-Propellant in Nitrogen at a Test-Gas Velocity of Mach 0.13 for Propellant Samples Prepared by Different Methods	312
77	Temperature-Sensing Element Resistance Data for Pyrex 7740 Heat Flux Gauge.	319
78	Wiring Diagram for Temperature Measurement with Heat Flux Gauges.	323
79	Thermal Conductivity Data for Pyrex 7740 Derived from Thermal Responsivity Data.	333
80	Thermal Conductivity Data for Pyrex Glass.	334
81	Assumed Temperature Dependence for Thermal Conductivity of Pyrex 7740.	335
82	Temperature Dependence of Heat Capacity for Pyrex Glass	337
83	Thermal Conductivity and Heat Capacity for Alumina .	338

Figure		Page
84	Data for Thermophysical Properties of Pyrex 7740 and Alumina Used for Calculations	340
85	Calculated Surface Temperature-Time Data for Heating of a Semi-Infinite Body of Pyrex 7740 with Temperature-Dependent Thermophysical Properties .	341
86	Effective Test Period in Shock-Tube Apparatus as Function of Mach Number of Incident Shock Wave for Different Flow-Control Orifices	347

LIST OF TABLES

Table		Page
1	Ignition Data for Cast Propellants F and G and Pressed Propellant CB at Low Radiant Fluxes . . .	349
2	Compositions of Propellant Systems	350
3	Ignition of F-Propellant in Nitrogen	355
4	Thermophysical Properties of Propellants and Propellant Ingredients.	361
5	Ignition Data for F-Propellant in Argon.	365
6	Ignition Data for F-Propellant in Air.	366
7	Ignition Data for Propellants O and P in Nitrogen. .	367
8	Ignition Data for S-Propellant in Nitrogen	369
9	Ignition Data for U-Propellant in Nitrogen	371
10	Strand Burning Rate Data for Propellants at 20°C . .	374
11	Ignition Data for U-Propellant in Argon and Oxygen .	375
12	Ignition Data for J-Propellant in Nitrogen	377
13	Ignition Data for Propellants AD and AE.	379
14	Ignition Data for Propellants in Catalyst Study. . .	381
15	Ignition Data for Pressed Propellants.	383
16	Ignition Data for Extended-Phase Propellants in Nitrogen.	385
17	Ignition Data in Dimensionless Form for Simple Thermal Ignition of Cast Propellants F and G, and Pressed Propellant CB	391
18	Data for Flow-Control Orifices	393
19	Properties of Heat Flux Gauges	394
20	Gas Temperatures behind Reflected Shock Waves in Air, Argon, and Oxygen.	395
21	Summary of Initial Temperature Rise Data for Heat Flux Gauges.	396
22	Summary of Heat Transfer Results	399

CHAPTER I

INTRODUCTION

In early research and development work on solid propellant rockets, so many problems faced the scientists and engineers that no great effort was directed toward understanding the ignition process; trial-and-error methods were employed to develop suitable ignition systems. With the arrival of the space age larger and more reliable rockets were required; the trial-and-error approach to igniter development could no longer be justified, and increased emphasis was placed on fundamental ignition research. As a result, in recent years several theories have been proposed to explain the behavior of solid propellants during the ignition process. Even though these ignition theories have undergone rather thorough development, reliable experimental data were not available to evaluate them critically.

The state-of-the-art of ignition of solid propellant rockets has advanced to keep pace with new propulsion systems through igniter development programs. Obviously, an igniter development program that requires testing of large rockets to determine ignition requirements necessitates a large expenditure for facilities and manpower. This becomes increasingly important as the size and complexity of propulsion systems grow. Also, with the development of new rocket propellants, a concurrent igniter development program is required. As more knowledge is obtained on the response of propellants to externally applied energy

and the nature of chemical reactions which control the ignition process, it will be possible to predict with greater confidence the igniter requirements for new propellants and rockets. Until we can predict the effect of new propellant ingredients on the ignition characteristics of a propellant, laboratory tests will still be required to support the igniter development engineer.

A complete study of rocket ignition should include a separate investigation of (1) the response of a propellant to externally applied energy and (2) the nature of the energy release from a rocket igniter. This information must then be coupled with other considerations, such as flame spread over the surface of the propellant grain and the rate of chamber pressurization for use in designing rocket igniter systems. The final proof of such an investigation would be the test firing of a rocket. Such a comprehensive study is outside of the scope of this study, but is required for those concerned with solid propellant rocket development.

The research described here was undertaken to further study ignition of composite solid propellants in an effort to learn more about the ignition process, and to provide experimental data for evaluating existing ignition theories. To achieve these goals a rather comprehensive study was made of the ignition characteristics of ammonium perchlorate solid propellants under convective heating.

The Department of Chemical Engineering at the University of Utah has been engaged in the study of solid propellant ignition and combustion for the past seven years. One part of this research program has been concerned with the ignition of composite solid propellants induced by

convective heating of the propellant surface. The primary objectives of the research described in this thesis were:

1. To study the ignition of composite solid propellants, containing ammonium perchlorate as the oxidant, by convective heating from hot gases in order to develop a clearer understanding of the ignition process.
2. To obtain experimental data on propellant ignition that would be useful to the engineer for designing ignition systems for solid propellant rockets.
3. To devise an ignition model that explains both the results of this work and the observations of other investigators.
4. To design and carry out ignition experiments which would provide information on the chemical reactions significant in the ignition process.
5. To study heat transfer in the test section used for ignition studies in order to provide a means of accurately calculating the externally applied heat flux to the propellant surface during ignition tests.
6. To study the effect on ignition of environmental factors such as (1) type of convective gas, (2) velocity of convective gas across the propellant surface, and (3) the magnitude of externally applied heat flux.
7. To study the roles of propellant ingredients in propellant ignition.

The research described here was sponsored by the United States Air Force Office of Scientific Research of the Air Research and Development

Command under Contract AF 49(638)-170, and Air Force Grants AF AFOSR 62-99, AF AFOSR 40-63, and AF AFOSR 40-64. Earlier work under Contract AF 49(638)-170 on solid propellant ignition is presented in the doctoral dissertations of A. D. Baer [6] and C. C. McCune [67], and a Department of Chemical Engineering Technical Report [80].

This study is primarily concerned with that aspect of rocket ignition that includes the response of the propellant to externally applied energy and the chemical processes which lead to steady combustion of the propellant. The ignition of composite solid propellants by convective heating is of more than academic importance, for many solid rockets utilize hot gases for ignition. Many rocket igniters also transfer energy by other modes of heat transfer, such as (1) by radiation from incandescent particles and hot gases and (2) by conduction from hot particles striking the propellant surface. Frequently, however, the primary process of heat transfer is by forced convection from hot, fast-moving gases. A specific example is the gas-generator-type igniter. Regardless of the type of igniter employed, the rate of energy transfer to the propellant surface is rapid, and complete ignition is achieved in 5 to 200 milliseconds. The rate of energy transfer to the propellant surface from such devices ranges from a low of perhaps 10 cal/(cm)^2(sec) to a high of about 300 cal/(cm)^2(sec).

The shock tube is a useful tool for ignition research by convective heating, providing in microseconds a supply of very hot gas that can be employed in readily controlled convective heating. In this work the hot gases generated in the shock tube were exhausted from the driven end of the tube through a constant area channel with the propellant

sample mounted in the wall. This test method provided convective heat fluxes of 20 to 160 cal/(cm)^2(sec) at the propellant surface.

The following discussion is a brief outline of the method of attack used in this study. The first phase of this study consisted of a thorough analysis of heat transfer in the constant area channel of the test section. Heat transfer at the test position was measured with a fast-response heat flux gauge (a thin-film, resistance thermometer on the surface of a glass or ceramic substrate). Three different substrate materials--Pyrex, Pyroceram, and alumina--with greatly different thermophysical properties were used so that the effect of thermal responsivity on the transient heat transfer process could be determined. Results from heat flux gauge measurements could be directly applied to calculating heat transfer to the propellant surface.

The second phase of this study included preparation of propellant samples and their subsequent testing in the shock-tube apparatus. All of the propellants studied contained ammonium perchlorate as the oxidant. Most of the propellants tested were castable propellants having a binder-fuel of polybutadiene-acrylic acid copolymer cured with an epoxy curing agent (Epon 828). Propellant formulations were varied to allow evaluation of the effect of ingredients on ignition characteristics and their role in the ignition process. Some of the compositional variables studied were: (1) ammonium perchlorate particle size, (2) concentration of ammonium perchlorate in propellants, (3) type of fuel--pressed propellants were made containing carbon black and paraformaldehyde as the fuels in place of the polymer, and

(4) different additives for promoting burning rate and decomposition of ammonium perchlorate.

In the final phase of this work, the experimental results were analyzed in terms of thermal ignition theory. It was found that this was the only ignition theory of the several considered that could adequately explain all of the experimental results. Numerical analysis of the governing partial differential equation which defines this model shows that results of ignition experiments, for propellants which undergo thermal ignition, can be represented by a straight line on a plot of externally applied heat flux versus the square root of ignition time on logarithmic coordinate paper. Furthermore, the slope of the straight line that best represents the experimental data is related to the activation energy of the key ignition reaction.

CHAPTER II

IGNITION THEORY

The ignition of a solid propellant is achieved through a combination of chemical and thermal processes which raise the propellant surface temperature and establish an environment which can support combustion reactions. These combustion reactions then become dominant, providing energy feedback to the propellant surface to sustain steady deflagration. A comprehensive theory of propellant ignition must consider the energy contributions to the ignition process both from the external environment and from exothermic chemical reactions at or near the propellant surface.

Because of the complexity of the constituents of a solid propellant, many combustion and ignition reactions are possible. Consider, for example, a simple ammonium perchlorate composite propellant composed of a mixture of oxidizer crystals, a rubbery binder-fuel, and a burning rate modifier. A few of the general types of chemical reactions that one might expect to be important during the ignition of a composite propellant in a neutral environment are:

1. Vaporization of the main propellant ingredients followed by exothermic reactions among these species in the gas phase.
2. Exothermic decomposition of ammonium perchlorate followed by gas-phase reactions among the decomposition products.

3. Heterogeneous surface reactions between the gaseous decomposition products of one ingredient and other, condensed-phase, ingredients.

Furthermore, if oxygen or other oxidizing gases were present, they could react in the gas phase with decomposition products or heterogeneously with condensed-phase ingredients.

An ignition theory which attempted to include all the possible chemical reactions and forms of energy feedback to the propellant surface would be prohibitively complex. However, it is to be expected that only one or two reactions would be "rate controlling" in the sense that they are the slow steps in the ignition process. For different propellant systems the rate controlling chemical reaction could be very different. A change in environmental test conditions, especially the heat flux level or ambient pressure, could also change the rate controlling process. As many rate controlling processes are conceivable, it is necessary to infer from experiment which chemical reactions are probably rate controlling under different test conditions. Only when such information is available can ignition characteristics of solid propellants be related to a realistic mathematical model.

Because of the complex nature of the ignition process and the observed influence of environmental factors on ignition, several ignition theories have been proposed to explain experimental observations. Each of the proposed ignition theories is characterized in terms of rate controlling processes. Foremost among these theories on composite solid propellant ignition are the following:

1. Gas-phase theory: The gas-phase theory of propellant ignition was proposed by McAlevy and Summerfield (see References 65 and 66). This theory assumes that propellant ingredients decompose by thermal processes and then undergo vigorous exothermic reaction in the gas phase, transferring energy back to the propellant. The rate controlling reactions are presumed to be those in the gas phase close to the propellant surface. Experimental evidence that supports this theory is that the presence of oxygen in the test gas used for convective heating experiments sometimes improves the ignitability of solid propellants. Also, in some ignition experiments a change in ambient pressure has been found to alter ignition characteristics.

2. Thermal theory: The thermal theory of ignition assumes that the rate of the ignition process is controlled by the temperature of the solid phase. For rapid heating of a propellant this would be the temperature at the surface of the propellant. While acknowledging the eventual appearance of exothermic gas-phase reactions in the late stages of the overall process, proponents of thermal theory believe that the gas-phase reactions appear very quickly after slower chemical processes in, or at least involving, the solid-phase ingredients that provide gaseous reactants. The net effect of these earlier reactions must be exothermic, though not necessarily strongly so. The key reactions in the ignition process become important

only near the end of the heating period. In a short period of time relative to the total heating period, the conditions prerequisite for sustaining deflagration reactions are established. The pioneering work on the thermal theory of ignition as applied to solid propellants was conducted by Frazer and Hicks [34] and Hicks[46], and by Altman and Grant [2]. More recent contributors were Baer and Ryan [6,8,9]; and Evans, Beyer, and McCulley [32].

3. Heterogeneous reaction theory: Anderson et al. [3] have suggested that the critical rate controlling reactions in the ignition process are spontaneous heterogeneous reactions between gaseous oxidizing species produced by the decomposition of ammonium perchlorate and the binder-fuel. The fact that solid propellants undergo hypergolic ignition by an extremely reactive oxidizer such as chlorine trifluoride without the application of external energy supports the hypothesis that heterogeneous surface reactions can be important in the ignition process.

In a later section on experimental results for ignition of composite propellants containing ammonium perchlorate, it will be shown that all experimental evidence gathered indicates the slow chemical step in the ignition process is the thermal ignition of ammonium perchlorate. It is concluded from the experimental studies conducted for this thesis that neither gas-phase nor heterogeneous-surface reactions are rate controlling in that they are the slow steps in the ignition process. On the contrary, if reactive species are present

at the propellant surface to support what appears to be gas-phase or heterogeneous-surface reactions, these are extremely fast reactions. For ignition experiments in which reactive species are generated at the propellant surface during the heating process, these species are involved in fast, exothermic reactions which contribute energy for heating the propellant surface. This energy affects propellant ignition by reducing the time required to bring the propellant surface to its thermal ignition temperature. Based on this work, it appears that environmental oxidizing gases also influence propellant ignition in this manner, that is, by heating the propellant surface through either heterogeneous reactions or gas-phase reactions near the surface with reactive species evolved from the propellant surface during heating. Reactions of the kind described above that are not rate controlling, but are found to be important in the ignition process under some test conditions, will be referred to as "secondary" ignition reactions.

In the remainder of this section the main features of the thermal ignition theory will be outlined, and the manner of its application to analysis and correlation of experimental data will be discussed.

DISCUSSION OF TERMINOLOGY

There are three terms used frequently in the discussion of solid propellant ignition--"ignition time," "ignition temperature," and "mean surface heat flux"--which need careful definition for the purposes of the discussion to be presented on solid propellant ignition.

Ignition Time

Ignition time in this work is defined as the time interval beginning with the first application of external energy to the propellant surface and ending with the appearance of a combustion flame as indicated by a light signal. When necessary, this will be referred to as a "real" ignition time.

In this work, the start of transient heating coincided with the arrival of the incident shock wave at the test position, and could be measured within an error of $\pm$ 10 microseconds. The onset of a combustion flame was determined by a photoelectric sensor (response time of about 100 microseconds) that viewed the surface of the test sample through a window. The direct signal from the light sensor and also the differentiated signal were displayed on the screen of an oscilloscope and recorded. Ignition was taken to occur at the time after the start of heating when the differentiated photocell signal was rising almost vertically. High-speed photography showed that at this time a combustion flame appeared at one or more locations on the propellant surface.

The validity of the time measurement requires further discussion in terms of ignition theory. To illustrate the difference between a "real" ignition time and a "theoretical" ignition time, the thermal model for ignition will be used. If the surface-temperature history of a propellant undergoing ignition is described by a one-dimensional, partial differential equation that includes terms for heat transfer to the surface both from externally applied heat flux and from the key thermal reaction, as is the case for simple thermal ignition, one may

define a "theoretical" ignition time as the time to reach either a preassigned surface temperature or a preassigned rate of change of surface temperature. The partial differential equation which describes the ignition process can then be integrated numerically for a given set of initial and boundary conditions to obtain a "theoretical" ignition time based on the preassigned cut-off conditions. Our "theoretical" criterion for ignition will be that the rate of change of the surface temperature reach an arbitrary but large value, say 10^6°C/(sec). The time it takes the propellant surface to reach this condition from the instant of the first application of external energy will be defined as the "theoretical" ignition time.

An idealized surface-temperature history for a semi-infinite slab of propellant undergoing simple thermal ignition is shown by Figure 1 and illustrates what is meant by a "real" ignition time. The "real" ignition time (t_i) corresponds to the time interval that starts with the first application of external heat and ends with the appearance of a luminous combustion flame at the propellant surface. As can be seen from Figure 1, during the greater part of the heating period, the propellant behaves as a passive solid and its surface temperature increases only as a consequence of the externally applied energy. The key exothermic chemical reaction, which is characteristic of the ignition process, is important only for a small fraction of the total heating period. During this short interval of time, the supply of energy from the reaction becomes much greater than that supplied externally and produces an accelerated rise in surface temperature which culminates with luminous gas-phase reactions.

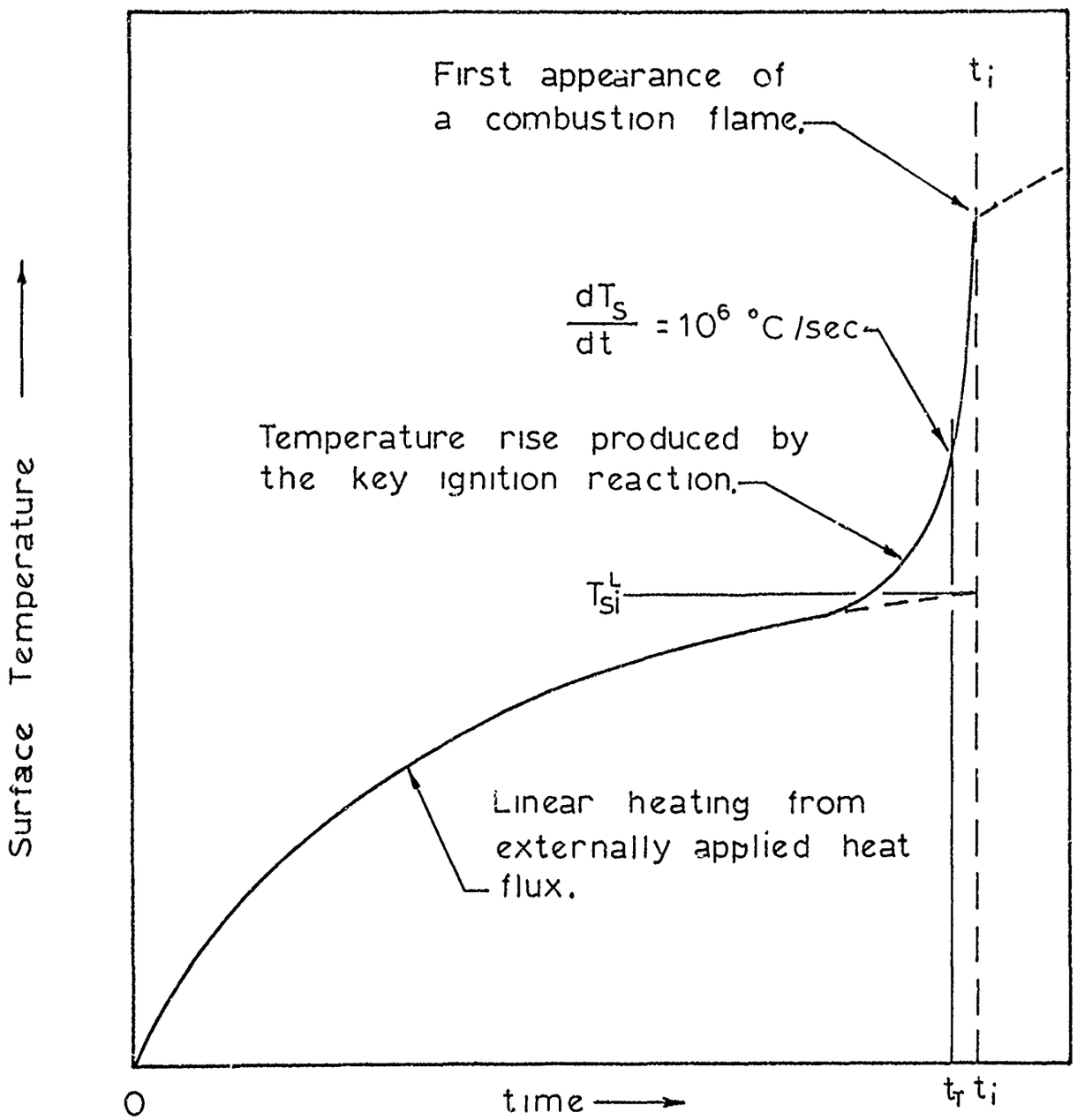

Figure 1

Idealized Surface-Temperature History for a Semi-Infinite Slab of Propellant Undergoing Simple Thermal Ignition.

The "theoretical" ignition time as defined above is indicated on Figure 1 by the vertical line at time t_T, and is compared with a "real" ignition time by the vertical dashed line labeled t_i. It is apparent that when the rate of change of surface temperature increases to a value of about 10^6°C/(sec), the propellant surface will reach its steady deflagration temperature (less than 1000°C) in much less than one millisecond. At this time the surface temperature for steady deflagration is only a few hundred degrees Centigrade higher than the actual surface temperature. As the total ignition time becomes shorter under higher external heat fluxes, the difference between the "real" time and the "theoretical" time will become a greater fraction of the total time.

In principle the above definition for "theoretical" ignition time should apply to all propellants which undergo thermal ignition regardless of the nature of the thermal and chemical processes which transfer heat to the surface. However, until equations can be written to describe all the thermal and chemical processes involved in ignition, it is not possible to calculate a "theoretical" ignition time when secondary ignition reactions are important. Even then a measured "real" ignition time would still be of great importance for assessing ignition characteristics of propellants.

Ignition Temperature

The ignition temperature (T_{si}) is the temperature at the propellant surface at the time ignition is observed. This is a defined temperature at time t_i and differs from the temperature at the propellant

surface during steady burning. Two different ignition temperatures, "ignition temperature for linear heating" and "thermal ignition temperature," are used in the discussion on propellant ignition. Neither temperature is a "real" temperature in that it can be measured experimentally.

The "ignition temperature for linear heating," T^L_{si}, is the temperature at ignition time, t_i, of the propellant surface; and it is calculated by the linear, one-dimensional heat conduction equation, assuming that the propellant behaves as a passive solid, its temperature rising only under the influence of externally applied heat flux up to the time of ignition. For propellants which undergo simple thermal ignition, that is, there is no contribution from secondary ignition reactions to help raise the propellant temperature, T^L_{si} is that shown by the temperature-time relationship of Figure 1. It can be seen from Figure 1 that the ignition temperature, T^L_{si}, is nearly the same irrespective of the ignition time used to describe it.

When secondary ignition reactions contribute part of the energy to produce thermal ignition of propellants, T^L_{si} still has precisely the same meaning as given above, but its significance in terms of the ignition process has changed. T^L_{si} now represents only the contribution to the temperature rise at the surface provided by the externally applied heat flux. This is shown by Figure 2.

The "thermal ignition temperature" (T^T_{si}) is the temperature on an absolute temperature scale to which the propellant surface must be raised before thermal ignition occurs regardless of the mode of heat transfer to the propellant surface. T^T_{si} is a weak function of the

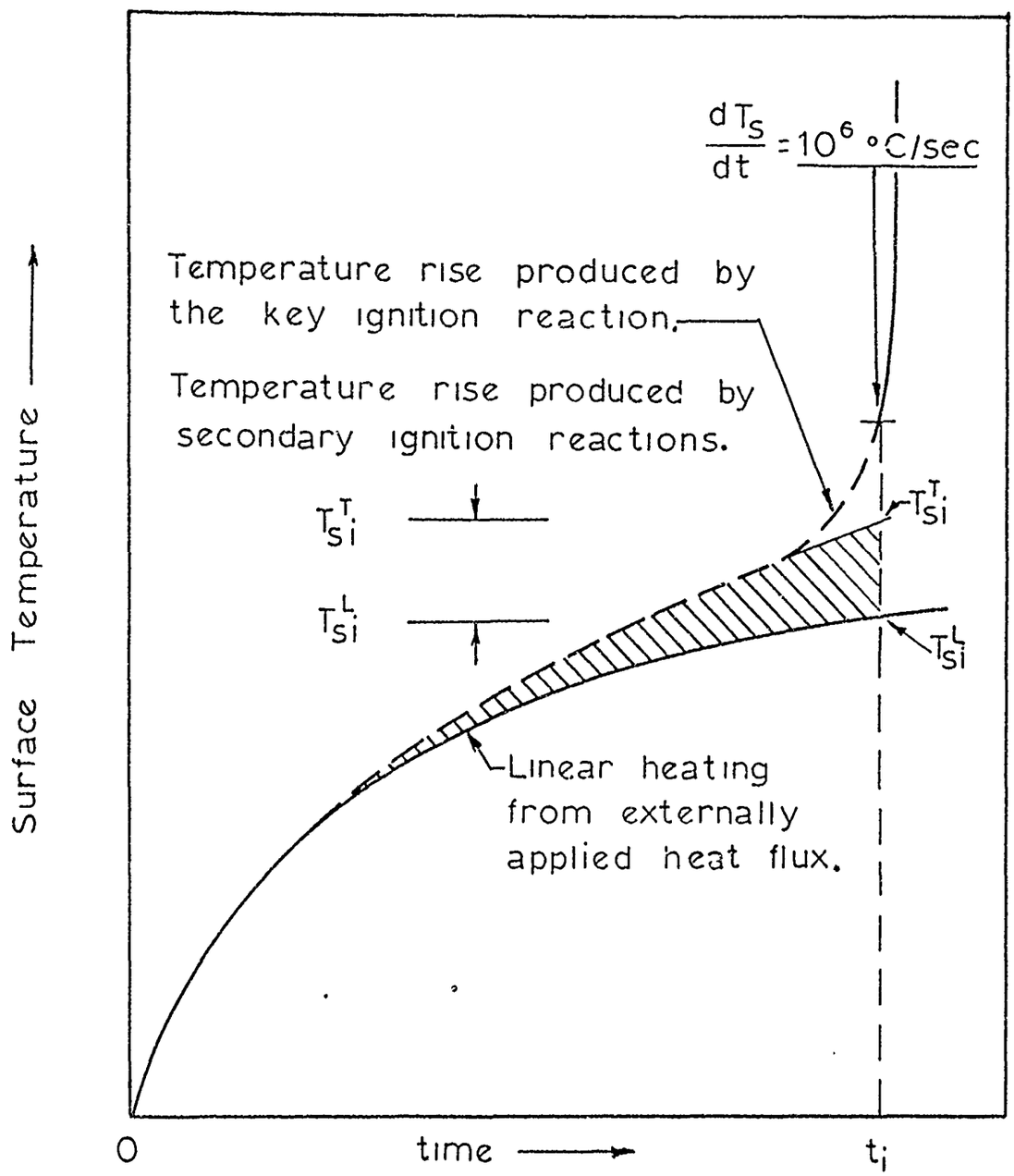

Figure 2

Idealized Surface-Temperature History for a Semi-Infinite Slab of Propellant Undergoing Thermal Ignition with Part of the Heat Flux at the Surface Supplied by Secondary Ignition Reactions.

total heat flux applied at the propellant surface and is characteristic of the propellant system. For simple thermal ignition, as described by Figure 1, T^T_{si} has exactly the same meaning and the same value as T^L_{si}. When secondary ignition reactions contribute energy for heating the propellant surface, as shown by Figure 2, the value of the thermal ignition temperature cannot be calculated directly unless the contribution from these reactions to the total applied heat flux can be ascertained. However, it will be shown later that this ignition temperature, T^T_{si}, can be calculated with only a measurement of ignition time under any experimental test conditions if the propellant system has been previously characterized under test conditions which produced simple thermal ignition of the propellant.

Baer [8] has predicted from thermal ignition theory, and has also shown experimentally, that the absolute thermal ignition temperature, T^T_{si}, is not dependent on the initial propellant temperature. This means that a propellant that ignites thermally will ignite at the same temperature, under a given applied heat flux, regardless of its initial uniform temperature. However, the ignition time will be a function of the initial temperature.

Mean Surface Heat Flux

The "mean surface heat flux," $\bar{F}$, as used in this thesis is the externally applied, constant surface heat flux which is required to bring the propellant to its ignition temperature (T^L_{si}) in the observed ignition time. This heat flux at the propellant surface is calculated by the following equation:

$$\bar{F}_s = \frac{\Gamma_p}{2} \left(\frac{\Pi}{t_i}\right)^{1/2} \left(T^L_{si} - T_o\right) \qquad (1)$$

Where Γ_p is the thermal responsivity of the propellant (the square root of the product of thermal conductivity, density, and heat capacity of the propellant).

t_i is the observed ignition time.

T_o is the initial uniform propellant temperature.

T^L_{si} is the ignition temperature for linear heating as previously defined.

The mean surface heat flux is the experimental heat flux for experiments conducted in a radiation or carbon-arc image furnace which give a very nearly constant heat flux at the propellant surface.

Surface heat flux has special significance in terms of thermal ignition theory. Thermal ignition theory predicts that a plot of experimental data in the form of $\ell n\ (\bar{F})$ versus $\ell n\ (t_i)^{1/2}$ can be represented by a straight line. The slope of this straight line is related to the activation energy of the key chemical reaction in the ignition process. This and other aspects of thermal ignition theory will be discussed in considerable detail in the next section.

All the experimental data on propellant ignition presented in the section on experimental results are graphed in the form of $\ell n\ (\bar{F})$ versus $\ell n\ (t_i)^{1/2}$. The characterization of ignition data on propellants in terms of heat flux at the surface and ignition time provides a means of representing experimental data obtained by different experimental methods in a unified manner regardless of the nature of the heat transfer process used to provide the heat flux.

THERMAL IGNITION

Altman and Grant [2] were perhaps the first to apply thermal ignition theory to experimental data. They studied the ignition of composite solid propellants by heating a slab of propellant electrically with an embedded wire. Using transient heating theory and the assumption of constant thermophysical properties for the propellant, a surface temperature at ignition was calculated from the experimentally determined ignition time. They found from this study that their propellant ignited when the surface temperature reached 390°C regardless of the rate of energy input to the embedded wire, a result that suggested that an exothermic reaction with a high activation energy was a rate controlling step in the ignition process. Altman and Grant predicted from theoretical considerations that this surface temperature at ignition should be a function of the applied heat flux and that the ignition temperature should increase with an increase in heat flux. However, because of the limited range of their experimental data, they could not establish a relationship between these variables.

The concept of an invariant ignition temperature, as used by Altman and Grant, is thermal ignition theory in its simplest form.

Thermal Ignition with Bulk-Phase Reactions

Hicks [46] carried out a numerical analysis of a thermal ignition model described by the following partial differential equation.

$$\rho c \frac{\partial T}{\partial t} = k \frac{\partial^2 T}{\partial x^2} + Z\, Q_v\, e^{-\frac{E_a}{RT}} \qquad (2)$$

$$\text{at } x = 0,\ F_s(0,t) = -k \frac{\partial T}{\partial x} = h\,(T_g - T_s)$$

$$\text{at } x = +\infty,\ \frac{\partial T}{\partial x} = 0,\ \text{all } t$$

$$\text{at } t = 0,\ T(x) = T_o,\ \text{all } x$$

where: k, ρ, and c are the thermal conductivity, density, and specific heat, respectively, for the propellant.

Z is the frequency factor and is characteristic of the rate controlling chemical reaction.

Q_v is the heat of reaction per unit volume of propellant.

E_a is the activation energy of this temperature-dependent reaction.

The basic assumptions for this model are:

1. Heat is transferred uniformly to the surface of a homogeneous, semi-infinite slab of propellant, initially at T_o, by a hot gas with a temperature (T_g) through a constant heat transfer coefficient (h).
2. The propellant thermophysical properties, k, ρ, and c are not temperature dependent.
3. The rate of the condensed-phase reactions is not dependent on concentration of ingredients.
4. There is no regression of the propellant surface or depletion of reactive propellant ingredients during ignition.

In his numerical analysis of this ignition model, which was intended to describe ignition of double-base propellants, Hicks considered a wide range of values for T_o, E_a/R, h, k, and ρc. He also considered the effect of cutting off externally applied energy before ignition occurred. For the case where energy was supplied until ignition occurred, ignition time was taken to be the time interval from the first application of energy until the calculated surface temperature reached a preassigned value. For this case he found that the rate of energy generation in the solid and at the surface by the key chemical reaction is related to that absorbed at the surface from linear heating by a constant at the time of ignition. This gives a criterion for ignition defined by the following expression:

$$K = \frac{Z\, Q_v\, e^{-E_a/R\, T^T_{si}}}{\rho c \left(\frac{\partial T^T_s}{\partial t}\right)_i + Z\, Q_v\, e^{-E_a/R\, T^T_{si}}} \qquad (3)$$

where K is a constant characteristic of the propellant system, and the subscript i denotes the expression is to be evaluated at time of ignition, t_i. Hicks assumed a value of 0.833 for K. Using this value, he found that ignition times calculated by Equation (3) differed by less than 10 per cent from values calculated numerically using Equation (2).

Baer [6] showed that it was not necessary to know the value for K in Equation (3) and, furthermore, this criterion for ignition could be put in a useful form for correlating and analyzing experimental data.

$$\frac{d\ \ell n\ (t_i)^{1/2}}{d\ \ell n\ \bar{F}_s} = S = -\left[\frac{\frac{E_a}{R}\left(T_{si}^T - T_o\right) - \left(T_{si}^T\right)^2}{\frac{E_a}{R}\left(T_{si}^T - T_o\right) + \left(T_{si}^T\right)^2}\right] \qquad (4)$$

From this expression it is seen that for ignition processes where thermal ignition of bulk-phase reactions is controlling, experimental data plotted in the form of $\ell n\ (\bar{F})$ versus $\ell n\ (t_i)^{1/2}$ can be represented by a straight line. The slope of this line is related to the activation energy, E_a/R, of the key chemical reaction. For a reaction having a finite activation energy the slope of the line will always be greater than -1.0 ($|S| < 1$). For a system having a very large activation energy, the slope of the straight line will approach - 1.0. For this condition, the concept of a unique ignition temperature is valid. Thus the criterion proposed by Altman and Grant is a limiting case of the Hicks criterion for ignition.

Baer [6] found that E_a/R was insensitive to variations in T_{si} over the range of temperatures normally associated with propellant ignition, and that Equation (4) agreed well with Hicks' numerical calculations for ignition times when the values of E_a/R were greater than 15,000°K. The major error in evaluating E_a/R from experimental data arises in determining the slope from an $\ell n\ (\bar{F})$ versus $\ell n\ (t_i)^{1/2}$ plot. This is true since the slope has a value only slightly greater than - 1.0 and E_a/R is proportional to 1.0 plus the value for the slope.

Evans, et al. [32] considered a thermal ignition model, which is basically the same as that proposed by Hicks, in connection with their study of the ignition of ammonium perchlorate-copper chromite-carbon

pellets under high radiant fluxes in a carbon-arc image furnace. In this work special care was taken to develop an ignition model which could be used for critically evaluating thermal ignition theory by a series of carefully controlled ignition experiments. The differential equation which was taken to describe the pellet heating process is:

$$\rho c(T) \frac{\partial T}{\partial t} = k \frac{\partial T}{\partial x^2} + Z\, Q_v(T)\, e^{-E_a/RT} \qquad (5)$$

$$\text{at } x = 0,\ F_s(0,t) = -k \frac{\partial T}{\partial x} = I\,(1 - r)$$

$$\text{at } x = +\infty,\ T(t) = T_o,\ \text{all } t$$

$$\text{at } t = 0,\ T(x) = T_o,\ \text{all } x$$

where I is the radiant flux received by the pellet and (1 - r) is the fraction of incident radiation absorbed by the pellet surface, r being the fraction reflected. The other symbols have their conventional meanings.

For this model it was assumed that:

1. Transmittance of radiant energy was negligible.
2. The pellet was a one-dimensional slab.
3. The pellet was homogeneous.
4. Surface regression could be neglected.

All of these assumptions were critically reviewed in terms of pellet properties.

Numerical solutions to Equation (5) were obtained for selected values of constant surface heat flux using experimentally determined values for k, ρ, c(T), Z, $Q_v(T)$, and E_a. An important feature of this

analysis was the use of kinetic data for the postulated key chemical reaction in the ignition process, the exothermic decomposition of ammonium perchlorate. The data used by Evans, et al. [32] were determined thermogravimetrically by Jacobs and Russell-Jones of the Imperial College, London. Temperature-dependent values for c and Q_v were used in this analysis. The regular numerical procedure for calculating the pellet surface temperature was modified to include the latent heat of phase transition for the crystalline ammonium perchlorate.

Thermal Ignition with Surface Reactions

Baer [6] used Equation (4) to calculate activation energies for ignition reactions from propellant ignition data obtained in a radiation furnace. He found that they were high by a factor of about two over that which would be expected for the key chemical reactions in the ignition process. Activation energies for three greatly different ammonium perchlorate propellants ranged from 57 to 80 kcal/(mole). It has been established that the activation energy for low-temperature decomposition of ammonium perchlorate is about 30 kcal/(mole), and that for the oxidation of hydrocarbons is of the same order of magnitude. He tentatively concluded from these observations that the ignition mechanism for composite propellants was different than that defined by Hicks' model, Equation (2).

In a subsequent analysis similar to that used for developing Equation (4), Baer [7,80] showed that if a surface reaction is assumed to be the key ignition reaction, then activation energies

calculated from experimental data were in the range expected. He derived the following equation:

$$\frac{d\ \ell n\ (t_i)^{1/2}}{d\ \ell n\ \bar{F}_s} = S' - \left[\frac{\frac{E_a}{R}\ (T^T_{si} - T_o) + (T^T_{si})^2}{\frac{E_a}{R}\ (T^T_{si} - T_o)}\right] \tag{6}$$

From his observations Baer [7,8,81,82] proposed that one can reasonably assume that a single surface reaction is controlling in the ignition process. The exact nature of this key chemical reaction could not be defined by the experimental data available, but appeared to be the low-temperature decomposition of the ammonium perchlorate. For the case where the propellant surface is subjected to a one-dimensional, constant external surface heat flux, F_s, the mathematical model which describes the relationship between temperature, time, and position in the propellant sample is:

$$\rho c\ \frac{\partial T}{\partial t} = k\ \frac{\partial^2 T}{\partial x^2} \tag{7}$$

$$\text{at } x = 0,\ F_T\ (0,t) = -\ k\ \frac{\partial T}{\partial x} = F_s + Be^{-E_a/RT}$$

$$\text{at } x = +\infty,\ T(t) = T_o,\ \text{all } t$$

$$\text{at } t = 0,\ T(x) = T_o,\ \text{all } x$$

Here the factor B is the product of the frequency factor, Z, and the energy released at the surface per unit area, Q_s, by the key chemical reaction. The other symbols have their conventional meaning. An important feature of this description is that the chemical energy

term is in the boundary condition Whereas Hicks considered a distributed homogeneous reaction, Baer considered the key reaction to be localized at the surface.

For the purpose of this analysis, Baer assumed that:

1. The propellant undergoing heating through a constant surface heat flux could be treated as a homogeneous, semi-infinite solid originally at a uniform temperature (T_o).
2. The thermophysical properties of the propellant, k, ρ, and c were not temperature dependent. Values determined experimentally at 60°C were used.
3. Negligible surface regression of the propellant surface occurred up to the time of ignition.
4. The rate of the surface reaction was not dependent on concentration of ingredients.
5. Activation energy, E_a, and heat of reaction, Q_s, are not temperature dependent.
6. That ignition of the propellant occurred when the heat flux contributed by the surface reaction was much greater than the applied surface heat flux.

Equation (7) was put into a dimensionless form and numerical solutions to the equation were obtained for a range of reasonable values for the parameters. The results of this analysis can be summarized as follows:

1. A plot of experimental ignition data in the form of $\ell n\ (\bar{F}_s)$ versus $\ell n\ (t_i)^{1/2}$ can be represented by a straight line with a slope greater than -1.0. The slope of this line,

to a good approximation, is only dependent on the activation energy for the key ignition reaction and the initial propellant temperature. The activation energy is related to the slope of the line by:

$$S = 4.2 \frac{RT_o}{E_a} - 1 \tag{8}$$

2. Ignition time (t_i) can be expressed in terms of the mean surface heat flux and propellant thermal properties by:

$$(t_i)^{1/2} = \frac{\Gamma_p (\Pi)^{1/2}}{2\bar{F}_s} \left[\frac{E_a/R}{1 - 1.04 \ln (\bar{F}_s/B)} - T_o \right] \tag{9}$$

It is seen from Equation (9) that for two propellants having the same activation energy and pre-exponential factor, B, but differing in thermal responsivity, their relative ignition times at a given surface heat flux are a function only of their thermal properties. This fact is an important one in the later discussion of results.

The surface energy for thermal ignition is defined as:

$$E_i = \int_0^{t_i} \bar{F}_s \, dt \tag{10}$$

and can be evaluated from Equation (9). For the case where the externally applied heat flux can be represented as a mean surface flux, $\bar{F}_s$, the ignition energy is:

$$E_i = \bar{F}_s \, t_i = \frac{(\Gamma_p)^2 \, \Pi}{4 \, \bar{F}_s} \left[\frac{E_a/R}{1 - 1.04 \ln (\bar{F}_s/B)} - T_o \right]^2 \tag{11}$$

The ignition model does not allow predicting the value for activation energy and the pre-exponential factor, B, but provides a method for determining these values for a propellant system from experimental data. Neither does the model predict an effect of pressure on ignition time; however, if it is found experimentally that pressure has an effect on ignition, it can be included later as a factor in B.

By examining the groups that appeared when Equation (7) was put into dimensionless form for numerical solution, Baer [8,82] found that ignition data for a series of propellants which have the same value of E_a/R and B, but have different thermophysical properties, should be represented by one straight line if the data are plotted in the form of a dimensionless surface heat flux ($\bar{F}^*$) versus a dimensionless ignition time (t_i^*) on logarithmic coordinate paper.

$$t_i^* = \frac{t_i}{(\Gamma_p)^2} \left(\frac{RB}{E_a}\right)^2 \tag{12}$$

$$\bar{F}^* = \bar{F}_s/B \tag{13}$$

Thus for a given surface heat flux and initial uniform propellant temperature (T_o), the value of t_i^* would be the same for all propellants which ignite thermally and have the same key ignition reaction, regardless of the value for thermal responsivity of the propellant. For a given value of t_i^* the thermal ignition temperature (T_{si}^T) would be the same for all propellants with the same values of E_a/R and B.

From this analysis it was also found that the method was still more general and that ignition data for propellants for which the activation energy of the key ignition reaction was the same, regardless of the values for B and Γ_p, could all be represented by the same straight line when experimental data are plotted in dimensionless form.

The mathematical model defined by Equation (7) was found to be in excellent agreement with experimental data for ignition of composite propellant under low radiant heat fluxes in the radiation furnace [8,82]. It was found by the research reported here that this model also describes the ignition process for composite propellants under high convective fluxes.

Thermal Ignition with Surface Heating from Secondary Ignition Reactions

Through the experimental studies on propellant ignition conducted for this thesis, it is now possible to see more clearly how secondary ignition reactions affect propellant ignition. Secondary ignition reactions are important in the ignition process under some test conditions in that they supply energy for bringing the propellant surface to its thermal ignition temperature.

Figure 3 shows how these secondary chemical reactions affect the ignition process. In this figure the solid-line curve (1) represents simple thermal ignition. Under an equivalent externally applied heat flux, the net effect of secondary reactions is to reduce the time required to bring the propellant to its thermal ignition temperature (T^T_{si}) as shown by the dashed-line curve (2). Based on the experimental work for this thesis, it appears, for ignition of propellants by

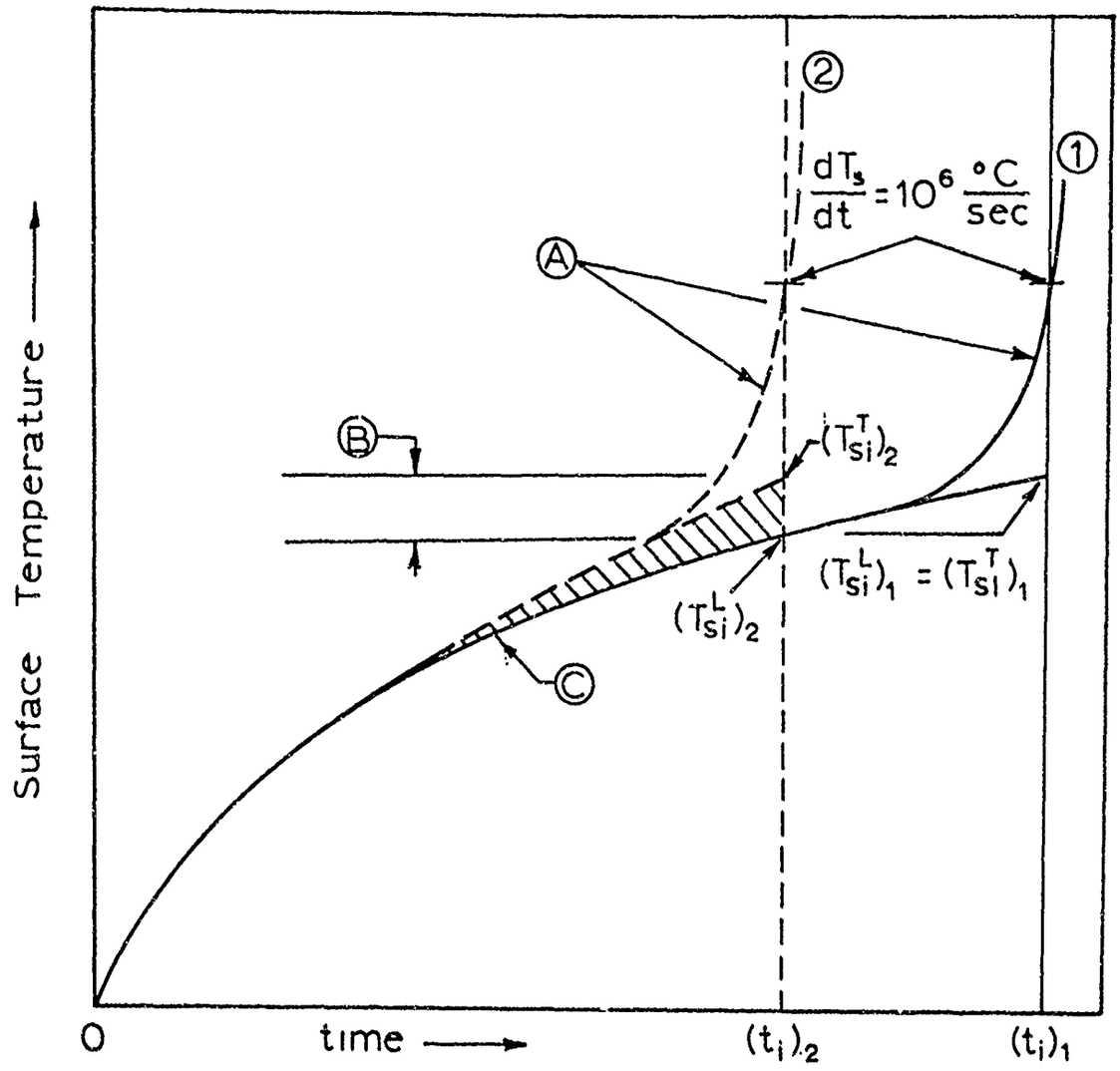

Figure 3

Surface-Temperature History for a Propellant Undergoing Thermal Ignition Illustrating the Effect of Secondary Ignition Reactions on the Ignition Process. Curve 1 is for Simple Thermal Ignition. Curve 2 is for Thermal Ignition with Part of the Heat Flux at the Surface Supplied by Secondary Ignition Reactions.

A. Temperature Rise Produced by the Key Ignition Reaction.
B. Temperature Rise Produced by Secondary Ignition Reactions.
C. Linear Heating From Externally Applied Heat Flux.

convective heating with a neutral gas, that these reactions are extremely fast gas-phase or heterogeneous-surface reactions involving only ammonium perchlorate decomposition products evolved during heating. These reactive species appear to be generated by two-dimensional heating of surface imperfections. The presence of secondary ignition reactions does not change the basic thermal ignition process, but affects ignition only by supplying part of the energy for heating the propellant surface.

The theory for thermal ignition of solid propellants has undergone much development, and it describes in considerable detail simple thermal ignition of propellants. However, except for the studies by Anderson, et al. [4], only a small amount of theoretical work has been done to include energy contributions from secondary chemical reactions in propellant ignition theory. Anderson and coworkers [4] have considered in much detail the heating of a propellant surface by exothermic, heterogeneous-surface reactions between an environmental oxidizer and the propellant binder-fuel. They considered two cases: (1) heating from exothermic reactions only and (2) heating from exothermic reactions in conjunction with externally applied heat flux. They were able to treat this problem since they could predict with reasonable precision the effect of oxidizer concentration on the surface reactions.

Thermal Ignition Theory and Composite Propellants

One of the assumptions required for the development of thermal ignition theory needs further discussion relative to its application to composite propellants.

This is the assumption that a composite propellant can be regarded as a truly homogeneous, semi-infinite solid at high heating rates. The transient heat conduction problem that applies to a composite solid of this kind does not appear to have been solved by either analytical or numerical methods, and no attempt was made to obtain a solution for this problem in the work for this thesis. Consequently, for the present, this assumption can only be discussed with semiquantitative arguments.

Take as an example a propellant which contains a very fine particle-size ammonium perchlorate, say a 15-micron (weight average) cut with particle diameters ranging from submicron size to 25 microns. Calculations show that the average thickness of the polymer film between particles would be less than a micron if there were no appreciable agglomeration of ammonium perchlorate particles. It is thus seen that for propellants which contain an appreciable fraction of fine ammonium perchlorate, the difference in thermal properties would not preclude the establishment of a fairly uniform temperature at the propellant surface. It has been observed experimentally that propellants containing the same ingredients, but with a different particle-size distribution of ammonium perchlorate in a bimodal blend, which always included an appreciable fraction of 15-micron ammonium perchlorate, exhibited essentially the same ignition characteristics under test conditions where simple thermal ignition of the propellant occurred.

For propellants with only a coarse particle-size ammonium perchlorate, the polymer film surrounding each particle would be much thicker and one would expect the temperature of the exposed polymer to

be as much as 50 to 100°C higher, depending on the particle size, than that for the surface of an ammonium perchlorate particle. Even so, one would expect, by analogy to the one-dimensional heat conduction problem (the bringing together of two semi-infinite solids of different thermal properties and at different temperatures) that a fairly uniform interface temperature would be established between the polymer and ammonium perchlorate particles at the surface. The thermal ignition temperature for a propellant with coarse particles would then be the interface temperature at the time ignition occurred.

CHAPTER III

EARLIER WORK ON PROPELLANT IGNITION

All ignition studies on propellant, regardless of the mode of heat transfer to the propellant surface or the nature of the environmental test conditions, reflect the response of a propellant system to external stimuli and reveal information about the important chemical processes in ignition. However, this section is restricted to a brief review of experimental work on ignition which is relevant to the work described in this thesis. Specific information from convective heating experiments and also information on propellant ignition obtained by different heating methods is integrated in the discussion of experimental results for propellants studied in the research for this thesis. Some of the work reviewed here has been reviewed previously by Summerfield and Hermance [89,43].

IGNITION BY CONVECTIVE HEAT FLUXES

Perhaps the earliest quantitative studies on the ignition of solid propellants by convective heat fluxes were reported by Churchill, Kruggel, and Brier [24]. In this work cylindrical grains of pyrocellulose and double-base propellants were exposed to cross-flow heating with hot nitrogen, oxygen, carbon dioxide, or mixtures of oxygen and nitrogen. The results of this study showed that the gas temperature, gas velocity, and composition of the test gas, if it contained oxygen, affected the time for ignition to occur. Some of

results on M-2 double-base propellant from this study are compared with data obtained in a pressurized furnace under radiant and free-convection heat transfer by Roth and Wachtell [78].

In general, the results under convective heating by Churchill et al. definitely show that gas-phase processes are important in the ignition of pyrocellulose and double-base propellants. However, the work of Roth and Watchell indicates that condensed-phase reactions also have a role in the ignition process for double-base propellants.

The first quantitative studies on the ignition of composite propellants by convective heat fluxes that are reported were conducted by Baer in a shock tube. The results of this work are reported in References 6 and 9. He studied ignition of propellant samples mounted in the wall of a test section at the end of the shock tube. The rate of energy transfer to the wall position was measured prior to making ignition tests. Several different ammonium perchlorate propellants and one ammonium nitrate propellant were studied. Baer found that compositional factors influenced propellant ignition, but he did not undertake a systematic variation of propellant ingredients. For ignition of these propellants under heat fluxes of 25 to 100 cal/$(cm)^2(sec)$, he found that ignition time was primarily dependent on heat flux at the propellant surface when air or nitrogen was used as the test gas. All propellants were tested under approximately the same gas velocity, and heat flux was varied by increasing the gas temperature and pressure. Pressure and temperature of the test gas had no observable effect on ignition time at a given heat flux. When

oxygen was used as the environmental gas, the time for ignition of the propellant to occur as observed by a photoelectric device was considerably shorter than in air or nitrogen at equivalent heat flux levels. Since ignition time was primarily dependent on heat flux at the propellant surface in air and nitrogen, it was concluded that ignition results on composite propellants could be correlated by the criterion for thermal ignition suggested by Hicks [46]. Baer also found that data obtained for ignition of the same propellants in a radiation furnace were in qualitative agreement with data obtained by convective heating. It was apparent, however, that hot, reactive gases, such as oxygen, greatly reduced the ignition time for propellants in convective heating tests. He suggested that the improved ignitability resulted from heating of the propellant surface by exothermic reactions between the binder-fuel and oxygen.

The work of Baer was extended by McCune [67,80] to slightly higher heat flux levels to obtain minimum ignition times in the range of one to two milliseconds. This work was conducted in a 4.0-in. diameter shock tube, rather than the 1 7/8-in. diameter tube used by Baer, to obtain more uniform gas properties behind the reflected shock. McCune also varied the test-gas velocity across the propellant through the use of different flow-control orifices downstream of the test position. The results of this study were in good agreement with Baer's earlier work, except that McCune observed that one of the propellants tested was more difficult to ignite as the velocity of the test gas across the surface of the propellant was increased.

In a more recent investigation, Hermance [43] studied ignition of ammonium perchlorate propellants by convective heating in both supersonic and subsonic gas streams. These ignition studies were conducted in a shock tunnel. In none of the tests at supersonic gas velocities, Mach 2.35, using test samples in the form of either a two-dimensional wedge or a cylinder with a hemispherical end, was steady deflagration of the propellant observed. However, some regions of luminosity were observed by high-speed photography for a wedge-shaped sample having a semi-vertex angle of 45° and for the hemisphere-cylinder-shaped sample. When regions of luminosity were observed they were always brighter when oxygen was the test gas. Examination of samples after tests showed changes in surface characteristics which resulted from exposure of the propellant to the high-temperature and high-velocity gases, but these surface features varied somewhat and were dependent on the shape of the test sample and test gas.

For subsonic flow tests, at a gas velocity of 60 ft/(sec), a propellant sample in the form of a flat plate with a sharp leading edge was ignited in test gases composed of pure oxygen, pure nitrogen, or mixtures of nitrogen and oxygen. Ignition occurred under all test conditions, but ignition was much faster at equivalent heat flux levels in gases that contained oxygen than in pure nitrogen. The effects of variable total gas pressure and subsonic flow velocities were not investigated in this study. Hermance concluded from these studies that the concept of a gas-phase mechanism controlling in the ignition process of composite propellants cannot be neglected. This conclusion was based, primarily, on the observed dependence of ignition

time on the concentration of oxygen in the test gas at subsonic flow conditions, and the fact that ignition followed by steady-state deflagration of the propellant never occurred for heating at supersonic flow conditions.

The most comprehensive experimental study on propellant ignition of those reported was that conducted by Bastress, Alan, and Richardson [10]. In this work they studied ignition of propellants in both radiant and convective heating experiments. In addition, they investigated the effect of solid particles and flame retardants in the convective gas on ignition. Also, they measured heat flux from practical propellant igniters and applied this information to the ignition of propellant grains.

The apparatus used for studying ignition in convective heating experiments was uniquely suited for this work. The propellant samples to be ignited were mounted in the wall of a long, rectangular test channel, 1.0-in. wide by 0.25-in. high. The channel wall was heated by the flow of hot gases from a gas-fueled combustion chamber. During start up of the combustion system, hot combustion gases were vented through two ports in the combustion chamber and were prevented from flowing into the test section by a diaphragm downstream of the propellant position. The test channel was also pressurized with helium during start up to prevent flow of combustion gases into the test section. When the diaphragm was ruptured, hot gases flowed through the test section and the flow rate was controlled by a nozzle at the exit section. Heat flux was monitored during each ignition run by wall-mounted thermocouples. Ignition was detected photoelectrically.

To study the effect of environmental factors, Bastress, et al. varied gas temperature, gas flow velocity in the test section (as high as Mach 1), and composition of the convective gases. They found that the most significant factor influencing ignition of the propellant was the rate of heat transfer to the propellant surface. In addition, as has been observed by most investigators, the presence of oxygen in the test gases reduced ignition time. In these tests and also for tests by radiant heat fluxes, little or no effect of pressure on ignition time was observed when the test pressure was varied from 30 to 135 psia. Since there was no test-period limitation in the apparatus used, ignition was studied over a wide range of heat fluxes with the maximum near 200 cal/$(cm)^2$(sec). Another significant observation was that ignition characteristics of the propellant were strongly dependent on surface roughness. It was also observed in this work that velocity of the gas in the test section influenced ignition and that ignition time increased with gas velocity at equivalent externally applied heat fluxes. For gas velocities less than Mach 0.2 in the test section, there was no noticeable change in ignition characteristics with a variation in gas velocity.

Bastress, Alan, and Richardson were primarily interested in developing experimental methods for obtaining ignition data which could be used for designing ignition systems. They did not attempt to relate their experimental observations on propellant ignition to a particular ignition theory. However, they did point out that the propellant surface does not remain unchanged during the heating process,

and that an ignition theory that describes solid propellant ignition must take into consideration the chemical and physical changes that occur at the propellant surface.

Lancaster [58] and Grant [41] studied composite propellant ignition using combustion gases from a gas-fueled combustor to heat the propellant surface. Hot gases were passed through the perforation of a cylindrical grain of propellant, before being exhausted to the atmosphere through a critical-flow nozzle. The results from these studies are summarized by Reference 40. To separate the effects on ignition of heat flux, pressure, and concentration of oxygen in the test gas, in one phase of this study ignition tests were conducted with the same heat-transfer rate at the propellant surface. The effect of pressure on ignition was studied over the range of 30 to 80 psia. The effect of oxygen on ignition was investigated by varying the amount of methane, nitrogen, and oxygen in the combustor feed in such a way that the temperature of the hot gases was the same for the series of tests. The concentration of oxygen was as large as 75 weight per cent of the test gas for some ignition runs. Both changes in pressure and concentration of oxygen in the test gas significantly influenced the ignition of propellants. In the experiments conducted by Lancaster and Grant, the ignition of propellants was followed by recording the pressure history in the chamber. The observed effects of pressure and oxygen concentration in the test gas on ignition were explained in terms of chemical processes in the gas phase.

Kling, Maman, and Brulard [55] have recently published their work on ignition of composite solid propellants by convective heating in a shock tube. The experimental apparatus they used was similar to that used by Baer [6] and McCune [67] in earlier studies, and is also very similar to that used for conducting research for this thesis. Kling, et al. [55] investigated the effect of gas velocity, which they varied over the range of 12 to 220 m/(sec), and the effect of oxygen concentration in the test gas, a mixture of nitrogen and oxygen. All tests were conducted under high pressures, 35 to 55 atmospheres, and at high convective heat fluxes which gave ignition of a wall-mounted propellant sample in less than 5 milliseconds in most tests. It was found from this study that both the velocity of the gas across the propellant surface and oxygen in the test gas affected propellant ignition. However, it was also noted that propellants of different composition responded differently to these environmental factors. Based on these studies, Kling, Maman, and Brulard concluded that the determining step in ignition of composite propellants is a process in the gas phase.

IGNITION BY RADIANT HEAT FLUXES

Beyer and Fishman [13] studied ignition of an ammonium perchlorate propellant with a polysulfide rubber binder in an arc image furnace. Ignition characteristics of this propellant were observed at pressures in the range of 0.0065 to 35 atmospheres and at radiant heat fluxes at the propellant surface of 5 to 75 cal/(cm)^2(sec). The first indication of luminosity at the surface was taken to be the

onset of ignition. Energy requirements for ignition were based on a "go/no-go" criterion. Beyer and Fishman found that the energy required to produce ignition was strongly dependent on the ambient pressure, particularly for pressures in the range of 0.1 to 5 atmospheres. They also found that the effect of pressure on ignition was more pronounced at higher heat flux levels. Beyer and Fishman also observed that the exposure time to induce ignition of the propellant was strongly dependent on the level of the externally applied heat flux for fluxes of 5 to 10 cal/$(cm)^2$(sec), and was a much weaker function of heat flux for fluxes in the range of 10 to 75 cal/$(cm)^2$(sec). In this work they also found an effect of oxygen on ignition. As the concentration of oxygen in the gas stream, which was passed through the ignition chamber, was increased, the external energy required to produce ignition of the propellant was greatly reduced. High-speed motion pictures taken by Beyer and Fishman, during ignition tests at atmospheric pressure and at high radiant heat fluxes, showed that a flame was first observed in the gas phase above the propellant surface which was followed by ignition at the propellant surface.

Price, et al. [77] report experimental data for ignition of different ammonium perchlorate propellants in an arc image furnace. The experimental work reported was conducted by the Bermite Powder Company and Stanford Research Institute. Much of the ignition data reported are for Propellant A-26, composed of the following ingredients: 25.0 per cent polybutadiene-acrylic acid copolymer, 75.0 per cent ammonium perchlorate (80 micron), and 1.0 part per hundred parts

propellant of copper chromite. For propellant A-26, ignition times were almost identical at pressures of 15 and 100 psia for equivalent radiant heat fluxes in the range of 5 to 20 cal/(cm)^2(sec) with air or nitrogen as the test gas. For low heat fluxes, 5 to 20 cal/(cm)^2 (sec), ignition time was strongly dependent on the heat flux level [$(t_i)^{1/2}$ was approximately proportional to $1/\bar{F}$]. For higher heat fluxes, 30 to 100 cal/(cm)^2(sec), ignition time was a weaker function of heat flux, but was now also dependent on the ambient test pressure.

Ignition data are reported in the paper by Price, et al. [77] for propellants with different additives and particle sizes of ammonium perchlorate. Ignition tests on these propellants were made at nominal pressures of 200 and 400 psia and at a radiant heat flux of 100 cal/(cm)^2 (sec). For propellants with no additives, a propellant with 15-micron ammonium perchlorate ignited much faster than a similar propellant with 80-micron ammonium perchlorate. For propellants which contained copper chromite, the effect of variations in particle size of the ammonium perchlorate was no longer significant. Both copper chromite and carbon black, in concentrations as low as 0.5 per cent in the propellant, significantly reduced ignition times below those observed for propellants without additives. In general, ignition times were longer at test pressures of 400 psia than at 200 psia; however, studies at different pressures for applied heat fluxes of 100 cal/(cm)^2(sec) showed that the ignition process was a complex function of test pressure and the effect of pressure was also related to the concentration of additives in the propellant.

Evans, Beyer, and McCulley [32] made a careful study of the ignition characteristics of pressed propellants, containing carbon black, copper chromite, and ammonium perchlorate, in a carbon-arc image furnace at heat fluxes of 9 to 63 cal/(cm)^2(sec). All ignition experiments were conducted at 25 atmospheres in nitrogen. The concentrations of copper chromite and carbon in the pellets were varied systematically to study the effect of compositional factors on ignition. The pellets tested were classified according to composition: (1) constant copper chromite plus carbon (5 per cent of the pellet), carbon was varied from 0 to 4 per cent; (2) constant copper chromite, concentration of copper chromite was held at 2.5 per cent and carbon content was varied from 0.5 to 4.5 per cent in equal increments; and (3) constant carbon, concentration of carbon was held at 2.5 per cent and copper chromite was varied from 0.5 to 4.5 per cent.

The experimental procedure employed by Evans, et al. was to determine for a given radiant heat flux the minimum exposure time, t_e, necessary to initiate a deflagration wave at the pellet surface. For t_e greater than t_i initiation occurred during exposure to the radiant heat flux, and for t_e equal to t_i a deflagration wave was initiated within one millisecond of the time that the energy pulse was cut off. The temperature of the pellet surface, at the time that a deflagration wave was initiated, was calculated using the experimentally determined values of t_i.

Evans, Beyer, and McCulley found that when carbon was added to the composition that ignitability of pellets was greatly improved.

For ignition of pellets which contained 5 per cent copper chromite and no carbon, the temperature at the pellet surface was about 380°C at t_i. When 1.0 per cent carbon was added replacing copper chromite the temperature of the pellet surface was only 260°C when the energy pulse was cut off. Variations in the concentration of copper chromite in the pellets from 0.5 to 4.5 (for pellets with 2.5 per cent carbon) reduced the surface temperature at t_i from 260°C to 240°C, respectively, a rather insignificant amount relative to the effect exhibited by variations in carbon content. They also found that for a given pellet composition the surface temperature at the instant that the application of external energy was terminated, t_e, an exposure time sufficient to initiate steady deflagration, was independent of the heat flux level.

In general, the experimental results reported by Evans, et al. were not in agreement with those predicted by thermal ignition theory. Pellets were found to ignite in a much shorter time at a given heat flux level than that predicted by theory. They concluded that the experimental ignition results obtained indicated that thermal ignition of material in the solid phase was not a prerequisite for initiation of a deflagration wave at the pellet surface.

Baer and Ryan [8,82] studied ignition of composite propellants in a radiation furnace at radiant heat fluxes of 1 to 13 cal/(cm)^2(sec). These low heat fluxes gave ignition times in the range of 0.2 to 25.0 seconds. Contributions from both radiation and free-convection heat transfer in the furnace were considered for calculating heat flux at the propellant surface during ignition tests. They found for ignition

at low radiant heat fluxes that ignition times for ammonium perchlorate - oxidized propellants were dependent only on the magnitude of externally applied heat flux, $\bar{F}$, and the initial uniform propellant temperature, T_o. The effect of ambient pressure on ignition was checked by subjecting an ammonium perchlorate-polysulfide rubber propellant to low heat fluxes in a sealed furnace and ignition times were measured at pressures in the range of 0.2 to 11.0 atmospheres. In another study on this propellant, the initial propellant temperature (T_o) was varied over the range of -60 to +60°C for ignition tests at atmospheric pressure. From this study it was found that the calculated linear heating temperature (T^L_{si}) at ignition for a given applied heat flux was essentially independent of the initial temperature (T_o)

In addition to the work described above, Baer and Ryan studied the effect of ingredients on propellant ignition. A group of propellants were made to study the effect of copper chromite concentration on the ignition characteristics of an ammonium perchlorate propellant with polybutadiene-acrylic acid rubber as the binder-fuel. They found that the ignitability of these propellants improved with incremental additions of copper chromite from 0 to 2 weight per cent. When the amount of copper chromite was increased from 2 to 4 per cent in the propellant, no further improvement in ignitability was observed. Experimental data for two of these propellants, propellant F (with 2 per cent copper chromite) and propellant G (with no copper chromite), have been retabulated in Table 1 of Appendix K from Reference 82, and are presented graphically in the form of $\ell n\ (\bar{F})$ versus $\ell n\ (t_i)^{1/2}$ by Figure 4. Complete compositional data for propellants F and G are

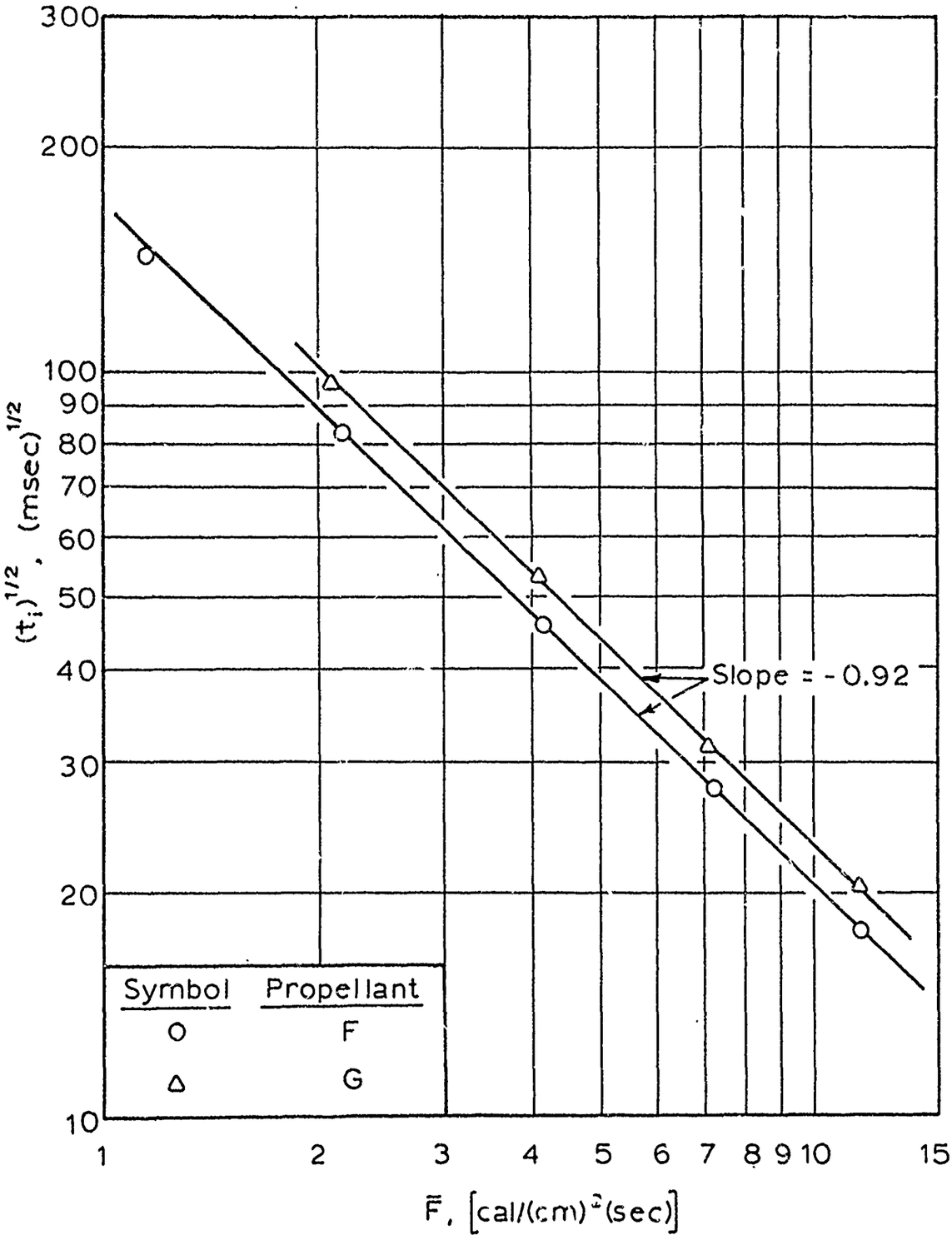

Figure 4

Ignition Data for Propellants F and G for Low Radiant Heat Fluxes at Atmospheric Pressure. (Data are from References 8 and 82).

given in Table 2. Propellants F and G were found to be slightly transparent to thermal radiation, and to ensure absorption of all radiant energy at the propellant surface, freshly cut surfaces were coated with a thin coat of carbon black. The results shown by Figure 4 are for propellant samples prepared in this manner. The difference in ignition times for propellants F and G at a given heat flux level represents the effect of copper chromite on the ignition process. It is interesting to note that both sets of data on the $\ell n\ (\bar{F})$ versus $\ell n\ (t_i)^{1/2}$ plot are represented by straight lines with slopes of -0.92.

Baer and Ryan also studied the ignition of pressed propellants containing only non-volatile fuels of carbon and graphite in a radiation furnace at low heat fluxes. All of the pressed propellants tested contained 2.0 weight per cent of copper chromite. They found, as was predicted by thermal ignition theory, that ignition data for all of the pressed propellants, although thermal properties were greatly different, can be represented by one straight line on logarithmic coordinate paper if the data are plotted in the form of a dimensionless surface heat flux ($\bar{F}^*$) versus a dimensionless ignition time (t_i^*) as defined by Equations (13) and (12), respectively. In addition, the ignition data in this dimensionless form for cast propellant F (with 2.0 per cent copper chromite) were represented by the same straight line that described ignition results for the pressed propellants.

In another experiment Baer and Ryan [8,82] studied the ignition of samples of F-propellant with square corners. They have shown by analytical solution of the heat conduction equation for two-dimensional heating of a semi-infinite (90°) corner that the temperature rise of a

semi-infinite corner would be twice that for the surface of a semi-infinite solid subjected to the same surface heat flux. From this analysis and considerations involving the propellant properties and thermal ignition theory, they predicted that the ignition time for a sample with a flat surface would be 3.6 times as long as that for a sample with a semi-infinite corner exposed to the same surface heat flux. The ratio of ignition times (ignition time for a flat surface divided by that for a semi-infinite corner) at the same surface heat flux was in excellent agreement with that predicted.

All of the ignition results on composite propellants reported by Baer and Ryan at low radiant heat fluxes were in substantial agreement with those predicted by thermal ignition theory. They concluded from this study on ignition of ammonium perchlorate propellants that the first step in the ignition process was the decomposition of ammonium perchlorate. The initial reaction is immediately followed by chemical reactions involving ammonium perchlorate decomposition products and the fuel.

CHAPTER IV

SHOCK-TUBE APPARATUS

The simple shock tube is a useful tool for studying ignition of solid propellants by convective heating in that it provides a means of producing hot gases for ignition tests in a few microseconds. Also, chemical composition, temperature, and pressure of test gases can be easily varied to specifications.

The shock-tube apparatus used for ignition studies on propellants in the research for this thesis is described in considerable detail in Appendix A. This shock tube had a diameter of 1 7/8 in., a driven section with a length of 15.5 ft., and a driver section with a length of 52.4 ft. The test section for convective heating experiments was mounted at the end of the driven section opposite the diaphragm position. Figure 5 is a cutaway sketch of the driven end showing the position of the test section. Figure 6 is an exploded view of the test section showing a propellant sample holder, flow-control orifice plate, and the quartz window through which propellant surfaces were viewed during ignition tests. Test procedures are described in Appendix B.

The test section has a constant-area flow channel, 1.15-in. long by 0.500-in. wide by 0.250-in. high, with a bell-shaped entrance region. The center of the test position at the wall of the flow channel is 0.50 in. from the intersection of bell-shaped entrance and the constant-area flow channel. The velocity of the hot, test gas through the test

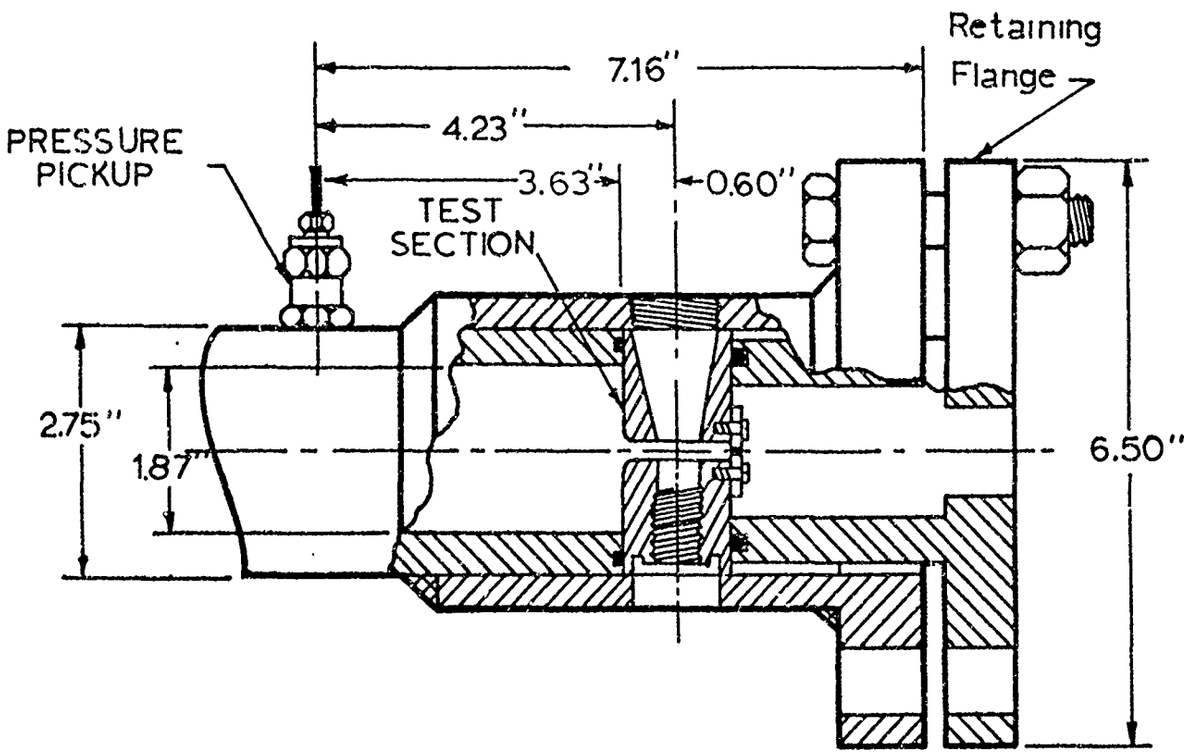

Figure 5

Cutaway Sketch of Driven End of Shock Tube Showing Position of the Test Section.

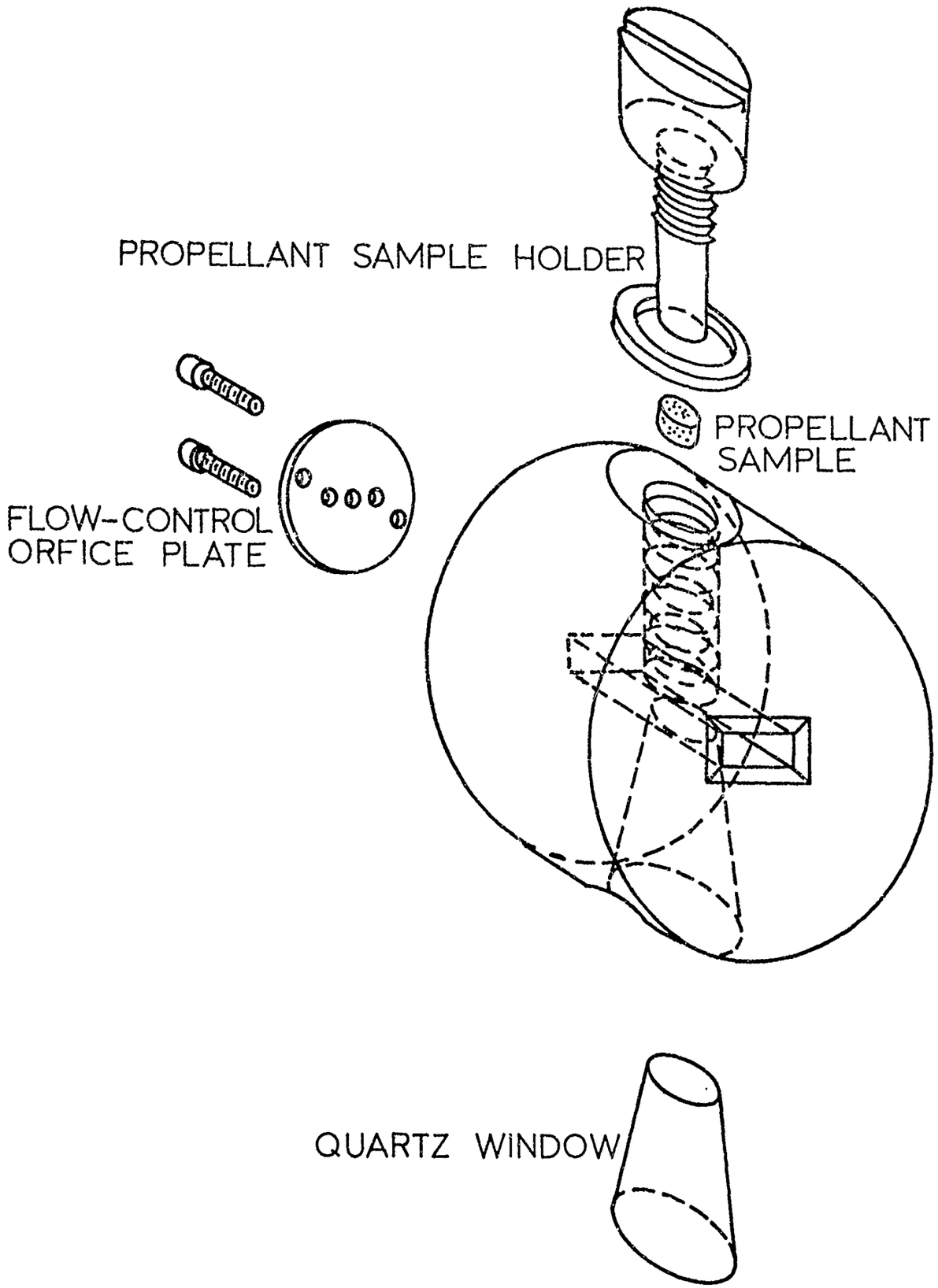

Figure 6

Sketch of Test Section

section was controlled by different critical-flow orifices at the outlet of the flow channel.

Since it was important to know the rate of heat transfer to the propellant surface during ignition tests, a series of studies were made on the shock-tube apparatus to provide data for calculating heat flux to the propellant surface. These studies included: (1) calibration of flow-control orifices at critical-flow conditions; (2) measurement of incident shock wave attenuation in the driven end of the tube so that the temperature of shock-heated gases could be calculated at the entrance to the test section; and (3) measurement of heat transfer at the test position for several initial shock-tube conditions and with different flow-control orifices for obtaining heat-transfer coefficients for heat transfer between the hot test gases and the wall of the flow channel at the test position. These preliminary studies for characterizing the shock tube are discussed in Appendix C.

HEAT TRANSFER TO WALL OF TEST SECTION

For critically evaluating ignition results on propellants with respect to thermal ignition theory, it was necessary to know the heat flux at the propellant surface to within about 5 per cent of its actual value during ignition tests. In a simple convective heating apparatus, the rate of heat transfer from a hot gas to the wall of a channel through which the gas is flowing can be predicted to within 10 per cent for steady-state conditions by conventional methods. For the shock-tube apparatus described briefly in the preceding section, the heat transfer process was not amenable to conventional analysis because of

complications introduced by the test section design and also the manner in which the hot, convective gases were produced. In general, the heat transfer process in the test section can be described as transient, convective heat transfer in the entrance region of a rectangular cross-section channel following the passage of a shock wave. Because of the specialized nature of the heat transfer problem, it was necessary to make a thorough experimental study of heat transfer to the wall of the test-section flow channel before starting ignition tests. The experimental conditions which were investigated in the heat-transfer study are summarized by Figure 7.

The following discussion is a brief summary of the results obtained from the study on heat transfer in the shock-tube apparatus. A thorough discussion of the experimental procedures and analysis of results for this study has been reserved for Appendix C. Heat transfer to the flow channel wall was measured with a heat flux gauge (a thin-film platinum resistance thermometer bonded to a glass or ceramic substrate) mounted flush with the channel wall. Heat flux gauge measurements were made at the same position in the test section as that used for ignition tests. The temperature-time relationships obtained from heat flux gauges for shock tube runs with air or argon as the convective gas were analyzed with the aid of transient heat-conduction theory. The results of this heat-transfer study were correlated in terms of shock parameters and gas properties in a form that could later be used for calculating the rate of heat transfer to propellant surfaces during ignition tests.

Figure 7

Range of Test Conditions for Heat Transfer Study

Test Variable	Test Gas: Air	Test Gas: Argon
Incident Mach No. at test section (M_E)	1.9 - 3.9	1.9 - 3.4
Gas temperature, T_g, (°K)	700 - 2300	900 - 2650
Driver pressure, P_o, (atm)	11, 18, 25	11, 18, 25
Area ratios[a] (A_{or}/A_{ts})	0.115, 0.227, 0.458 0.964	0.227
Mach No. of gas flow through test section (M_{ts})	0.07, 0.13, 0.28, ca. 1.0	0.13
Mean gas velocity through test section, U, m/(sec)	45 - 800	75 - 140
Mass flow rate through test section, G, $g/(cm)^2(sec)$	10 - 180	20 - 70
Reynolds No. at test position[b] (Re_x)	23,000 - 870,000	30,000 - 170,000
Heat flux at test position, $\bar{F}$, $cal/(cm)^2(sec)$	10 - 120	10 - 80
Heat gauges	Pyrex, alumina, Pyroceram	Pyrex, Pyroceram

[a]Flow area of control orifice divided by area of test section flow channel (see Table 18).

[b]Reynolds Number based on distance from leading edge (center of heat flux gauge 1.27 cm. from leading edge).

It was found from this study, as was observed previously by Baer [6,9] that the transient heating process at the wall could be represented by an instantaneous temperature rise produced by the incident and reflected shock waves as they moved through the test section, followed by a one-dimensional heating of a semi-infinite solid through a constant surface heat transfer coefficient. The equation which describes this heating process and also completely describes the temperature-time data obtained from heat flux gauges is:

$$\frac{T_s - T_j}{T_g - T_j} = (1 - e^{N^2} \operatorname{erfc} N), \quad N = \frac{h(t)^{1/2}}{\Gamma} \tag{14}$$

Where T_s, T_j, and T_g are the time-dependent surface temperature, temperature of the gauge surface immediately following the passage of the reflected shock wave, and temperature of the gas, respectively. For temperatures defined on an absolute temperature scale, T_j is:

$$T_j = T_o + \Delta T_o, \ (^\circ K) \tag{15}$$

Where T_o is the initial uniform wall temperature and ΔT_o is the instantaneous temperature rise produced by passage of the shock wave.

For the test section illustrated by Figure 6, heat transfer coefficients, h, for heat transfer from the test gas to the wall at the test position were correlated in terms of the gas stagnation temperature, $T_g(^\circ K)$, and the mass flow rate, $G[g/(cm)^2(sec)]$, of the gas flowing through the test-section channel. Experimental heat transfer coefficients were represented within 6 per cent by the following equations:

For air, oxygen, and nitrogen:

$$h = 1.435 \times 10^{-4} (T_g)^{0.3} (G)^{0.905}, \ [\text{cal}/(\text{cm})^2(\text{sec})(°\text{K})] \tag{16}$$

For argon:

$$h = 4.05 \times 10^{-4} (G)^{1.06}, \ [\text{cal}/(\text{cm})^2(\text{sec})(°\text{K})] \tag{17}$$

Where T_g is in °K, and G has the units cal/(cm)^2(sec).

The initial instantaneous temperature rise (ΔT_o) at the flow-channel wall produced by the incident and reflected shocks was found to be a function of: (1) the Mach number of the incident shock wave, (2) the pressure behind the reflected shock (P_4), (3) the thermal responsivity of the heat flux gauge substrate material, and (4) the area of the flow control orifice. For air as the test gas, it was found that ΔT_o at the gauge surface could be represented by the following relationships (these relationships are also applicable to nitrogen and oxygen):

For A_{or}/A_{ts} greater than 0.458:

$$\Delta T_o = 0°\text{K} \tag{18}$$

For A_{or}/A_{ts} less than 0.458:

$$\Delta T_c = 13.66 \left(\frac{P_4}{P^*}\right)^{1/2} \left(\frac{\Gamma^*}{\Gamma}\right)\left(1 - \frac{A_{or}}{A^*}\right) (M_E - 1.20), \ (°\text{K}) \tag{19}$$

Where P* is a reference pressure having a value of 10 atmospheres.

Γ^* is the thermal responsivity of the Pyrex heat flux gauge having a value of 0.0366 cal/(cm)^2(sec)$^{1/2}$(°K).

A^* is the flow area of flow-control orifice No. 1 with an area of 0.369 $(cm)^2$.

A_{or} and A_{ts} are the areas of flow control orifices and test section, respectively, $(cm)^2$.

M_E is the value of the Mach number of the incident shock wave at the test end of the driven section.

Heat transfer runs were made using only one flow-control orifice when argon was used as the test gas. For flow control orifice No. 3 (area ratio of 0.227), the initial temperature rise could be approximated by:

For M_E less than 2.35:

$$\Delta T_o = 0°K \tag{20}$$

For M_E greater than 2.35:

$$\Delta T_o = 11.1 \left(\frac{P_4}{P^*}\right)^{1/2} \left(\frac{\Gamma^*}{\Gamma}\right) (M_E - 2.35), \ (°K) \tag{21}$$

Once the nature of the heat transfer process in the test section was known, the information from this study was applied directly for calculating heat transfer to propellants during ignition tests as described in the following section.

HEAT TRANSFER TO PROPELLANTS

As mentioned earlier, thermal ignition theory predicts that ignition data for propellants which ignite thermally can be represented by a straight line if data are plotted in the form of $\ln(\bar{F})$ versus

$\ln (t_i)^{1/2}$. The mean surface heat flux ($\bar{F}$) is calculated assuming the propellant undergoes linear heating, up to the time that ignition is observed, under only the influence of externally applied energy. The ignition time (t_i) is a real time which is measured with a photocell.

During ignition tests on propellant, ignition time (t_i) was measured with an RCA 1P40 gas photodiode. The signal from the photocell and from the Kistler, Model 601, pressure pickup were recorded from an oscilloscope screen with a Polaroid camera. With this information and the measured incident shock velocity, gas temperature and mass flow rate of the gas in the test section were calculated. From known relationships between Mach number and the initial temperature rise behind the reflected shock (Equations (18) and (19) for air, nitrogen, or oxygen) and from the relationship between mass flow rate and heat transfer coefficient at the test section wall, Equation (16), the ignition temperature for linear heating (T^L_{si}) was calculated using Equation (14). For this calculation of T^L_{si}, it was assumed that the propellant thermophysical properties were constant during the heating process and the values measured at 60°C were used. It was also assumed that the propellant is a homogeneous, semi-infinite solid. It will be shown later that the assumption of constant thermophysical properties for the propellant is a reasonable one, and variations of these properties with temperature do not greatly alter the calculated heat flux at the propellant surface. The thermophysical properties of all propellants investigated in this ignition study are given in Table 4. Thermophysical properties of several propellants were determined

experimentally, and for the others, properties were estimated from data on the individual ingredients or from data on similar propellants. The experimental methods used for determining thermophysical properties of propellants are described in Appendix D.

Using this calculated value for T_{si}^{L}, Equation (1) was then used to calculate the mean externally applied heat flux to the propellant surface.

$$\bar{F} = \frac{\Gamma_p}{2} \left(\frac{\Pi}{t_i}\right)^{1/2} \left(T_{si}^{L} - T_o\right) \qquad (1)$$

where T_o is the initial uniform propellant temperature, °K. For this calculation, the propellant is assumed to behave as a passive solid, and undergoes heating to its ignition temperature without the crystalline phase change. Very little is known about the kinetics of the crystalline phase transition from the orthorhombic to the cubic crystal structure at approximately 240°C. The DTA analysis on ammonium perchlorate by Bohon [19] indicates that this is a slow transition and occurs over a fairly wide temperature range (approximately 20°C). Jacobs and Kureishy [48] indicate that the transition temperature for this transformation is displaced even at a rather slow heating rate of 200°C/(min.). Evans, Beyer, and McCulley [32] included the heat of phase transition, 2.7 kcal/(mole), in their calculations of surface-temperature histories for pressed propellants. The results of these calculations by Evans, et al. are shown graphically in Figure 3 of Reference 32. The effect of the crystalline transformation on the calculated ignition temperature is not very large. It can be shown

from considerations related to transient heat conduction theory that the heat of phase transition, if the transition actually took place, would decrease the calculated ignition temperature by about 10°C. Since ammonium perchlorate is the primary constituent in all propellants, even if the phase change did occur, the results for different propellants would still be comparable and the calculated heat fluxes would be lower by 2 or 3 per cent than those calculated without consideration of the phase transition.

A detailed example of the procedure used for calculating ignition temperature and externally applied heat flux to propellant surfaces, as described above, is presented in Appendix E.

CHAPTER V

IGNITION OF F-PROPELLANT

An extensive study was made of the ignition of F-propellant by convective heat fluxes. This propellant was selected for extensive study since a number of related combustion studies of it have been concluded or are in progress. Some of these related studies were on low- and high-frequency combustion instability [11,25,73]. Also, research has been conducted on flame spread and flame extinguishment using this propellant [29,67,69,70]. In addition, ignition of F-propellant had been previously studied by low radiant heat fluxes [8,82]. Some preliminary results on F-propellant ignition have been published previously in References 51 and 83.

F-propellant was composed of 80 per cent ammonium perchlorate (equal fractions of 15- and 200-micron cuts), 18 per cent PBAA binder-fuel, and 2 per cent copper chromite (Harshaw Catalyst, Cu 0202P). All of the propellant samples used in convective heating experiments were prepared by casting freshly mixed propellant directly into the cavity of the sample holder (See Figures 6 and 75). The method used for processing propellant and filling of sample holders is described in Appendix F. The cavity of the sample holder was overfilled so that a fresh surface could be cut immediately before ignition tests with a new single-edge razor blade. Photomicrographs of a cut surface of F-propellant are shown by Figures 8a and 8b. The white spots on the

a. 5X Magnification

b. 24X Magnification

Figure 8

Photomicrographs of a Freshly Cut Surface of F-Propellant.

surface are fractured ammonium perchlorate crystals and the dark spots are crystals which were perfectly cut in the plane of the surface. It was not possible to cut perfectly smooth surfaces on samples of F-propellant with a razor blade as shown by Figure 8, and it is estimated that the surface roughness was of the order of 20 to 30 microns.

The ignition of F-propellant is described on the following pages. In general, the ignition data discussed in this section were obtained in the research for this thesis, but some experimental data from other studies are included to complete the picture of F-propellant ignition.

TEST VARIABLES FOR IGNITION OF F-PROPELLANT IN THE SHOCK TUBE

Thermal ignition theory predicts that ignition data for propellants that ignite thermally should be represented by a straight line if the data are plotted in the form of $\ln(\bar{F})$ versus $\ln(t_i)^{1/2}$, and the slope of this straight line is related to the activation energy of the key ignition reaction, Equation (8). Baer and Ryan [8,82] have shown that ignition results on F-propellant obtained by subjecting the propellant to low radiant heat fluxes in a radiation furnace were in excellent agreement with those predicted by thermal ignition theory. Although ignition data have been obtained on similar ammonium perchlorate propellants in both convective heating and radiant heating experiments in previous work reported by Baer [6] and Bastress, et al. [10], in none of this earlier work was there found to be more than qualitative agreement among data obtained by different experimental methods. As a consequence, it has not been

previously possible to arrive at any firm conclusions about the ignition process for ammonium perchlorate propellants.

Since thermal ignition theory suggests a simple relationship between the heat flux level applied to a propellant surface and ignition time, F-propellant was subjected to a variety of test conditions at convective heat fluxes in the range of 20 to 160 cal/(cm)^2(sec). As already mentioned, considerable effort was expended to obtain reliable heat transfer data in the shock tube apparatus which would provide a basis for assessing quantitatively the heat flux at the propellant surface during ignition tests.

In order to observe the true response of F-propellant to externally applied convective heat fluxes, most of the ignition tests were conducted with nitrogen or argon as the test gas. It is well known from the previous work of Baer [6], McCune [67], Bastress, et al. [10], Hermance, et al. [43], and Kling, et al. [55] that oxidizing species in the test gas significantly affect the ignitability of ammonium perchlorate propellants in convective heating experiments.

The heat flux at the propellant surface in convective heating experiments is dependent on the following parameters for a given test gas:

$$\bar{F} = f\ (T_g,\ U,\ P) \qquad (22)$$

Because of the strong dependence of heat flux on the parameters, T_g, U, and P, these parameters cannot be varied independently without also changing level of applied heat flux to the propellant surface. It is seen that if each of the parameters, T_g, U, and P, also affect

the propellant ignition one cannot separate the individual contributions of $\bar{F}$, T_g, U, and P to the ignition process. To alleviate this problem, both argon and nitrogen were used as test gases in ignition experiments. It can be shown through considerations involving the thermophysical properties of argon and nitrogen that to produce equivalent heat fluxes at a propellant using these two gases, at a given pressure, P, the temperature must be several hundred degrees higher for argon than for nitrogen. Because of the difference in molecular weights of the two gases, the velocity, U, for argon through the test-section flow channel, for the same flow-control orifice, is very nearly the same for a given value of heat flux, although the temperatures for the two gases are different. Therefore, through the use of argon and nitrogen, the gas temperature could be varied independently to determine its effect on ignition.

Mass flow rate, G, also appears as a test variable in convective heating experiments, and is dependent on T_g, U, and P. Except for determining heat flux to the propellant surface, the mass flow rate would not be expected to influence independently propellant ignition unless mass transfer processes were also important.

NATURE OF EXPERIMENTAL DATA

During ignition runs using the shock tube for producing hot gases, pressure in the shock tube near the test section was monitored with a Kistler, Model 601, quartz pressure pickup and the surface of the propellant was viewed with an RCA 1P40 gas photodiode. The electrical signals from these instruments were displayed on the screen of an

oscilloscope and permanently recorded with a Polaroid camera. Some oscilloscope records obtained from ignition runs on F-propellant are shown by Figure 9.

Figures 9a and 9b are records obtained from ignition runs at low gas velocities in the test section, Mach 0.07 and 0.13, respectively. Data derived from the ignition tests from which these records were obtained are given in Table 3. Ignition time as determined from these records is the time after the first application of energy that the differentiated photocell signal begins to rise very rapidly. This corresponds to the development of steady deflagration at some location on the surface and a rapid spreading of the flame over the surface. This observation was verified by high-speed motion picture studies of F-propellant ignition which are described in another section. The light intensity is much greater for low Mach number runs as indicated by the continual downward movement of the direct light signal. At Mach 0.28, Figure 9c, the light intensity drops off sharply after about 10 milliseconds. This corresponds to the arrival of cold driver gas at the test position. At Mach 1.0, Figure 9d, the light intensity is very low because of the thin flame zone, and the light signal returns to its base-line as burning is quenched when cold driver gases enter the test section, after about 6 or 7 milliseconds, in this case. The time of arrival for the incident shock wave at the test section which coincides with the start of heating, is usually shown by a small pip on differentiated light signals, see Figure 9a.

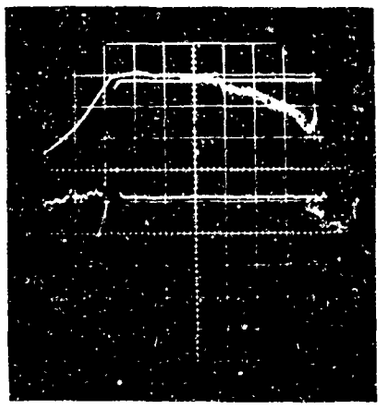

a. Run No. 29-12-4.
Gas Velocity: Mach 0.07.
Heat Flux: 28 cal/(cm)^2(sec).
Ignition Time: 34.4 msec.

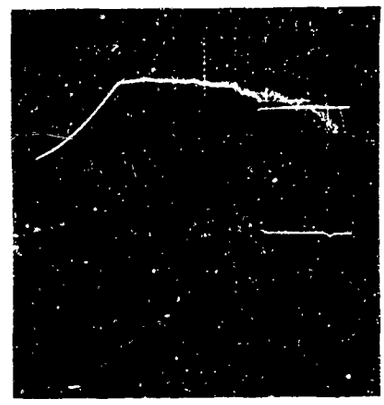

b. Run No. 212-24-2.
Gas Velocity: Mach 0.13.
Heat Flux: 43 cal/(cm)^2(sec).
Ignition Time: 13.8 msec.

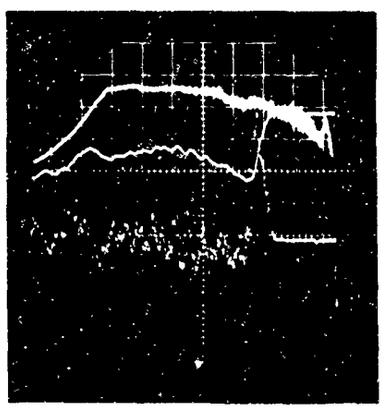

c. Run No. 31-2-9.
Gas Velocity: Mach 0.28.
Heat Flux: 68 cal/(cm)^2(sec).
Ignition Time: 9.3 msec.

d. Run No. 43-2-9.
Gas Velocity: Mach 1.0
Heat Flux: 127 cal/(cm)^2(sec).
Ignition Time: 3.7 msec.

Figure 9

Oscilloscope Records of Pressure Pickup and Photocell Signals for Ignition Runs on F-Propellant at Various Test Conditions. Time Base (Right to Left), 5 msec/(div.), all Records. The Trace that Starts at the Lower Left on Each Record is the Pressure Trace, 50 psi/(div.). Traces Starting at the Top and Center of Each Record are the Direct and Differentiated Photocell Signals, Respectively.

With the data from these records and a measurement of the incident shock velocity in the driven section, the procedures already described are used for calculating the heat flux applied to the propellant surface. Data for all ignition runs on F-propellant in nitrogen, including those for which ignition did not occur, are tabulated in Table 3 of Appendix K. For runs during which no ignition was detected, an ignition time, t_i, a surface temperature for linear heating of the propellant, T^L_{si}, and a heat flux value, $\bar{F}$, are given which correspond to the end of the test period that was determined by heat flux gauge measurements. The test period is terminated either by the arrival at the test position of the reflected rarefaction wave or by the depletion of processed gases.

In Table 3 and other tables of ignition data, the information under heading Propellant Code describes the propellant composition. For example, the first letter identifies the propellant. The number following the letter, such as F-5, denotes the batch number. All propellants were made in small batches and sometimes, if many tests were to be performed, several batches were required since some of the samples were always discarded because of imperfections. The letter following the batch number, for example F-30M, means the propellant was a modification of the original composition. In this case the letter M indicates that the fine particle size (15-micron) ammonium perchlorate was obtained from a different supplier.

All of the other symbols used for headings in Table 3 are defined in the Table of Nomenclature of Appendix L. A sample calculation,

describing the method used for obtaining the calculated results given in Table 3, is presented in Appendix E.

IGNITION IN NITROGEN

In this section the experimental data for ignition of F-propellant by convective heat fluxes with nitrogen as the test gas are presented and analyzed. The important environmental factors studied in this phase of the work on F-propellant ignition were heat transfer rate to the propellant and velocity of the test gas across the propellant surface. Applied heat fluxes were studied over the range of 30 to 160 cal/(cm)^2(sec). It is estimated that the mean heat flux at the propellant surface could be calculated to within about 5 per cent of its actual value. Gas velocity through the test section ranged from 50 to 800 m/(sec). Ignition tests were conducted at pressures of 14 to 25 atmospheres, and temperatures of the convective gas were varied from 1000 to 2000°K.

Description of Experimental Results

Ignition at Low Gas Velocities

For the purpose of this discussion low gas velocities are velocities of the convective gas through the test-section channel with Mach numbers (M_{ts}) of 0.07, 0.09, and 0.13. Since shock-tube operating conditions are varied to produce different heat-flux levels, the only variable which is not influenced by these changes for a given critical-flow orifice at the downstream end of the flow channel is the Mach number of the test gas. In this case, because c_p/c_v for the gas is not a strong function of temperature, the Mach number to an excellent

approximation is dependent only on area ratios (A_{or}/A_{ts}). It is thus convenient to present ignition results from convective heating experiments as a plot of ℓn ($\bar{F}$) versus ℓn $(t_i)^{1/2}$ for values of constant Mach number. The data for F-propellant are presented in this manner by Figure 10 for Mach numbers of 0.07, 0.09, and 0.13. The data graphed in Figure 10 are also given in Table 3, and are only for regular F-propellant. Propellant surfaces exposed to convective heating were cut immediately before each run with a new single-edged razor blade.

The first ignition runs on F-propellant in the shock tube were conducted at low gas velocities, 50 to 115 m/(sec) as shown by Figure 10. When the data from these tests were compared to the results obtained on F-propellant in the radiation furnace at low heat fluxes [8,82] (shown by the uppermost straight line of Figure 10 which is an extrapolation of the radiation furnace results given by Figure 4), it was found that all data from convective heating tests fell below the line defined by the radiation furnace results for ignition at atmospheric pressure. This was contrary to expectation since it was believed that the ignition results at low radiant heat fluxes represented simple thermal ignition of F-propellant. Also no pressure effect on ignition was observed. The data shown by Figure 10 were obtained at pressures of 14 to 25 atmospheres, and no stratification of the data was found that could be attributed to a pressure effect on ignition. Furthermore, the temperature of the hot nitrogen passed over the propellant surface was in the range of 1000 to 2000°K, approximately the same range of temperatures as that used for radiation furnace tests.

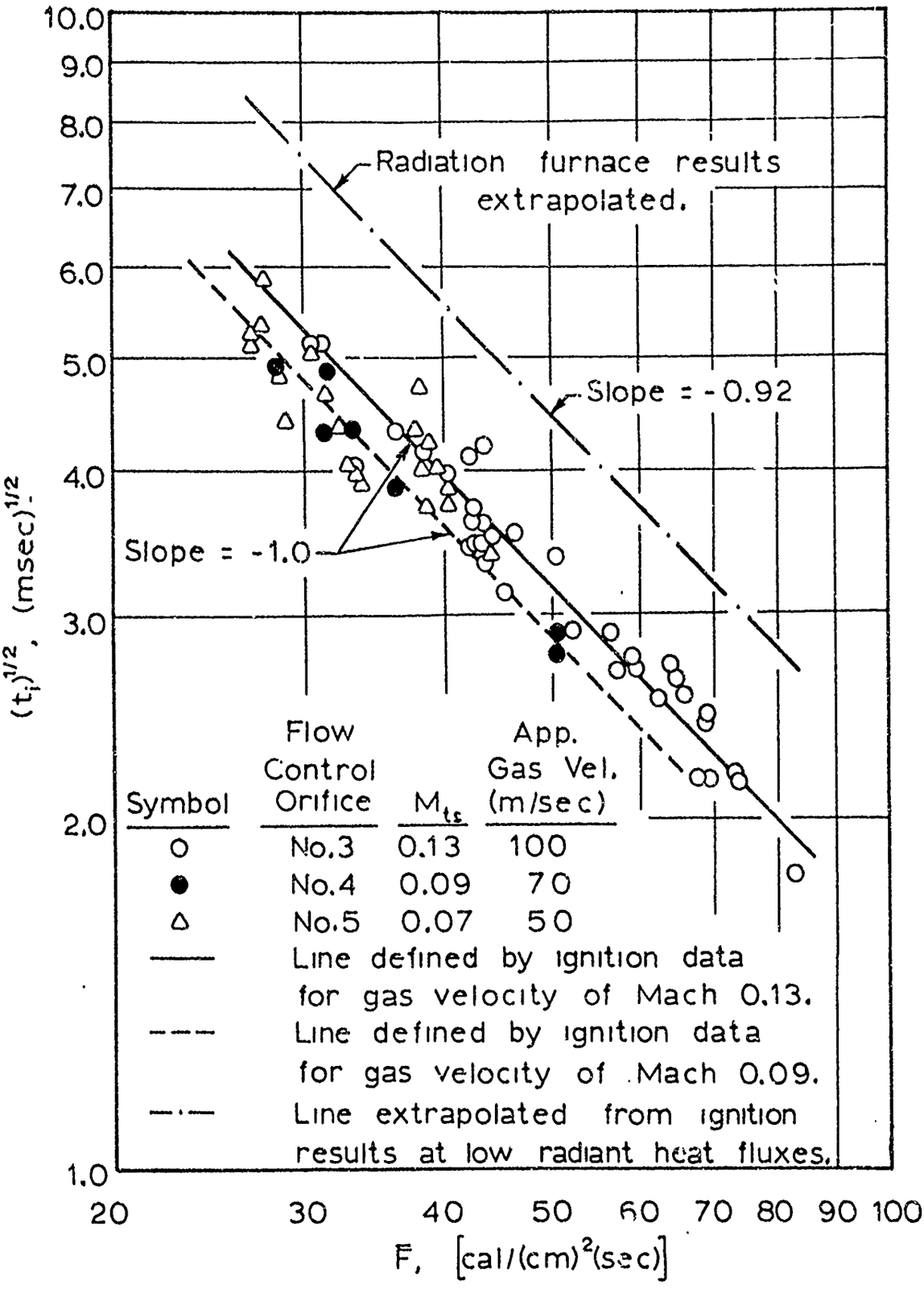

Figure 10

Ignition Data for F-Propellant in Nitrogen at Low Gas Velocities For Pressures of 14 to 25 Atmospheres.

It appeared that the only test variable which was greatly different from those encountered in radiation furnace tests was the gas velocity over the propellant surface. However, one would expect that velocity of the test gas would have an adverse effect on ignition, and that ignition times would be longer at equivalent heat fluxes in a convective heating experiment than in a radiant heating experiment where the propellant would be surrounded by a stagnant gas. In other words, reactive species formed at the propellant surface would not be swept away in the fluid stream as in a convective heating experiment.

Except for the difference in ignition times for F-propellant in the shock tube and radiation furnace, the only significant trend shown by the data obtained by convective heating was that F-propellant was more difficult to ignite as the velocity of the gas across the propellant surface was increased. This effect can be seen by comparing ignition data of Figure 10 at Mach 0.07 and 0.09 with those obtained at Mach 0.13. Even though it was not possible to arrive at any conclusions about the ignition process from the data at low gas velocities, it was interesting to note that the data plotted in the form of $\ell n\ (\bar{F})$ versus $\ell n\ (t_i)^{1/2}$ were well represented by straight lines with a slope of -1.0. This result is in qualitative agreement with thermal ignition theory.

Ignition at Intermediate Gas Velocities

In the next set of experiments on F-propellant the velocity of the gas across the propellant surface was increased to Mach 0.20 and 0.28, actual gas velocities of about 150 and 210 m/(sec).

respectively. Ignition data for Mach 0.20 and 0.28 are shown on the $\ell n\ (\bar{F})$ versus $\ell n\ (t_i)^{1/2}$ plot of Figure 11 along with data obtained at Mach 0.13 and a straight line representing the extrapolated radiation furnace results on F-propellant.

The effect of higher gas velocities was to further lengthen ignition time over that observed for equivalent heat fluxes at Mach 0.13. Again the data were well represented by straight lines with slopes of -1.0. The fact that gas velocity has such a large effect on ignition strongly suggested that gas-phase or heterogeneous-surface reactions were participating in the ignition process; and as the gas velocity was increased, reactive species at or near the propellant surface were being diluted by the fast-moving, inert gases. If gas-phase species were important in the ignition process, such an effect would be expected. Although the results at higher gas velocities were of interest, it was still not possible to understand why F-propellant ignited faster by convective heating than by radiant heating.

Ignition at High Gas Velocities and the Ignition Paradox

As a final test of the effect of gas velocity, ignition runs were made on F-propellant at Mach 1.0; actual gas velocities through the flow channel were in the range of 700 to 800 m/(sec). For these tests no flow-control orifice was used downstream of the test position and flow of hot gas from the shock tube was controlled entirely by the open area of the flow channel. This was a critical test of thermal ignition theory for if gas-phase or heterogeneous-surface reactions were

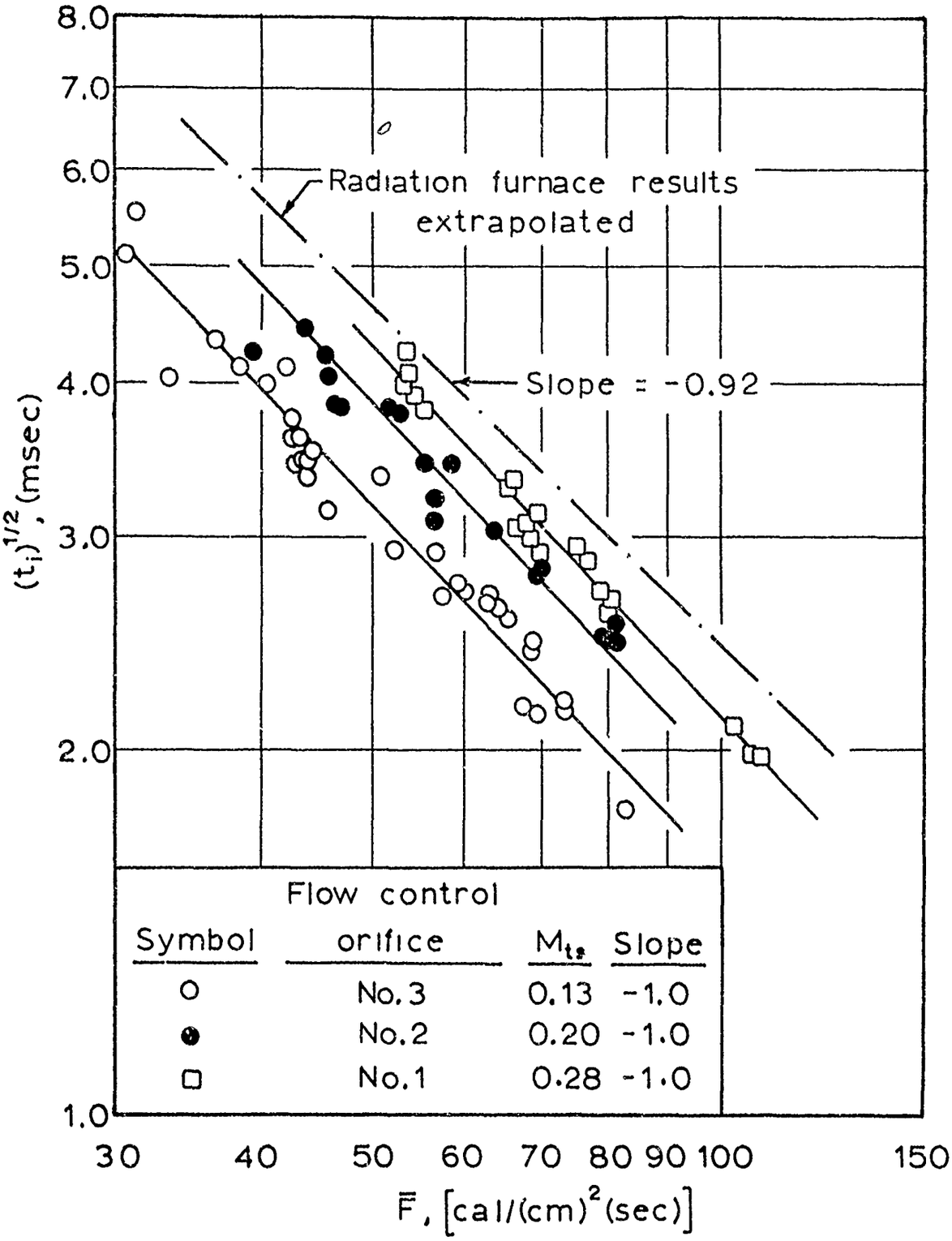

Figure 11

Ignition Data For F-Propellant in Nitrogen at Intermediate Gas Velocities for Pressures of 20 to 25 Atmospheres.

the key processes in the ignition of F-propellant, it would be expected that the F-propellant would not ignite at Mach 1.0.

It was found that F-propellant ignited at Mach 1.0; however, steady burning was later extinguished when cold driver gases mixed with the test gas and flowed through the test section. When the data for the three tests at Mach 1.0 were graphed on logarithmic coordinate paper in the form of $\bar{F}$ versus $(t_i)^{1/2}$, the data points were well represented by the straight line which was extrapolated from the results in the radiation furnace. The ignition data for tests at Mach 1.0 in the shock tube are compared to those obtained in the radiation furnace on Figure 12.

The results at Mach 1.0 were unexpected for they showed that F-propellant ignites by a simple thermal ignition process only at very high gas velocities, and they suggested that at lower gas velocities propellant ignition was accelerated by a supplementary mechanism. If it were assumed, on the other hand, that gas-phase or heterogeneous surface reactions involving the production of reactive species at the surface were controlling in the ignition process, it was again impossible to explain the result, for the data showed that at higher gas velocities the relative effect of gas velocity on ignition was diminished. This result would not be expected if gaseous species were necessarily involved in the ignition process. The ignition paradox was finally resolved when it was found that variations in gas velocity did not affect the ignition of propellants which had very smooth surfaces. This result suggested that the improved ignitability of F-propellant at low gas velocities was related to imperfections produced at the

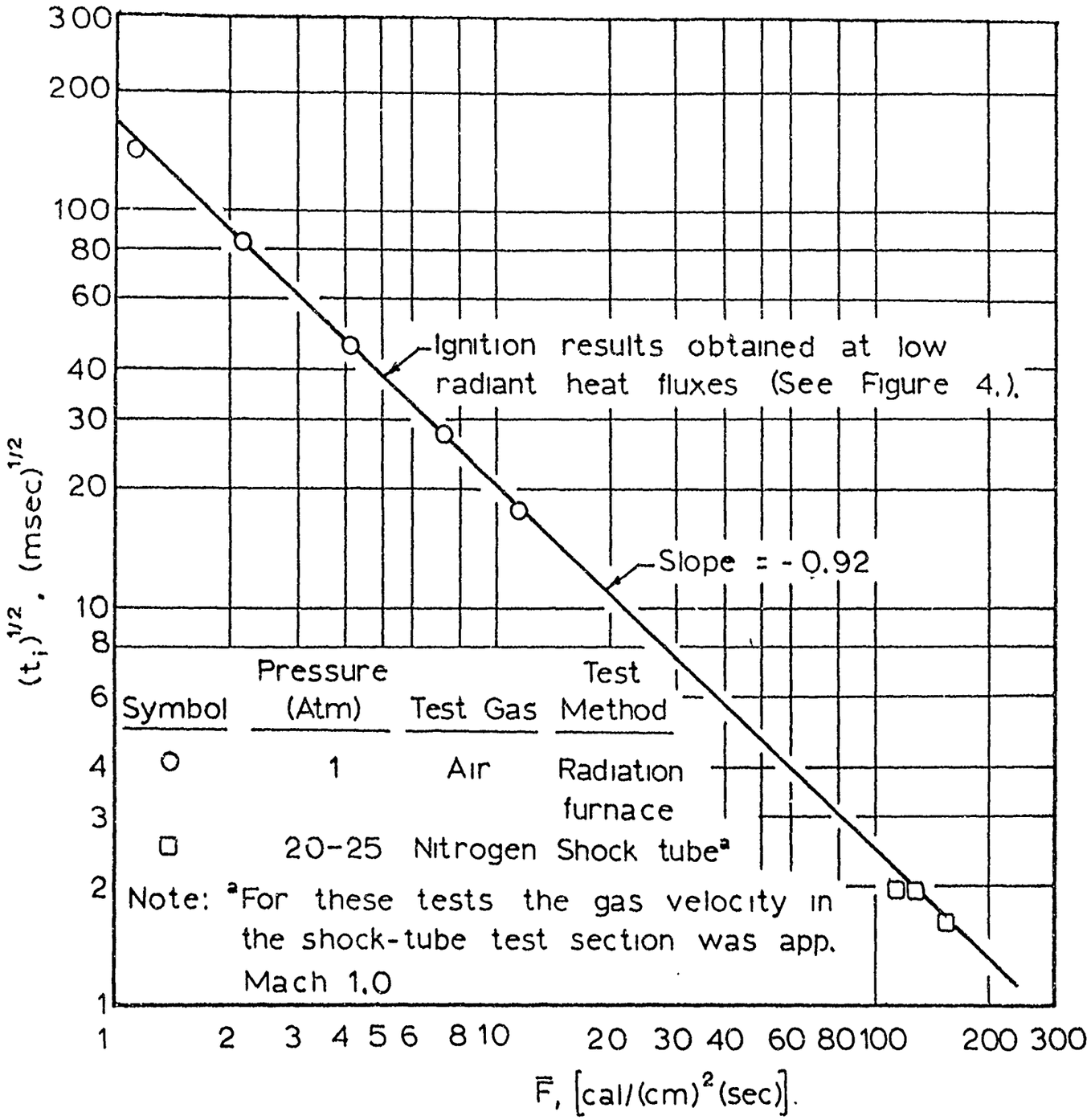

Figure 12

Ignition Data for F-Propellant Obtained by Different Methods.
(Simple Thermal Ignition of F-Propellant)

propellant surface during the preparation of samples for ignition tests. The importance of this finding with respect to thermal ignition theory will be discussed in subsequent sections.

Effect of Test Variables on Ignition

From the experimental results presented by Figures 10, 11, and 12 it is seen that the test variable which has the most significant effect on the ignitability of F-propellant in a neutral environment (neutral in that the test gas contains no reactive gases) is the rate of heat transfer to the propellant surface. This is shown by the relationship between heat flux ($\bar{F}$) and ignition time (t_i) for ignition tests at different Mach numbers. It was found that $(t_i)^{1/2}$ was directly proportional to $1/\bar{F}$ for ignition at low gas velocities.

A second variable which was found to affect the ignitability of F-propellant for convective heating was the velocity of the test gas through the test section. The gas velocity effect is shown by the sets of ignition data at different constant Mach numbers in Figures 10 and 11. Here the Mach number (M_{ts}) is that for the bulk gas velocity in the test-section flow channel. It is shown by these data that the relative effect of gas velocity on ignition time diminishes as gas velocities are increased, and at Mach 1.0, ignition data obtained in the shock tube were in substantial agreement with those obtained in the radiation furnace. From the velocity effect observed, it is predicted that at a threshold Mach number of 0.50, corresponding to a test section velocity of about 400 m/(sec), the ignitability of F-propellant would no longer be significantly

influenced by gas velocity and that ignition data obtained above Mach 0.5 would be represented by the line on an $\ell n\ (\bar{F})$ versus $\ell n\ (t_i)^{1/2}$ plot defined by radiation furnace results and the data obtained at Mach 1.0.

To better illustrate the effect of gas velocity on the ignition F-propellant, average values of $(t_i)^{1/2}$, as defined by the constant Mach number lines of Figures 10, 11, and 12, have been plotted in Figure 13 as a function of M_{ts} for different constant values of externally applied heat flux, $\bar{F}$. It will be shown later that this velocity effect can be linked with imperfections on the propellant surface and that when a very smooth-surfaced propellant is tested, the effect of velocity on ignition is negligible.

A third test variable which was found to affect the ignition of F-propellant was the temperature of the convective gas. This effect of gas temperature cannot be gleaned from the data presented by Figures 10, 11, and 12 for it is subtly concealed by the velocity effect. However, it will be shown, and this discussion is also reserved for another section, that when high-temperature argon was used as the convective gas, propellants with surface imperfections ignite in considerably less time at equivalent gas velocities and heat fluxes in argon than in nitrogen. The gas temperature effect on ignition can be exposed by comparing data for ignition tests in argon and nitrogen because the thermophysical properties of argon are considerably different from those of nitrogen; as a consequence, for a given heat flux, the gas temperature of argon is several hundred degrees Kelvin higher than that for nitrogen. The net result of this difference in

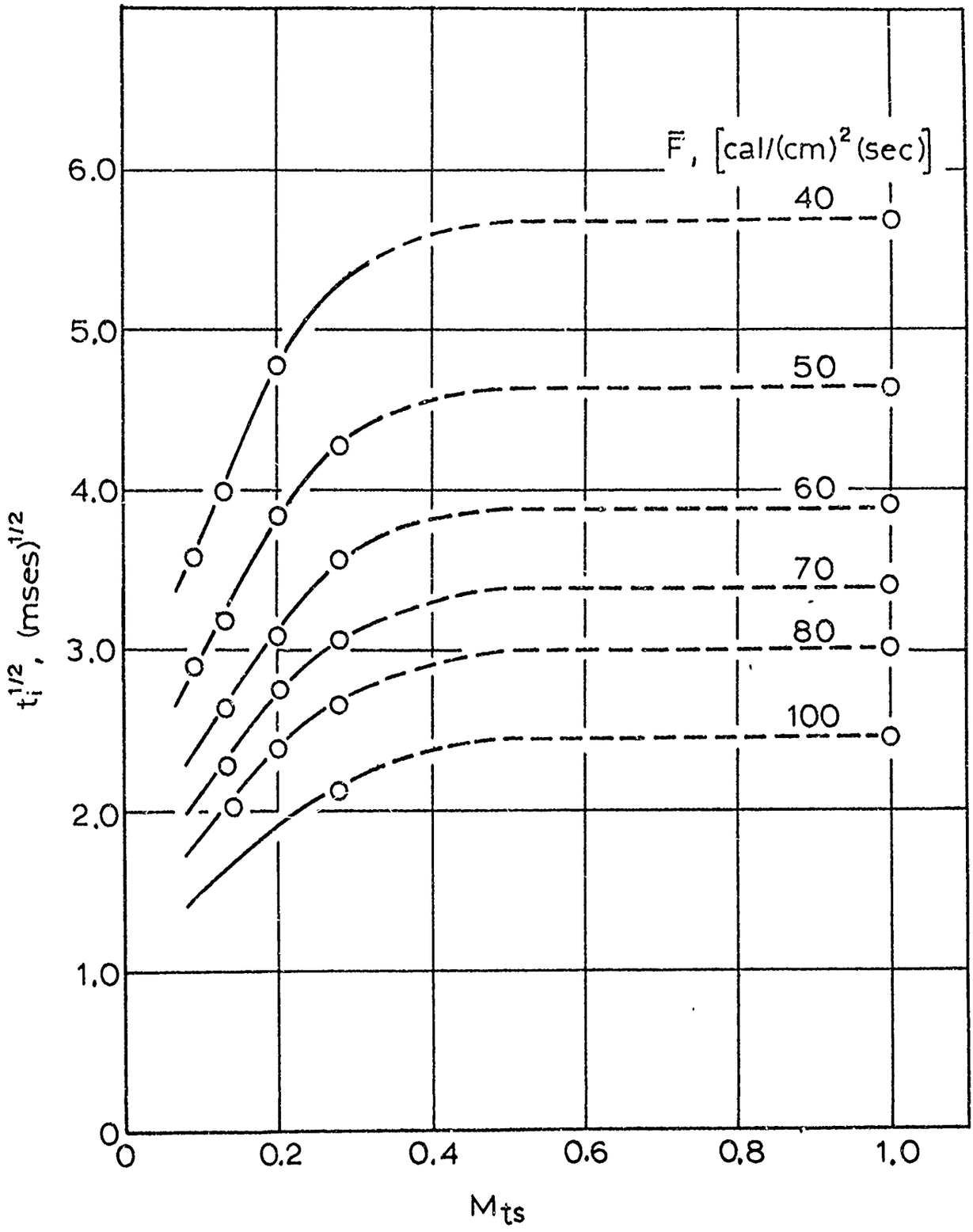

Figure 13

Effect of Gas Velocity on Ignition Time of F-Propellant for Different Values of Externally Applied Heat Flux in Nitrogen. (This Graph is a Cross-Plot of the Results Given By Figures 10, 11, and 12). M_{ts} is the Mach Number of the Test Gas in the Flow Channel of the Test Section.

gas properties is that the temperature of the convective gas can be varied independently of U, P, and $\bar{F}$ in ignition experiments. The effect of gas temperature on the ignition of ammonium perchlorate propellants diminishes as test velocities are increased and propellant surfaces are made smoother.

It should be pointed out that no measurable effect of pressure on ignition of F-propellant was observed in this shock tube work when the test pressure was varied over the range from 14 to 25 atmospheres. This is in general agreement with earlier work by Baer [6] and McCune [67], and also with that of Bastress, et al. [10]. Under high radiant fluxes (75 to 100 cal/(cm)^2(sec)) produced by an arc image furnace, some investigators (see for example, References 13 and 77) have observed that changes in ambient pressure greatly influence ignition of ammonium perchlorate propellants even at fairly high pressures. These observations have not been confirmed by Bastress, et al. [10], for they found even at very high fluxes (greater than 100 cal/(cm)^2 (sec)) in an ar image furnace that there was little or no pressure effect on ignition for pressures in the range 30 to 135 psia.

Discussion of Results with Respect to Ignition Theory

Simple Thermal Ignition of F-Propellant

As indicated earlier, it was found that at very high gas velocities through the test section, in this case about Mach 1.0 (actual gas velocities of 720 to 800 m/(sec)), surface imperfections no longer influence the ignition of catalyzed ammonium perchlorate propellants,

and ignition characteristics can be described by simple thermal ignition theory. In Figure 12 the results of ignition tests on F-propellant at high gas velocities are compared with data obtained by careful experiments under low radiant fluxes of 1 to 13 cal/(cm)^2(sec). These data are plotted as $\ell n\ (\bar{F})$ versus $\ell n\ (t_i)^{1/2}$. As these results show, the straight line which defines ignition under low radiant fluxes when extrapolated is in remarkable agreement with the data for high convective fluxes (115 to 155 cal/(cm)^2(sec)). Detailed data for ignition of F-propellant by convective heat fluxes are given in Table 3. The data for ignition at low radiant fluxes were presented previously in References 8 and 82, and have been retabulated in Table 1 and are graphed in Figure 4.

The data at low radiant fluxes were obtained in a radiation furnace at atmospheric pressure with air as the environmental gas. Special care was taken to ensure that all radiant energy intercepted by the surface was absorbed at the surface of the propellant. This was accomplished by coating the sample surface with a very thin coat of carbon black. Both radiant and free-convection heat transfer to the surface were considered in calculating the surface heat flux. Although tests on F-propellant under radiant heating were only conducted at atmospheric pressure, experiments on a similar ammonium perchlorate propellant showed no effect of pressure on ignition when the pressure was varied from 0.2 to 11.0 atmospheres [8,82]. Also, in similar tests under low radiant fluxes, no effect of the gaseous environment was found when air and nitrogen were used.

Some additional comments are required with regard to the results given by Figure 12. To start with we will assume that the line which defines ignition in the radiation furnace and that for convective heating at Mach 1.0 (Figure 12) represents the true ignition characteristics of F-propellant and that F-propellant ignites by a simple thermal ignition process. Under these conditions, one-dimensional heating of the surface, ignition characteristics of F-propellant are described by the ignition model proposed by Baer, Equation (7); the ignition time for a given one-dimensionally applied surface heat flux is given by Equation (9):

$$(t_i)^{1/2} = \frac{\Gamma_p (\Pi)^{1/2}}{2\bar{F}} \left[\frac{E_a/R}{1 - 1.04 \ln(\bar{F}/B)} - T_o \right] \qquad (9)$$

Where t_i has the dimensions of seconds and $\bar{F}$ those of cal/(cm)^2(sec).

With the aid of Equation (8) and using an initial propellant temperature (T_o) of 300°K, it was found for the data given by Figure 12 that E_a/R is about 15,500°K which corresponds to an activation energy for the key ignition reaction of 30.8 kcal/(mole). It is interesting to note that this value is in reasonable agreement with activation energies obtained for the thermal decomposition of ammonium perchlorate containing copper chromite. See for example the results of Jacobs and Russell-Jones, reported by Evans, et al. [32]. The activation energies they report are in the range of 31 to 32 kcal/(mole) for the low-temperature (200 to 280°C) decomposition of ammonium perchlorate. This value for the activation energy also corresponds to that observed for the uncatalyzed, low-temperature decomposition

of ammonium perchlorate [15,37]. The pre-exponential factor, B, has a value of 4.45×10^{10} cal/(cm)^2(sec) for the data of Figure 12.

Also there is a uniquely defined thermal ignition temperature associated with each value of externally applied flux that must be reached before runaway surface reactions are initiated that bring about the transition to steady deflagration. This ignition temperature can be calculated from the transposed form of Equation (1):

$$T_{si}^{T} = T_o + \frac{2\bar{F}}{\Gamma_p} \left(\frac{t_i}{\pi}\right)^{1/2} \tag{23}$$

The straight line which represents the ignition data for F-propellant on the $\ln(\bar{F})$ versus $\ln(t_i)^{1/2}$ plot of Figure 12 for low radiant fluxes and for convective heating at high gas velocities is defined by the following equation for an initial uniform propellant temperature of approximately 300°K.

$$t_i = 28.94/(\bar{F})^{1.84} \tag{24}$$

Where t_i has the units of seconds and $\bar{F}$ the units cal/(cm)^2(sec).

By combining Equations (23) and (24), we find (for F-propellant upon taking T_o to be 300°K and using the value for thermal responsivity of the propellant at 60°C, 0.0212 cal/(cm)^2(sec)$^{1/2}$(°K)) that the thermal ignition temperature, T_{si}^{T}, can be expressed as a function of either the mean surface heat flux or the measured ignition time by the following equations:

$$T_{si}^{T}\ (°K) = 300°K + 286.1\ (\bar{F})^{0.08} \tag{25}$$

$$T_{si}^{T}\ (°K) = 300°K + 443.4/(t_i)^{0\ 0435} \tag{26}$$

Where $\bar{F}$ has the units of cal/(cm)^2(sec) and the ignition time (t_i) is in milliseconds. It is seen from Equation (26) that the thermal ignition temperature for F-propellant can be calculated directly from an experimentally determined ignition time.

This background information on the ignition of F-propellant for test conditions under which it ignites by a simple thermal ignition process provides a starting point for a discussion of how environmental factors affect propellant ignitability. If a propellant ignites in a shorter time at low gas velocities than at high gas velocities for a given externally applied heat flux, then factors other than one-dimensional heating of the surface from hot, convective gases must be important in bringing the propellant surface to its thermal ignition temperature, T^T_{si}. See Figure 3. In other words, heat flux in an amount which is the difference between that required to bring the propellant to its ignition temperature in the observed ignition time and that which is supplied externally by one-dimensional, convective heating from hot gas is generated at or near the propellant surface.

Thermal Ignition of F-Propellant with Secondary Ignition Reactions

Analysis of the Ignition Process. During ignition studies on F-propellant and other ammonium perchlorate propellants it was found that propellants with rough surfaces ignited faster in convective heating experiments at low gas velocities than at high gas velocities. (Furthermore, as will be shown, the ignition of smooth-surfaced propellants was not influenced by gas velocity.) In the ignition experiments on other propellants, compositions were varied, surface

characteristics were changed, and different types of ammonium perchlorate decomposition catalysts were tested. In view of the numerous experimental observations on the ignition of propellants, which will be discussed in subsequent sections, it was found that the following processes appear to be important in providing part of the total heat flux required to bring the propellant to its thermal ignition temperature when imperfections are present on the propellant surface:

1. Two-Dimensional Heating of Surface Imperfections. The presence of imperfections on the propellant surface, such as fractured ammonium perchlorate particles and pits formed by pulling of ammonium perchlorate particles from the surface during cutting of a propellant surface for ignition tests, provides sites for two-dimensional convective heating. The amount and magnitude of this surface roughness is related to the size of the ammonium perchlorate particles in the propellant. In preparing a propellant surface containing large particles of ammonium perchlorate (some particles were as large as 400 microns in diameter in F-propellant), it was impossible to cut an aerodynamically smooth surface. One can cut through some of the large ammonium perchlorate particles, as shown by Figure 8, flush with the plane of the propellant surface. Some of the particles are fractured and others with their bases near the cutting plane are pulled from the propellant matrix. Most of the surface defects are below the plane of the cut surface. It is estimated that the surface roughness of a freshly prepared sample of F-propellant is of the order of 20 to 30 microns. But in some cases pits as deep as 50 microns were observed. Each

surface was examined microscopically before tests and when extremely rough surfaces were found the sample was discarded.

Baer [8,82] has shown through an analytical solution of heat conduction equations and by experiments on propellants that for heating of a 90-degree, semi-infinite propellant corner the temperature rise at the corner is twice as large for a given heat flux as for one-dimensional heating of a propellant surface. From this work by Baer, it appears that two-dimensional heating of surface imperfections could contribute to raising the total surface temperature more rapidly by heat conduction laterally from a higher temperature hot spot at the surface. However, since heating times to produce ignition were very short, usually less than 25 milliseconds in this work, one would not expect this effect to be of great importance. It is expected that the greatest contribution from two-dimensional heating would be the generation of reactive species in these regions of higher temperature at the surface. These reactive species could then undergo exothermic reactions and provide energy to supplement external flux. It is unlikely that localized ignition would be initiated at these localized hot spots until a sizable portion of the surface surrounding it (say of the order of several square millimeters) is heated to its ignition temperature. This would be particularly true at high gas velocities in the test section.

2. Heterogeneous-Surface Reactions. Another source of energy for heating the propellant surface could come from heterogeneous-surface reactions. The true nature of these reactions is not known, but one can

speculate about these reactions, and then look for evidence in data from ignition experiments for postulating a reaction mechanism. As suggested in the previous paragraph, two-dimensional heating of exposed rough edges of ammonium perchlorate particles would raise the temperature of the individual particles above that of the mean surface temperature and thus provide decomposition products which are capable of undergoing further reaction. Such reactive species, including perchloric acid, ammonia, and other ammonium perchlorate decomposition products characteristic of the low-temperature decomposition reaction, could undergo further exothermic reaction at reactive sites on the surface. Also, oxidizing species in the decomposition products of ammonium perchlorate might react heterogeneously with the binder-fuel or with pyrolized hydrocarbon fragments at catalyst sites. Studies by Cummings and Hall [27] showed that the perchloric acid-methane reaction gave flame speeds about three times as fast as that for the oxygen-methane flame. This shows that ammonium perchlorate decomposition products are extremely effective oxidizing agents.

Heterogeneous-surface reactions appear to be important since ammonium perchlorate propellants containing catalysts, such as iron oxide and copper chromite, ignite much faster at a given heat flux level under convective heating than do uncatalyzed propellants. This comparison is based on relative ignitability of the two types of propellants under radiant and convective fluxes. It is known that both iron oxide and copper chromite are good oxidation catalysts. These catalysts would not be expected to be in the gas phase at low

surface temperatures (200 to 400°C). Consequently, it appears that these catalysts affect the ignition of propellants under convective heating by catalyzing surface reactions. For heterogeneous-surface reactions which depend upon transport of reactive species, an increase in the gas velocity would decrease their effectiveness, and at very high gas velocities no contribution for heating the surface would be expected from this source.

Baer [8,82] has shown in radiation furnace tests that an increase in the concentration of copper chromite catalyst (from 2.0 to 4.0 per cent) does not improve the ignitability of a propellant system. The effect of the concentration of copper chromite on ignition over the range reported by Baer was not studied under convective heating where the effect of catalyst concentration may be more important and provide clues as to the nature of secondary ignition reactions. It needs to be emphasized that secondary ignition reactions are only important during ignition of propellants with surface imperfections.

3. Gas-Phase Reactions. Still another source of energy for raising the propellant surface temperatures would be gas-phase reactions among ammonium perchlorate decomposition products or between ammonium perchlorate decomposition products and gaseous polymer fragments. Here again surface imperfections would be important in providing localized hot spots where gaseous reactants are generated, also for providing flame holders for gas-phase reactions. Gas-phase reactions would not be as effective in providing energy feedback to the surface as surface reactions, but if the gas-phase reactions were strongly

exothermic they could add significantly to the surface heat flux. The fact that temperature of the convective gas has an effect on ignition time at a given externally applied surface heat flux indicates that gas-phase reactions are important at lower gas velocities. On the other hand, if gas-phase reactions are important, one would expect a sizable pressure effect on ignition. Such an effect on ignition has not been observed in this work. It is possible, however, that reactive species undergo further gas-phase reaction at the rate at which they are generated. If this were true, it would not be possible to detect a pressure effect on ignition at low gas velocities. The energy contribution from gas-phase reaction would be influenced by the gas velocity. As the gas velocity is increased, reactive species would be diluted and surface imperfections would be less effective as flame holders, and at extremely high gas velocities their contribution to the surface heat flux would be negligible.

It appears that secondary ignition reactions, be they gas-phase or heterogeneous-surface reactions, are not highly exothermic and occur at rather low temperatures. It was shown by a high-speed motion picture study of F-propellant ignition which is described in another section that no luminosity was observed at the propellant surface until ignition occurred and a combustion flame appeared. This was true even when ignition occurred at several locations on the surface. Only for a few of the tests did motion pictures reveal a dull, reddish glow a few frames before a combustion flame became visible. It is possible that gas-phase or surface reactions were not visible because

of the high film speeds. It might be fruitful to examine ignition of propellants at low film speeds in order to detect such reactions. Such experiments would be more revealing under convective heating where background radiation does not interfere. With respect to these secondary ignition reactions, it is well known, and it can easily be verified by heating of an ammonium perchlorate crystal on a hot plate, that the flame associated with reaction of the decomposition products has a very low luminosity. This reaction, however, if catalyzed at the surface of the propellant could contribute significantly to the surface heat flux, and yet not be visible on a high-speed motion picture film or be detectable with a photocell.

To summarize these observations with respect to the ignition results given by Figures 10 and 11 for F-propellant in nitrogen at low and intermediate gas velocities, it appears that two-dimensional heating of surface imperfections followed by heterogeneous-surface reactions and gas-phase reactions augments the surface heat flux and helps bring the propellant surface to its ignition temperature.

Effect of Secondary Ignition Reactions at Intermediate and High Gas Velocities. With reference to Figure 11, the lines which have been drawn to describe the data for Mach numbers of 0.13, 0.20, and 0.28 all have a slope of -1.0. This is in contrast with the slope of the line which describes the data obtained in a radiation furnace and that for convective heating at high gas velocities (Figure 12). This line has a slope of -0.92. Obviously, assigning a slope of a -1.0 to these data is somewhat arbitrary, and the true slope cannot

be established within perhaps 5 per cent. Also, it is seen from the plot of experimental data, that if a curve-fitting technique were used, each set of data, corresponding to a given Mach number, would have a different slope. It is apparent, however, that lines having a slope of -1.0 describe these data reasonably well. Also, for other propellants having compositions similar to F-propellant for which more consistent data were obtained, there was a strong indication that the slope of the lines is very close to a -1.0.

The reason that the slope of the line for lower gas velocities is different from that observed for ignition in the radiation furnace and ignition at high gas velocities is that both velocity and the temperature of the convective gas influence ignitability. The effect of gas temperature is to rotate the set of data (for a given Mach number) clockwise and that of velocity to rotate a given set of data counter-clockwise. The net effect is that for these propellants the slope of the line which describes a set of data is in qualitative agreement with that defined by radiation furnace results. It is thus seen that where gas velocity and gas temperature influence ignition, the magnitude of their effect on the ignition process will determine the slope of the straight line which defines the data. Therefore, the slope of the line can be either greater or less than a -1.0. In fact it may be found that the data cannot be represented by a straight line. This will depend on the nature of the dependence of secondary ignition process on gas velocity and gas temperature.

The implications of these preceding statements are not readily apparent by examination of the results given by Figures 11 and 12,

and further clarification is required. This is true because, as already mentioned, the effects on ignition of both gas temperature and gas velocity across the propellant surface are encompassed by the individual sets of data for a given Mach number. The ignition data for pressures other than 20 to 25 atmospheres have been excluded from Figure 11, but are included in Figure 14 for ignition at Mach 0.13. This was not done because there appears to be a pressure effect on ignition, but because one of the test variables, mass flow rate, G, in the test section is strongly dependent on pressure. By exclusion of lower pressures there is a continuous range of variables from left to right (from low to high surface heat fluxes) for each set of data given by Figures 11 and 12. The range of these variables is summarized by Figure 15. Here the first set of numbers corresponds to low heat fluxes and the second set to high heat fluxes.

It is seen from the data of Figure 15, which were taken from Table 3, that heat flux increases continuously with an increase in both gas velocity and gas temperature for a given Mach number when the test pressure is not a variable. The effect of velocity is to lengthen ignition time and that of gas temperature is to shorten ignition time for a given surface heat flux. It is not possible to detect an effect of mass flow rate, G, on ignition time, other than its influence, accounted for in computing $\bar{F}$, on the total heat transfer process from the hot, convective gases. The mass flow rate which is included in Reynolds number for the fluid stream defines the form and the thickness

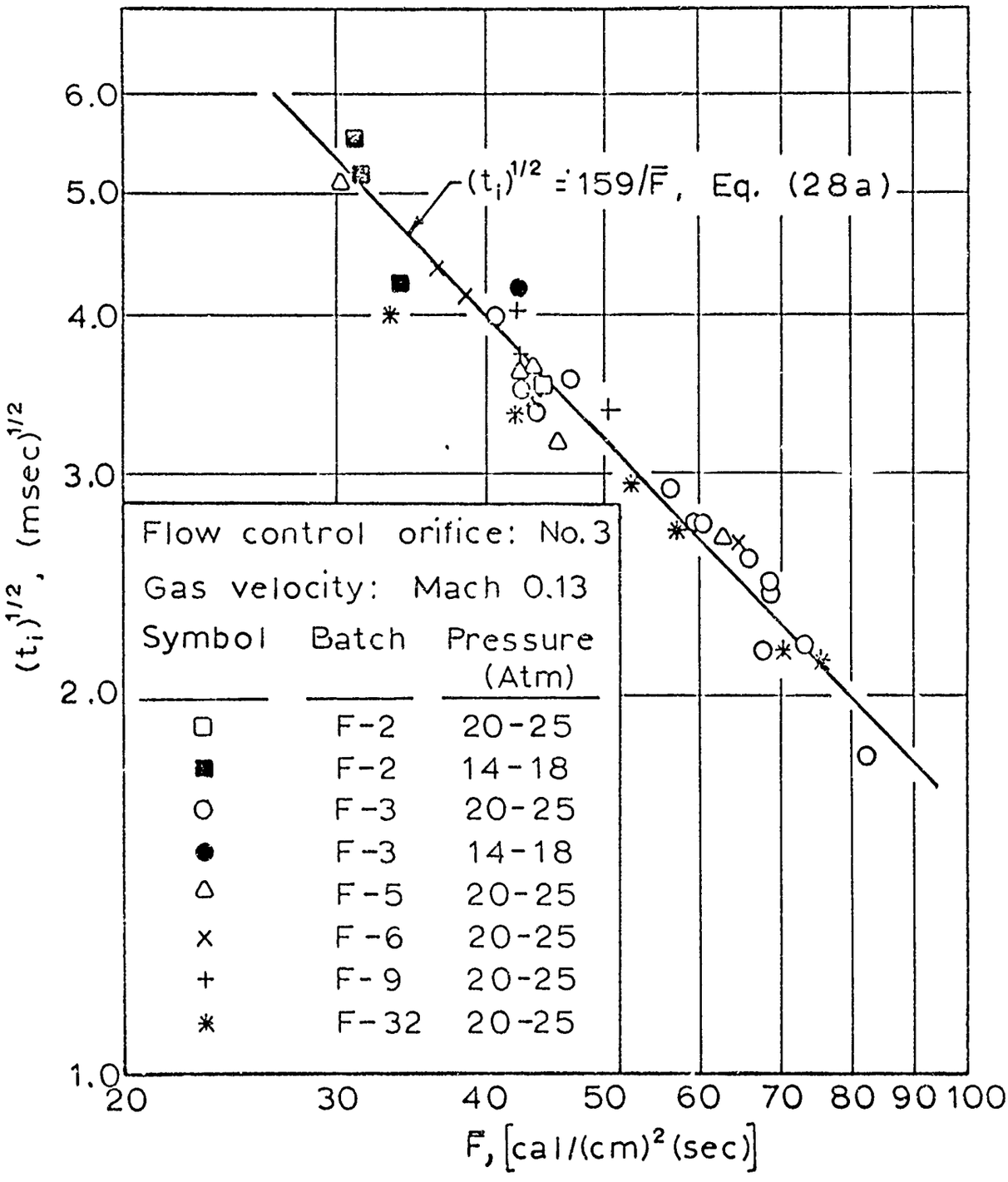

Figure 14

Ignition Data for F-Propellant in Nitrogen at a Test-Gas Velocity of Mach 0.13 for Pressures of 14 to 25 Atmospheres. (A Comparison of Ignition Data for Different Batches of Propellant.)

Figure 15

Range of Experimental Variables for Data Presented in Figures 11 and 12

Mach No.[a]	Temperature of Convective Gas, T_g, (°K)	Velocity of Convective Gas, U, (m/(sec))	Mass Flow Rate in Test Section, G, (g/(cm)^2(sec))
0.13	1000 - 2000	90 - 115	70 - 45
0.20	1000 - 2000	130 - 165	100 - 70
0.28	1000 - 1800	185 - 235	130 - 95
1.0	1500 - 1900	720 - 805	160 - 140

[a]Mach Number at test position is only a function of area ratio.

of the wall boundary layer. But again any relationship between boundary layer thickness and propellant ignition is not evident, and such an effect if it existed could not be separated from the effects of other variables in this study. Other experiments would be required to define the influence of boundary layer thickness on ignition. One indication that there is no effect on ignition of mass flow rate is that ignition data for lower test pressures, as shown by Figure 14, are well defined by the same line which describes the data for higher pressures. If, however, it were assumed that there was an effect of mass flow rate on ignition, then a pressure effect equal in magnitude, but opposite in direction, would be required to give the observed correlation. Without some other form of definitive experimental evidence, we must conclude that pressure and mass flow rate do not influence the ignition process as we describe it.

Figure 14 presents all the data on F-propellant ignition for a gas velocity of Mach 0.13 in the test section. These data are presented in the conventional manner, $\ell n\ (\bar{F})$ versus $\ell n\ (t_i)^{1/2}$. This figure also shows data for lower test pressures (14 to 18 atmospheres) as well as those already given by Figure 11. The ignition data for lower pressures, as shown by Figure 14, cannot be separated from those at higher pressures (20 to 25 atmospheres). Since externally applied heat flux is directly related to gas temperature and gas pressure, it was not possible to obtain experimental ignition data at test pressures lower than 14 atmospheres because of the test-time limitation in the shock tube. Because of the lower heat fluxes for lower operating pressures, heating of the propellant sample was terminated by the arrival of the reflected rarefaction wave or mixing of cold driver gas with the hot test gas before the propellant surface could be brought to its ignition temperature.

Data from six batches of F-propellant are included in the data of Figure 14. Precautions were taken to produce uniformly mixed propellants, but it is well known by those who process propellants that rigid quality control is required to process composite propellants with consistent burning rates. For ignition variations in processing procedures have no apparent effect on the ignitability of a given propellant composition.

Assuming there are no effects which influence propellant ignition other than gas velocity, gas temperature, and externally applied heat flux, it should be possible to separate the temperature effect for the

data given by Figure 11, if the effect is the same for Mach numbers of 0.13, 0.20, and 0.28. The velocity effect can be removed by adjusting all data to the line which describes the Mach 1.0 results, and then by manipulating the data to give a slope of -0.92 it should be possible to uncover the effect of gas temperature on ignition. Incidentally, it is observed that the velocity effect can be substantially removed from the data given by Figure 11 if $(t_i)^{1/2}$ is divided by a factor $(U/U^*)^{0.25}$ where U^* is a fictitious threshold velocity having a value of about 400 meters/second. This arithmetic analysis has not been carried out for the data given by Figure 11, since the result would only apply to this or a very similar propellant system and the answer would not be universally applicable. However, for those who have need for such information for designing a rocket ignition system, such analysis would yield an excellent approximation for engineering applications. A word of caution is required, however, since these data are for a cut propellant surface and ignition behavior for a cast propellant surface of the same propellant composition might be different. Other aspects of surface properties will be discussed in a later section.

Finally, for the experimental data at each Mach number for propellants having similar thermophysical properties (Γ_p) and the same initial temperature (T_o), the ignition time can be expressed by the equation of the straight line which defines the data on an $\ell n\ (\bar{F})$ versus $\ell n\ (t_i)^{1/2}$ plot:

$$(t_i)^{1/2} = C_i(\bar{F})^n \qquad (27)$$

For those cases where the slope, n, has a value of -1.0, ignition characteristics of propellants can be compared directly in terms of the coefficient, C_i. The data of Figure 11 can then be defined by the following expressions:

at Mach 0.13:

$$(t_i)^{1/2} = 159/\bar{F} \qquad (28a)$$

at Mach 0.20:

$$(t_i)^{1/2} = 192/\bar{F} \qquad (28b)$$

at Mach 0.28:

$$(t_i)^{1/2} = 213/\bar{F} \qquad (28c)$$

Where t_i is in milliseconds and $\bar{F}$ has the units of $cal/(cm)^2(sec)$. These simplified expressions provide a means for comparing ignition data at a given test-section Mach number for propellants which have similar thermophysical properties and under test conditions where secondary ignition reactions are important. Under this condition ignition time cannot be expressed by Equation (9) for simple thermal ignition.

The ignition data on F-propellant obtained in the radiation furnace and for convective heating when secondary ignition reactions are not important (simple thermal ignition) can also be represented by a simplified expression:

$$(t_i)^{1/2} = 170/(\bar{F})^{0.92} \qquad (29)$$

To briefly summarize the main points in the foregoing discussion, it appears that two-dimensional heating of surface imperfections and its associated effects, which include heterogeneous-surface and gas-phase secondary ignition reactions, provide additional heat flux to bring the propellant surface more quickly to its ignition temperature. These effects are dependent on gas velocity and gas temperature. At high gas velocities these secondary chemical reactions are no longer important, and propellant ignition is determined only by the externally applied heat flux and the key ignition reaction. Additionally the slope of the line which defines the data for low gas velocities on a $\ell n\ (\bar{F})$ versus $\ell n\ (t_i)^{1/2}$ plot is also dependent on gas velocity and gas temperature.

At higher gas velocities this observation is no longer valid and experimental data obtained by convective heating are in excellent agreement with low-flux data obtained in a radiation furnace under carefully controlled experimental conditions. It should be pointed out that when secondary ignition reactions contribute energy for heating the propellant surface, the externally applied heat flux calculated by the method described previously does not represent the total heat flux at the propellant surface, but the values reported are an excellent approximation to the amount transferred from the hot gas. This is true since the heat is transferred at a rate proportional to the difference between gas and surface temperatures and the propellant surface temperature rise brought about by the aid of secondary ignition reactions is small compared to the gas-surface difference.

Effect of Secondary Ignition Reactions at Low Gas Velocities. The results discussed here are for test gas Mach numbers of 0.07 and 0.09 corresponding to actual gas velocities of approximately 50 and 65 m/(sec), respectively. (Because of heat flux-test time limitations in the shock-tube apparatus, propellant samples could not be ignited at lower gas velocities.) The results of these ignition experiments at low gas velocities for F-propellant are given by Figure 10 and the data are tabulated in Table 3. Data for all test pressures which range from 14 to 25 atmospheres are included in this figure, but are not specifically identified. The results at low gas velocities are compared with those obtained at Mach 0.13.

It is seen that a decrease in test gas velocity to Mach 0.09 further increases the ignitability of F-propellant. At a lower gas velocity, Mach 0.07, no further improvement in ignitability is observed. For the results at lower gas velocities, the incremental change in Mach number is much less than at the higher velocities, thus the relative separation for each set of data would be expected to be less. Because of the large amount of scatter in experimental data for tests at Mach 0.07 and the limited range of heat fluxes that could be investigated, it is not possible to define these results by a straight line on the $\ell n\ (\bar{F})$ versus $\ell n\ (t_i)^{1/2}$ plot. Experimental data for Mach 0.09 and 0.07 are presented in separate graphs in Figures 16 and 17, respectively. The experimental data for Mach 0.09 are defined on the $\ell n\ (\bar{F})$ versus $\ell n\ (t_i)^{1/2}$ plot by:

$$(t_i)^{1/2} = 144/\bar{F} \qquad (28d)$$

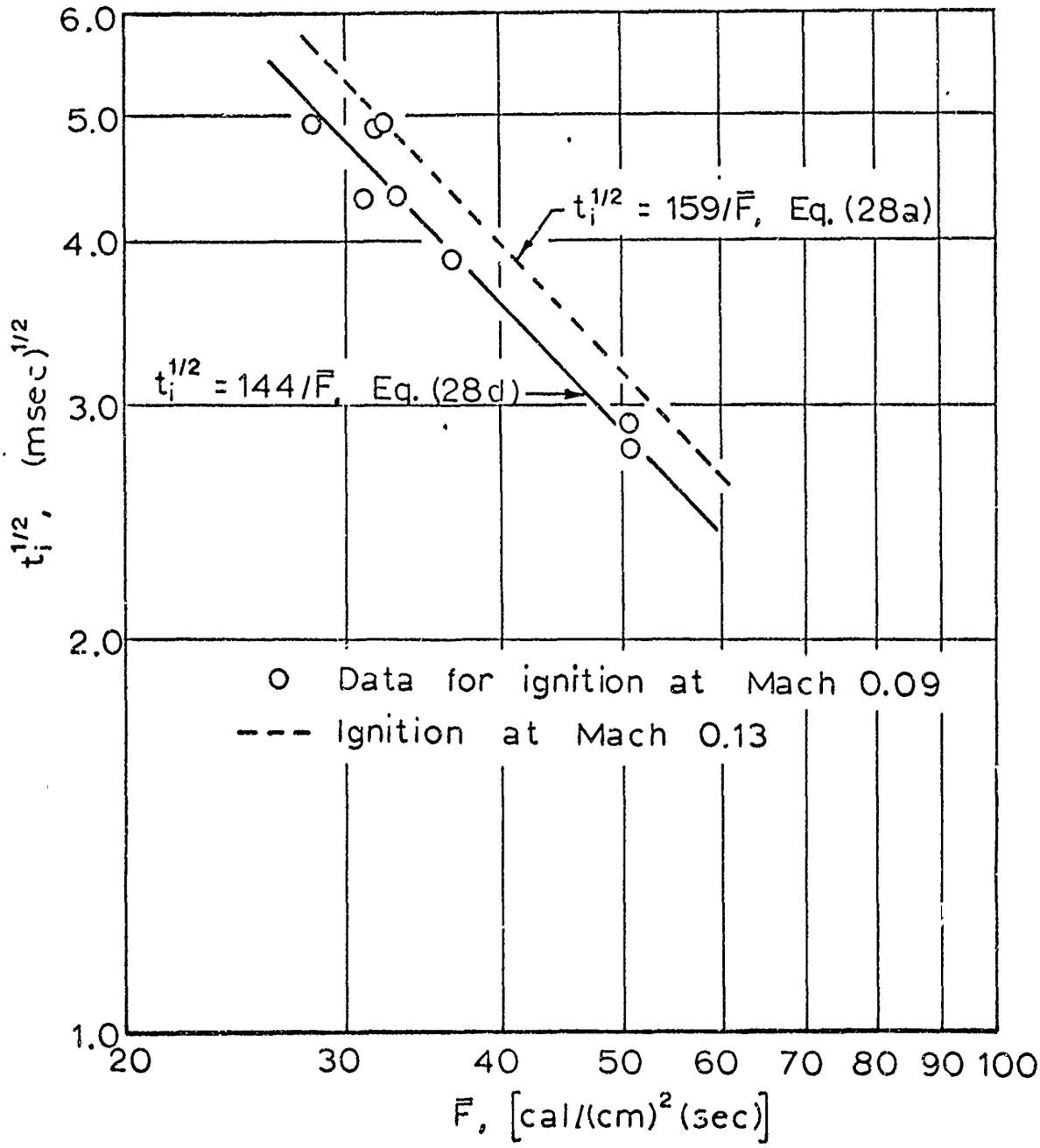

Figure 16

Ignition Data for F-Propellant in Nitrogen at a Test-Gas Velocity of Mach 0.09 for Pressures of 20 to 25 Atmospheres.

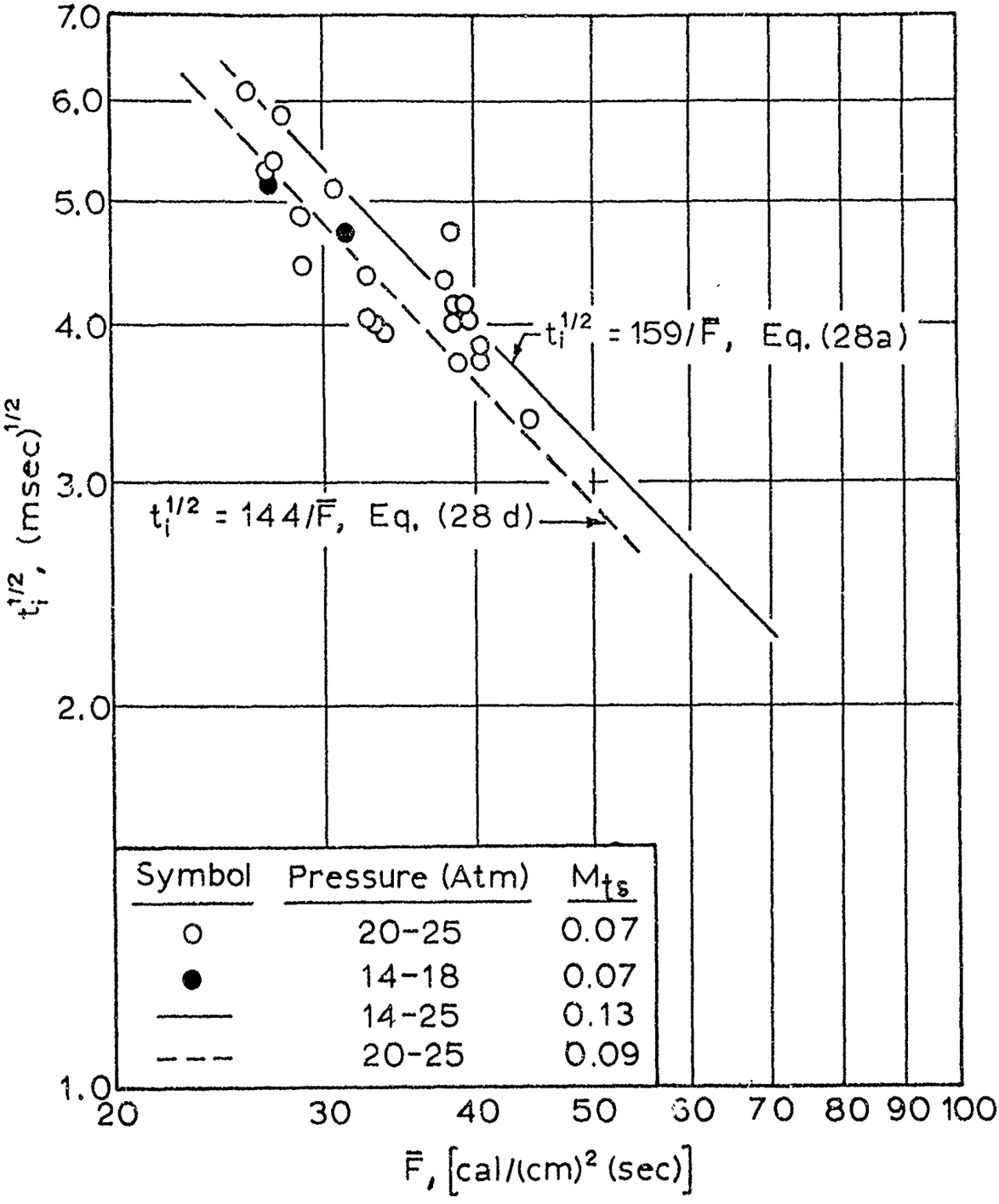

Figure 17

Ignition Data for F-Propellant in Nitrogen at a Test-Gas Velocity of Mach 0.07 for Pressures of 14 to 25 Atmospheres.

compared to the data at Mach 0.13 which are represented by:

$$(t_i)^{1/2} = 159/\bar{F} \tag{28a}$$

The reason for the large amount of scatter in experimental data at Mach 0.07 is not known; however, much of the scatter appears to be caused by surface imperfections. Also, it was observed (see Figure 68) on temperature-time data from heat-flux gauges, that some small fluctuations in temperature occurred during runs at Mach 0.07 that were not observed at higher Mach numbers. This is apparently associated with the heat transfer mechanism in the entrance region of the test section at low gas velocities and is not fully understood. It is also possible that at low gas velocities thermal ignition of two-dimensionally heated individual crystals is possible. If this were true, even fairly small variations in surface roughness would have a large effect on ignitability at low velocities. Further studies will be required to resolve this problem.

The fact that no further improvement in propellant ignitability occurred for the lower gas velocity (Mach 0.07) indicates that at lower convective heating rates with this propellant, secondary reactions are limited by the rate at which reactive species are generated in contrast to limiting conditions at higher gas velocities where these reactions are limited by dilution of reactive species.

It is noted from the data of Table 3 that F-propellant was not ignited when the convective gas temperature was lower than about 1000°K. Calculated results indicate this was not a true gas temperature effect, but was the result of test limitations in the shock tube. At

low gas temperatures the test time in the shock tube was insufficiently long to bring the propellant surface to its ignition temperature. This can be seen by noting the calculated propellant surface temperatures at which the test period was terminated and comparing these values to surface temperatures of propellants which ignited under the same gas velocities (Table 3). There is some experimental scatter among these data, but all of the propellants which did not ignite had surface temperatures in the same range or lower than those which did ignite. It would be of interest to pursue the effect of gas temperature to very low temperatures, perhaps 500 or 600°K, to see if secondary chemical reactions still contribute energy to the ignition process with convective heating. It would appear that at low gas temperatures, surface reactions would not be important and propellant ignition times would be in agreement with radiation furnace results for a given externally applied heat flux.

IGNITION IN ARGON

With a monatomic gas such as argon, higher gas temperatures can be obtained for a given incident Mach number in the shock tube than for nitrogen. This was important in the work described here because the higher gas temperature could be attained without a trade-off in test time, and, as mentioned earlier, the gas temperature could be varied independently of the test pressure (P) and gas velocity (U). The relationship between the mean surface heat flux ($\bar{F}$) and gas temperature (T_g) for ignition of F-propellant in argon and nitrogen is shown graphically by Figure 18 for gas velocities of Mach 0.13

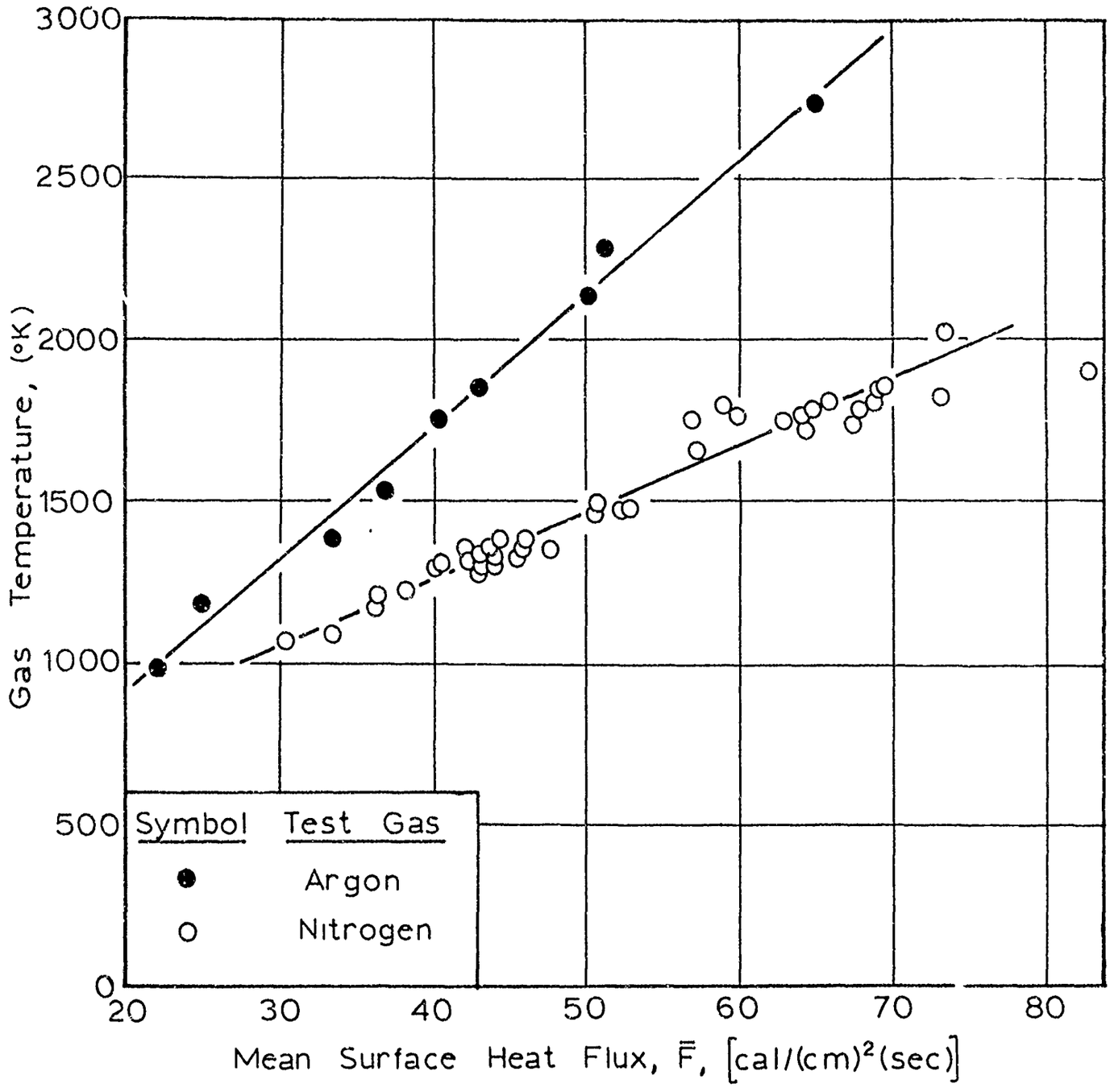

Figure 18

Variation of Surface Heat Flux with Gas Temperature for Ignition of F-Propellant at Pressures of 20 to 25 Atmospheres in Nitrogen and Argon at a Test-Gas Velocity of Mach 0.13.

through the test section and by Figure 19 for Mach 0.27 in argon and Mach 0.28 in nitrogen. The data for preparing these graphs were taken directly from tables of ignition data, Table 3 for ignition in nitrogen and Table 5 for ignition in argon. It should be noted that the temperature behind the reflected shock wave in a shock tube cannot be calculated precisely. (The method used for calculating the temperature behind a reflected shock wave in this work is described in Appendix C.) This does not preclude the use of a calculated gas temperature for determining the externally applied heat flux to a propellant surface, if local heat transfer coefficients are measured at the test position, but it does limit the usefulness of this temperature for estimating the effect of gas temperature on the ignition process.

Experimental data for ignition of F-propellant (Batch F-32) in argon are given in Table 5 and are presented graphically in Figure 20 in the form of an $\ln(\bar{F})$ versus $\ln(t_i)^{1/2}$ plot. The data are for test gas velocities of Mach 0.13 and 0.27 and convective heat fluxes of 20 to 95 cal/(cm)^2(sec). The ignition results on F-propellant in nitrogen are represented in Figure 20 by a solid line for tests at Mach 0.28 and by a dashed line for tests at Mach 0.13. The individual data points for ignition of Batch F-32 at Mach 0.13 in nitrogen are included in Figure 20 for comparison with data obtained in argon. There is some scatter among the ignition data for tests in argon which precludes fitting a straight line to the data. However, the data for tests in argon are sufficiently consistent to show that the ignition of F-propellant is affected by gas temperature at relatively

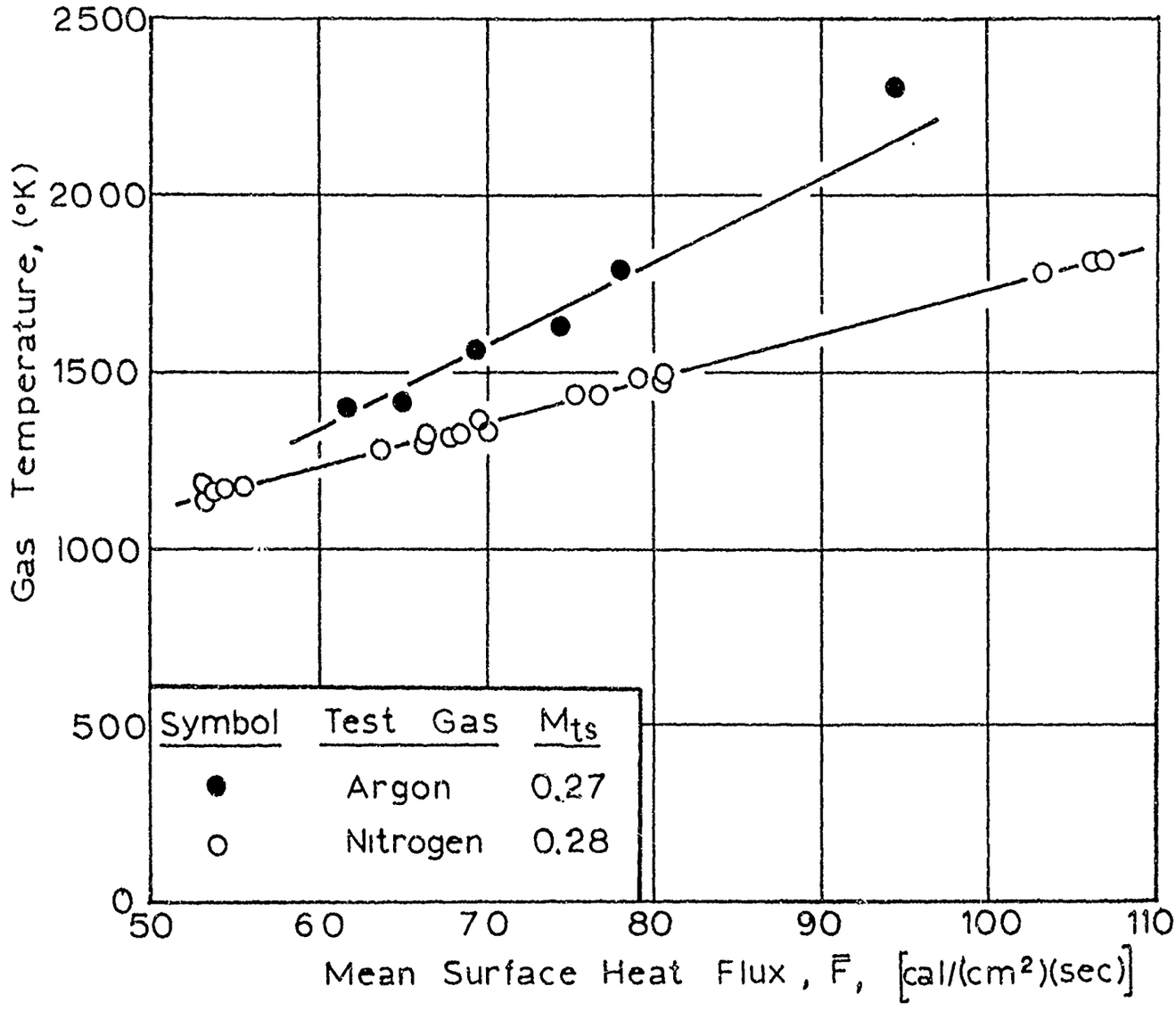

Figure 19

Variation of Surface Heat Flux with Gas Temperature for Ignition of F-Propellant at Pressures of 20 to 25 Atmospheres in Nitrogen at Mach 0.28 and in Argon at Mach 0.27.

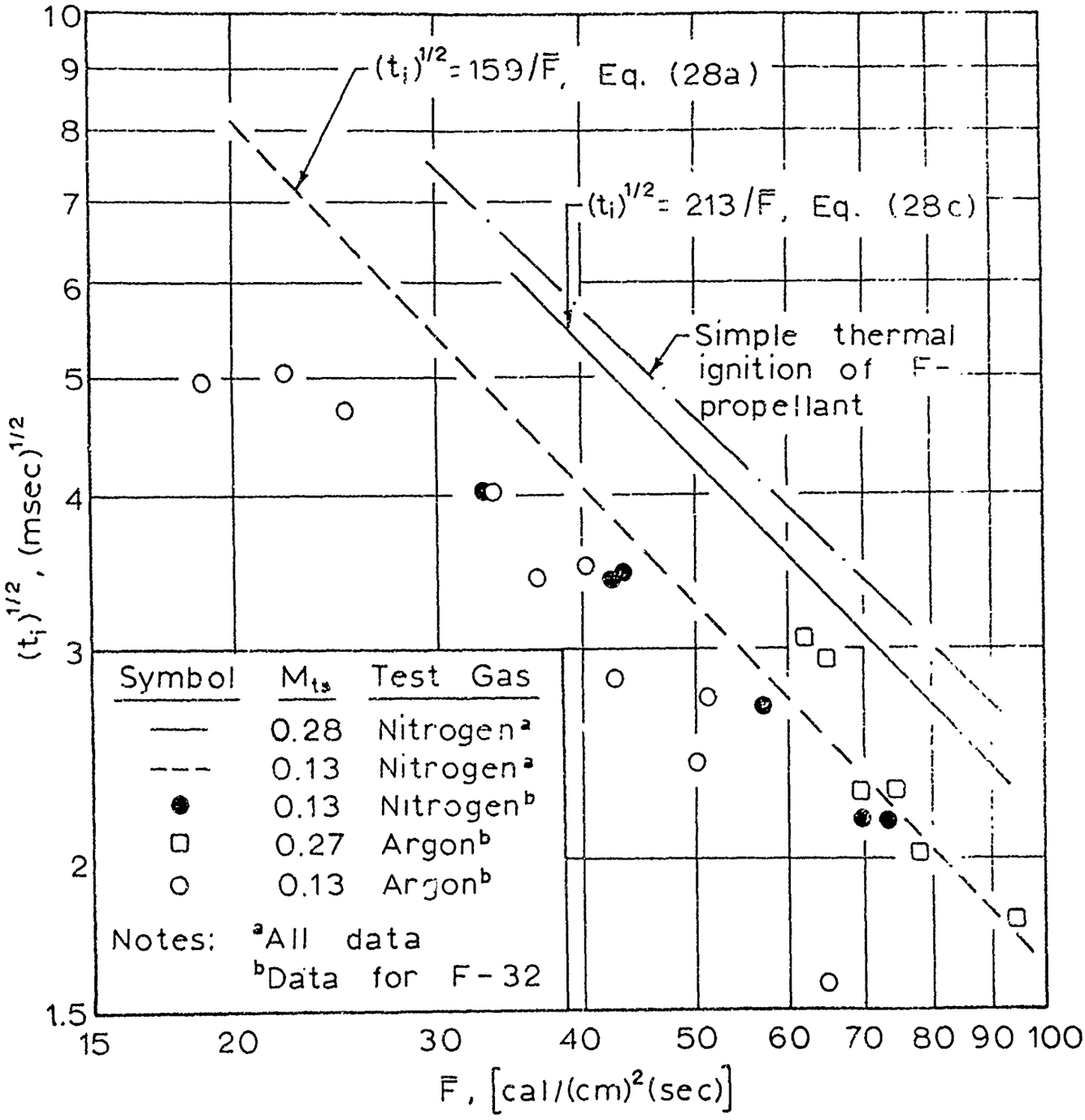

Figure 20

Ignition Data for F-Propellant (Batch F-32) in Argon for Pressures of 20 to 25 Atmospheres. (A Comparison of Ignition Results in Argon and Nitrogen.)

low gas velocities. Except for tests at low heat fluxes, the data show a larger difference in ignition times for runs in argon and nitrogen at the highest heat fluxes, test conditions under which the temperature difference is also greater. Consequently, the best straight line representing the data in argon would have a slope with an absolute value greater than 1.0. This is in accordance with an earlier observation that if ignition times are compared at the same gas velocities for propellants with rough surfaces, the effect of increasing gas temperature at a given externally applied heat flux should be a shortening of ignition time.

Because the temperature of the convective gas was found to alter the ignition characteristics of F-propellant, it was concluded that secondary ignition reactions, either gas-phase or heterogeneous-surface reactions, participate in the ignition process at relatively low gas velocities. These secondary ignition reactions contribute energy for bringing the propellant surface more rapidly to its ignition temperature. The gas-temperature effect on ignition is only important when propellants have surface imperfections, for it was found in ignition experiments on propellants with very smooth surfaces that the effect of gas temperature on ignition was almost negligible.

The large amount of scatter among the experimental data for tests in argon also appears to be related to surface imperfections. For test in argon on propellants with smoother surfaces which will be discussed in a later section, the experimental data were much more consistent than those obtained on F-propellant. It would be expected,

based on the results of ignition tests at Mach 1.0 in nitrogen, that even for a propellant with a rough surface, the effect of gas temperature on ignition would diminish with an increase in gas velocity; and at some threshold velocity, variations in gas temperature would no longer affect the ignition process. The ignition data on F-propellant in argon were not obtained over a sufficiently wide range of gas velocities to observe a decrease in the effect of gas temperature.

IGNITION IN AIR

Ignition runs on F-propellant in air were made at a gas velocity of Mach 0.13 for convective heat fluxes of 30 to 70 cal/(cm)^2(sec).

Baer [6], McCune [67], Kling, et al. [55], Bastress, et al. [10], and Hermance, et al. [43] had previously studied the ignition of composite propellants in convective heating experiments using reactive test gases, and found that propellants ignite much faster in oxygen than in air or nitrogen. The propellants studied by Baer and McCune had essentially the same ignition characteristics in air and nitrogen. However, all of the propellants tested by Baer and McCune contained a relatively fine particle-size oxidant that facilitated the preparation of fairly smooth surfaces.

In the study made for this thesis on ignition of F-propellant in air, it was found that ignition times were faster in air than in nitrogen for equivalent applied heat fluxes. Ignition data for F-propellant in air at Mach 0.13 are tabulated in Table 6 and are presented in the form of $\ell n\ (\bar{F})$ versus $\ell n\ (t_i)^{1/2}$ by Figure 21. The ignition results in nitrogen at Mach 0.13 are represented by the dashed line in Figure 21.

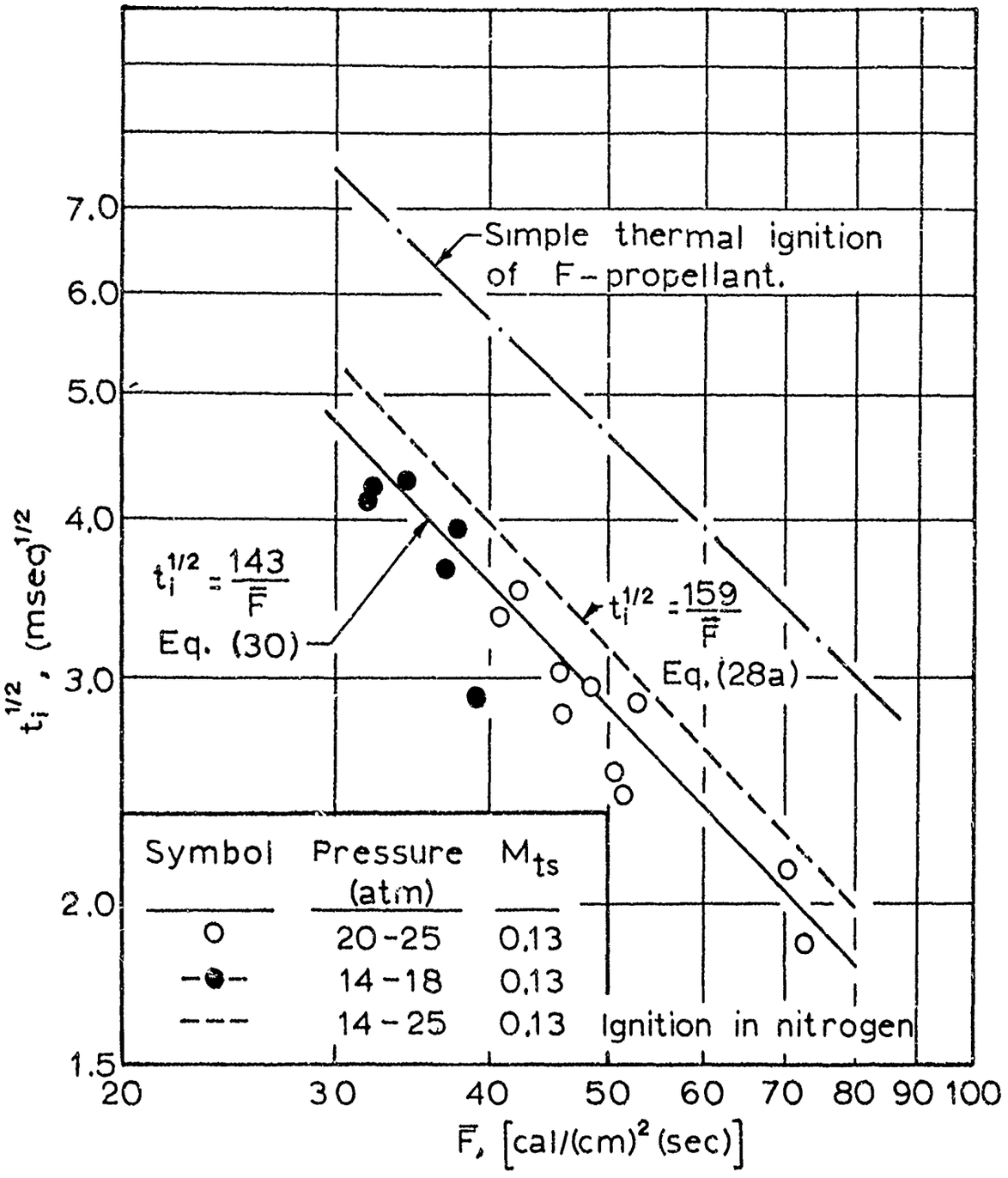

Figure 21

Ignition Data for F-Propellant in Air for a Test-Gas Velocity of Mach 0.13 for Pressures of 14 to 25 Atmospheres. (A comparison of Ignition Results in Air and Nitrogen.)

The data for ignition at Mach 0.13 in nitrogen and air, respectively, are represented by the following equations:

$$(t_i)^{1/2} = 159/\bar{F} \tag{28a}$$

$$(t_i)^{1/2} = 143/\bar{F} \tag{30}$$

Where $\bar{F}$ has the units of cal/(cm)^2(sec) and t_i is in milliseconds.

From this result, it appears that the oxygen in the air participated in the secondary ignition process, increasing the exothermicity of the reaction process, which helped bring the propellant surface to its ignition temperature in a shorter period of time. This result is in agreement with our earlier supposition that the ignitability of propellants with rough surfaces should be improved through exothermic reactions between the environmental gas and reactive species generated at the surface.

McCune [67] has shown that for higher gas velocities (about Mach 0.3) and for propellants with fairly smooth surfaces that even pure oxygen does not have a large effect on ignition. In another section, the ignition of propellants in reactive gases is discussed in more detail, and it is shown that for propellants with smooth surfaces, even at rather low gas velocities, high-temperature oxygen does not affect the ignitability of ammonium perchlorate propellants.

HIGH-SPEED MOTION PICTURE STUDIES OF F-PROPELLANT IGNITION

As a means of determining where on the propellant surface ignition was initiated in terms of the development of a luminous flame and also to observe the ignition process with respect to possible clues as to

the ignition mechanism, several ignition tests were observed by photographing the propellant surface with a Fastax, high-speed, motion picture camera. These studies were also conducted as a check on the validity of photocell measurements as a means of detecting ignition. For these runs film speeds of 2200 to 4700 frames per second were used.

The results of this study showed that at low gas velocities, Mach 0.13, across the propellant surface, ignition occurred at one or more positions on the propellant surface, and then spread rapidly across the surface. Ignition at low-gas velocities, in tests photographed, was always initiated at the center or at the trailing edge of the sample which had a circular cross-section of 3/8-in. diameter. Because of entrance effects in the short test section, heat transfer should be higher at the leading edge of the sample. The reason that ignition occurs at the trailing edge may be due to the fact that the boundary layer is colder at the leading edge from flow of the hot gases over the metal wall in the entrance region of the test section. This explanation could be checked by making the entrance to the test section of material having thermophysical properties similar to that of the propellant. Bastress [10] noted a similar effect, and when longer samples were used ignition time was somewhat less and the effect of gas velocity was not as pronounced. These observations may also suggest that the boundary layer is changing its form because of surface roughness. However, the same effect was observed for both F-propellant with very large particle-size ammonium perchlorate

(200 micron) and for propellants AD and AE with a finer particle-size ammonium perchlorate (85 micron). In fact for the propellants containing the smaller particle-size ammonium perchlorate, ignition in all tests photographed occurred close to the trailing edge.

Prints from one of the high-speed motion picture films taken during ignition of F-propellant are shown by Figure 22. The ten frames shown are for the two-millisecond period beginning with the appearance of a luminous zone on the propellant surface. This test was conducted in air with a gas velocity in the test section of about 100 m/(sec), Mach 0.13. For these prints the leading edge of the sample is at the top. The pressure in the test section was about 20 atmospheres, the gas temperature was 1800°K, and the externally applied surface heat flux was approximately 50 cal/$(cm)^2$(sec). Ignition time was less than 10 milliseconds. These photographs were taken through a quartz window opposite the propellant test position and are views of the entire propellant surface. Since no external lighting was used, surface details are not visible. It is interesting to note the number of positions on the surface at which ignition occurred.

Figure 23 shows photographs of ignition of F-propellant at a higher gas velocity (Mach 0.28). For these photographs the leading edge is at the bottom. In this test the gas temperature was 1600°K and the mean surface flux was about 80 cal/$(cm)^2$(sec). Ignition time was approximately 6 milliseconds.

Prints of high-speed photographs for ignition of F-propellant at Mach 1.0 are shown by Figure 24. For this run the gas temperature

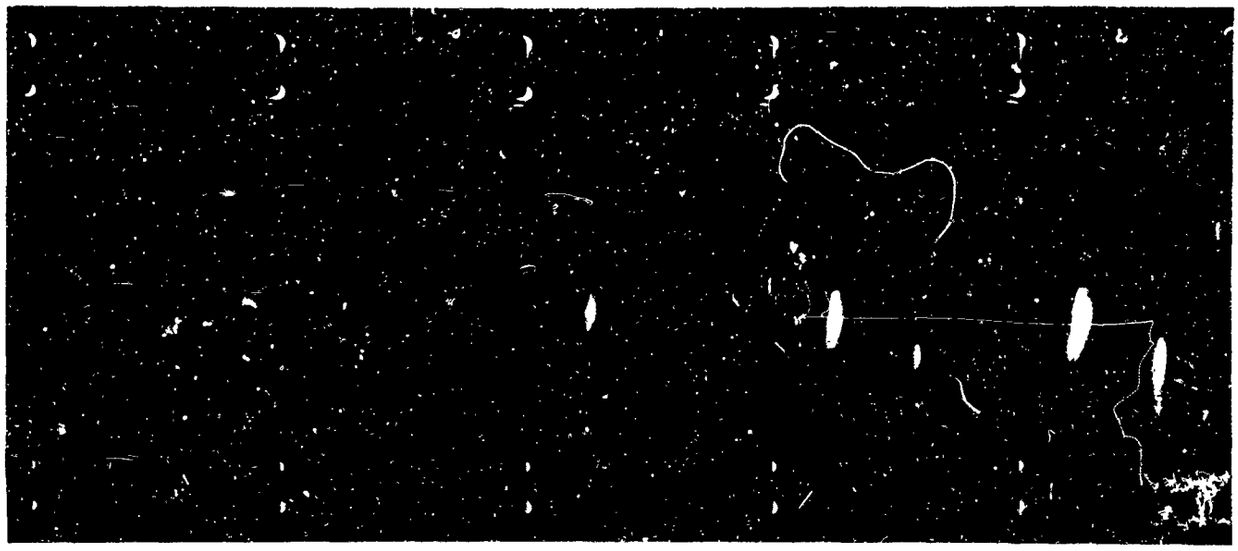

0.0 0.22 0.44 0.66 0.88 msec.

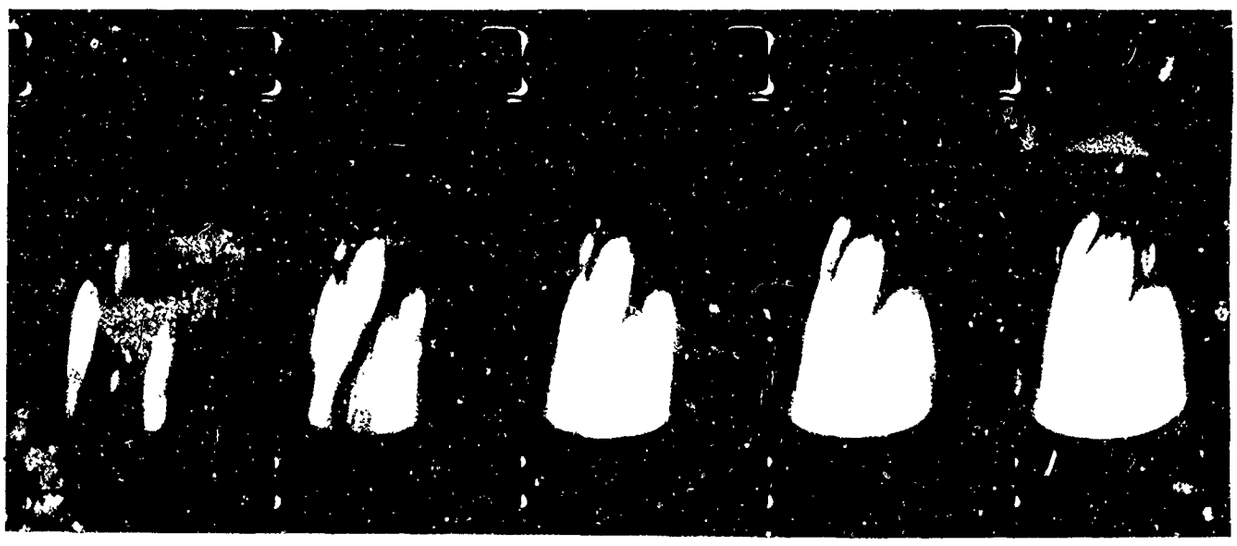

1.10 1.32 1.54 1.76 1.98 msec.

Figure 22

Photographs of F-Propellant Ignition in Air at a Test-Gas Velocity of Mach 0.13. Run No. 47-15-3, Propellant F-62M, Gas Temperature: 1800 °K, Mean Surface Heat Flux: 50 cal/(cm)^2(sec), Film Speed: 4600 frames /(sec). The Leading Edge is at the Top of Prints.

0.0 0.22 0.44 0.66 0.88 msec.

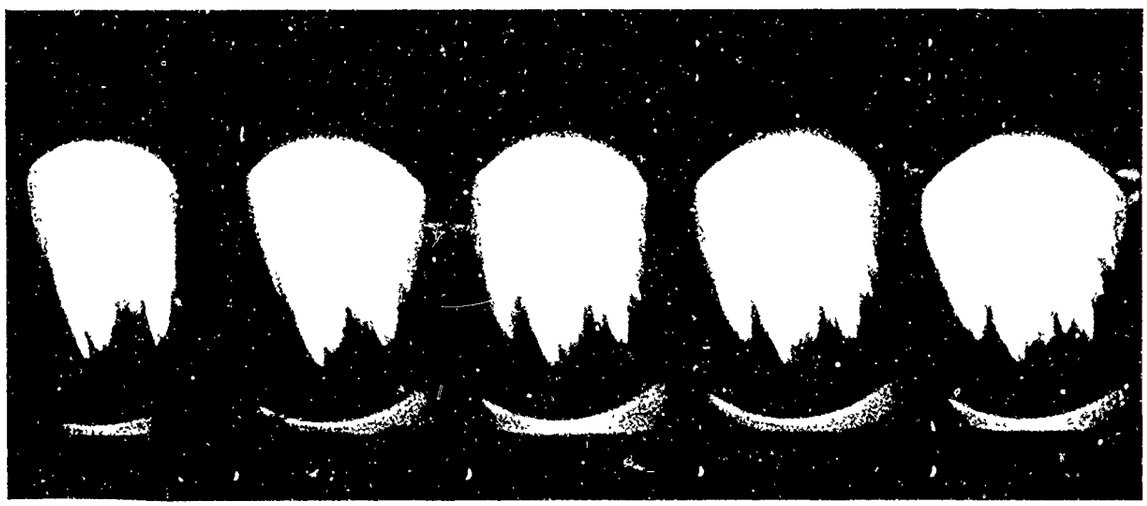

1.10 1.32 1.54 1.76 1.98 msec.

Figure 23

Photographs of F-Propellant Ignition in Air at a Test-Gas Velocity of Mach 0.28. Run No. 47-23-4, Propellant F-62M, Gas Temperature: 1600°K, Mean Surface Heat Flux: 80 cal/(cm)^2(sec), Film Speed: 4600 frames/(sec). The Leading Edge is at the Bottom of Prints.

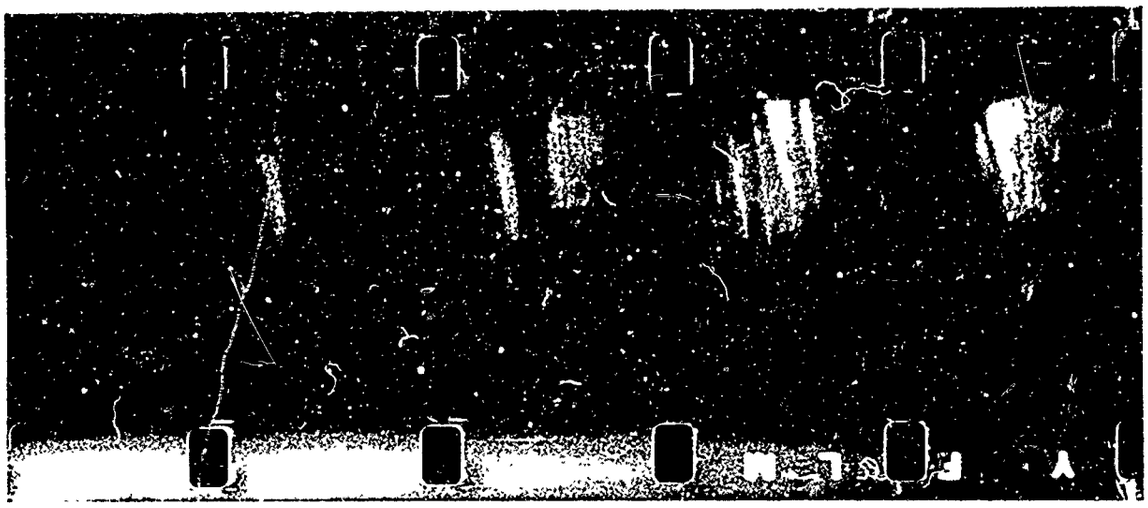

0.0 0.22 0.44 0.66 0.88 msec.

1.10 1.32 1.54 1.76 1.98 msec.

Figure 24

Photographs of F-Propellant Ignition in Air at a Test-Gas Velocity of Mach 1.0. Run No. 47-16-3, Propellant F-62M, Gas Temperature: 1800°K, Mean Surface Heat Flux: 130 cal/(cm)^2(sec), Film Speed: 4600 frames/(sec). The Leading Edge is at the Bottom of Prints.

was 1800°K and the mean surface heat flux was about 130 cal/(cm)^2(sec). Ignition occurred within 5 milliseconds under these conditions. The leading edge of the sample is at the bottom of the photograph. Because of the high gas velocity, the flame zone is extremely thin and it is possible to see on some of the frames small hot spots which appear to be burning particles of ammonium perchlorate. Again, as was the case for lower gas velocities, ignition occurred near the center of the propellant sample. It was found that for all tests at Mach 1.0, propellant burning was always extinguished when the cold driver gas entered the test section. This occurred after 5 milliseconds for the test described here. Extinguishment of the deflagration process is to be expected since the exothermic decomposition of ammonium perchlorate alone cannot provide sufficient energy to sustain steady deflagration of the propellant under these conditions without energy feedback from gas-phase or surface reactions. Since reactive gaseous species are swept away by the high velocity gas, external application of energy is required. It was found for some of the tests at Mach 1.0 that a small flame was stabilized downstream of the leading edge of the sample holder on the propellant surface and continued to burn locally after cold gases moved into the test section.

Samples of F-propellant which were recovered from tests at high gas velocities, when burning was quenched by the flow of cold driver gases into the test section, showed that large particles of ammonium perchlorate protruded above the surface in the downstream region with only a slight change in the appearance of the surface near the leading

edge. Photomicrographs of a propellant surface after a test at Mach 1.0 are shown by Figure 25. Photomicrographs of a freshly cut surface are shown by Figure 8.

The fact that large ammonium perchlorate particles were exposed at the surface during tests at high gas velocities (Mach 1.0) indicate that at least a quasi-steady deflagration process was initiated at the surface before being quenched by the arrival of cold driver gases at the test position. Substantial changes of the propellant surface, as shown by Figure 25, were found on recovered samples only when a strong photocell signal was observed during an ignition test.

SUMMARY

The most significant result obtained from the study on ignition of F-propellant under convective heating was that only for very high gas velocities across the propellant can the ignition process be described as simple thermal ignition. Under this test condition ignition characteristics of F-propellant under convective heating can be compared directly with those for ignition of F-propellant under low radiant fluxes. At low gas velocities this propellant still ignites thermally, but some of the energy for bringing the propellant to its thermal ignition temperature is supplied by secondary ignition reactions. As a consequence, F-propellant is easier to ignite by convective heating under low gas velocities than at very high gas velocities. It is shown that this improved ignitability at low gas velocities can be related to the surface characteristics of the propellant sample.

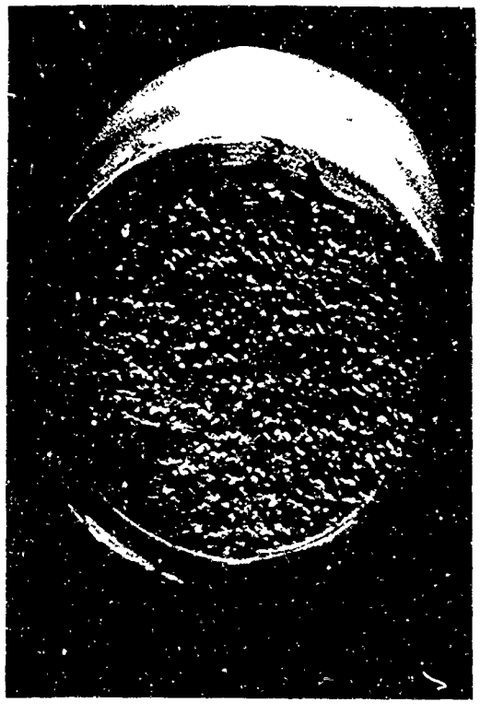

a. 5X Magnification

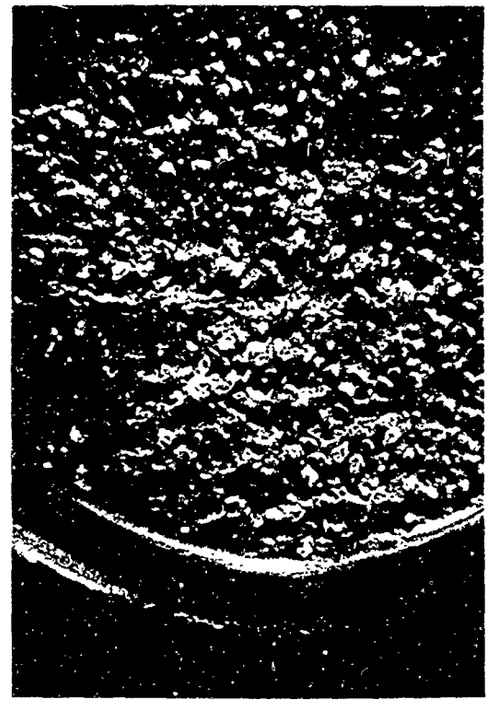

b. 10X Magnification

Figure 25

Photomicrographs of the Surface on a Sample of F-Propellant Recovered from an Ignition Test in Nitrogen at a Test-Gas Velocity of Mach 1.0. Run No. 43-19-1, Gas Temperature: 1500°K, Mean Surface Heat Flux: 115 cal/(cm)^2(sec), Leading Edge at Left.

Surface imperfections are produced during the preparation of samples for ignition tests if large particles of ammonium perchlorate (greater than about 50 microns in diameter) are present in the propellant. The magnitude of this surface roughness increases with the size of the ammonium perchlorate particles in the propellant.

At low gas velocities across the propellant surface, processes associated with these surface imperfections provide energy in addition to that supplied externally by one-dimensional heat transfer from the hot test gas. Consequently, the surface temperature of the propellant increases more rapidly than one calculates for one-dimensional heating. Some of the additional heating occurs by heat conduction from surface imperfections which have been heated two-dimensionally. However, the greater part of the additional heating comes from secondary ignition reactions. By two-dimensional heating of surface imperfections, reactive species generated at local hot spots on the surface react in the gas phase or heterogeneously at the propellant surface to supply energy for heating the propellant surface.

At higher gas velocities these effects which are attributable to exothermic reactions become less important, as the reactive species that participate in these reactions are swept away in the inert gas stream. Also, surface heating which occurs through heat conduction from two-dimensionally heated surface imperfections appears to be less important at high gas velocities. In short, high velocity erases the two-dimensional effect due to surface roughness, providing, in effect, the one-dimensional situation of a smooth surface.

If a gas-phase reaction were the key process in the ignition of ammonium perchlorate propellant, such as F-propellant, one would also expect the velocity of the test gases to influence ignition. However, contrary to the above observations, one would then expect the ignition delay to increase continually with gas velocity until some threshold velocity were reached beyond which no ignition would occur. Such an effect is observed in the ignition of double-base propellants where gas-phase processes are known to be important. In the ignition studies made by Churchill, Kruggel, and Brier [24] on double-base propellants under convective heating, ignition was observed to take place in the gas phase with subsequent flashback of the flame to the propellant surface. Prior to ignition, Churchill and coworkers observed etching of the cylindrical propellant grain under the influence of the convective gas, and in some studies the propellant decomposed completely without the appearance of a flame. The decomposition of the propellant grains without apparent ignition occurred at high gas flow rates and low gas temperatures. Unpublished results at the University of Utah have shown that under high convective heat fluxes in a shock tube some double-base propellants cannot be ignited, but examination of the surface of the propellant sample after a test always showed considerable surface regression.

From the results of work on the ignition of F-propellant and other ammonium perchlorate propellants conducted for this thesis, it was found that all observed ignition phenomena could be explained by thermal ignition theory. On the other hand, if it were assumed that

the key ignition process involved gas-phase or heterogeneous-surface reactions, it would be impossible to provide a consistent explanation of the observed ignition characteristics of composite propellants for tests under different environmental conditions.

CHAPTER VI

IGNITION OF OTHER CAST PROPELLANTS

The studies on propellant ignition described in this chapter were conducted primarily to investigate the effect of compositional variables on ignition. These studies also provided the information necessary to verify our earlier hypothesis that the improved ignitability of some propellants at low-gas velocities was linked with imperfections at the propellant surface, and provided information about the role of secondary ignition reactions in the thermal ignition process.

IGNITION OF PROPELLANTS CONTAINING COPPER CHROMITE

The studies on propellants containing copper chromite included an investigation of the effect on ignition of: (1) particle-size distribution of ammonium perchlorate in a bimodal blend, (2) concentration of ammonium perchlorate, and (3) different single particle-size cuts of ammonium perchlorate in the propellant.

Ignition of Modified F-Propellant

The "modified" F-propellant was different from what we previously have called "regular" F-propellant in that a new lot of 15-micron ammonium perchlorate was used in the bimodal mixture in making the modified propellant. It was found that after cure the modified propellant was softer than the regular propellant, and consequently, it

was more difficult to cut smooth surfaces on it. The effect of increased surface roughness was to improve the ignitability of this propellant over that for regular F-propellant at low test-gas velocities. This was additional evidence for associating improved ignitability of propellants with surface imperfections.

The lot of 15-micron ammonium perchlorate used in the regular F-propellant was obtained from Thiokol Chemical Corporation, Brigham City, Utah. This fine particle-size ammonium perchlorate was apparently made by grinding a much coarser material, then screening the ground material to obtain a 15-micron cut. The new lot of 15-micron ammonium perchlorate that was used in the modified propellant was obtained from American Potash and Chemical Corporation. A careful microscopic particle-size analysis of the two lots of perchlorate revealed that both lots had a similar particle-size distribution. The only apparent difference in physical appearance between the two lots was that the perchlorate obtained from American Potash and Chemical Corporation was more bulky and the small particles were clustered in soft agglomerates. It appeared that the clustering of particles was produced by an electrostatic effect and was not due to caking, for the agglomerates could be dispersed rather easily.

Upon comparing cut surfaces for the two propellants microscopically, it was found that surfaces on the modified propellant were much rougher than those on regular F-propellant. The surface roughness of the modified propellant was estimated to be of the order of 30 to 40 microns as compared to a surface roughness of about 20 to 30 microns for regular F-propellant. The modified propellant was softer,

and the fine particles were not held as firmly in the propellant matrix as they were in the regular propellant. During the cutting of new surfaces on modified F-propellant, it was noticed that some of the large particles in the propellant matrix (average diameter of about 200 microns) were raised and rotated a small amount as the cutting edge of the razor blade was moved through the propellant. This produced a rougher surface and a larger number of fractured particles.

At low gas velocities in nitrogen, modified F-propellant ignited faster than regular F-propellant at equivalent externally applied heat fluxes. However, ignition characteristics of the two propellants were identical at Mach 1.0. The experimental ignition data for modified F-propellant are included in Table 3 with data for the regular F-propellant and are identified by an "M" following the batch number. The data for gas velocities of Mach 1.0, 0.28, and 0.13 are presented graphically by Figure 26. The results for regular F-propellant at gas velocities of Mach 0.13 and 0.28 are shown in Figure 26 by the dashed lines which represent the data given by Figure 11. The ignition of modified F-propellant at lower gas velocities, Mach 0.09 and 0.07, are given in Figure 27.

As was the case for regular F-propellant, the slopes of the lines which defined ignition data for modified F-propellant at low gas velocities on an $\ell n\ (\bar{F})$ versus $\ell n\ (t_i)^{1/2}$ plot were assumed to have values of -1.0. The results on ignition of these two propellants are compared by Figure 28 as a tabulation of coefficients in the equations

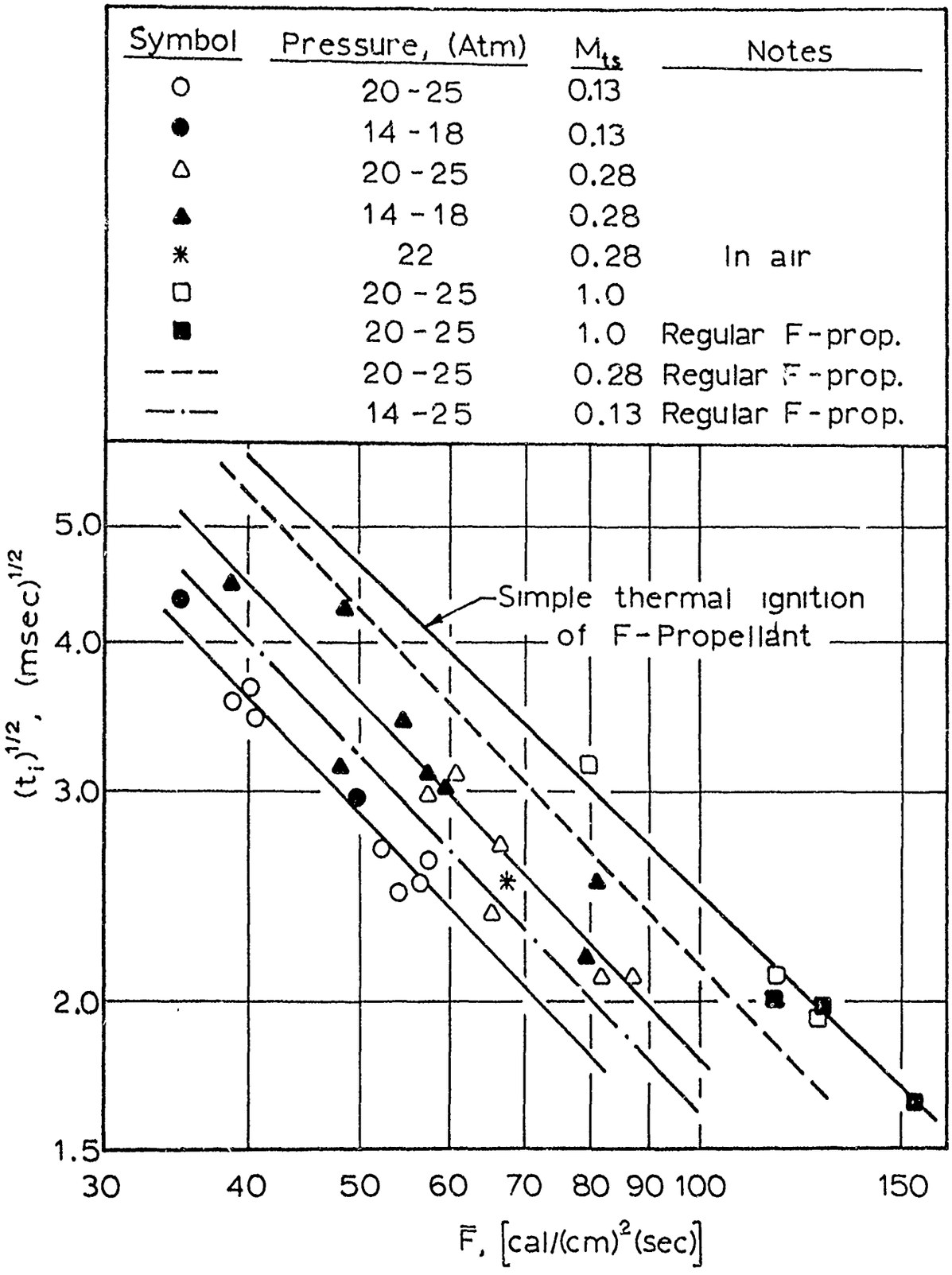

Figure 26

Ignition Data for Modified F-Propellant in Nitrogen at Intermediate and High Gas Velocities for Pressures of 14 to 25 Atmospheres. (A Comparison of Ignition Results with Those for Regular F-Propellant.)

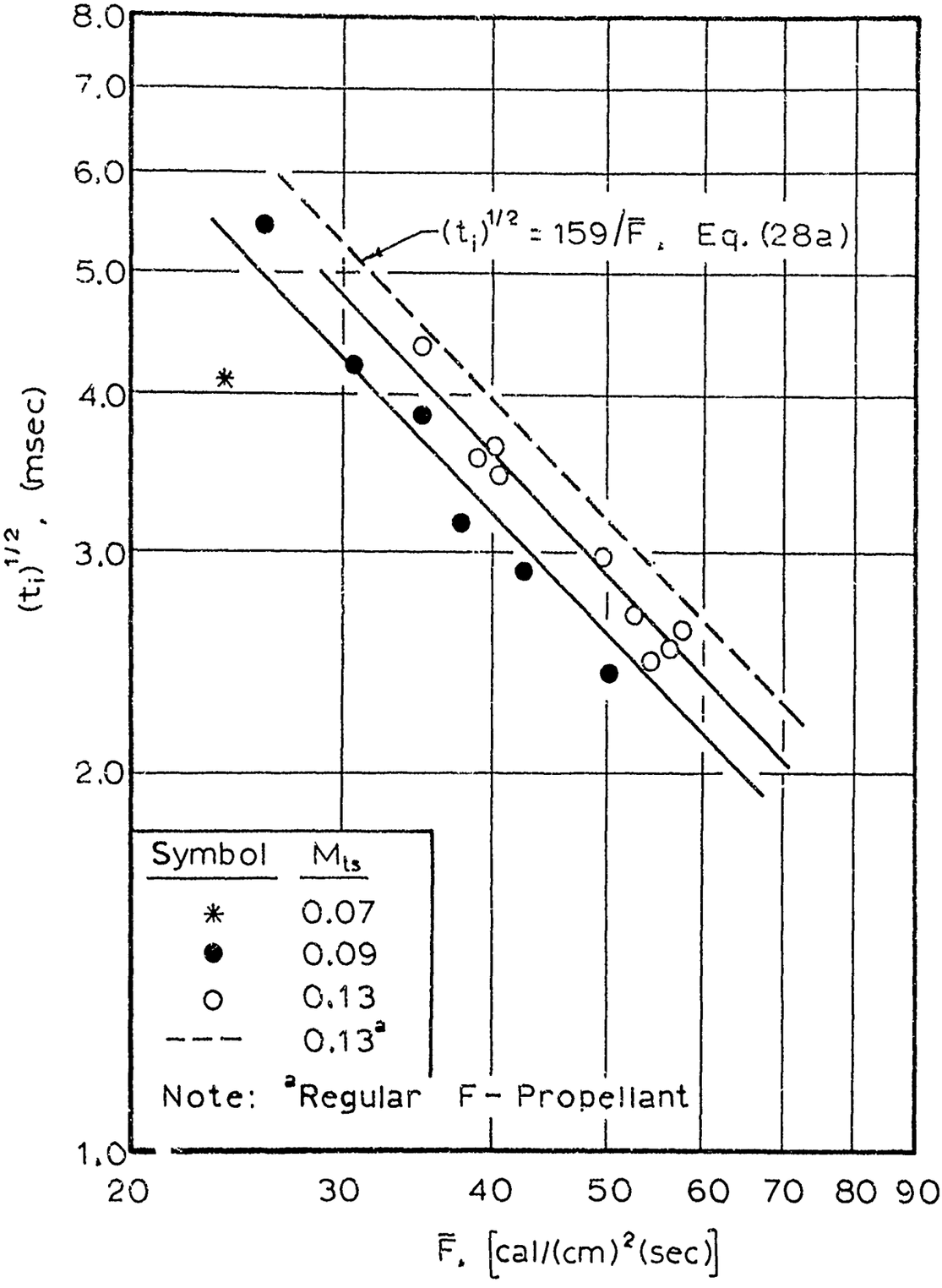

Figure 27

Ignition Data for Modified F-Propellant in Nitrogen at Low Gas Velocities for Pressures of 14 to 25 Atmospheres.

for the straight lines that represent the ignition data, Equation 27, on a graph of $\ell n\ (\bar{F})$ versus $\ell n\ (t_i)^{1/2}$ for gas velocities of 0.09, 0.13, and 0.28.

Figure 28

Comparison of Ignition Results in Nitrogen for Regular and Modified F-Propellant

Mach No. (M_{ts})	Coefficient, C_i, defined by Equation (27)[a]	
	Regular F-Propellant	Modified F-Propellant
0.28	213	179
0.13	159	144
0.09	144	129

[a] $(t_i)^{1/2} = C_i(\bar{F})^n$ (27)

Where t_i is in milliseconds and $\bar{F}$ has the units cal/(cm)^2(sec).

Although it was found that modified F-propellant ignited faster in tests at Mach 0.28, 0.13, and 0.09 than the regular propellant, this propellant was difficult to ignite at Mach 0.07. Three ignition runs were made at Mach 0.07 on the modified propellant at heat flux levels that ignited regular F-propellant. Out of the three samples, only one ignited, and it ignited in a much shorter time than did the regular propellant under similar test conditions. This data point is included with other ignition data for low Mach numbers in Figure 27. It was expected that the modified propellant, because of its greater surface roughness, would have ignited faster and more consistently

at all heat fluxes at low gas velocities. Additional experiments will be required to establish the ignition characteristics of the modified propellant at very low gas velocities

The Effect of Particle-Size Distribution and Loading of Ammonium Perchlorate

In an early phase of the study on propellant ignition, two propellants were processed for the purpose of assessing the effect on ignition of varying the ratio of coarse and fine particle sizes of ammonium perchlorate, and the total loading of ammonium perchlorate (percentage of ammonium perchlorate) in the propellant. These two propellants were similar to regular F-propellant in that the same ingredients were used, but were incorporated into the propellant in different proportions (see Table 2). Propellant O had the same loading of ammonium perchlorate but the ratio of 15-micron to 200-micron perchlorate was 3:1 in place of the 1:1 ratio used in F-propellant. Propellant P had an oxidizer loading of 75 per cent with the same particle-size distribution as that in F-propellant. This last propellant was made to investigate the effect of oxidizer loading on ignition and to provide a standard for comparing ignition data for propellants containing only one particle-size cut of ammonium perchlorate. Propellants with a single particle-size cut were not castable for loadings of 80 weight per cent ammonium perchlorate.

The experimental data on propellants O and P are given in Table 7, and presented graphically in Figures 29 and 30, respectively. The data for these propellants show that neither of the compositional changes affected the ignitability of these propellants relative to the

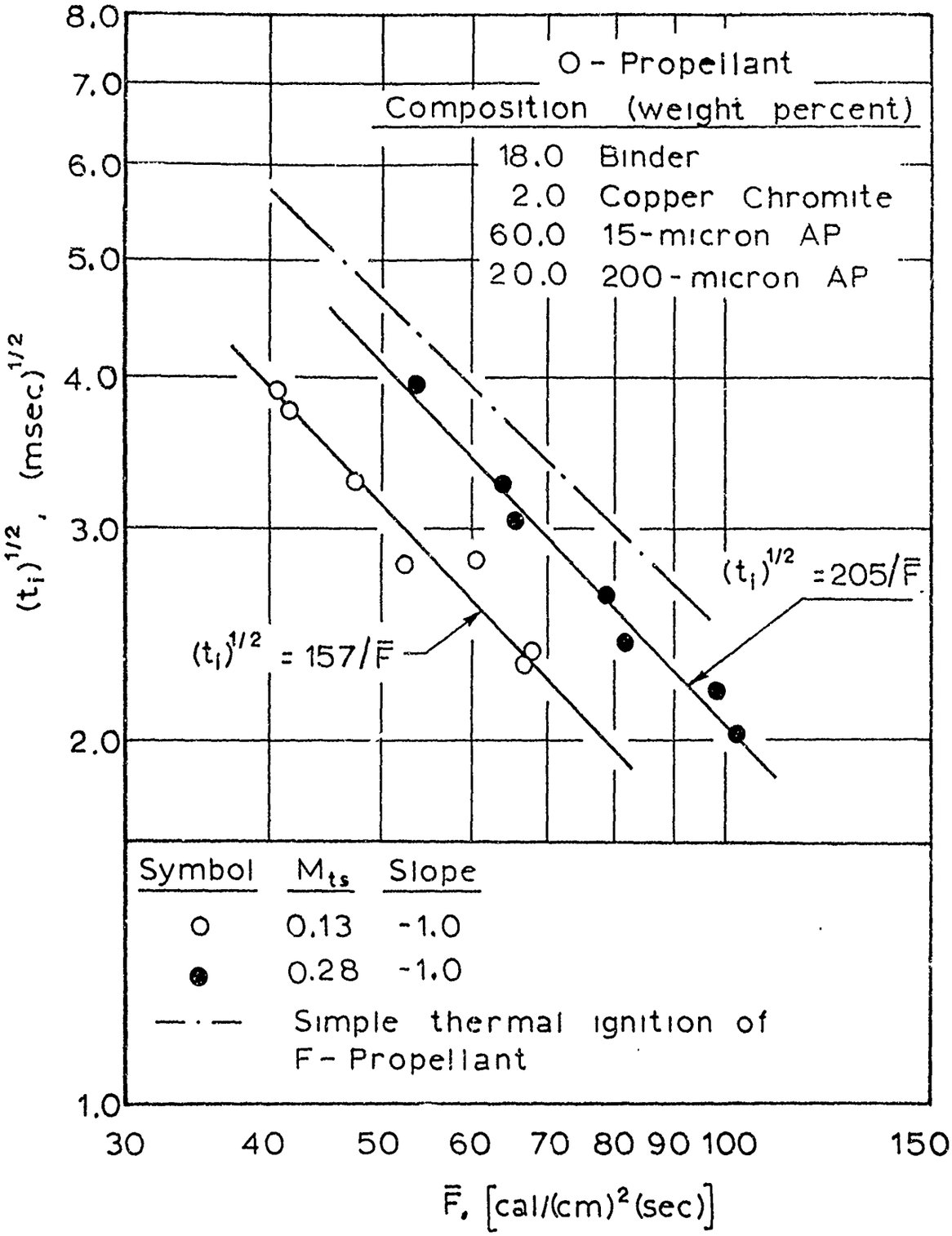

Figure 29

Ignition Data for O-Propellant in Nitrogen for Pressures of 20 to 25 Atmospheres.

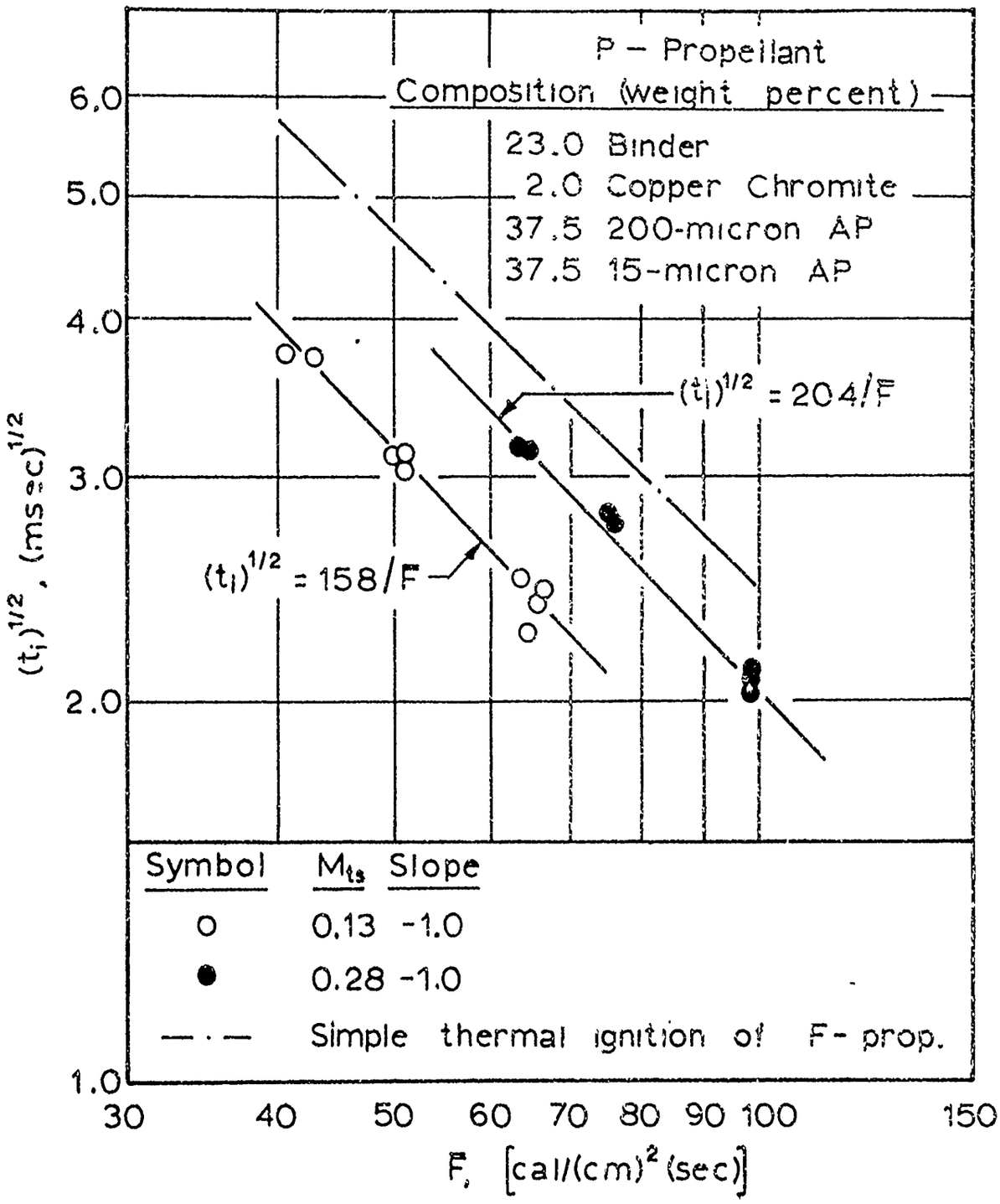

Figure 30

Ignition Data for P-Propellant in Nitrogen for Pressures of 20 to 25 Atmospheres.

ignition characteristics exhibited by F-propellant under the same test conditions. Again, the slope of the straight line which represents the experimental data for these two propellants at relatively low gas velocities is approximately -1.0. The ignition results for propellants O and P are compared by the coefficient, C_i, of Equation (27) with those for propellant F in Figure 31. Ignition results can be compared directly in this manner for all the propellants have similar thermophysical properties (see Table 4).

Figure 31

A Comparison of Ignition Results in Nitrogen for Propellants F, O, and P

Propellant	F	O	P
Oxidizer level (weight per cent)	80	80	75
Ratio of 15-micron to 200-micron AP	1:1	3:1	1:1
Coefficient, C_i, defined by Equation 27[a] (for n = -1.0)			
M_{ts} = 0.13:	159	157	158
M_{ts} = 0.28:	213	205	204

[a] $$(t_i)^{1/2} = C_i(\bar{F})^n \qquad (27)$$

Where t_i is in milliseconds and $\bar{F}$ has the units cal/(cm)^2(sec).

It is seen from Figure 31 that the ignition characteristics were very nearly the same at a given gas velocity for all three propellants. Although the ignition results for propellants F, O, and P when plotted

in the form of $\ln(\bar{F})$ versus $\ln(t_i)^{1/2}$ were similar, it was found that samples of P-propellant with the 75 per cent loading of ammonium perchlorate were sometimes extinguished during tests at Mach 0.28 when the cold driver gas entered the test section. For both propellants F and O some decrease in the intensity of the light signal was observed for tests at Mach 0.28 when cold gas entered the test section, but in none of these tests was the propellant extinguished. Figure 9c is an oscilloscope record for an ignition run with F-propellant at Mach 0.28 showing a change in light intensity when cold gas begins to flow through the test section.

Neither propellant O nor propellant P was tested at Mach 1.0, and consequently it is not possible to compare results for simple thermal ignition of these propellants. The fact that propellants F, O, and P exhibited similar ignition characteristics at relatively low gas velocities indicates that neither the concentration of ammonium perchlorate in the propellant nor the distribution of particle sizes affects the ignition process. The reason that propellants F, O, and P had similar ignition characteristics at Mach 0.28 and 0.13 can be attributed to the presence of the large particle-size ammonium perchlorate. With even a few large particles in the propellant, one cannot cut a smooth surface since some of the larger particles are always fractured or some of the particles with their bases near the surface are pulled from the propellant matrix. These imperfections provide sites for two-dimensional heating and generation of reactive species which eventually contribute heat flux for bringing the propellant surface, at least locally, to its ignition temperature. It is

shown in the next section that when no large ammonium perchlorate particles are present, the ignition characteristics at low gas velocities are very different.

The Effect of Ammonium-Perchlorate Particle Size

It was found in this study that neither gas velocity, gas temperature, nor oxygen in the test gas affected ignition of propellants containing only fine particle-size ammonium perchlorate. For U-propellant with 15-micron ammonium perchlorate, the only factor that influenced ignition was the magnitude of the externally applied heat flux. For all test conditions U-propellant exhibited ignition characteristics which were in substantial agreement with those for simple thermal ignition of F-propellant.

Ignition of Propellants S and U in Nitrogen

Two propellants were processed with different single particle-size cuts of ammonium perchlorate to determine the effect of particle size on ignition by convective heat fluxes. Propellants S and U contained single cuts of ammonium perchlorate with average particle diameters of 85 and 15 microns, respectively.

S-Propellant. Ignition data for S-propellant in nitrogen for gas velocities of Mach 0.13 and 0.28 are given in Table 8 and are presented graphically in Figure 32. These data, as were the data for propellants F, O, and P, are well represented on an $\ln(\bar{F})$ versus $\ln(t_i)^{1/2}$ plot by a straight line with a slope of -1.0. Ignition times for S-propellant are in substantial agreement with those observed for propellants

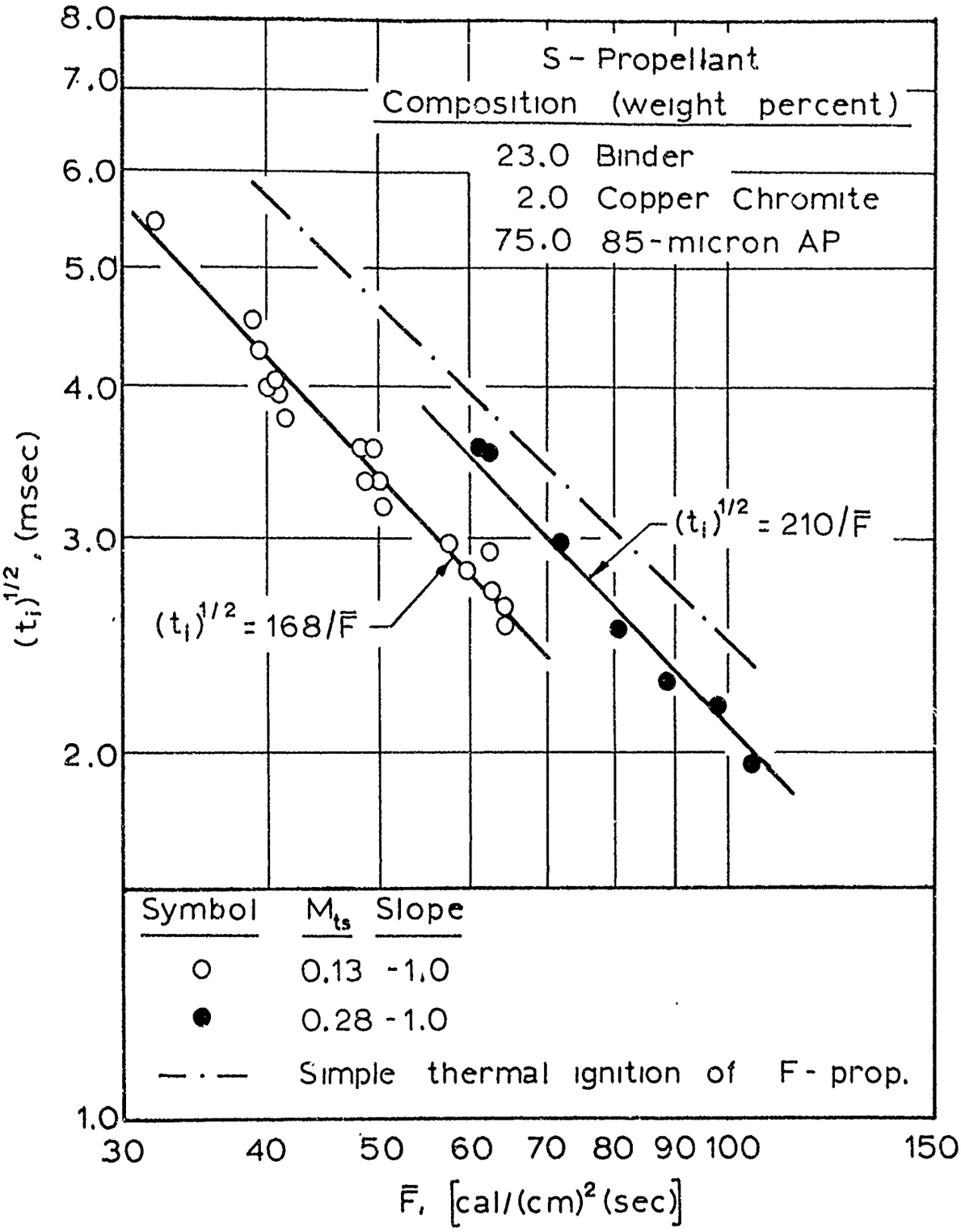

Figure 32

Ignition Data for S-Propellant in Nitrogen for Pressures of 20 to 25 Atmospheres.

F, O, and P at equivalent gas velocities and externally applied heat fluxes. For some runs, as was observed on P-propellant, samples of S-propellant were extinguished at Mach 0.28 when cold gases entered the test section. The surface roughness of S-propellant was estimated to be of the order of 10 to 15 microns.

U-Propellant. For U-propellant containing 15-micron ammonium perchlorate, it was possible to obtain very smooth surfaces on propellant samples by cutting away the excess propellant with a razor blade. Figure 33a shows a photomicrograph of a freshly cut surface of U-propellant. This can be compared to a cut surface on F-propellant by Figure 8a. It was estimated that the surface roughness of a carefully prepared sample of U-propellant was of the order of 5 microns. The ignition data for U-propellant in nitrogen at pressures of 20 to 25 atmospheres are given in Table 9 and are shown graphically in Figure 34.

Data shown in Figure 34 represent tests on 5 batches of U-propellant. Of the 5 batches, batch U-5 had the most uniform distribution of ammonium perchlorate particles. Before mixing, all of the ammonium perchlorate was passed through a 270-mesh screen to remove agglomerates or caked particles larger than about 50 microns in diameter. No agglomerates larger than 50 microns were found at a freshly cut surface of propellant U-5.

It is observed by examining the data given in Figure 34 that most of the data points for tests at Mach 0.28 and Mach 1.0 fall on or near the line which represents simple thermal ignition of F-propellant,

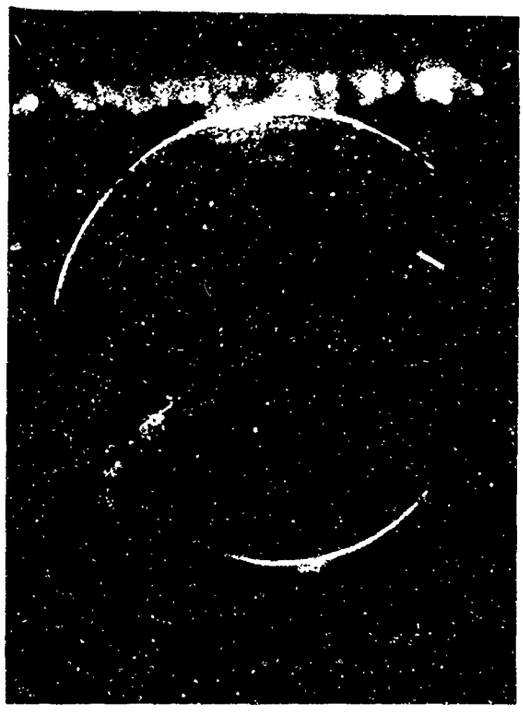

a. Freshly Cut Surface (5X).

b. After Ignition Run (5X). Run No. 53-18-2, Test-Gas Velocity: Mach 1.0, Leading Edge of Sample at Right.

Figure 33

Photomicrographs of Surfaces on Samples of Propellant U-5.

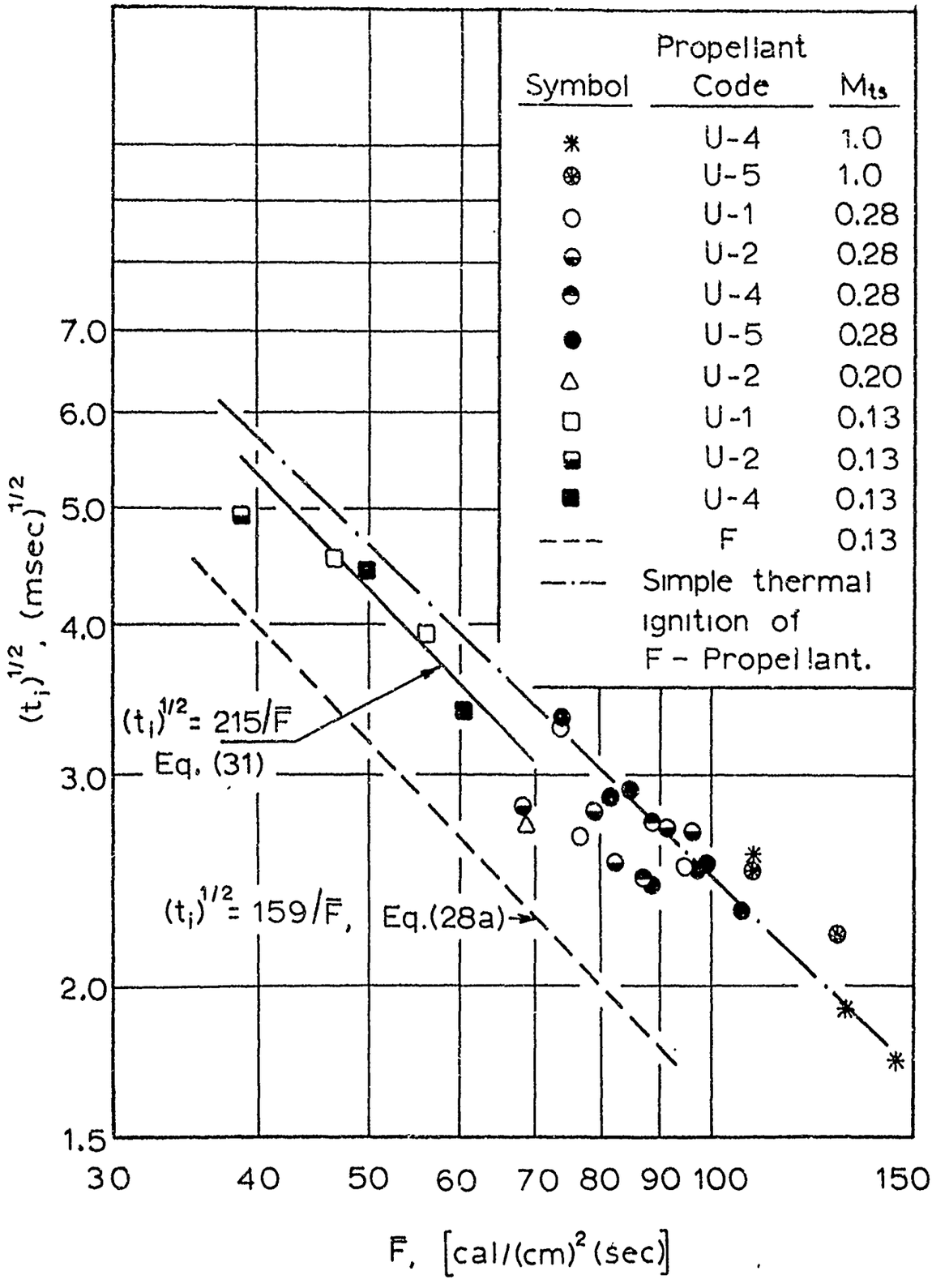

Figure 34

Ignition Data for U-Propellant in Nitrogen for Pressures of 20 to 25 Atmospheres.

and there is no significant effect of gas velocity on ignition as shown by the concentration of data points for all gas velocities near the line on the $\ell n\ (\bar{F})$ versus $\ell n\ (t_i)^{1/2}$ plot defined by the equation [where t_i is in milliseconds and $\bar{F}$ has the units cal/(cm)^2(sec)]:

$$(t_i)^{1/2} = 170/(\bar{F})^{0.92} \tag{29}$$

All of the data points for tests at Mach 0.13 are below this line and are represented by:

$$(t_i)^{1/2} = 215/(\bar{F}) \tag{31}$$

It should be noted, however, as is shown by the data tabulated in Table 9, that several runs at Mach 0.13 did not produce ignition of propellant samples because of the heat flux-test time limitation in the shock tube. The minimum test time at Mach 0.13 was about 25 milliseconds for a heat flux of 40 cal/(cm)^2(sec) and about 15 milliseconds for an externally applied heat flux of 60 cal/(cm)^2(sec) as shown by Figure 35. It appears that several of the samples with smoothest surfaces did not ignite at Mach 0.13 because of this limitation. Otherwise, it would be expected that some of the data points for tests at Mach 0.13 would have been near or above the line defined by Equation (29). Since several samples did not ignite at Mach 0.13, no tests were conducted on U-propellant at lower gas velocities, conditions under which test times would not be adequate to bring the propellant surface to its thermal ignition temperature. The line which represents ignition of F-propellant at Mach 0.13 is included on the plot of data for U-propellant in Figure 34 for use in comparing ignition results for the two propellants.

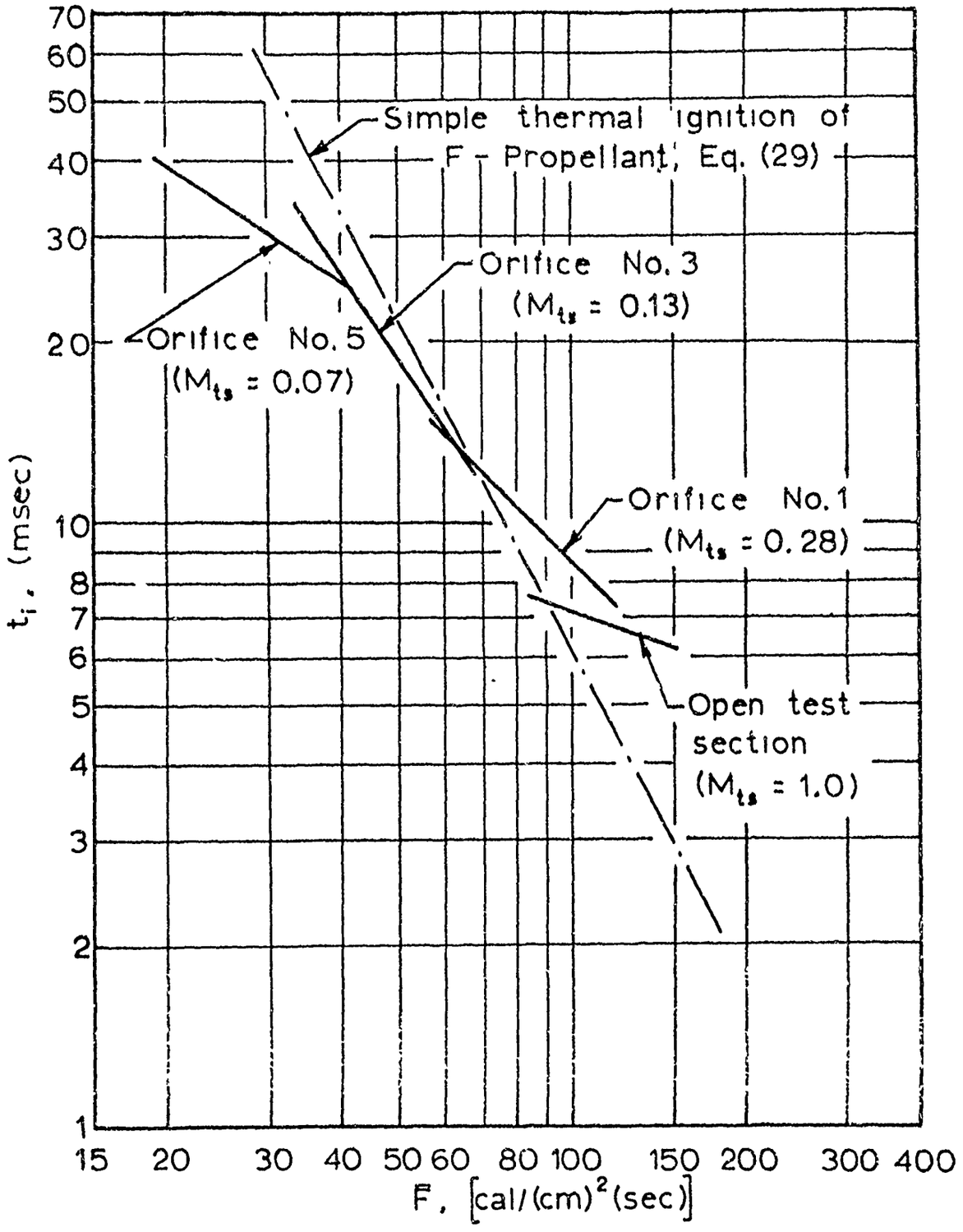

Figure 35

Approximate Test Time in Shock-Tube Apparatus for Various Flow-Control Orifices Compared with the Heat Flux-Ignition Time Relationship for Simple Thermal Ignition of F-Propellant. (These Results are for Tests in Nitrogen and for a Driver-Gas Pressure of Approximately 350 psig.)

There is also a test-time limitation for tests at Mach 0.28 and 1.0; however, the limiting condition is in the area above the line defined by Equation (29). The approximate total test time in the shock tube apparatus for various flow-control orifices downstream of the test section is shown by the graph of Figure 35. For Mach 0.28 the available test time is about 9 milliseconds for an externally applied heat flux to the propellant surface of 100 cal/(cm)^2 (sec). Since the test time at higher gas velocities (greater than about Mach 0.20) is determined by the time it takes for the hot gases to be exhausted through the test section, this test time can be longer or shorter than that shown by Figure 35, depending on how well the contact surface in the driven end of the shock tube is matched for a given test run. The method used for estimating the length of available test time for a shock tube run is described in Appendix J.

It was observed during tests on propellant U-5 that ignition was not produced for some runs at Mach 0.28 and 1.0, although calculated ignition temperatures (see Table 9) indicated that temperature of the propellant surface had reached its thermal ignition temperature, calculated from Equation (25), before termination of the test period as defined by the information given in Figure 35. Since some of the samples did not ignite and others had ignition times slightly longer than would be expected for the applied heat flux levels, it appears that cold driver gases were entering the test section sooner than was expected (based on the information of Figure 35) for some of the runs. Depending on the amount of cold gas that mixed with the hot gases

near the end of the run, ignition times were longer than expected or ignition did not occur.

The fact that all the ignition data for U-propellant lie near the line which describes simple thermal ignition of F-propellant shows that when surface imperfections are no longer important in providing two-dimensional heating, followed by secondary ignition reactions, the ignition time for ammonium perchlorate propellants is dependent only on the magnitude of the externally applied heat flux and the kinetics of the key ignition reaction. For a propellant with a smooth surface, the surface temperature increases primarily under the influence of externally applied heat flux, ignition characteristics are in substantial agreement with those for ignition by low radiant fluxes. It is interesting to note that a line with a slope of -0.92 represents the data for ignition of U-propellant at Mach 0.28 and Mach 1.0.

Summary of Ignition Results on Propellants S and U in Nitrogen

Ignition results for propellants S and U at intermediate gas velocities (Mach 0.13 and 0.28) in nitrogen are compared by the coefficients, C_i, of Equation (27) with those for propellants F, P, and S in Figure 36. All propellants have similar thermal properties and tests were conducted on samples having approximately the same initial temperature (T_o).

From the information given by Figure 36, it appears that ignitability does not improve at relatively low gas velocities as surface roughness is increased in the range of 10 to 30 microns. For a greater surface roughness (about 30 to 40 microns) as was found on surfaces of

Figure 36

A Comparison of Ignition Results for Propellants F, P, S, and U
(For Ignition in Nitrogen at Mach 0.13 and 0.28)

Propellant	F	P	S	U
Oxidizer Level (Weight per cent)	80.0	75.0	75.0	75.0
Particle Size (Weight per cent)				
200 micron	40.0	37.5	-	-
85 micron	-	-	75.0	-
15 micron	40.0	37.5	-	75.0
Estimated surface roughness (microns)	20-30	20-30	10-15	5
Coefficient, C_i, defined by Equation (27)[a] (for n = -1.0)				
M_{ts} = 0.13:	159	158	168	215
M_{ts} = 0.28:	213	204	210	-[b]

[a] $(t_i)^{1/2} = C_i(\bar{F})^n$ (27)

Where t_i is in milliseconds and $\bar{F}$ has the units cal/(cm)^2(sec).

[b] Ignition results are represented by Equation (29).

modified F-propellant (see Figure 26), ignition times were shorter for equivalent convective heat fluxes than those observed for propellants O, P, and S, and regular F-propellant. For propellants with smooth surfaces, such as U-propellant, changes in gas velocity do not significantly alter ignition characteristics of the propellant, and

data for all gas velocities can be represented by one straight line on a plot of $\ln(\bar{F})$ versus $\ln(t_i)^{1/2}$.

The results presented here are not conclusive with respect to the effect of particle size on simple thermal ignition of ammonium perchlorate propellants. Propellants F and U both contain 15-micron ammonium perchlorate, and as we have shown at high gas velocities (for simple thermal ignition) both propellants have very nearly the same ignition characteristics. This could mean that the simple thermal ignition process for these propellants is strongly dependent on the fine particle-size ammonium perchlorate. However, there is no evidence from this study that particle size of the ammonium perchlorate affects the simple thermal ignition process. S-propellant with a larger, single particle-size of ammonium perchlorate was not tested at the higher gas velocity (Mach 1.0), conditions under which propellants F and U ignite by a simple thermal ignition process. Further experimental work will be required to fully establish the effect of particle size on simple thermal ignition, if such an effect exists.

The experimental data on U-propellant at Mach 0.28 and Mach 1.0 and that on F-propellant at Mach 1.0 represent simple thermal ignition of ammonium perchlorate propellants containing 2.0 per cent copper chromite catalyst. The effect on ignition of copper chromite concentration was not studied in the research for this thesis; however, earlier work by Baer [8] at low radiant heat fluxes showed that ignitability does not change significantly with a change in the level

of copper chromite as long as some is present in the propellant. The effect of catalysts on ignitability of propellants will be discussed in greater detail in another section.

As a final observation on the results reported in this section it was shown that the ignitability of propellants cannot be related to their steady-state burning rates. U-propellant had the highest burning rate of the propellants tested (see data given by Table 10); however, when ignition results for different propellants are compared at conditions under which propellants ignite by simple thermal ignition (compare ignition results of U-propellant with those of F-propellant at high gas velocities) there are no significant differences in ignition characteristics.

To summarize the information presented in this section, it is seen that particle size of ammonium perchlorate per se does not appear to affect the simple thermal ignition process of propellants containing ammonium perchlorate, but the ignition characteristics of these propellants at lower test-gas velocities are modified by the nature and size of surface imperfections which are produced at the surface during preparation of samples for tests. The surface roughness is related to the size of the particles in the propellant in that when larger particles are present, more surface imperfections are created by fracturing of large particles and the pulling of some of the particles from the propellant matrix. Two-dimensional heating at these imperfections generates reactive species which undergo further exothermic reactions at the propellant surface or in the gas phase near the surface and

supply part of the heat flux for bringing the propellant to its thermal ignition temperature.

Ignition of U-Propellant in Argon and Oxygen

Description of Experimental Data. Ignition tests were made in high-temperature argon and oxygen to provide data which could be used for critically evaluating the ignition process for ammonium perchlorate propellants. It had already been shown by the results described in the last section that for propellants with smooth surfaces, ignition time was a function only of the initial uniform propellant temperature and the magnitude of the externally applied heat flux to the propellant when nitrogen was used as the test gas. From this earlier work it was apparent that if the temperature of the convective gas or oxygen in the test gas did not influence the ignition of U-propellant, it could be concluded that the basic ignition process for ammonium perchlorate propellants is simple thermal ignition.

Ignition tests were made on propellant U-4 in argon and on propellant U-5 in pure oxygen. Ignition data obtained in these gases are given in Table 11. Data for runs with argon at gas velocities of Mach 0.13 and 0.27 are compared with all the data obtained in nitrogen by the $\ln(\bar{F})$ versus $\ln(t_i)^{1/2}$ plot of Figure 37. Ignition data for propellant U-5 in pure oxygen at gas velocities of Mach 0.28 and 1.0 are compared with data obtained in nitrogen in Figure 38.

It is seen from Figure 37 for ignition of U-propellant in argon that ignition times in argon are in good agreement with those observed

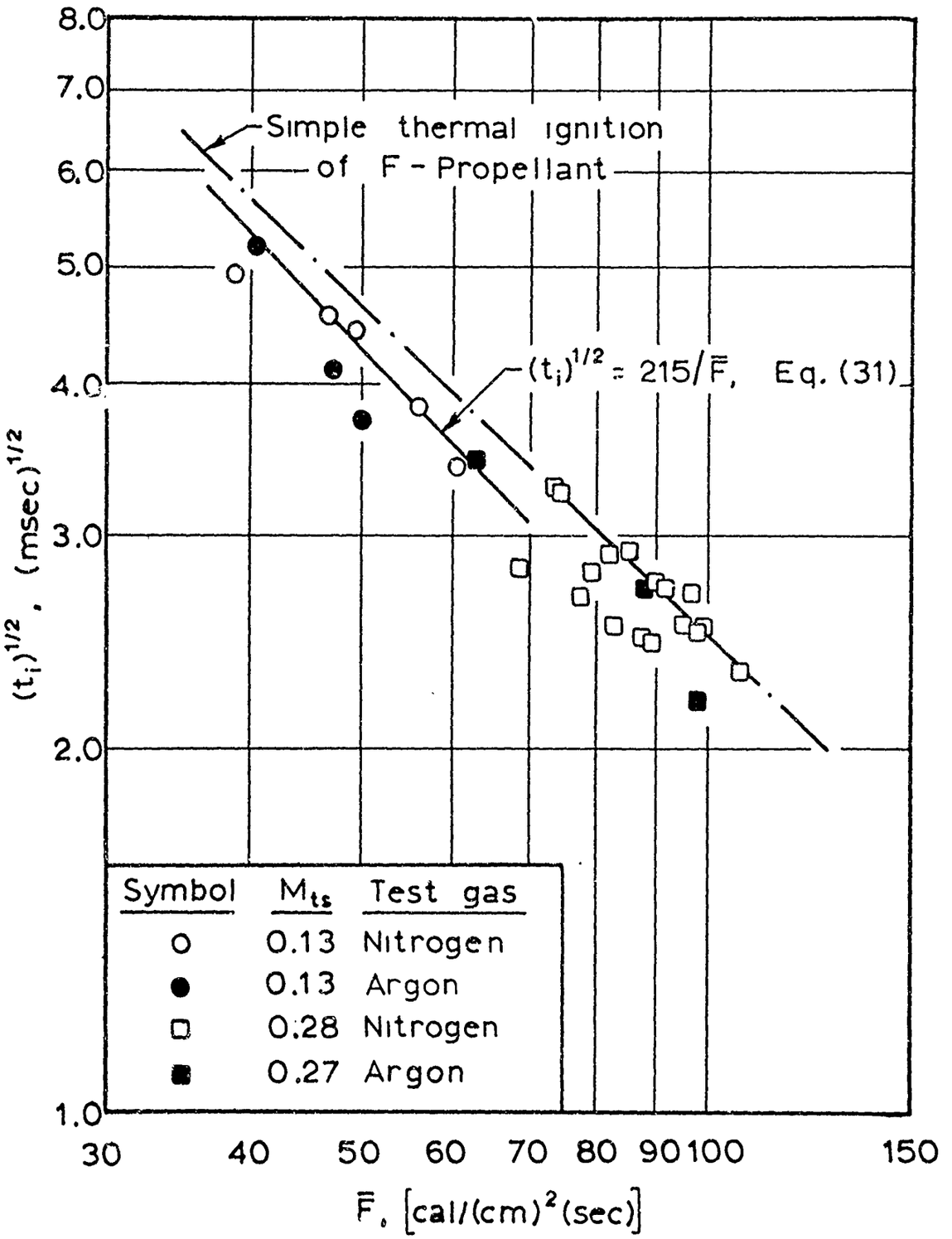

Figure 37

Ignition Data for U-Propellant in Argon at Test-Gas Velocities of Mach 0.13 and 0.27 for Pressures of 20 to 25 Atmospheres. (A Comparison of Ignition Results in Nitrogen and Argon.)

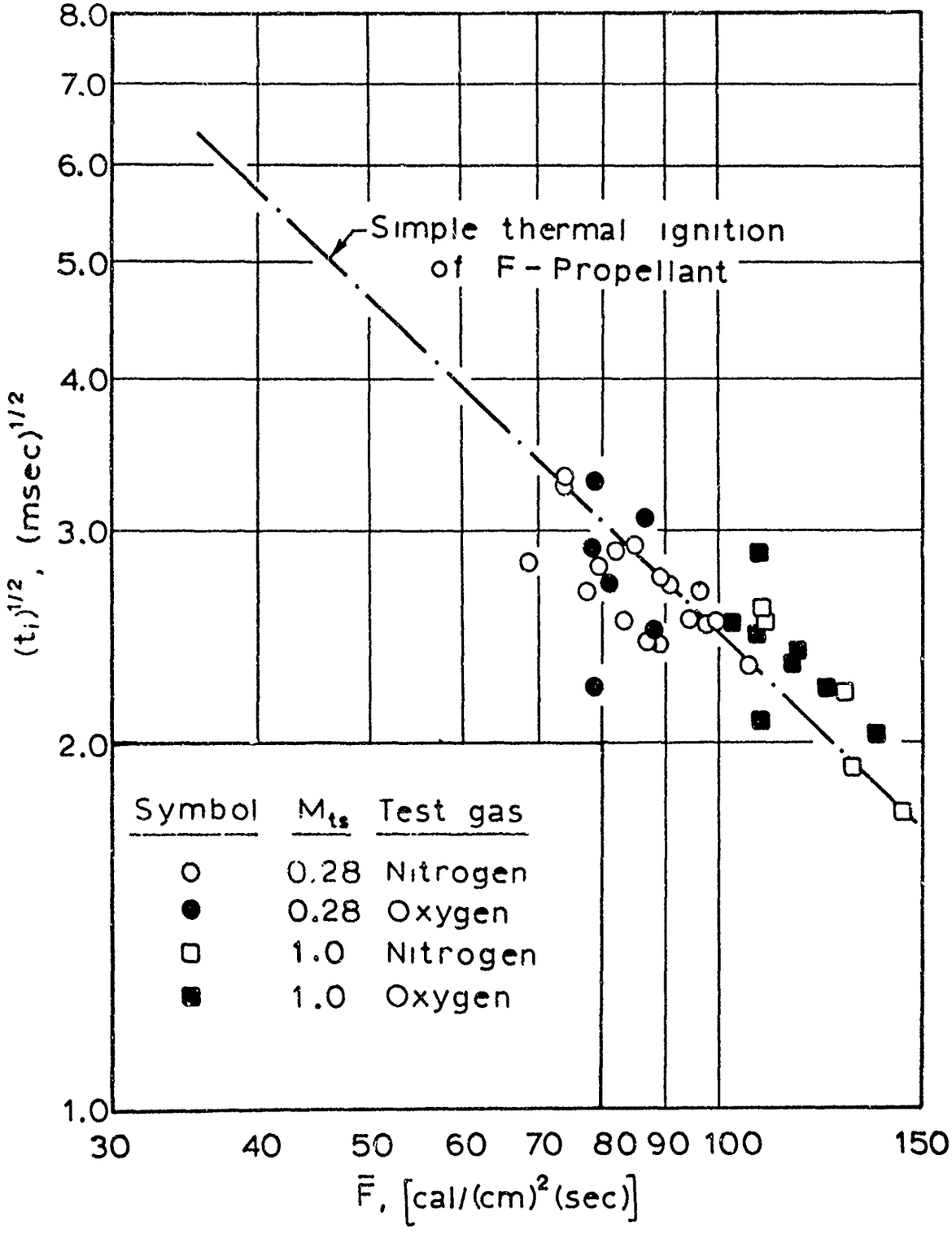

Figure 38

Ignition Data for U-Propellant in Oxygen at Test-Gas Velocities of Mach 0.28 and 1.0 for Pressures of 20 to 25 Atmospheres. (A Comparison of Ignition Results in Nitrogen and Oxygen.)

for ignition in nitrogen at equivalent heat fluxes. For these tests, as for the ignition tests on F-propellant, the gas temperatures were much higher for equivalent externally applied heat fluxes in argon than in nitrogen. The difference in gas temperature for a given heat flux between argon and nitrogen at Mach 0.13 and 0.28 would be almost the same as that for the ignition of F-propellant shown by Figures 18 and 19. Upon comparing results for ignition of F-propellant in argon and nitrogen (compare data of Figure 37 with data given in Figure 20), it is seen that there is no appreciable difference in ignition times for tests in argon and nitrogen with U-propellant; however, F-propellant ignited considerably faster in argon than in nitrogen for equivalent heat fluxes.

The data for ignition of U-propellant in oxygen were in remarkable agreement with data for ignition in nitrogen as shown by Figure 38. Not only are the data for ignition in oxygen and nitrogen the same, but all ignition data fall near the line on the $\ell n\ (\bar{F})$ versus $\ell n\ (t_i)^{1/2}$ plot that describes simple thermal ignition of F-propellant. Another interesting feature of the ignition tests in oxygen was that samples of propellant U-5 could not be ignited at Mach 0.13 (see Table 11), test conditions under which secondary ignition reactions at the propellant surface involving the environmental oxygen would most likely contribute energy for heating the propellant surface. It was mentioned in a previous section that propellant U-5 contained the most uniform distribution of ammonium perchlorate of the 5 batches tested, and consequently cut surfaces were the smoothest on samples of this propellant. Because of the smoother surfaces, more consistent data were

obtained and most of the data points were grouped near the line which represents simple thermal ignition of F-propellant. It was also found, as was observed on tests in nitrogen, that some samples of propellant U-5 did not ignite in oxygen at Mach 0.28 and 1.0. For some of these tests calculated surface temperatures at the end of the test period, as estimated from temperature-time data obtained from heat flux gauge measurements, were higher than the predicted thermal ignition temperature of U-propellant calculated by Equation (25). However, as was already mentioned, it was not always possible to predict precisely the length of available test time for a given shock tube test. If, for example, the contact surface between the driven and driver gases is not well-matched, movement of the contact surface relative to the tube can shorten the time that hot gases are available at the test position. Since time required for ignition of propellant U-5 was near that for the minimum test period in the shock tube (see Figure 35), it appears that some of the tests were terminated by the flow of cold driver gas into the test section before the propellant reached its ignition temperature.

It was also observed during ignition tests on propellant U-5 in oxygen and nitrogen that burning of the samples was quenched during tests at Mach 1.0 when cold driver gas entered the test section. This was not a unique feature of U-propellant, but occurred during tests for all propellants during tests at Mach 1.0. Figure 33b shows a photomicrograph of a propellant surface for the sample recovered from Run No. 53-18-2. This test was conducted in oxygen with a gas

velocity of Mach 1.0 (about 685 m/sec) at a heat flux of 124 cal/(cm)^2 (sec). This photomicrograph shows that a considerable amount of propellant was consumed before the sample was extinguished. This shows, as mentioned previously, that at least a quasi-steady deflagration wave can be sustained with high gas velocities across the propellant surface as long as some of the energy is supplied externally.

Discussion of Results. The results of this study on U-propellant show that for propellants with very smooth surfaces, ignition of the propellant takes place by a simple thermal ignition process, and ignition results are in excellent agreement with those predicted by thermal ignition theory; in particular, the ignition model described by Equation (7) for the key ignition reaction localized at the propellant surface. For propellants with very smooth surfaces, the surface temperature of the propellant increases only under the influence of one-dimensional heat transfer. For a propellant with a smooth surface there is no two-dimensional heating and the entire surface rises uniformly. As a consequence of the lower uniform temperature, reactive species are produced at a much slower rate at the surface than, for example, at the surface of F-propellant during ignition. Therefore, the temperature of the convective gas does not influence the ignitability of U-propellant. The fact that high-temperature oxygen under high pressures, 20 to 25 atmospheres, does not affect ignition of U-propellant is strong evidence that heterogeneous attack of the propellant surface by an oxidizing gas is not an important chemical process in the ignition of some ammonium perchlorate propellants.

On the other hand, oxygen has been observed by several investigators to influence the ignitability of ammonium perchlorate propellants in convective heating experiments, particularly propellants with rough surfaces. This observation strongly suggests that when oxygen is present in the test gas it affects propellant ignition through exothermic reactions with gaseous decomposition products which are generated by two-dimensional heating of surface imperfections. For propellants with rough surfaces, it is these secondary ignition reactions, either in the gas phase or at the surface, which supply part of the energy for bringing the propellant to its thermal ignition temperature.

IGNITION OF PROPELLANTS CONTAINING IRON OXIDE

Since iron oxide is known to be an excellent burning rate catalyst, comparable to copper chromite in its ability to enhance the burning rate of ammonium perchlorate propellants, a few propellants were made in which a fine particle-size iron oxide was used as the catalyst. The iron oxide used in these propellants was a pigment-grade material, Code R-1599, obtained from C. K. Williams and Company.

Ignition of J-Propellant in Nitrogen

The first propellant tested that contained iron oxide was J-propellant. Except for the catalyst, J-propellant had the same composition and particle size of ammonium perchlorate as regular F-propellant. Freshly cut surfaces of J-propellant were of the same order of roughness as those observed on regular F-propellant.

Experimental data for J-propellant are given by Table 12 and are graphed in the form of $\ell n\ (\bar{F})$ versus $\ell n\ (t_i)^{1/2}$ in Figure 39 for test-section Mach numbers of 0.07, 0.13, and 0.28. The ignition times for Mach 0.13 and 0.28 are very nearly the same as those for regular F-propellant at equivalent heat fluxes. The data are well represented by straight lines with slopes of -1.0.

The equations for the straight lines which represent the ignition data for J-propellant on a plot of $\ell n\ \bar{F}$ versus $\ell n\ (t_i)^{1/2}$ in nitrogen are as follows:

at Mach 0.28:

$$(t_i)^{1/2} = 213/\bar{F} \tag{32a}$$

at Mach 0.13:

$$(t_i)^{1/2} = 162/\bar{F} \tag{32b}$$

at Mach 0.07:

$$(t_i)^{1/2} = 132/\bar{F} \tag{32c}$$

Where t_i is in milliseconds and $\bar{F}$ has the units $cal/(cm)^2(sec)$. The equations that represent ignition data at Mach 0.28 and Mach 0.13, Equations (32a) and (32b), respectively, can be compared directly to those that represent ignition of F-propellant at these gas velocities, Equations (28c) and (28a), respectively. It is seen that ignition characteristics of F-propellant and J-propellant were almost the same at these test conditions.

One rather significant difference in ignition characteristics of J-propellant from that of regular F-propellant is the improved ignitability of J-propellant at Mach 0.07. For F-propellant at

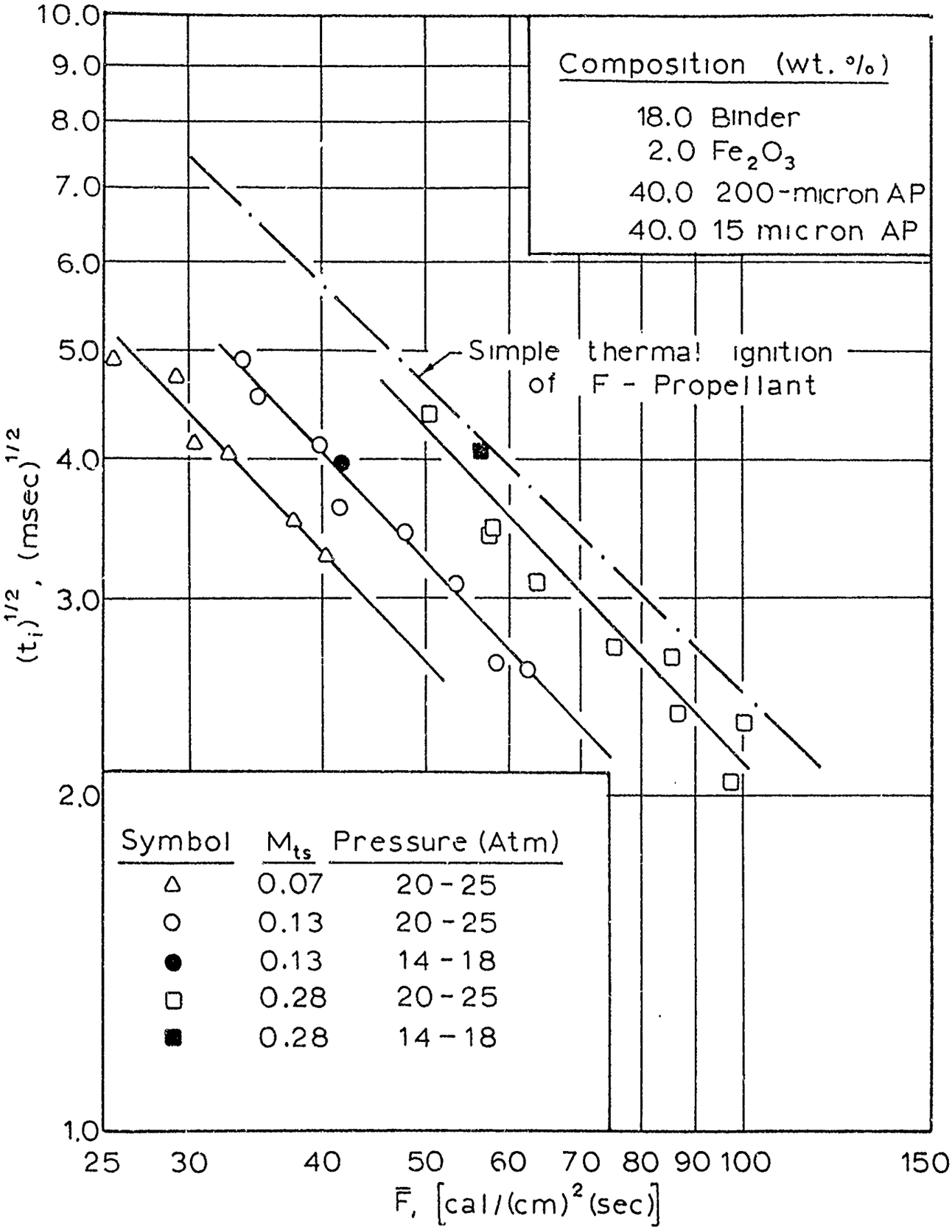

Figure 39

Ignition Data For J-Propellant in Nitrogen for Pressures of 14 to 25 Atmospheres.

Mach 0.07 (see Figure 10), the ignition data could not be separated from those obtained at Mach 0.09 and 0.13, and there was considerable scatter among the experimental data. On the other hand, the data for ignition of J-propellant at Mach 0.07 are very consistent, but ignition times were considerably shorter for a given heat flux than those observed for regular F-propellant. This apparently indicates a difference in the secondary ignition process for the two propellants and cannot be explained at this time.

It was found during ignition tests that samples of J-propellant were sometimes extinguished by cold driver gas entering the test section for runs at Mach 0.28. As was noted earlier, this never occurred during tests on F-propellant, although the photocell signal indicated a change in light intensity when cold gases entered the test section.

In the discussion on page 60, the method for calculating the rate of heat transfer to the propellant surface during an ignition test was described. At that time it was pointed out that the value for thermal responsivity, Γ_p, used in these calculations was that obtained experimentally or estimated for the propellant at 60°C. The use of a constant value for propellant thermal responsivity was justified by the argument that all propellants have similar properties and have high loadings of ammonium perchlorate. Therefore, even though the thermal properties are a function of temperature, one can compare ignition data for all propellants in terms of ignition time and externally applied heat flux to the surface. It would be desirable to include the temperature dependence of thermal properties in all heat

flux calculations, and this will be required as experimental and analytical procedures become more refined. To obtain some indication of the order of magnitude of the error in heat flux calculations which are calculated using the assumption of constant thermal properties, a second set of heat flux calculations was made on the ignition data for J-propellant. For these calculations an average value of heat capacity was taken for ammonium perchlorate for the temperature range 300° to 540°K. This higher value for heat capacity increased the thermal responsivity for J-propellant from 0.0206 to 0.0224 cal/(cm)^2 (sec)$^{1/2}$(°K). Heat fluxes calculated using the latter value for Γ_p are given by the second set of values for several ignition tests on J-propellant in Table 12. In all cases the difference in the calculated heat fluxes for the two values of Γ_p is less than two per cent. This shows that the assumption of constant thermal properties for heat flux calculations is a reasonable one.

Effect of Ammonium-Perchlorate Particle Size, Catalyst Concentration, and Cure Time

Two propellants were processed with different concentrations of iron oxide catalyst (R-1599), 2.0 and 5.5 per cent in propellant AD and AE, respectively. See Table 2 for propellant compositions. These propellants were made from one batch. The batch was started with the composition for propellant AD which was mixed by the regular procedure. When processing of propellant AD was completed, part of the propellant was removed for filling sample holders. More catalyst was added to the portion remaining in the mixer and the propellant was mixed for an additional 15 minutes. This procedure gave a propellant with a lower

concentration of oxidizer; however, it was already known that oxidizer level in the propellant does not have an effect on ignition. Two sizes of ammonium perchlorate, 85 and 15 micron in equal percentages, were used in propellant AD and AE. Propellant AD can be compared directly with J-propellant with respect to particle size of the oxidizer.

Ignition data for propellants AD and AE are given in Table 13. The data for these propellants for a test-gas velocity of Mach 0.13 are plotted in Figure 40. It can be seen from the data plotted in Figure 40 that increasing the iron oxide level from 2.0 to 5.5 per cent did not change ignition characteristics, and the data for propellants AD and AE can be represented by a single straight line. In contrast with the results for J-propellant, the data for propellants AD and AE on an $\ell n\ (\bar{F})$ versus $\ell n\ (t_i)^{1/2}$ plot are represented by a straight line with a slope of -0.68.

$$(t_i)^{1/2} = 50.5/(\bar{F})^{0.68} \tag{33}$$

Where t_i is in milliseconds and $\bar{F}$ has the units $cal/(cm)^2(sec)$. In fact, it appears that these data would be better represented by a curved line having a slope of about -1.0 at lower heat fluxes and with a somewhat lower slope at larger values of heat flux.

The effect of cure time on ignition was also investigated for propellant AE. The normal curing condition used for all propellants was 7 days at 80°C. Several samples of propellant AE were removed from the oven after 12 hours at 80°C and tested. These data are also included in Figure 40. These samples ignited somewhat faster

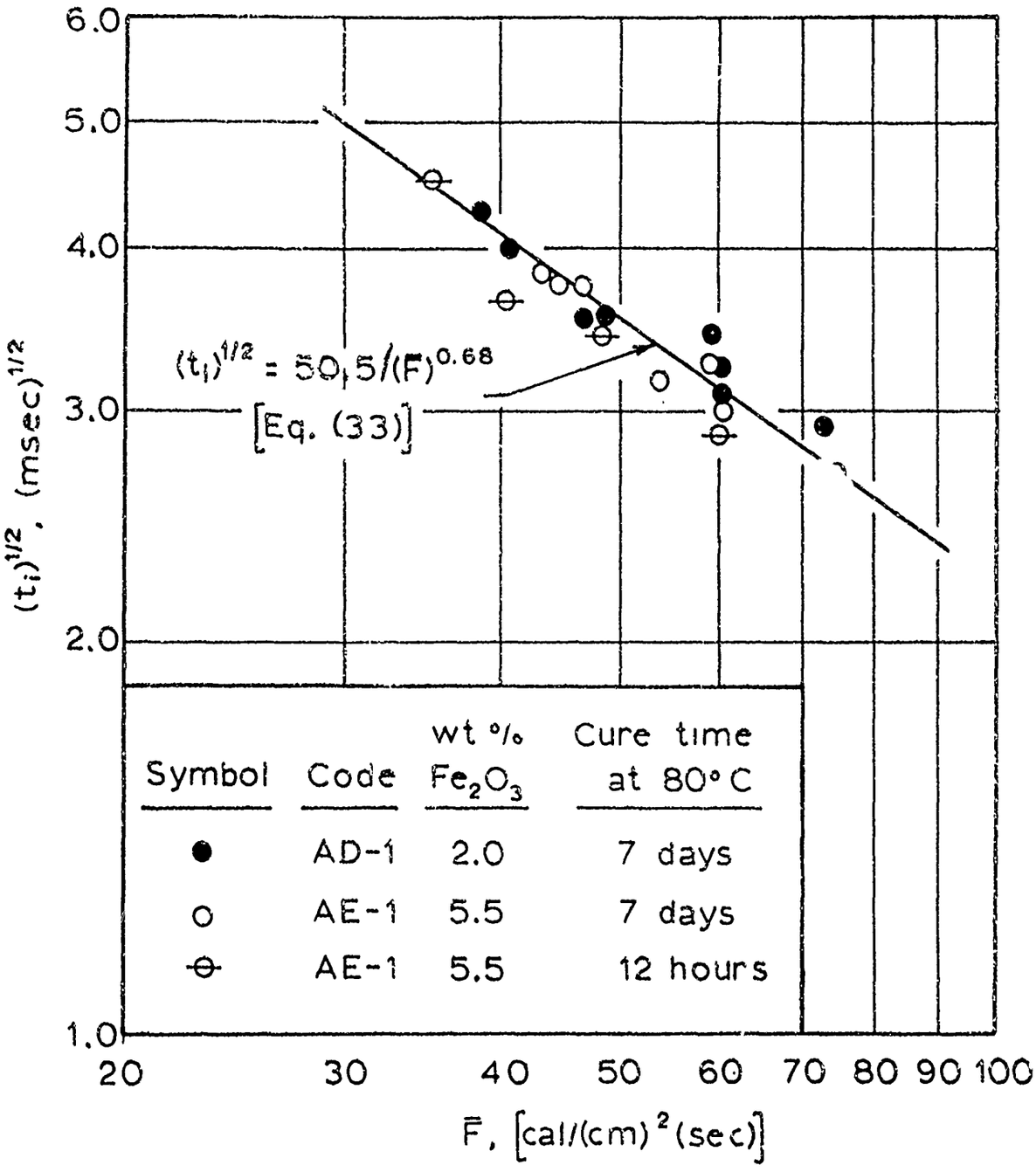

Figure 40

Ignition Data for Propellants with Different Concentrations of Iron Oxide and Different Cure Times for Ignition in Nitrogen at a Test-Gas Velocity of Mach 0.13 and Pressures of 20 to 25 Atmospheres.

than those for propellant cured for 7 days at 80°C. However, it is believed that this effect is not related to the state of cure, but rather to the difference in surface characteristics of the propellants cured for different times. For the propellant cured only 12 hours at 80°C, the polymer was still somewhat tacky and it was difficult to prepare surfaces without pulling some oxidizer particles from the propellant matrix. The results of this study indicate that the state of cure of the polymer does not significantly affect ignition of ammonium perchlorate propellants.

At higher gas velocities, Mach 0.28, the ignition data for propellants AD and AE can be represented by the same straight line with a slope of -1.0 (see Figure 41) which also represents ignition data for J-propellant at Mach 0.28, Equation (32a). It is also interesting to note (see Figure 41) that the one data point obtained at Mach 1.0 for propellant AE lies near the straight line which represents simple thermal ignition of F-propellant.

The effect of particle size of ammonium perchlorate on ignition of propellants containing an iron oxide catalyst is shown by Figure 42 for ignition at Mach 0.13 and by Figure 43 for ignition at Mach 0.28. Data for X-propellant with 2.0 per cent iron oxide and a single particle-size cut of ammonium perchlorate (70 micron) is included with data for propellants J and AD. Experimental data for X-propellant are given in Table 14.

In Figure 42 the dashed line represents ignition results on J-propellant at Mach 0.13. It is interesting to note that at low heat fluxes in the range of 40 to 50 cal/(cm)^2(sec) this line also represents

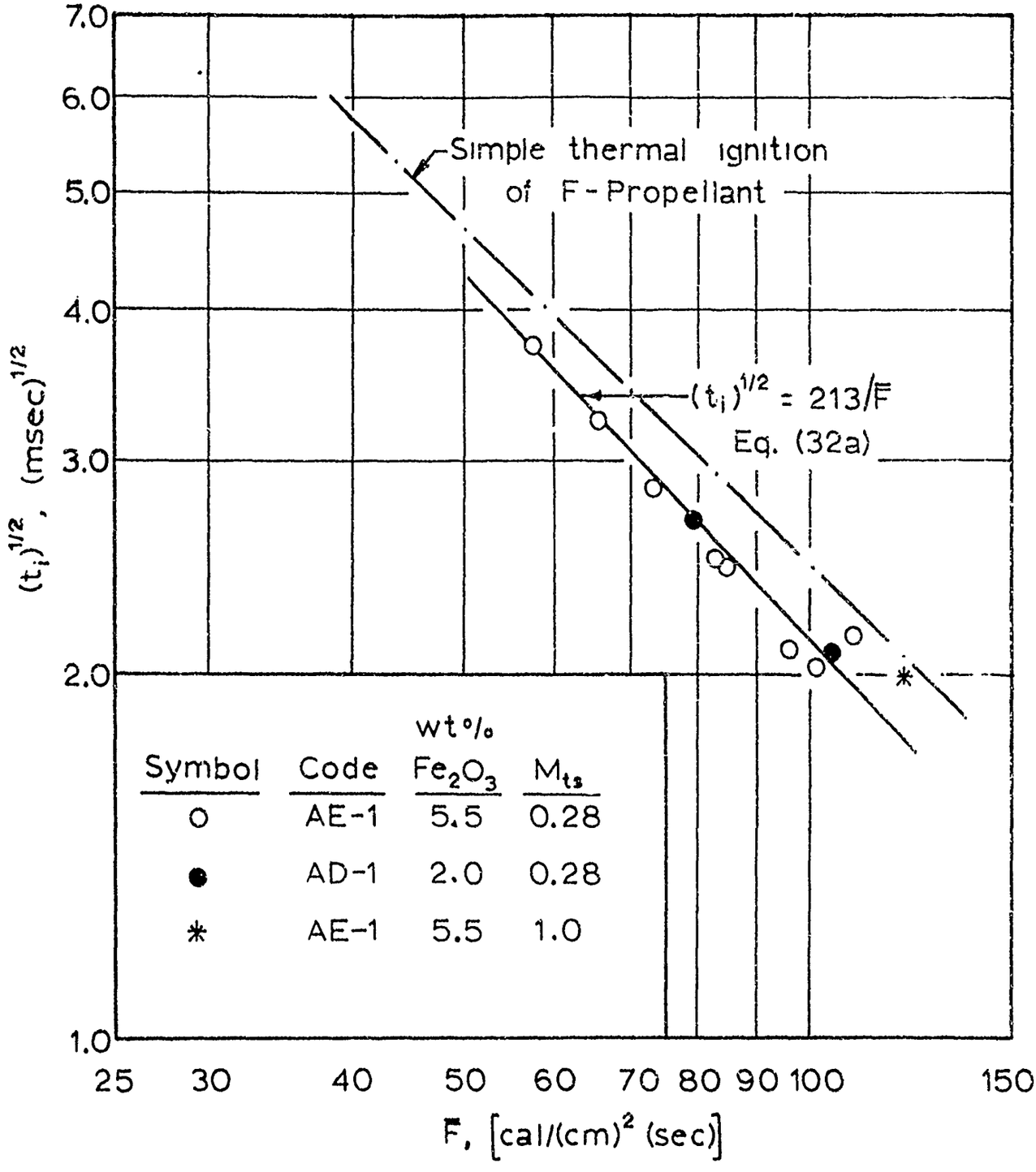

Figure 41

Ignition Data for Propellants with Different Concentrations of Iron Oxide for Ignition in Nitrogen at Intermediate and High Gas Velocities and Pressures of 20 to 25 Atmospheres.

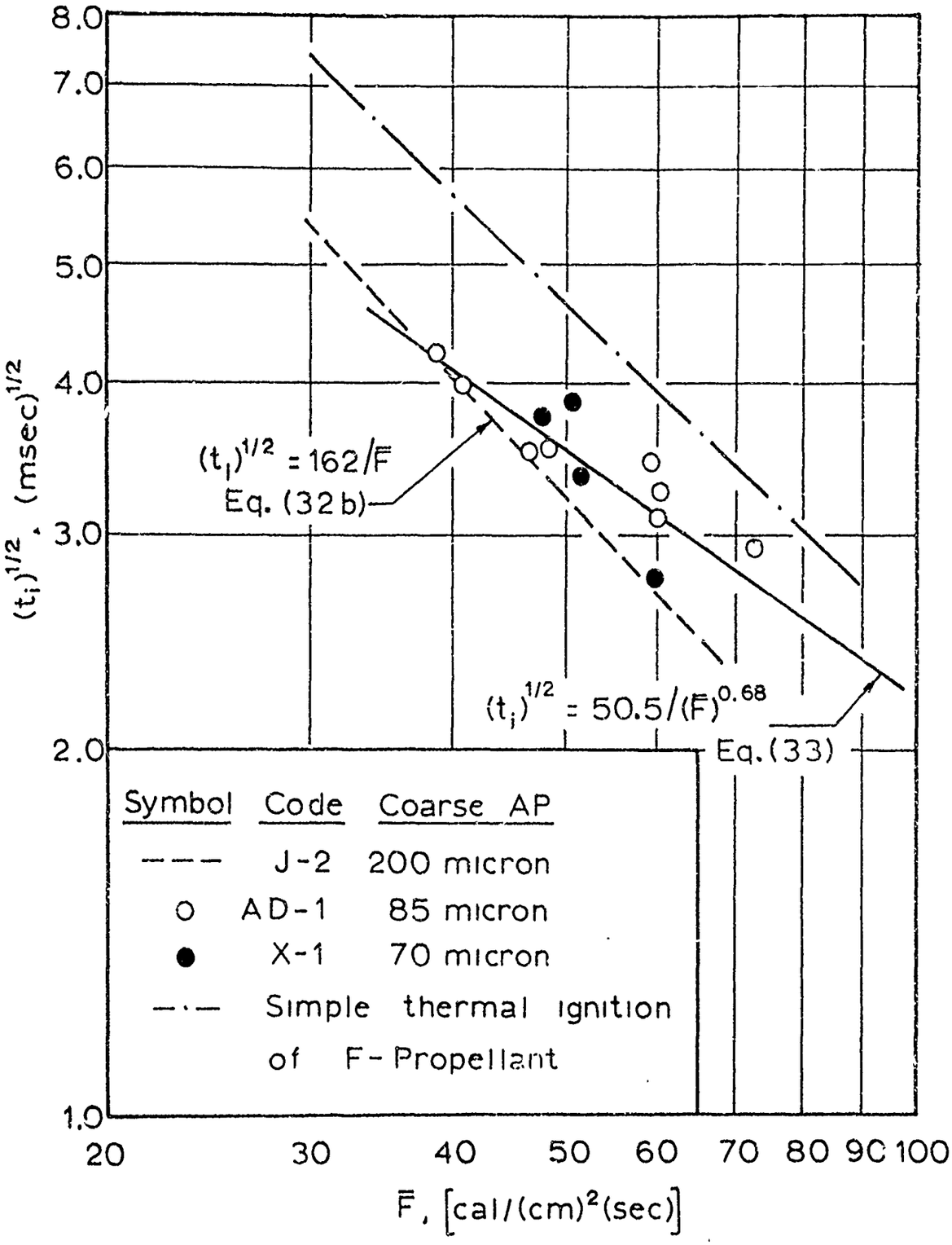

Figure 42

Ignition Data for Propellants Containing 2.0 per Cent Iron Oxide, but Different Particle Sizes of Ammonium Perchlorate, for Ignition in Nitrogen at a Test-Gas Velocity of Mach 0.13.

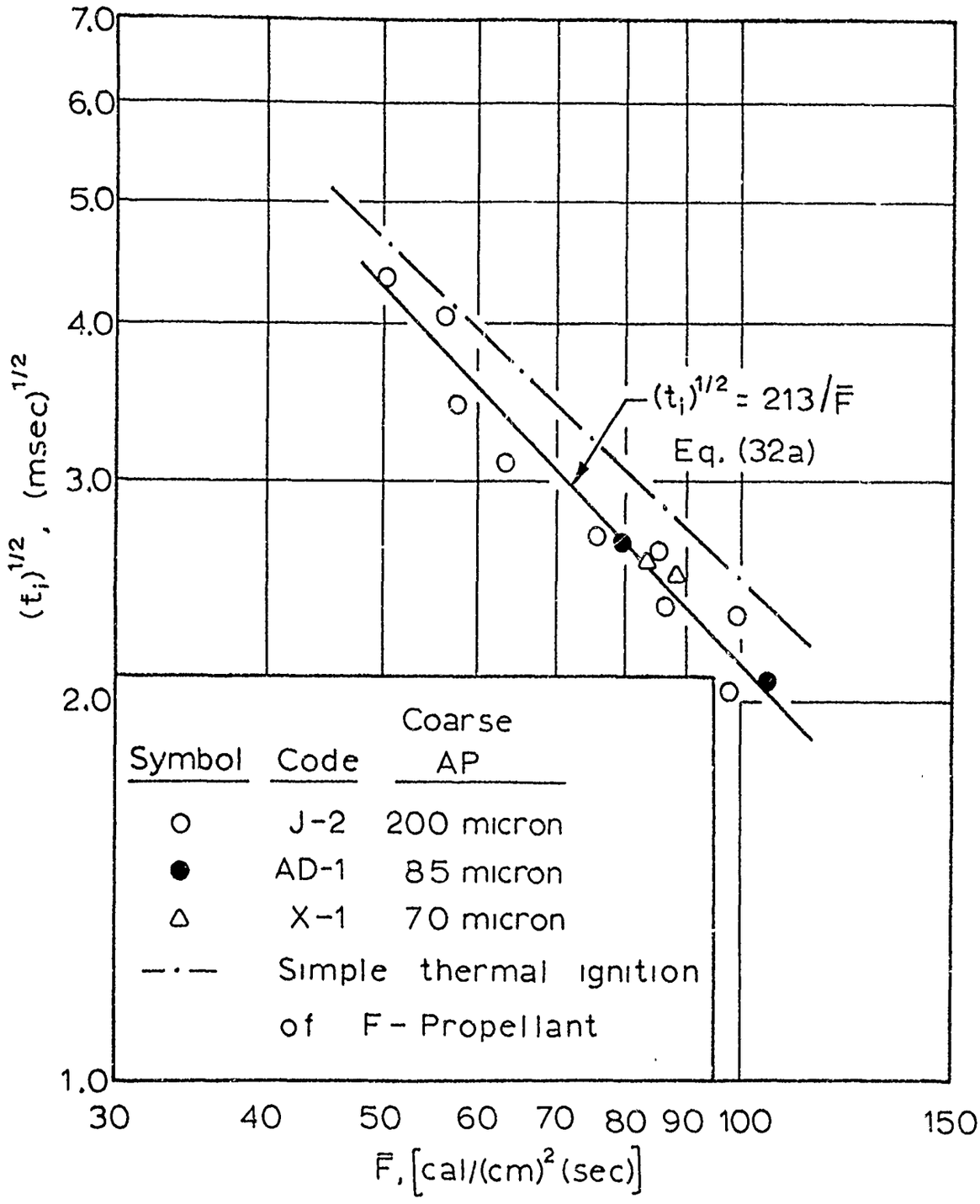

Figure 43

Ignition Data for Propellants Containing 2.0 Per Cent Iron Oxide, but Different Particle Sizes of Ammonium Perchlorate, for Ignition in Nitrogen at a Test-Gas Velocity of Mach 0.28.

ignition data for propellant AD. But at higher heat fluxes, 50 to 70 cal/(cm)^2(sec), the ignition times for propellant AD are a weaker function of heat flux. The data for X-propellant do not correspond well to data for either propellant J or AD. The data on X-propellant are too limited, however, to draw any conclusion about its ignition characteristics.

For ignition at Mach 0.28, Figure 43, data for all three propellants with 2.0 per cent iron oxide are well defined by the straight line with a slope of -1.0 which represents ignition of J-propellant, Equation (32a). There is no apparent difference in the ignition characteristics of these propellants with different particle sizes of ammonium perchlorate at Mach 0.28.

An obvious extension of the work described in this section would be to study ignition of propellants containing iron oxide and a finer particle size of ammonium perchlorate at lower gas velocities. Neither propellant AD nor propellant AE could be ignited at gas velocities lower than Mach 0.13 because of limitations in the test apparatus which have already been described.

Ignition of Propellant AD in Argon

Several ignition runs were made on samples of propellant AD using argon as the test gas at Mach 0.13. These data are tabulated in Part II of Table 13 and are compared graphically with ignition data in nitrogen by Figure 44. The data obtained on propellant AD in argon are reasonably consistent and show that the best straight line that represents the data has a slope of -0.79. The equations which

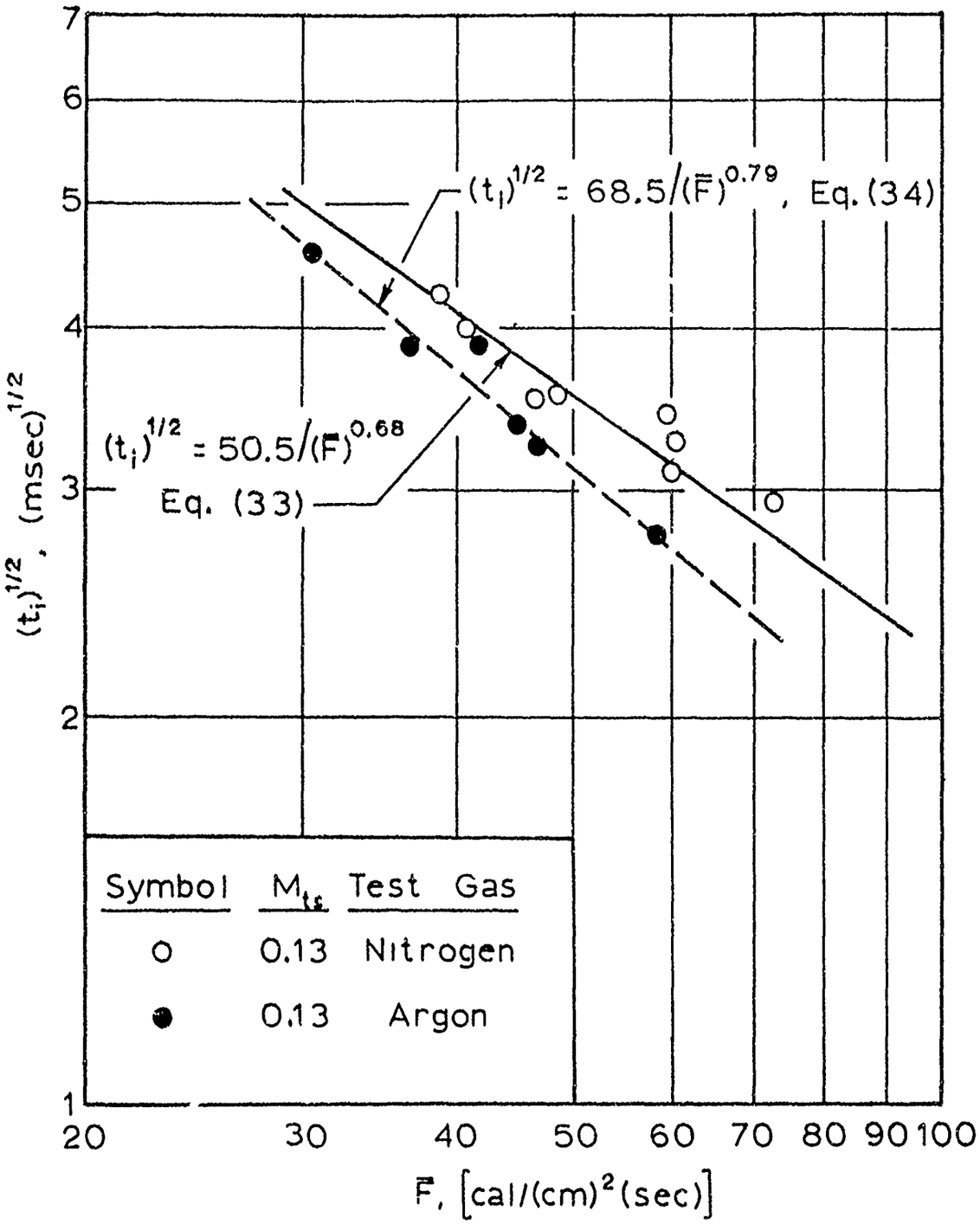

Figure 44

Ignition Data for Propellant AD in Argon at a Test-Gas Velocity of Mach 0.13 for Pressures of 18 to 25 Atmospheres.
(A Comparison of Ignition Data Obtained in Argon and Nitrogen.)

represent ignition of propellant AD in nitrogen and argon are:

For nitrogen:

$$(t_i)^{1/2} = 50.5/(\bar{F})^{0.68} \tag{33}$$

For argon:

$$(t_i)^{1/2} = 68.5/(\bar{F})^{0.79} \tag{34}$$

Where t_i is in milliseconds and $\bar{F}$ has the units cal/(cm)^2(sec). As was mentioned earlier in the discussion of ignition results on F-propellant in argon, if there is an effect of gas temperature on ignition, the slope of the line which represents the experimental data should be steeper for tests in argon. A comparison of ignition results on propellant AD in argon with those for propellant F in argon (Figure 20) shows that there is a smaller gas temperature effect on ignition of propellant AD than was observed for F-propellant. This difference in ignition characteristics between propellants F and AD can be attributed to difference in surface characteristics of the two propellants. Because of the finer particle-size oxidizer in propellant AD, a smoother surface could be cut on this propellant.

The ignition results for propellant AD in argon and nitrogen at Mach 0.13 show that the line which defines ignition data on an $\ell n\ (\bar{F})$ versus $\ell n\ (t_i)^{1/2}$ has a slope with an absolute value considerably less than 1.0. The exact significance of the lower slope for data on propellants AD and AE at Mach 0.13 is not readily apparent, but appears to be related to the dependence of secondary ignition reactions on gas velocity and gas temperature. As was mentioned earlier on page 93, one might expect gas temperature and gas velocity to affect

secondary ignition reactions in such a way that the slope of the line which defines experimental data on $\ell n\ (\bar{F})$ versus $\ell n\ (t_i)^{1/2}$ plot can be either less than or greater than -1.0. It would also be expected that the type of catalyst used in the propellant would alter the kinetics of the secondary ignition reactions. It will be shown later that of the catalysts tested in this research, only iron oxide and copper chromite were found to greatly enhance ignitability of propellants at low test velocities.

Ignition of Propellants AD and AE in Oxygen

A few samples of propellants AD and AE that remained after tests in nitrogen and argon were tested in pure oxygen at a pressure of 20 atmospheres. The ignition data obtained from these tests are tabulated in Part III of Table 13 and are plotted in Figure 45 where they are compared with ignition results in nitrogen. In contrast with the data obtained on U-propellant, propellants AD and AE ignited much faster for equivalent heat fluxes in oxygen than in nitrogen. The faster ignition times in oxygen were expected for propellants AD and AE since the surface roughness was greater on samples of these propellants, of the order of 10-15 microns, than on samples of U-propellant. As a consequence of the surface roughness, propellant decomposition products are generated by localized heating at the sites of surface imperfections. These decomposition products undergo more vigorous exothermic reactions at or near the surface when environmental oxygen participates in the reaction process. The net result is a higher rate of energy production at the propellant surface which helps

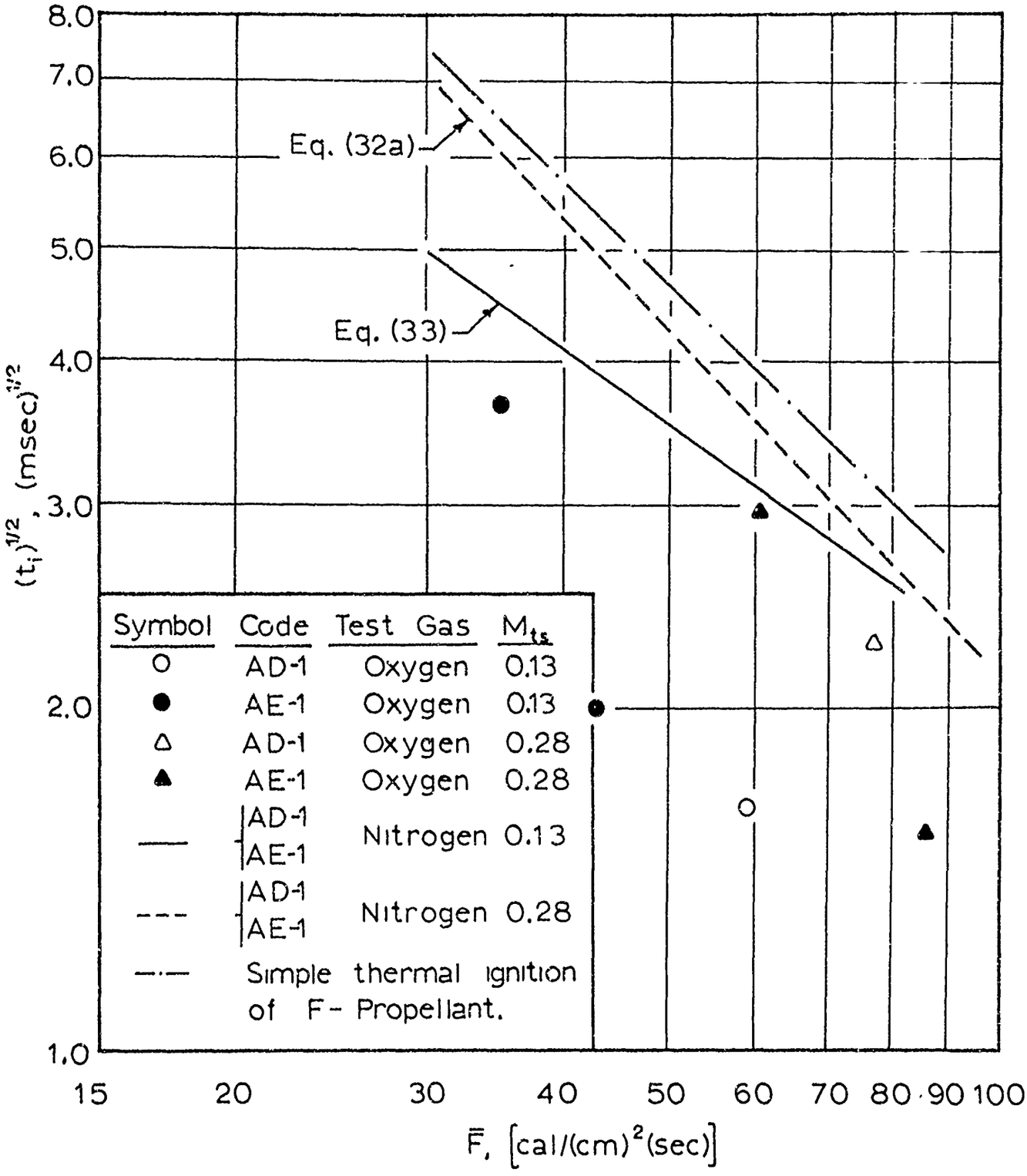

Figure 45

Ignition Data for Propellants AD and AE in Oxygen at a Pressure of 20 Atmospheres. (A Comparison with Ignition Results in Nitrogen.)

bring the propellant more rapidly to its thermal ignition temperature. It is to be expected, although not shown by the data of Figure 45, that at higher gas velocities, somewhere in the range of Mach 0.3 to Mach 1.0, that the effect of environmental oxygen on ignition would become less important. This would take place when gas velocity becomes great enough to prevent the secondary reaction processes at the propellant surface. Reactive species would be swept away by high velocity gases before undergoing reaction and the propellant surface would be heated only by one-dimensional heat transfer from the hot test gas.

APPARENT ROLE OF CATALYSTS IN THE IGNITION PROCESS

Thermal decomposition studies on ammonium perchlorate at fairly low heating rates relative to those encountered in solid propellant ignition show that several metal oxides, in otherwise pure ammonium perchlorate, are very effective in increasing the rate of the low temperature (200-350°C) decomposition reaction. Some of these metal oxides are also effective in catalyzing the complete decomposition of ammonium perchlorate at low temperatures. Thermal decomposition studies on pure ammonium perchlorate at low temperatures by Bircumshaw and Newman [14,15] and by Galwey and Jacobs [37] show that ammonium perchlorate decomposes directly from the solid phase at low temperatures and under low ambient pressures by the following exothermic reaction:

$$2NH_4ClO_4(s) \rightarrow 4H_2O + Cl_2 + 3/2\ O_2 + N_2O \qquad (35)$$

The exact reaction mechanism by which the crystal undergoes decomposition directly to gaseous products does not appear to be completely

understood. The low-temperature decomposition of pure ammonium perchlorate starts at discrete nuclei on the surface of a crystal at the junction of mosaic blocks, then propagates through the intergranular material, and terminates after about 30 per cent of the original sample has decomposed [37]. The addition of some metal oxides to the ammonium perchlorate, even in low concentrations, greatly accelerates the low-temperature decomposition reaction and also lowers the temperature at which ammonium perchlorate will undergo spontaneous deflagration or thermal explosion. The temperature at which thermal explosion occurs is sometimes referred to as an autoignition or critical temperature.

Low-temperature decomposition studies on ammonium perchlorate are very useful in that they provide data on the reaction kinetics of the important decomposition reactions. However, since most of these studies are conducted under a high vacuum or at atmosphere pressure, we know very little about the effect of pressure on the decomposition reaction. Also, at low temperatures where the rate of decomposition is slow, the decomposition reaction is essentially isothermal since the rate of energy generation by the exothermic decomposition reaction is slow and heat is conducted to the surroundings without significantly raising the temperature of the perchlorate sample. However, in some experimental work [48], a small amount of self-heating has been reported for pure ammonium perchlorate during the initial, accelerative phase of the decomposition process. The heating rates used for low-temperature decomposition studies are much slower than those encountered

in ignition work and as a consequence in ignition experiments energy from solid-phase decomposition provides self-heating of the perchlorate.

Effect of Catalysts on the Thermal Decomposition of Ammonium Perchlorate

Bircumshaw and Newman [14] in their studies on low-temperature decomposition of ammonium perchlorate in the presence of catalysts noted that manganese dioxide greatly increased the rate of decomposition of ammonium perchlorate at 230°C and complete decomposition of the ammonium perchlorate occurred at this temperature. In this same paper, it was reported that ferric oxide and calcium oxide were less effective decomposition catalysts than manganese dioxide, and aluminum oxide exhibited no catalytic effect on the decomposition process.

Galwey and Jacobs studied the effect of carbon [38] and manganese dioxide [36] on the low-temperature thermal decomposition of ammonium perchlorate. Below 240°C, carbon at concentrations of 3.5, 5.5, and 17 per cent showed very little, if any, effect on the decomposition of ammonium perchlorate. Also, most of the carbon was found in the solid residue after tests. The activation energy for the low-temperature decomposition reaction in the presence of carbon was found to be about 32 kcal/(mole). Above 260°C, for pellets containing 20 per cent carbon, the decomposition reaction accelerated rapidly, resulting in a mild explosion which ruptured the pellet. The scattered particles then underwent slow thermal decomposition. Thermal decomposition of ammonium perchlorate containing 10 per cent manganese dioxide was studied over the temperature range of 137 to 212°C. The decomposition

reaction was found to proceed by two successive stages. The first stage was the catalyzed decomposition of ammonium perchlorate followed by uncatalyzed decomposition as the area of contact between the catalyst and ammonium perchlorate crystals became smaller. The activation energy for the catalyzed decomposition was about 32 kcal/(mole).

Jacobs and Kureishy [48,49] have shown that pellets composed of ammonium perchlorate and cuprous oxide will undergo self-heating in low-temperature decomposition studies, which under certain test conditions will lead to thermal explosion of the pellet. The transition from self-heating to thermal explosion is dependent on the mass of the pellet, temperature at which the experiment is conducted, and concentration of cuprous oxide in the pellet. This experimental work showed that the process that leads to thermal explosion can proceed by one of two reaction mechanisms. One mechanism is the thermal decomposition of ammonium perchlorate with concurrent oxidation of cuprous oxide by free oxygen liberated in the decomposition process. In this process heat generated by the oxidation of cuprous oxide can bring the pellet to its thermal explosion temperature. If this first process does not produce a thermal explosion, catalysis of ammonium perchlorate decomposition by cupric oxide formed in the first reaction can produce self-heating which terminates with a thermal explosion. Here again the initiation of a thermal explosion depends on the test temperature, mass of the pellet, and the concentration of cupric oxide.

Kuratani [57] investigated the effect of metal compounds, in low concentrations, on the thermal decomposition of ammonium perchlorate

and also their effect on the autoignition temperature of ammonium perchlorate. This work can be summarized as follows:

1. Cupric oxide, cuprous oxide, cuprous chloride, and zinc oxide were found to promote both the low- and high-temperature decomposition processes for ammonium perchlorate. Of these metal compounds, zinc oxide was found to be most effective material for lowering the autoignition temperature of otherwise pure ammonium perchlorate. The autoignition temperature of pure ammonium perchlorate is about 430°C, but when zinc oxide was mixed with the ammonium perchlorate the autoignition temperature was lowered to 250°C for pellets of equal mass.
2. Nickel oxide (NiO) and chromic oxide were found to promote primarily the low-temperature decomposition reaction.
3. Manganese dioxide and copper chromite were found to be most effective as high-temperature decomposition catalysts.
4. Aluminum oxide, titanium oxide, ferric oxide, and vanadium pentoxide had no significant catalytic effect on the thermal decomposition processes for ammonium perchlorate.

In the paper by Kuratani, the low-temperature reaction is thermal decomposition of ammonium perchlorate below 350°C.

Other studies on the decomposition of ammonium perchlorate which appear to be significant with respect to ignition of solid propellants were those conducted by Hermoni and Salmon [45]. They found that carbon, manganese dioxide, and copper chromite catalyze reactions in the solid phase. In another publication by Hermoni and Salmon [44]

they report that nickel oxide (Ni_2O_3) and mixtures of cobalt oxides (Co_2O_3 plus Co_3O_4) are good low-temperature decomposition catalysts for ammonium perchlorate. Chromic oxide was found to be less effective than nickel or cobalt oxides.

Solymosi and Révész studied the effect of zinc oxide [86] and ferric oxide [87] on the thermal decomposition of ammonium perchlorate. It was found that the addition of zinc oxide to ammonium perchlorate, even in concentrations as low as 0.1 weight per cent, significantly lowered the autoignition temperature and increased the rate of the low-temperature decomposition [86]. The activation energy for the low-temperature decomposition catalyzed with zinc oxide was approximately 32 kcal/(mole). Ferric oxide was found to have only a small catalytic effect on the rate of thermal decomposition of ammonium perchlorate in the temperature range of 210 to 240°C. In the temperature range of 245 to 300°C with small concentrations of ferric oxide, 2.0 to 12.5 per cent, the rate of decomposition of ammonium perchlorate was not significantly different from that for pure ammonium perchlorate. Only at test temperatures above 300°C did small concentrations of ferric oxide accelerate the rate of decomposition of ammonium perchlorate [87]. The activation energy for the low-temperature reaction catalyzed by ferric oxide was about 31 kcal/(mole), a value which is typical of the low-temperature decomposition process.

Ignition of Propellants Containing Different Catalysts

Since much information was available on the catalyzed decomposition of ammonium perchlorate, although there are some inconsistencies

between results reported by different investigators, it appeared that some information about ignition process of propellants could be obtained by making ignition tests on propellants containing different catalysts. The compositions of the propellants used in this study are summarized in Figure 46. Complete compositional data on these propellants are given in Table 2.

Figure 46

Compositions of Propellants Tested in Catalyst Study

Propellant	Ammonium Perchlorate[a]	Binder	Catalyst
Y	75.0	23.0	2.0 Zinc Oxide
Z	74.0	23.0	2.0 Zinc Oxide 1.0 Ferric Oxide
AA	75.0	23.0	2.0 Chromic Oxide
AB	75.0	23.0	2.0 Cuprous Oxide
AC	74.0	23.0	2.0 Cuprous Oxide 1.0 Philblack E
AD	75.0	23.0	2.0 Ferric Oxide

[a]A 50-50 blend of 15-micron and 85-micron ammonium perchlorate.

Samples of propellant with freshly cut surfaces were exposed to convective heat fluxes in the range of 40 to 130 cal/(cm)^2(sec). As already indicated (see Figure 35) there is a test-time limitation at different heat fluxes resulting from termination of the test period by the arrival of the head of the reflected rarefaction wave at the test position or at high gas velocities by mixing of cold driver gas

with the test gas. Except for propellant AD, ignition data obtained on propellants in these tests are tabulated in Table 14 and are shown graphically in Figure 47. The ignition data for propellant AD are given in Table 13.

In this study it was found that only propellant AD containing two per cent iron oxide could be ignited at all test conditions. Propellant Z with two per cent zinc oxide and one per cent iron oxide would not ignite at a heat flux less than 50 cal/(cm)^2(sec) because of test limitations already described. Ignition times were as much as 50 per cent longer for propellant Z than for propellant AD at equivalent heat fluxes.

Propellants Y and AA containing zinc oxide and chromic oxide, respectively, gave some indication of ignition as shown by a small deflection of the photocell signal at the times indicated in Table 14. This small amount of luminosity was only observed at heat flux levels of about 100 cal/(cm)^2(sec) or higher. The time for the appearance of the photocell deflection, which did not lead to steady deflagration of propellants Y and AA, was about the same as that for propellant Z containing, in addition to zinc oxide, one per cent ferric oxide.

One sample of propellant AB containing 2.0 per cent cuprous oxide ignited and completely burned at a heat flux of 90 cal/(cm)^2(sec), but a subsequent run at a heat flux level of 110 cal/(cm)^2(sec) gave only a slight photocell deflection and the sample was not completely burned.

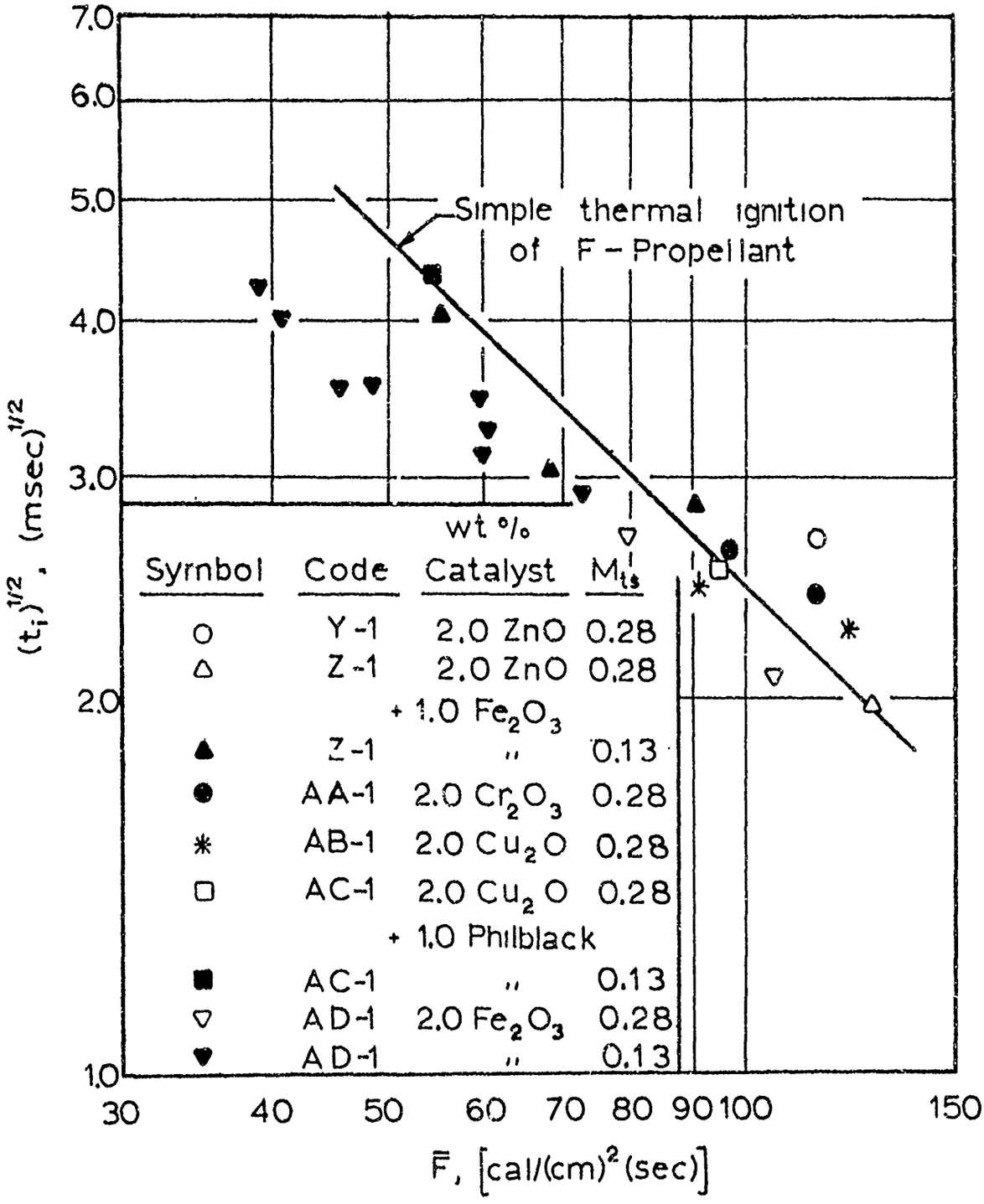

Figure 47

A Comparison of Ignition Data for Propellants with Different Catalysts.

Propellant AC with cuprous oxide as well as carbon black gave strong light signals for both conditions tested. Ignition times were close to those for propellants with other catalysts; however, one sample ignited at a much lower heat flux than was found for the propellant catalyzed with cuprous oxide alone. More data were not obtained on propellant AC because the samples were not entirely homogeneous. Some of the cut surfaces had rather large agglomerates of carbon black.

Examination under a microscope of surfaces of propellants which did not ignite showed that for all samples which gave photocell deflections there was some regression of the propellant surface. For the propellant containing only zinc oxide there was considerable charring of the polymer for runs at high heat fluxes even when no light signal was observed. All of the propellants tested at high heat fluxes showed some surface discoloration, although in several cases no deflection of the photocell signal was observed.

Because of the test-period limitation in the shock tube, it was not possible to completely define the ignition characteristics of these propellants. The fact that several of the propellants gave a photocell deflection, indicating that thermal ignition had occurred at the surface but did not undergo transition to steady deflagration, indicates that catalysts other than iron oxide were not effective in catalyzing secondary ignition reactions which supply part of the energy for heating the propellant surface. It would be expected that if these tests could have been conducted at lower gas velocities, all of these propellants would have undergone steady deflagration at the

times when photocell deflections were observed. Baer [page 80, 6] observed in his studies on propellant ignition that one of the propellants tested ignited but did not undergo steady deflagration at test-gas velocities of about 100 m/(sec), equivalent to Mach 0.13 in this study. However, at a lower gas velocity, 50 m/(sec), the propellant samples ignited and burned.

In addition to the propellants described above, an uncatalyzed propellant, propellant G, and a propellant containing two per cent Sterling VR carbon black, propellant GB, were tested. Both of these propellants had the same particle-size distribution of ammonium perchlorate as F-propellant. See Table 2 for complete compositional data for these propellants. No indication of ignition, as monitored by a photocell, was observed during ignition tests on propellants G and GB. Data for ignition runs on these propellants are given in Table 14. Samples recovered from tests showed a small amount of surface regression, and a number of the larger oxidizer crystals were opaque after tests, an indication that some intergranular decomposition of ammonium perchlorate had occurred. For G-propellant some charred polymer was found on propellant surfaces. For tests at higher heat fluxes [greater than 90 cal/(cm)^2(sec)] and at high gas velocities, Mach 0.28 and 1.0, the polymer at the surface of G-propellant was more charred than for runs at lower heat fluxes and gas velocities. In some of these tests a thin coat of carbonaceous material deposited on the trailing edge of the sample holder.

Although G-propellant did not ignite in convective heating tests, ignition data for G-propellant were obtained experimentally by Baer

[8,82] at low radiant fluxes, 1-12 cal/(cm)^2(sec), in a radiation furnace at atmospheric pressure Experimental data from Reference 82 have been retabulated in Table 1 for propellants F and G, and are plotted in Figure 4. For ignition studies in the radiation furnace, freshly cut propellant surfaces were coated with a very thin layer of carbon black to eliminate reflectivity and to ensure that all radiant energy was absorbed at the surface. By comparing ignition results with propellants which were not coated with carbon black, and considering the effect of surface absorbtivity on heat transfer to the surface, it was shown that the thin layer of carbon black did not catalyze the ignition process. The experimental data presented by Figure 4 for propellants F and G are well represented by straight lines with slopes of -0.92 on the $\ell n\ (\bar{F})$ versus $\ell n\ (t_i)^{1/2}$ plot. The results from this study by Baer show that the addition of copper chromite to this propellant system affects the simple thermal ignition process.

The equations for the lines which represent the data for propellants F and G in Figure 4 for an initial temperature of 300°K are given by:

For F-propellant:

$$(t_i)^{1/2} = 170/(\bar{F})^{0.92} \tag{29}$$

For G-propellant:

$$(t_i)^{1/2} = 193/(\bar{F})^{0.92} \tag{36}$$

By combining Equations (23) and (36), it is found that the thermal ignition temperature as a function of the externally applied heat flux for G-propellant is:

$$T_{si}^{T}(°K) = 300°K + 333.9\ (\bar{F})^{0.08} \qquad (37)$$

where $\bar{F}$ has the units of cal/(cm)^2(sec).

If it is assumed that ignition results at low radiant fluxes can be extrapolated to higher heat fluxes for G-propellant, this was shown to be a valid assumption for F-propellant, then it can be shown through the use of Equation (37) that in none of the convective heating tests on G-propellant was the surface temperature T_{si}^{L}, (see Table 14) sufficiently high at the end of the test period to ensure thermal ignition of G-propellant.

Discussion of Results from Catalyst Study

It is interesting to note that except for ferric oxide and copper chromite, none of the other catalysts tested were very effective in increasing the ignitability of ammonium perchlorate propellants at low gas velocities. With respect to the preceding discussion on G-propellant, it appears that some of these catalysts may have exhibited some catalytic activity, but all of them were less effective than iron oxide at gas velocities of Mach 0.13 and Mach 0.28. Of the catalysts included in this study, zinc oxide appeared to be the most effective catalyst, based on thermal decomposition studies, for promoting low-temperature decomposition of ammonium perchlorate and also lowering the spontaneous ignition temperature. It is possible that cuprous oxide did not contribute to the low-temperature decomposition of ammonium perchlorate in ignition tests because of the fast heating rate. As suggested by Jacobs and Kureishy [48], the self-heating of

ammonium perchlorate in the presence of cuprous oxide results from energy liberated by the oxidation of cuprous oxide to cupric oxide. Experimental results by Hermoni and Salmon [45] had indicated that chromic oxide was not an effective low-temperature decomposition catalyst for ammonium perchlorate, but appeared to be a catalyst for reactions in the gas phase. Carbon black did not exhibit any observable catalytic effect on propellant ignition. Neither propellant GB containing carbon black nor propellant G ignited in convective heating tests.

Although zinc oxide, cuprous oxide, and chromic oxide did not exhibit strong catalytic activity, when compared to iron oxide and copper chromite, it is of interest to note that propellants which contained these materials gave indications of ignition at times which were in qualitative agreement with data for simple thermal ignition of F-propellant. See Figure 47. None of these materials appear to catalyze secondary ignition reactions, but only affect the simple thermal ignition process. On the other hand, iron oxide and copper chromite catalyze secondary ignition reactions at or near the surface in addition to their effect on the simple thermal ignition process.

One reason that ammonium perchlorate decomposition catalysts may not be effective in increasing the ignitability of propellants, as would be expected based on studies of thermal decomposition of ammonium perchlorate, is that most of the catalyst, as well as the ammonium perchlorate crystals, is coated with a thin film of polymer which prevents intimate contact between ammonium perchlorate crystals and the catalyst powder. It was found that copper chromite exhibits

essentially the same catalytic activity in cast propellants with a PBAA binder-fuel and in pressed propellants with carbon black as the fuel. The ignition results on pressed propellants are described in a subsequent section. A comparison of the results on pressed propellants and cast propellants containing copper chromite indicated that separation of the catalyst from ammonium perchlorate crystals did not change the ignition characteristics for the two kinds of propellants. However, this does not mean that other ammonium perchlorate decomposition catalysts, which have been shown through thermal decomposition studies on ammonium perchlorate to have greater catalytic activity than copper chromite, will not produce different ignition characteristics when incorporated in cast or pressed propellants. A critical test of this hypothesis would require ignition tests on cast and pressed propellants containing a very effective ammonium perchlorate decomposition catalyst.

Since iron oxide and copper chromite were the only catalysts tested which significantly increased the ignitability of propellants at low gas velocities, it appears that these catalysts have an additional role in the ignition process besides catalyzing the decomposition of ammonium perchlorate. One of these catalysts, iron oxide, according to Kuratani [57], and Solymosi and Révész [87], is not an extremely effective catalyst for the low-temperature decomposition reaction. It is known, however, that both iron oxide and copper chromite are excellent combustion catalysts. Copper chromite, although used primarily as a hydrogenation catalyst, was found by Cannon and Welling [21]

to be an excellent combustion catalyst for automotive exhaust gases which contain extremely small concentrations of hydrocarbons and carbon monoxide. Copper chromite exhibited catalytic activity at 185°C, and completely oxidized all combustible material at 265°C [21]. Arden, Powling, and Smith [5] have observed in studies on the burning of ammonium perchlorate that copper chromite appears to catalyze the decomposition of nitric oxide. The catalytic decomposition of endothermic oxides of nitrogen at the propellant surface could be an important secondary ignition process for supplying additional heat flux to the propellant surface during convective heating ignition of propellants with rough surfaces. Levy and Freidman [60] also found that copper chromite appears to catalyze gas-phase reactions in the steady deflagration of ammonium perchlorate containing only copper chromite. It is suggested by Levy and Freidman that in steady deflagration the flame zone is sufficiently close to the surface so that copper chromite particles protruding from the surface of the propellant extend into the flame zone. This type reaction, according to the definition used here, would be catalysis of heterogeneous surface reactions. This kind of reaction would be an effective secondary ignition process at low test-gas velocities since energy would be liberated at the surface where it would be utilized more effectively in bringing the propellant to its thermal ignition temperature. This role of the catalyst appears to be most realistic since both copper chromite and iron oxide are much too stable to enter the gas phase at the low temperatures found at the propellant surface during the transient ignition process.

Based on the foregoing observations, the following classes of chemical reactions appear to be important in the ignition process:

1. The most important and the key ignition reaction for ammonium perchlorate propellants is the low-temperature, thermal decomposition of ammonium perchlorate at the propellant surface. This reaction, whether catalyzed or uncatalyzed, ultimately determines the ignition characteristics of ammonium perchlorate propellants. The fact that the activation energy, as determined from ignition experiments where propellants ignite by a simple thermal ignition process, is about 30 kcal/(mole) strongly suggests, but is not positive proof, that the low-temperature decomposition of ammonium perchlorate is the key chemical reaction in the ignition process. Other possible ignition reactions could have similar activation energies. However, with respect to other ammonium perchlorate decomposition reactions, it does not appear that the high-temperature decomposition of ammonium perchlorate is important in the simple thermal ignition process. This high-temperature reaction has a higher activation energy and also requires an induction period which would appear to rule out its participation in the fast ignition process when the entire propellant surface is heated uniformly. However, for propellants with rough surfaces some of the perchlorate crystals may be heated to a sufficiently high temperature to undergo high-temperature thermal decomposition after the intermosaic

material at the surface has undergone decomposition. Furthermore, catalysis of the low-temperature reaction does not change its activation energy because the decomposition process is apparently controlled by an electron transfer process which is still the limiting process in the presence of most catalysts.

2. One class of secondary chemical reactions which appears to be important in the ignition process of ammonium perchlorate propellants is exothermic reactions among ammonium perchlorate decomposition products or between oxidizing species of perchlorate decomposition products and polymer fragments that are pyrolized during the heating process. When copper chromite or iron oxide is present in a propellant system, it catalyzes the low-temperature, exothermic decomposition reaction of ammonium perchlorate as well as secondary ignition reactions. The contribution of copper chromite to the simple thermal ignition process can be estimated by comparing ignition data for propellants F and G obtained in the radiation furnace (Figure 4), test conditions under which catalyzed gas-phase or heterogeneous surface reactions are not important in providing energy for heating the propellant surface. However, under convective heating, where two-dimensional heating of surface imperfections takes place and localized hot spots occur, reactive species are produced at the surface of the propellant. This effect, in addition to the normal

low-temperature decomposition of ammonium perchlorate, provides reactive species which then undergo further exothermic reactions, perhaps at catalyst sites. It is suspected that localized heating of perchlorate crystals leads to thermal ignition of some of the ammonium perchlorate crystals before the surrounding propellant surface is brought to its ignition temperature. However, since these particles have been heated at a very rapid rate, only a thin surface layer is thermally ignited on larger crystals. This does not lead to ignition of the propellant surface until adjacent areas are brought to the propellant's thermal ignition temperature, but this process does provide gaseous species for secondary reactions.

Thermal ignition of small individual crystals would suggest the appearance of an ammonium perchlorate decomposition flame and even some participation by the binder-fuel surrounding the crystal. If an ammonium perchlorate decomposition flame appeared without the participation of the binder-fuel in the reaction, it might not be possible to detect localized thermal ignition with a photocell, since the decomposition flame is not very luminous. During some of the tests on catalyzed propellants, small deflections were seen on the differentiated photocell signal several milliseconds before the propellant ignited. One of the more unusual photocell signals of this kind is shown by the oscilloscope record in Figure 48a. The small deflections which are more apparent on the differentiated

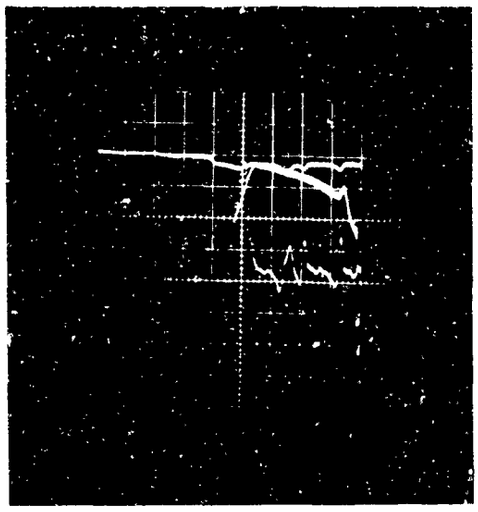

a. Run No. 46-17-2 in Argon.
Gas Temperature: 1314°K,
Heat Flux: 31 cal/(cm)^2(sec).
Ignition Time: 21 msec.

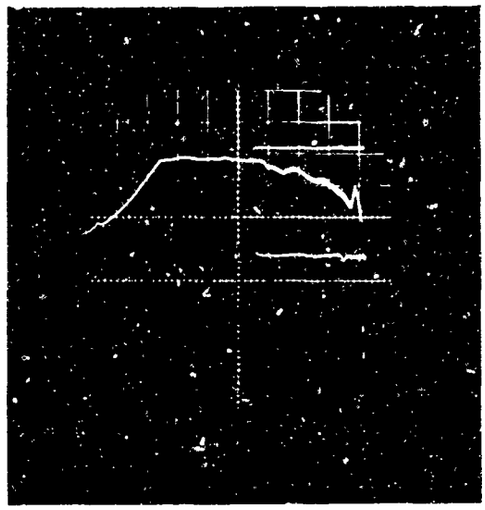

b. Run No. 46-15-4 in Nitrogen.
Gas Temperature: 1313°K,
Heat Flux: 39 cal/(cm)^2(sec).
Ignition Time: 18 msec.

Figure 48

Oscillographs for Ignition Runs on Propellant AD Showing Different Kinds of Ignition Characteristics. Traces starting at Top and Center are for the Direct and Differentiated Photocell Signals, Respectively.
Time Base: 5 msec/(div.) (Right to Left).

signal suggest that the luminosity at the propellant surface was produced by thermal ignition of individual crystals accompanied by reactions involving the polymer. Figure 48b is a normal light trace for the same propellant.

In addition to the preceding observation, high-speed motion pictures on some ignition runs in the shock tube have shown a dull, reddish glow at the propellant surface a few frames before a combustion flame was observed. This was only observed in about 5 per cent of ignition runs that were viewed photographically. It appeared that the glow at the surface before a flame appeared was produced by catalyzed surface reactions. Ignition characteristics of the kind shown by Figure 48a, localized ignition that was subsequently extinguished, were not observed on any of the motion picture films.

3. Another class of secondary ignition reactions which could be important in the ignition process are those in which the binder-fuel is an active participant. These reactions would include the heterogeneous attack on the polymer by reactive oxidizing species from the decomposition of ammonium perchlorate. It would be expected that this kind of reaction would be catalyzed by an oxidation catalyst in the propellant.

Allen and Pinns [1] have shown that conventional solid propellants can be ignited by the heterogeneous attack of a reactive oxidizer on the propellant. In their work they used

liquid and gaseous chlorine trifluoride as the oxidant. Allen and Pinns did observe, however, that propellants which contained a PBAA binder were more difficult to ignite than those with polysulfide or polyurethane binders.

Hermance [43] studied the ignition and combustion of a polyester-styrene resin under convective heating by oxygen and by mixtures of oxygen and nitrogen in a shock tunnel. He found that consistent ignition results on the pure polymer were obtained only if the test gas contained concentrations of oxygen greater than about 50 per cent. The results of these studies by Hermance indicate that heterogeneous attack by molecular oxygen on the binder-fuel may not be an important reaction process for raising the temperature of the propellant surface to its ignition temperature.

From the experimental work conducted for this thesis, it is not possible to completely assess the role of the binder-fuel in the ignition process. It appears, however, since propellants containing either polymer or carbon black as the fuel exhibit almost identical ignition characteristics, that exothermic reactions involving the binder-fuel are not important in the ignition process. It is suggested that reactions involving the fuel become important only after thermal ignition of the ammonium perchlorate. This aspect of ignition will be discussed in more detail in the section on pressed propellants.

CHAPTER VII

SPECIAL STUDIES ON PROPELLANT IGNITION

To supplement the experimental studies on the ignition of cast propellants with cut surfaces, several special propellants were made for study in the shock tube apparatus. Some of the different kinds of propellants studied in these experiments were:

1. Cast propellants with polymer-rich surfaces.
2. Cast propellants with polymer-rich surfaces that were salted with 15-micron ammonium perchlorate.
3. Pressed propellants of ammonium perchlorate and solid fuels.
4. Extended-phase propellants made from pellets of pressed ammonium perchlorate and different polymer-fuels.

IGNITION OF PROPELLANTS WITH POLYMER-RICH SURFACES

An exploratory study was made to determine the ignition characteristics of propellants with polymer-rich surfaces. In rocket ignition the propellant surface which is exposed to ignitor action is usually a smooth surface which was formed when the uncured propellant was cast around a mandrel to give the desired burning-surface geometry. This surface is polymer-rich and very few, if any, of the ammonium perchlorate crystals are visible at the surface. In the preceding chapters, the discussion on propellant ignition was devoted entirely to cast propellants with cut surfaces. The brief study

described here was made to obtain information on how a polymer-rich layer at the propellant surface affects the ignition process.

The cast propellants used in this study were processed in the same manner as those used in other studies. See Appendix F. However, after the propellant was cast into the cavity of the sample holder, all excess propellant was wiped away on a Teflon sheet to leave a smooth surface flush with the lip of the sample holder. The propellant samples were then cured for seven days at 80°C. When the samples were brought to oven temperature, a polymer-rich layer formed at the surface which covered all of the ammonium perchlorate particles with a thin film of polymer. When the samples had cured and were removed from the oven, the propellant surface was no longer flat; a small amount of shrinkage had occurred that gave a slightly concave surface. It is not believed that these polymer-rich surfaces are identical to cast surfaces, but ignition characteristics of propellant samples prepared by this method should be very nearly the same as those for a propellant grain with a surface formed by casting propellant around a mandrel.

Experimental data for some of the propellants with polymer-rich surfaces studied are plotted in Figure 49. These data are for F-propellant in nitrogen and air, P-propellant in nitrogen, and U-propellant in nitrogen, all at a test-gas velocity of Mach 0.13. The experimental ignition results for F-propellant samples with cut surfaces in nitrogen at Mach 0.13 (see Figures 10 and 11) are represented by the straight line in Figure 49. Data for ignition of F-propellant

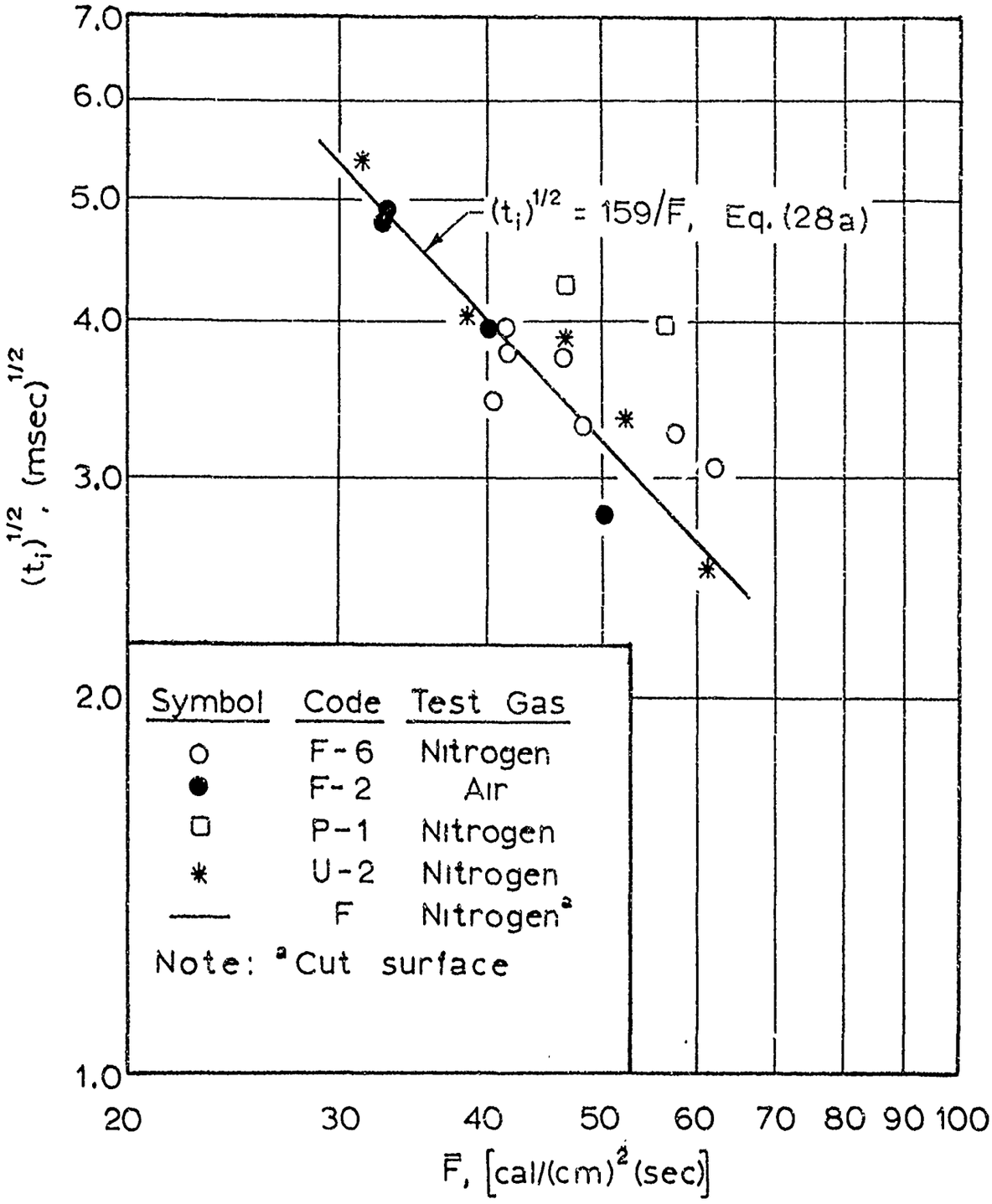

Figure 49

Ignition Data for Samples of Propellants F, P, and U with Polymer-Rich Surfaces at a Test-Gas Velocity of Mach 0.13.

samples with polymer-rich surfaces in nitrogen and air are tabulated in Table 3 (Part II) and Table 6 (Part II), respectively. Similar data for propellants P and U are given in Table 7 (Part II) and Table 9 (Part II), respectively.

For calculating externally applied heat flux to the surface of these polymer-rich samples, it was assumed that the thermophysical properties of the polymer-rich surface were the same as those for a cut surface. Obviously, this cannot be so, but if the other extreme is considered in which the thermophysical properties of the polymer are used, it is found that the calculated externally applied heat flux is only 5 to 10 per cent less than for the assumption that the surface has the same properties as the propellant. For the assumption of polymer properties controlling the rate of heat transfer, see Tables 3 and 6, the calculated ignition temperature (T^L_{si}) is 50 to 100°C higher than for the initial calculations in which propellant properties were used.

Neither assumption about the thermal properties of the polymer-rich surface is adequate to describe the heat transfer through the polymer film at the surface into the body of the propellant. It appeared from studies on propellants with cut surfaces that the only heat flux value which is really important is that which describes the heat flux at the surface of the ammonium perchlorate particles. For calculating the heat flux at the surface of the oxidizer crystals for these propellant samples, it would be necessary to know the thickness of the polymer film at the surface. Since no special precautions were

taken to ensure a uniform film thickness and the thickness of the polymer layer is not known, a more rigorous analysis of the heat transfer problem was not justified in this work. A thorough study of propellants with polymer-rich surfaces would necessarily include the ignition of samples with a thin-polymer film of known thickness on the freshly cut surface of cured propellant. Then, knowing the properties of the polymer film and propellant, one could use unsteady-state heat transfer theory to calculate the heat flux at the polymer-propellant interface during an ignition run. The surface layers of a cast propellant grain should also be examined to obtain information about the distribution of ammonium perchlorate particles near the surface. Until more information can be obtained about the properties of a polymer-rich film, the method used here for calculating externally applied heat flux to the propellant surface will provide a useful comparison of the ignition characteristics between propellants with freshly cut surfaces and those with polymer-rich surfaces.

Upon examining the data given in Figure 49, it is seen that samples of F-propellant with polymer-rich surfaces have nearly the same ignition characteristics as samples with cut surfaces, and the ignition times at equivalent heat fluxes are essentially the same in both nitrogen and air. It is also interesting to note that U-propellant, which was more difficult to ignite than F-propellant in tests with cut surfaces at low gas velocities, has essentially the same ignition characteristics as F-propellant when ignition data for polymer-rich surfaces are compared. The apparent reason for this anomalous behavior is that both

propellants contain a 15-micron cut of ammonium perchlorate. U-propellant contains only a 15-micron cut of ammonium perchlorate, whereas F-propellant contains equal proportions (by weight) of a 15-micron and a 200-micron cut of ammonium perchlorate. As would be expected, only fine perchlorate particles remain suspended in the polymer-rich film when samples are placed in the oven, and the concentration of these particles is less in the thin-polymer layer than it is in the main body of the propellant. Since each of these fine particles (the largest being only a few microns in diameter) is surrounded by a rather thick film of polymer, relative to that in the main body of the propellant, the temperatures of these particles increase at about the same rate as that of the polymer at the surface. It has already been mentioned that for the assumption that polymer properties control heat transfer to the surface, the calculated surface temperature, T^{L}_{si}, is 50 to 100°C higher than that for a cut propellant surface at ignition. Therefore, the small ammonium perchlorate particles suspended in the polymer reach their thermal ignition temperature more rapidly than would be expected if the polymer film were considered to be a thermal barrier slowing down the rate of heat transfer to the main body of the propellant. Because of this effect, both propellants U and F with polymer-rich surfaces give almost identical ignition times. It would be expected that the cast surface of a propellant grain would have a similar distribution of particles resulting from flow of the freshly processed propellant along the wall.

Two data points for ignition runs on samples of propellant P with a polymer-rich surface are also included in Figure 49. This

propellant is similar to F-propellant in that it has the same catalyst content and particle-size distribution of ammonium perchlorate, but has 5 per cent more polymer. The longer ignition times for samples of propellant P relative to those for propellant F are attributed to the fact that because of the lower loading of ammonium perchlorate, even some of the finer particles of oxidizer settled from the layer of polymer at the surface before the propellant cured, thus providing a slightly thicker polymer film over all particles. This was verified by cutting thin layers from the surface of a sample which extended above the lip of the sample holder and comparing them with similar slices from F-propellant. Ignition data for samples of P-propellant with cut surfaces were nearly the same as those for F-propellant at Mach 0.13 and 0.28 (see Figure 30).

Figure 50 shows the effect of oxidizer particle size on ignition of propellants with polymer-rich surfaces at a test-gas velocity of Mach 0.13. Propellants S and U contained single particle-size cuts of ammonium perchlorate, 85-micron and 15-micron, respectively. The data for S-propellant are given in Table 8, Part II. The two straight lines on the graph represent the data for propellants S and U with cut surfaces, see Figures 32 and 34, respectively. It is seen from these data that samples of U-propellant with polymer-rich surfaces ignite faster than samples with cut surfaces at equivalent heat fluxes. On the other hand, S-propellant samples with polymer-rich surfaces are more difficult to ignite than samples with cut surfaces. This observation is in agreement with our earlier supposition. Because S-propellant contains larger particles, 85 microns in diameter on the

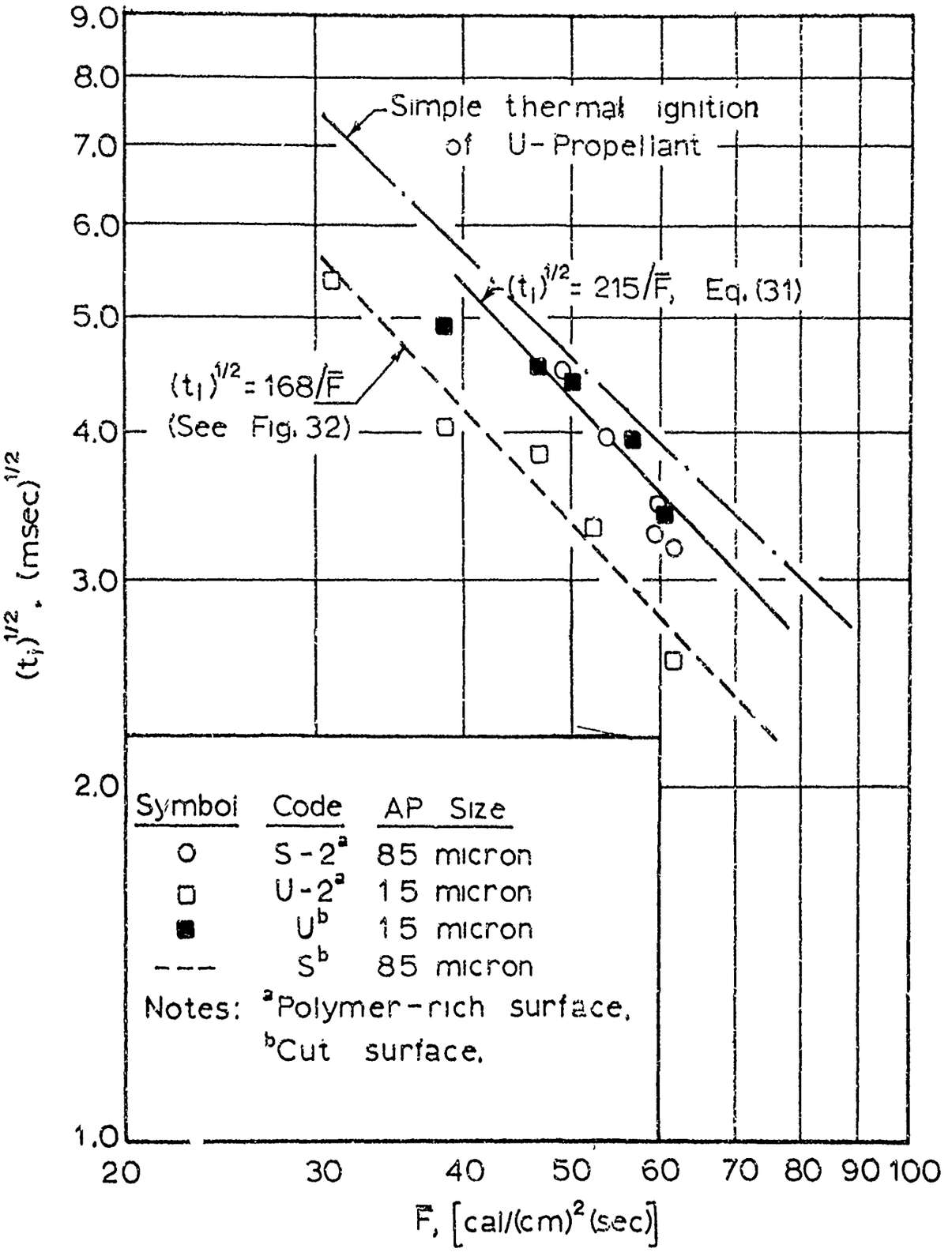

Figure 50

Effect of Ammonium-Perchlorate Particle Size on Ignition Time For Propellants with Polymer-Rich Surfaces at a Test-Gas Velocity of Mach 0.13 in Nitrogen.

average, even though the polymer is heated faster, the 85-micron particles still partially fulfill the requirements for a semi-infinite solid and consequently their surface temperatures increase at a slower rate than those for finer particles embedded in the polymer.

Data for higher gas velocities, Mach 0.28, for propellants S and U are given in Figure 51. Again, although there is a shift to longer ignition times because of velocity effects, S-propellant has longer ignition times at equivalent heat fluxes than U-propellant. The results for U-propellant with polymer-rich surfaces at Mach 0.28 are in reasonable agreement with those for samples with cut surfaces (see Figure 34). The dashed line in Figure 51 represents ignition results on samples of S-propellant with cut surfaces at Mach 0.28 (see Figure 32). The continuous line represents simple thermal ignition of propellants F and U with cut surfaces (see Figures 12 and 34, respectively).

The effect of gas velocity on ignition for propellant samples with polymer-rich surfaces can be seen by comparing data for the same propellants in Figures 50 and 51. The effect of gas velocity on ignition at low Mach numbers is about the same order of magnitude as that for propellant samples with cut surfaces. For samples with smooth, polymer-rich surfaces, one would not expect an effect of gas velocity on ignition. However, none of the propellant samples used in this study had perfectly smooth surfaces. Although all of the ammonium perchlorate particles were coated with polymer, there were always a few areas where individual crystals in the case of S-propellant and

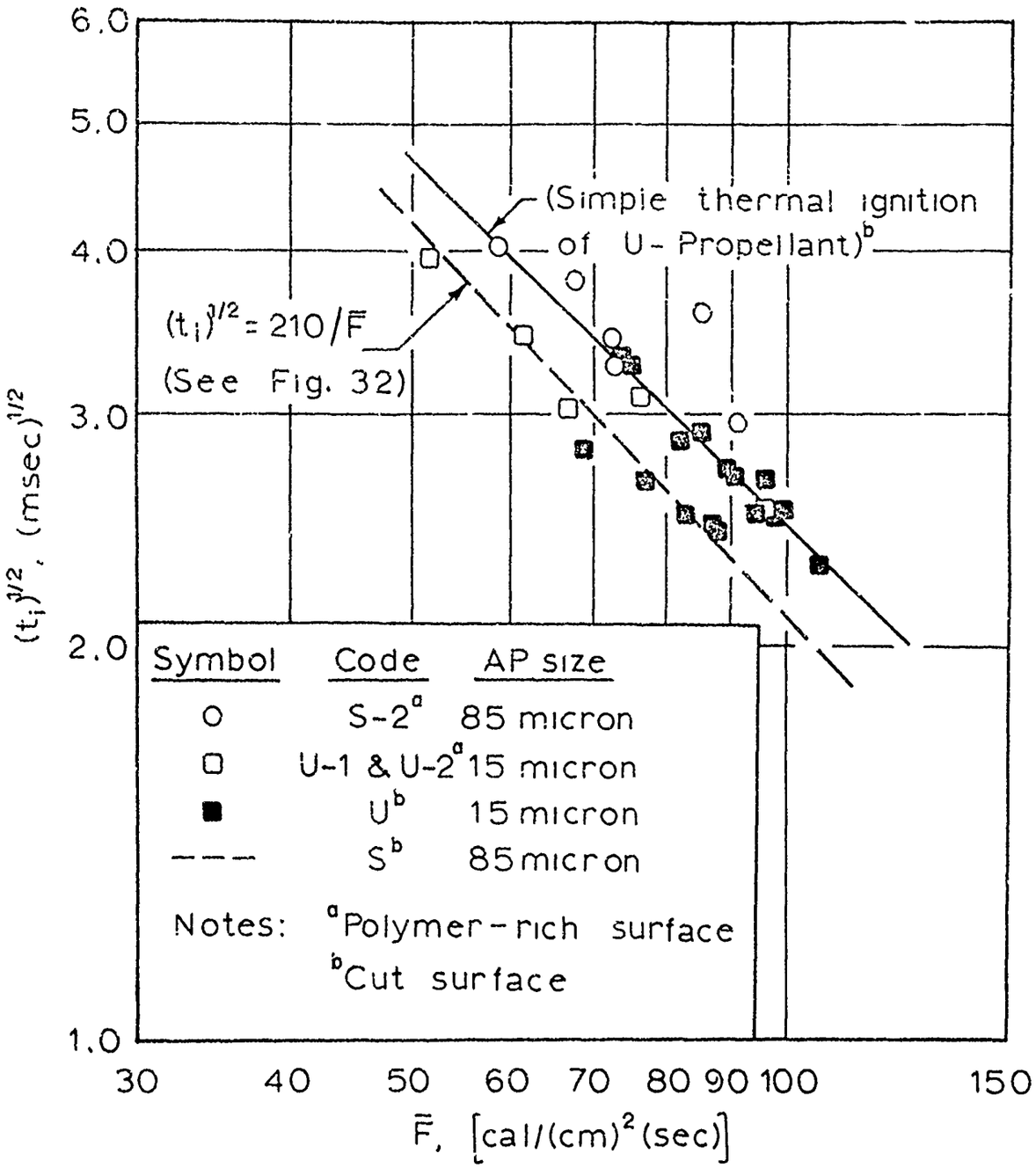

Figure 51

Effect of Ammonium-Perchlorate Particle Size on Ignition Time for Propellants with Polymer-Rich Surfaces at a Test-Gas Velocity of Mach 0.28 in Nitrogen.

agglomerates of small particles in the case of U-propellant that extended a small distance above the mean surface level. And as already mentioned, contraction of the sample upon removing it from the oven always left a slightly concave surface. This surface imperfection could be essentially eliminated by modifying the sample holders so that the propellant could be cast from the back side with the face of the holder pressed tightly against a very smooth surface. Since the work presented here was of an exploratory nature, all of the details with regard to sample preparation were not fully developed.

In another part of this study on samples with polymer-rich surface, thickness of the polymer-rich film over the ammonium perchlorate crystals at surface was reduced before samples were cured. This was accomplished by placing benzene on the surface of the sample, and then absorbing off the benzene and dissolved polymer. Ignition data at Mach 0.13 in nitrogen for samples of S-propellant with the modified polymer-rich surfaces are compared to data with those having as-cast, polymer-rich surfaces in Figure 52. Experimental data for these two types of samples are tabulated in Table 8 (Parts II and III). As would be expected, the samples with a thinner polymer film at the surface had shorter ignition times than samples with as-cast, polymer-rich surfaces at equivalent heat fluxes. Data for ignition of S-propellant with polymer-rich surfaces at Mach 0.28 are also included in Figure 52. The straight lines represent ignition results for samples of S-propellant with cut surfaces (see Figure 32).

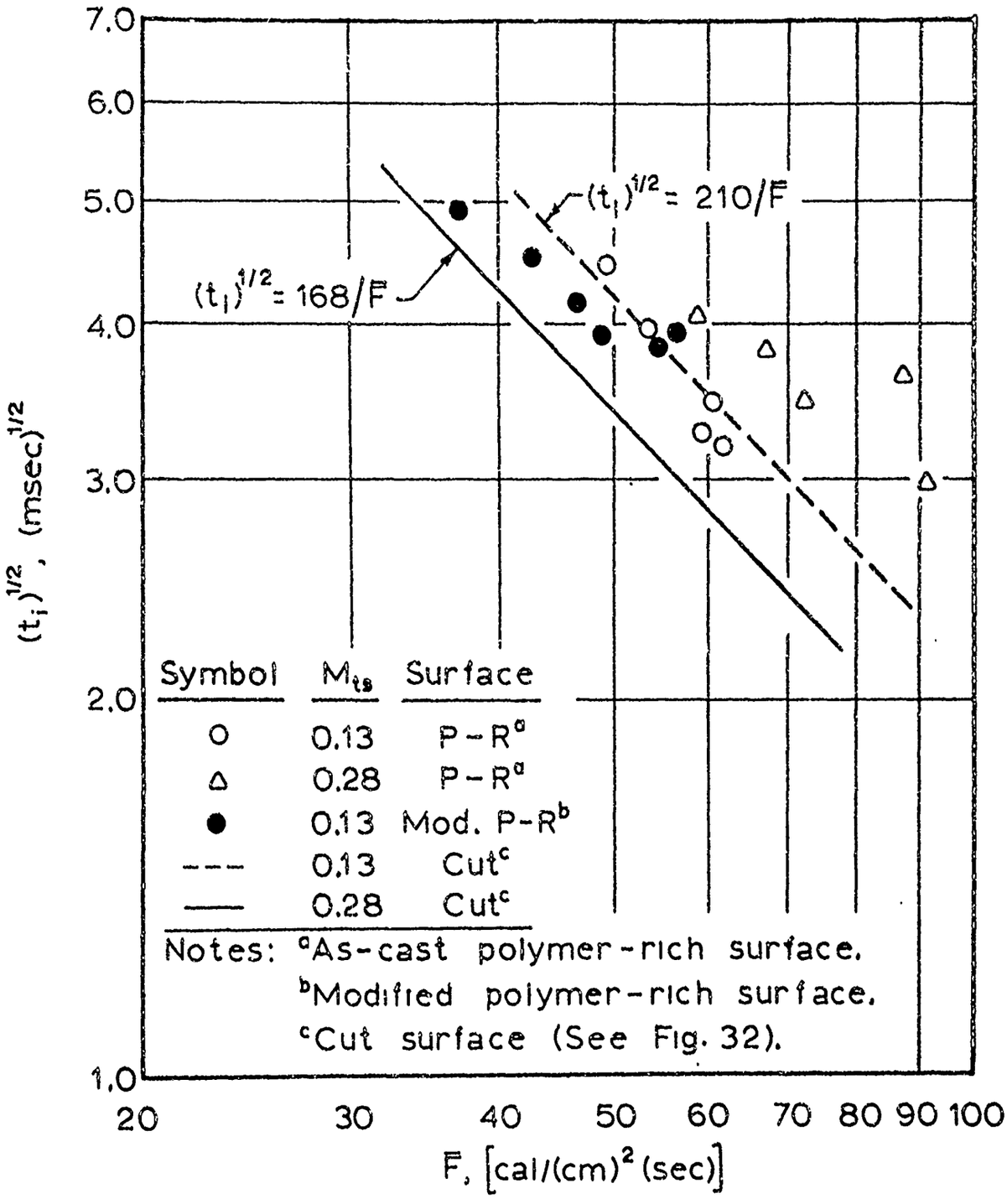

Figure 52

Effect of Polymer-Film Thickness and Test-Gas Velocity on Ignition Time for Samples of S-Propellant with Polymer-Rich Surfaces in Nitrogen.

IGNITION OF PROPELLANTS WITH SALTED, POLYMER-RICH SURFACES

As a special study to investigate the effect of surface roughness on ignition, several samples of propellant were prepared by salting polymer-rich surfaces of U-propellant with 15-micron ammonium perchlorate. Two procedures were used in preparing the samples. The first procedure was to salt a polymer-rich surface by sifting onto the surface 15-micron ammonium perchlorate through a 270-mesh screen as soon as the smooth surface was prepared. With this procedure, the polymer still formed a thin film over all the ammonium perchlorate crystals and agglomerates as soon as the samples were placed in the curing oven. This occurred even though a considerable number of the agglomerates extended above the surface. The second procedure for preparing samples was to salt the polymer-rich surface after the propellant had been in the curing oven for three hours at 80°C. When this was done, a much thinner film of polymer formed on the crystals and agglomerates, and some of the agglomerates were not completely covered with polymer. Photomicrographs of a salted, polymer-rich surface prepared by the second method and of a cut surface of U-propellant are shown in Figure 53a and b, respectively.

Ignition data obtained in nitrogen for samples of U-propellant with surfaces prepared by these methods are compared graphically with data for polymer-rich surfaces and cut surfaces in Figure 54 for a test-gas velocity of Mach 0.13 and in Figure 55 for a test-gas velocity of Mach 0.28. Ignition data for samples of U-propellant with salted surfaces are given in Parts III and IV of Table 9.

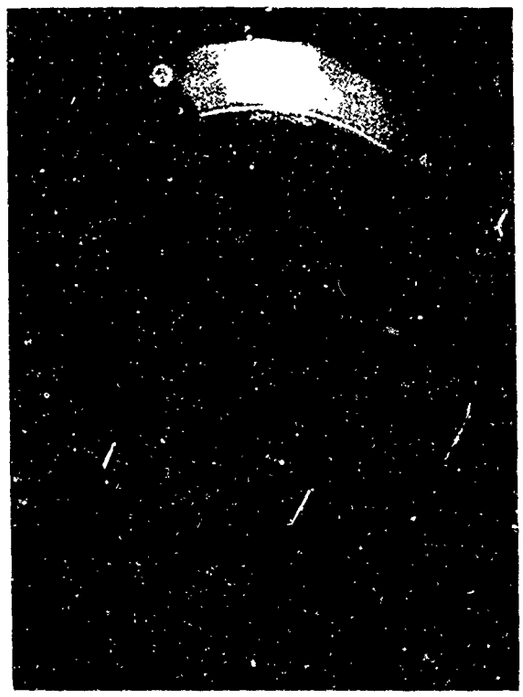

a. Polymer-Rich Surface Salted 3 Hours After Start of Cure (5X).

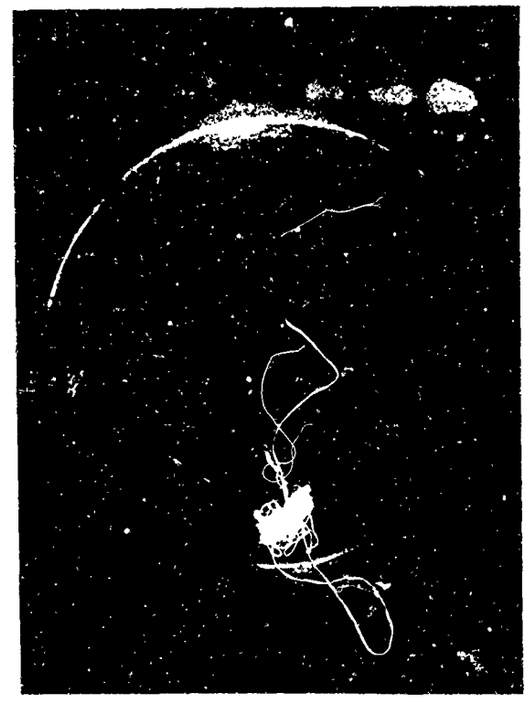

b. Surface Cut with Razor Blade (5X).

Figure 53

Photomicrographs of Surfaces on Samples of U-Propellant Prepared by Different Methods.

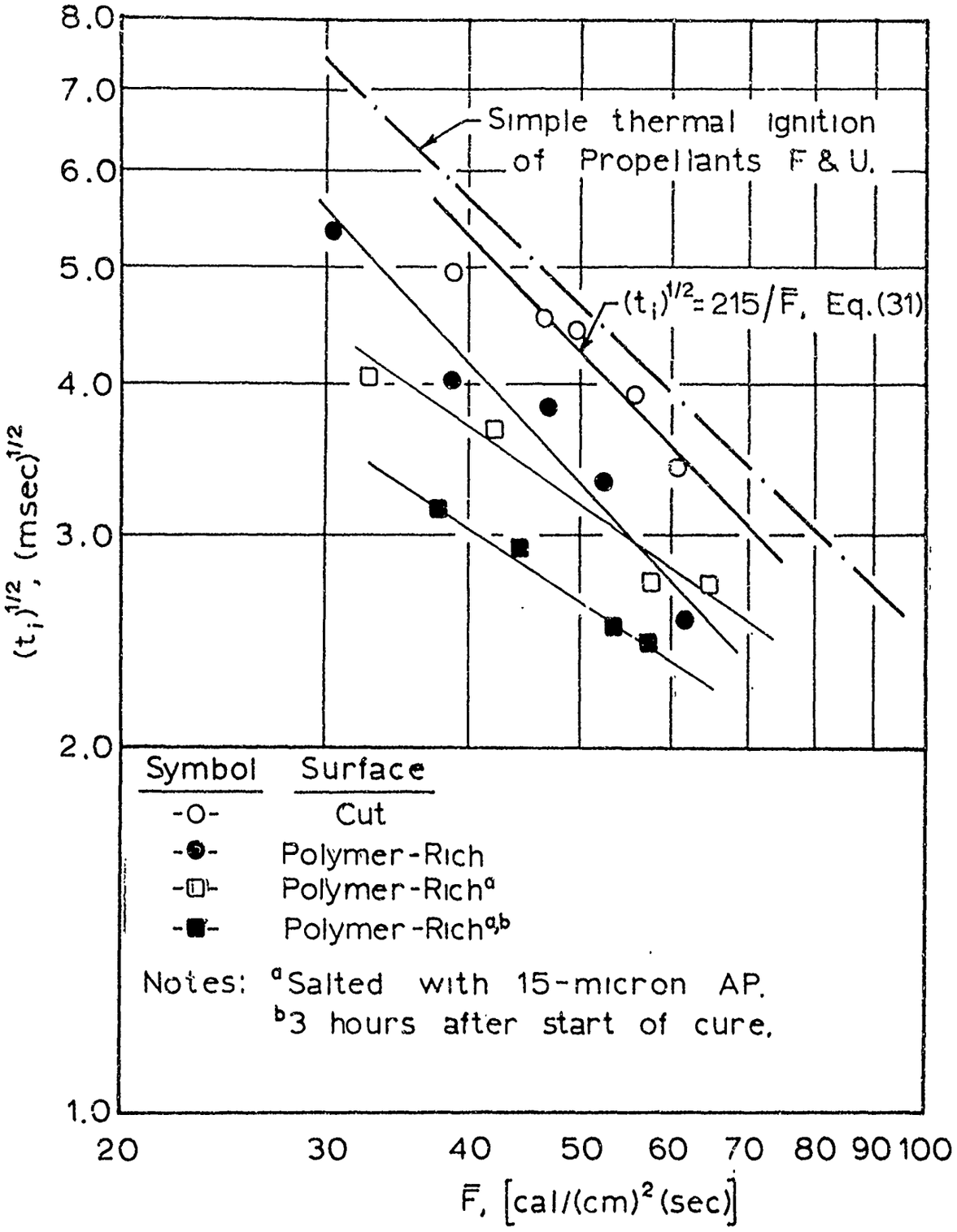

Figure 54

The Effect of Surface Conditions on Ignition Time for U-Propellant in Nitrogen at a Test-Gas Velocity of 0.13.

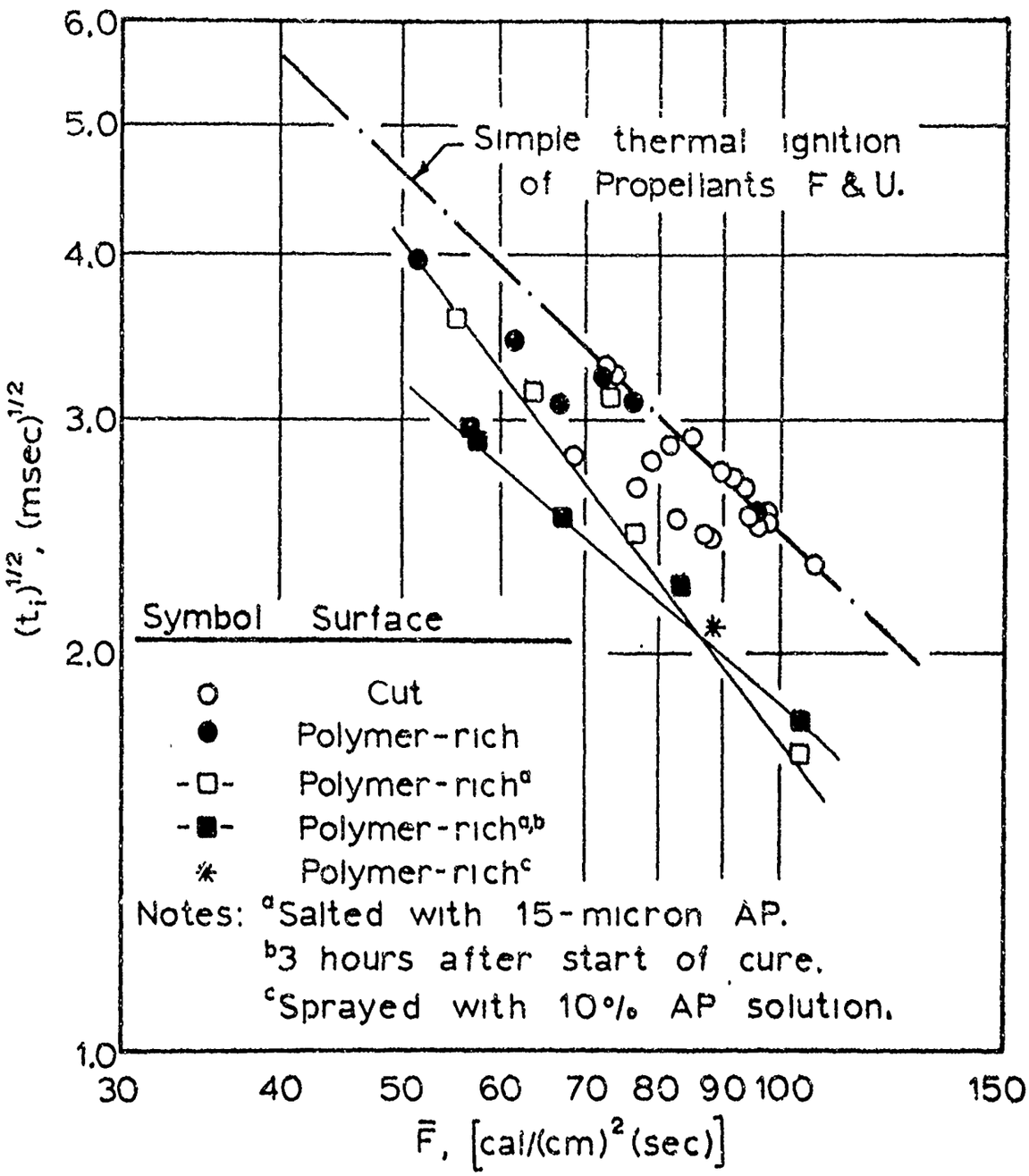

Figure 55

The Effect of Surface Conditions on Ignition Time for U-Propellant in Nitrogen at a Test-Gas Velocity of 0.28.

Only a few general statements can be made concerning the ignition characteristics of these propellants. The ignition results for propellant samples prepared by salting a polymer-rich surface with 15-micron ammonium perchlorate are identified by the narrow lines in Figures 54 and 55. These were drawn primarily for comparing data and the significance of the slopes of these lines is not apparent at this time. The only obvious conclusion which can be attached to these results is that surface roughness produced by salting the propellant surface improves the ignitability of U-propellant. The samples with salted surfaces which had exposed crystals and agglomerates of ammonium perchlorate had the shortest ignition times at a given heat flux. It appears that the improved ignitability of these samples is produced by two-dimensional heating of exposed ammonium perchlorate crystals and associated secondary ignition reactions which rapidly bring the propellant to its ignition temperature. It is seen by comparing these data with those for samples of F-propellant with cut surface (Figure 11) that the propellant with exposed ammonium perchlorate particles ignited considerably faster than F-propellant at equivalent heat fluxes and at the same Mach number.

Also, as a part of this study, a single ignition run was made on a propellant sample that was prepared by spraying a 10 per cent ammonium perchlorate solution on a hot, polymer-rich surface. This was done after the sample had cured for three hours at 80°C. By using an aspirator to spray the solution, it was found that very small crystals formed immediately on the surface of the sample as the water evaporated.

This single ignition test is represented by the star symbol in Figure 55. Ignition time was about the same as that for propellants with a salted surface. But in this case the surface roughness was not greatly different from that for the polymer-rich surface.

IGNITION OF PRESSED PROPELLANTS

A number of pressed propellants were prepared for study in the shock-tube apparatus. Compositions for pressed propellants are given in Part II of Table 2. Through the use of pressed propellants, it was possible to greatly alter physical and chemical properties of the fuel used in the propellant, and thus obtain information on the role of the fuel in the ignition process. All of the pressed propellants were made by thoroughly blending dry ingredients and then pressing the powder into a cylindrical pellet, 3/8 inch in diameter by 3/8 inch long, under a pressure of 100,000 psig. If a small amount of moisture was added to the dry powder, the densities of the pellets were greater than 95 per cent of theoretical based on the densities for individual ingredients. Pellets of pressed propellants were placed in the cavity of the sample holder by pressing or by bonding an undersized pellet. The material which extended above the lip of the molder was removed by sanding with a fine-grit silicon carbide paper. Ignition data for propellants discussed in this section are given in Table 15.

Pressed Propellants of Ammonium Perchlorate and Copper Chromite

Propellants containing only ammonium perchlorate and copper chromite were difficult to ignite, and consequently no quantitative results were obtained from shock tube tests because of the test time-heat flux

limitation. Propellant B was pressed from a mixture containing 96 per cent ammonium perchlorate and 4 per cent copper chromite. In one of the two tests on propellant B at a heat flux of 55 cal/(cm)^2(sec) a deflagration wave was initiated at the pellet surface, but it was found upon examining the recovered sample that ignition occurred at flaws at the pellet surface. One initiation site was a small void at the interface between the pellet and epoxy-resin bonding agent at the leading edge of the pellet. A second initiation site was an agglomerate of copper chromite at the surface. From these two sites, a deflagration wave moved downstream over the pellet surface. The deflagration process was apparently intensified downstream by energy generated by continued burning at the ignition site. Because of the test time-heat flux limitation in the shock tube no additional tests were made on propellant B.

Pressed Propellants with Carbon Black Fuel

Ignition of Propellant CB

Propellant CB was the first of two kinds of pressed propellants tested which contained carbon black as the fuel. Ignition tests were conducted previously on this propellant in a radiation furnace by Baer [8,82] at heat fluxes of 1-12 cal/(cm)^2(sec). The data for ignition under radiant fluxes have been retabulated from Reference 82 in Table 1. Propellant CB contained 82 per cent ammonium perchlorate, 16 per cent carbon black (Philblack E from Phillips Petroleum Company), and 2 per cent copper chromite, the same concentration of

catalyst that was used in F-propellant. The carbon black used in this propellant was heated for two hours at 1000°C to remove all volatile components.

Samples for ignition tests were prepared either by pressing pellets directly into sample holders or by bonding the pellets in sample holders with an epoxy resin. It was found that the epoxy resin surrounding the pellet did not alter the ignition characteristics of pellets and smoother surfaces could be obtained with bonded samples. Surfaces on the pellets were smoothed by removing the last few millimeters of excess material with a 600-A, silicon carbide paper.

Two batches of CB pellets were manufactured. The first of these, CB-1, contained a number of carbon black agglomerates, some as large as 100 microns in diameter, that appeared as soft spots at the pellet surface. For the second batch of pellets, CB-2, a different procedure was used for blending ingredients. All of the fine particle-size ammonium perchlorate, carbon black, and copper chromite were thoroughly blended by sifting the mixture of powders through a 270-mesh screen three times, and then thoroughly blending with the coarse particle-size ammonium perchlorate. The powder was then moistened by spraying with an atomizer. Pellets produced by this method had densities about 10 per cent higher than those produced by the first method. Samples were not dried after pelleting, but were held in a desiccator until used.

Ignition data for pellets of propellant CB-2 in nitrogen and oxygen for convective heating at Mach 0.28 are presented graphically in Figure 56 with ignition data obtained in a radiation furnace at low

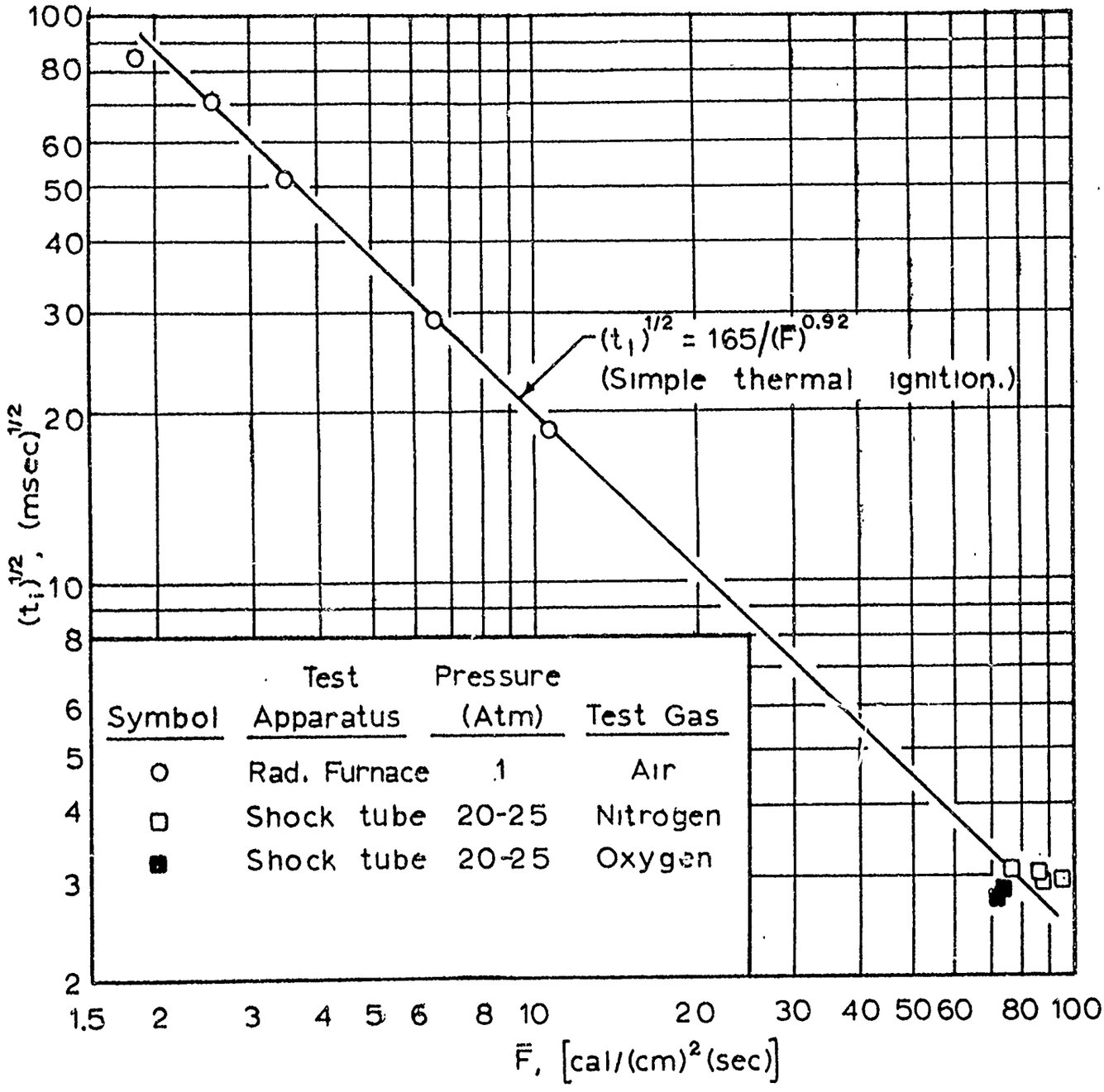

Figure 56

Ignition Data for Pressed Propellant CB (with Carbon Black Fuel) at Low-Radiant and High-Convective Heat Fluxes.

heat fluxes. The data for individual tests are given in Table 15. As was observed earlier for F-propellant, ignition data from convective heating experiments at high heat fluxes are represented on a plot of $\ell n\ (\bar{F})$ versus $\ell n\ (t_i)^{1/2}$ by the straight line extrapolated from the results obtained in the radiation furnace at low heat fluxes.

It can be seen by comparing the equations for the straight lines which describe simple thermal ignition of propellants F and CB on $\ell n\ \bar{F}$ versus $\ell n\ (t_i)^{1/2}$ plots that both systems have nearly the same ignition characteristics:

For F-propellant:

$$(t_i)^{1/2} = 170/(\bar{F})^{0.92} \qquad (29)$$

For CB-propellant:

$$(t_i)^{1/2} = 165/(\bar{F})^{0.92} \qquad (38)$$

Where t_i is in milliseconds and $\bar{F}$ has the units $cal/(cm)^2(sec)$.

F-propellant and CB-propellant have nearly the same thermal properties (see Table 4), and the slope of the lines which represent ignition data for the two propellants on an $\ell n\ \bar{F}$ versus $\ell n\ (t_i)^{1/2}$ plot is the same. This suggests that the key ignition reaction is the same for both propellants. Since carbon black does not appear to catalyze ammonium perchlorate decomposition and most certainly does not undergo rapid oxidation at the low temperatures associated with the transient heating process, it appears as suggested by Baer [8] that the fuel is not an active participant in the ignition process, but reactions involving the fuel become important only after thermal ignition of the ammonium perchlorate. Since pellets of propellant CB-2 had very

smooth surfaces, the ignition results at a test gas velocity of Mach 0.28 apparently represent simple thermal ignition for this propellant. This ignition result would be analogous to that obtained on samples of U-propellant with smooth cut surfaces. No tests were made at gas velocities greater than Mach 0.28 on propellant CB.

For tests in oxygen on propellant CB-2, the pellets were bonded in the sample holders with Fleck's phosphoric acid-copper cement to preclude reactions between the bonding agent and the environmental oxygen. The surfaces of the pellets used in these tests were reasonably smooth, showing only shallow scratches that were produced by the 600-A silicon carbide paper. The effect of oxygen on the ignition process, as shown by Figure 56, was relatively small at Mach 0.28.

All of the ignition data obtained on propellant CB-1 and CB-2 for convective heating are presented in Figure 57. The tests on pellets of propellant CB-1 gave fairly short ignition times relative to data obtained from tests in the radiation furnace and on pellets of propellant CB-2. As mentioned earlier, this was expected since some rather large agglomerates of carbon black were found at the surfaces of CB-1 pellets that prevented preparation of smooth surfaces. Some of the pellets of propellant CB-2 which were observed under a microscope to have small surface cracks and other surface imperfections also ignited faster. On the other hand, all pellets of propellant CB-2 which appeared to be free of surface imperfections gave ignition times in reasonable agreement with the extrapolated line on the $\ell n\ (\bar{F})$ versus $\ell n\ (t_i)^{1/2}$ plot from ignition data in the radiation furnace.

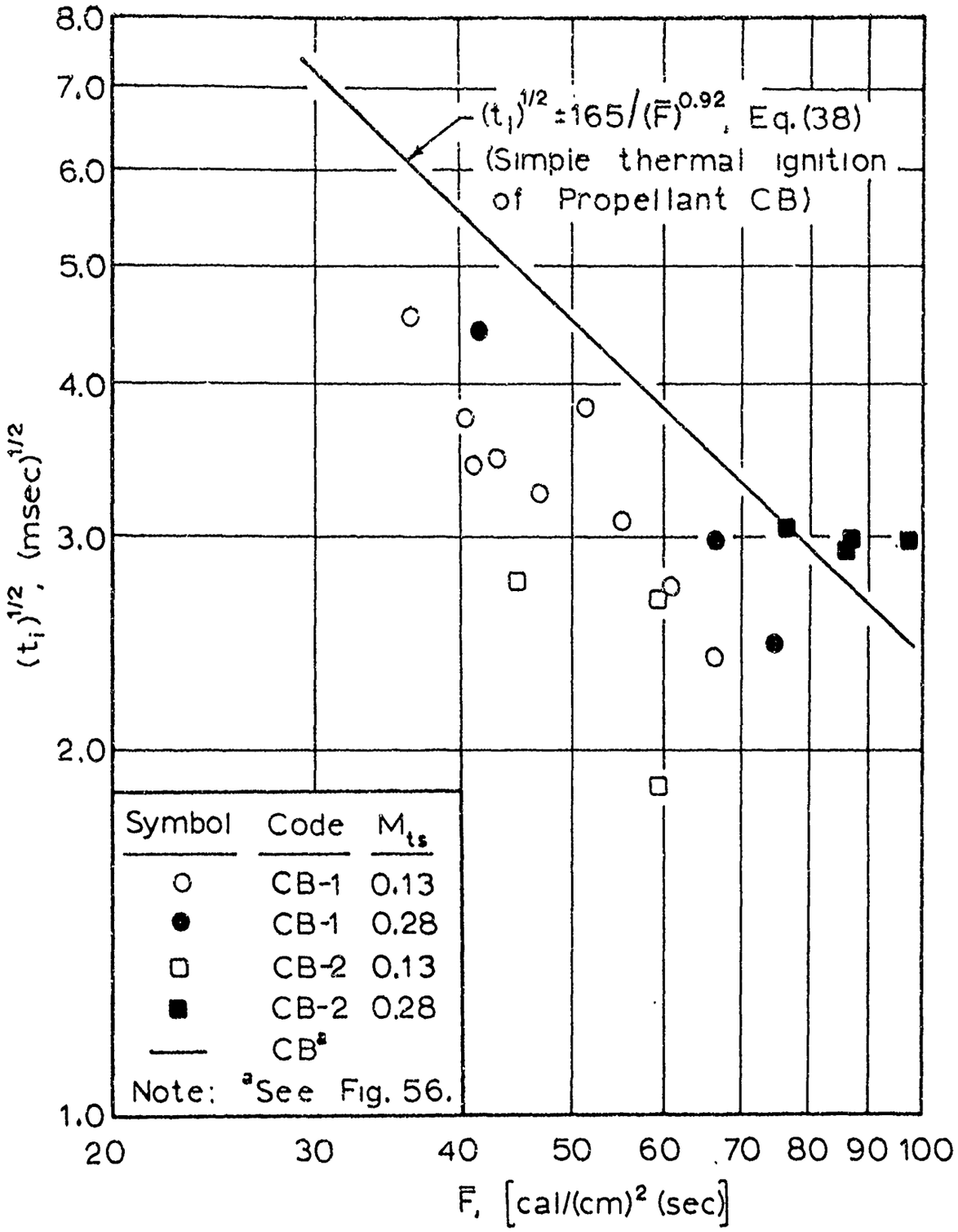

Figure 57

Ignition Data for Pressed Propellant CB in Nitrogen at Test-Gas Velocities of Mach 0.13 and Mach 0.28.

These ignition results on propellant CB with smooth and rough surfaces are consistent with the results obtained on cast propellants, and show that secondary ignition reactions can be important for raising the propellant surface temperature even though a volatile fuel is not present in the propellant. This observation suggests that the reactive species generated at the surface by two-dimensional heating of surface imperfections, which are subsequently involved in secondary reactions, are primarily ammonium perchlorate decomposition products.

Ignition of Propellant E

One additional propellant containing carbon black (Sterling VR from the Cabot Corporation) was pressed into pellets for ignition tests. Propellant E had the same composition as one of the pelleted compositions used by Evans [32] for ignition tests in the arc image furnace. Propellant E contained 4.5 per cent Sterling VR carbon black, 2.5 per cent copper chromite, and 93 per cent of ammonium perchlorate of two different particle sizes. See Table 2 for compositional details.

It was found that pellets of propellant E with very smooth surfaces were difficult to ignite by convective heat fluxes in the shock tube. Indications of ignition were only obtained during two of nine tests attempted with oxygen and nitrogen as the test gas. One pellet which had a relatively rough surface ignited in a rather short exposure time in nitrogen. The only other pellet which gave a photocell deflection was for a test in oxygen. The two data points obtained in these tests have been plotted in Figure 58. The straight line on the graph is

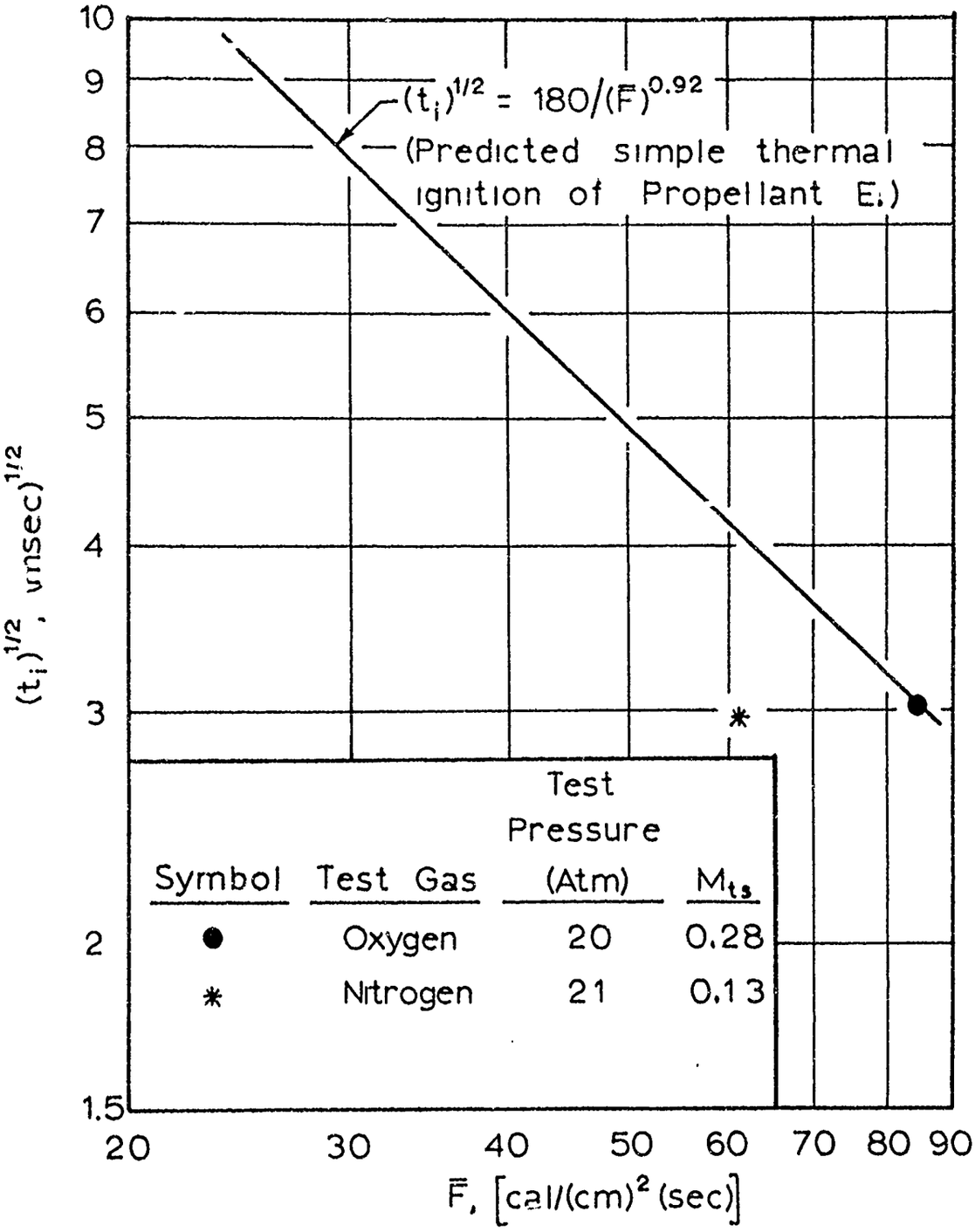

Figure 58

Ignition Data for Pressed-Oxidant Propellant E.

that estimated for simple thermal ignition for a pellet having the thermal properties of propellant E and the same key ignition reaction as propellant CB. This line was estimated with the aid of Equation (9) and experimental ignition data on propellant CB. It is interesting to note that the result for the one test in oxygen lies very close to the predicted line. Since additional data could not be obtained on propellant E, ignition results are not compared to those of Evans on a propellant of the same composition in the arc image furnace.

Pressed Propellants Containing Paraformaldehyde Fuel (Propellant D)

This propellant, except for the type fuel, had the same composition as propellant CB. Paraformaldehyde was selected as the fuel for this propellant because of its low sublimation temperature. Paraformaldehyde has a sublimation pressure of one atmosphere at 120°C. If the fuel in the propellant is important in the ignition process, it would be expected that a highly volatile fuel would greatly increase the ignitability of a given propellant system.

Ignition data obtained from tests on pellets of propellant D are given in Figure 59. Pellets were either pressed or bonded into the sample holders. It was found that pressing of pellets into the holders produced chipping at the edges which resulted in early ignition. When samples were bonded into sample holders and surfaces were finished with a fine silicon-carbide paper, ignition times were in good agreement with data for propellant CB-2 containing carbon black. It was assumed for purposes of analyzing ignition data that the thermophysical

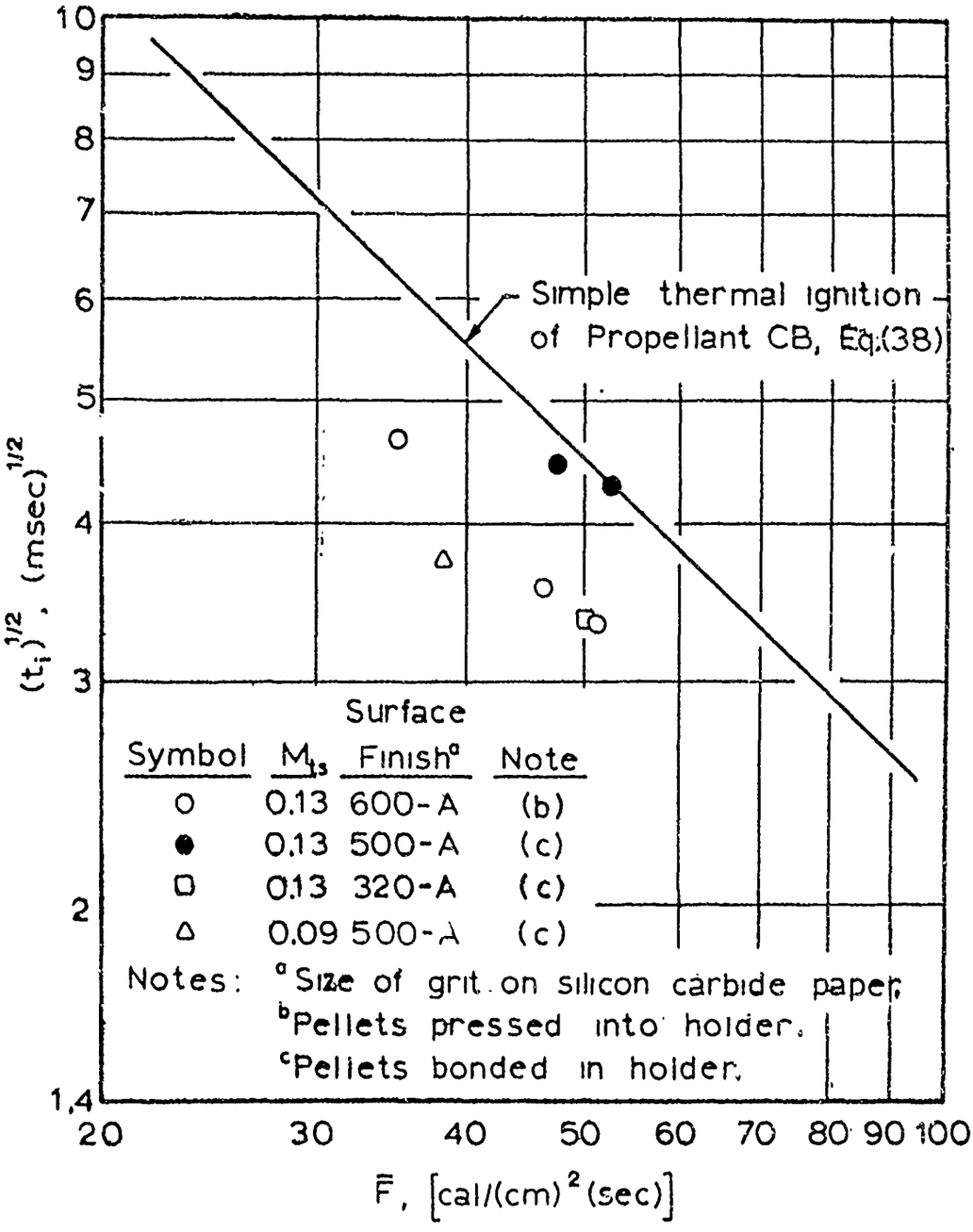

Figure 59

Ignition Data for Pressed Propellant D (with Paraformaldehyde Fuel) in Nitrogen.

properties for pellets of propellant D were the same as those for propellant CB.

The ignition results on Propellant D when compared to those for pressed propellant CB and cast propellant F show that the type of fuel used has no apparent effect on the ignition characteristics of propellants containing ammonium perchlorate oxidizer. This evidence further supports the conclusion arrived at earlier that the low-temperature, exothermic decomposition of ammonium perchlorate is the key reaction in the ignition process.

IGNITION OF EXTENDED-PHASE PROPELLANTS

This study on extended-phase propellants was undertaken to investigate the role of ingredients in the ignition process. It appeared from other work that if the polymer and ammonium perchlorate could be segregated into extended phases in a propellant system, it would be possible to obtain information on their respective contributions to the ignition process.

For preliminary studies, samples were prepared by bonding a half-cylinder of pressed ammonium perchlorate into the sample holder and then filling the remainder of the free volume with uncured propellant binder. Figure 60a shows a photomicrograph of a propellant sample prepared in this manner. Other samples were prepared by drilling small holes in the face of a mounted pellet and then filling the holes with uncured polymer (see Figure 60c). Some samples were prepared by placing the polymer directly on the surface of the pellet. This was done by placing a small drop of polymer at one or more locations on

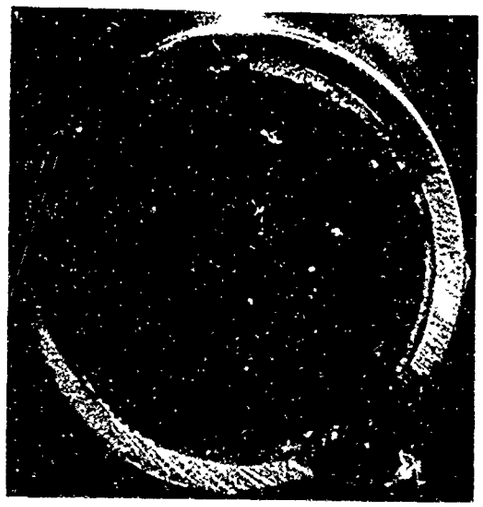

a. Before Test.

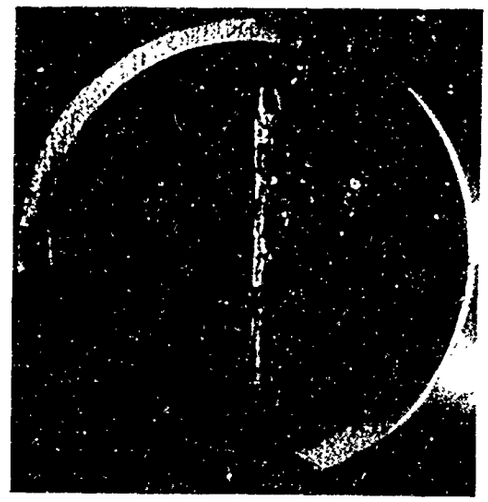

b. After Test.

c. Before Test.

d. After Test.

Figure 60

Photomicrographs (5X) of Surfaces on Extended-Phase Propellants. Gas Flow Across Surface was from Left to Right. Samples were prepared from Cylinders of Pressed Propellant B and F-Propellant Binder. Photomicrographs a and b are for Run No. 41-20-3. Photomicrographs c and d are for Run No. 41-25-5.

surface, or by diluting the polymer with a solvent and painting a thin coat on the face of the pellet. When curable polymers were used, samples were cured at 80°C for seven days. Information on sample preparation and results of ignition tests on these propellants are summarized in Table 16.

For ignition tests on samples made from half-cylinders of pressed oxidant, precautions were taken to ensure proper alignment of samples in the test section so that effects of gas flow could be ascertained. No special precautions were taken to align samples prepared by different methods in the test section, but the direction of flow of the hot gas over the surface was always noted.

Two types of pressed oxidant, propellants A and B, were studied. Propellant A was pressed from pure ammonium perchlorate, and propellant B was pressed from a powder composed of 96 per cent ammonium perchlorate and 4 per cent copper chromite. When samples prepared from half-cylinders of propellant A and F-propellant binder were tested, small cracks appeared at the surface of the pellet, but no evidence of ignition was ever observed as monitored by a photocell, even though F-propellant binder contained 10 per cent of copper chromite. This result indicated that only catalysts in the oxidant phase affect propellant ignition. Samples prepared from pellets of propellant B with 4 per cent copper chromite were used for all subsequent tests. The polymers used in these tests were F-propellant binder, G-propellant binder, and Krylon brand acrylic resin.

One of the interesting features of shock tube tests on extended-phase propellants was that deflagration of propellants was always

extinguished either by the arrival of the reflected rarefaction wave or by the mixing of cold driver gas with the test gas. The recovered samples could then be examined microscopically to determine where deflagration was initiated. Photomicrographs of surfaces of two recovered samples are shown by Figure 60b and d.

All of the relevant information for ignition tests on extended-phase propellants, including a description of microscopic observations of propellant surfaces after the tests, is given in Table 16.

The results of this study showed that extended-phase propellants made from half-cylinders of pressed propellant B ignited more consistently and in shorter times when the hot, convective gases flowed over the polymer first. Under these test conditions, when ignition occurred, the pellet of pressed propellant always ignited at the polymer-pellet interface. From this location the deflagration wave spread downstream over the pellet surface. When the samples were rotated 180° so that hot gases passed over the pellet face first upon entering the test section, ignition never occurred at the pellet-polymer interface, but when the sample ignited, ignition always occurred at imperfections at the pellet surface or at the interface between the pellet and the epoxy resin bonding agent. For this test condition ignition times were always longer. For samples prepared by filling cavities in the face of the pellet with polymer or when small buttons of polymer were placed on the surface of the pellet, ignition occurred at the downstream polymer-pellet interface and then spread over the pellet surface. This is shown by the photomicrograph of Figure 60d.

The fact that ignition almost always started at the polymer-pellet interface when the hot gas flowed over the polymer first is consistent with results on cast propellants. Since the thermal properties of the polymer and binder are considerably different, the surface temperature of the pellet would be highest at the interface and ignition would be expected to occur at this location. A second reason that deflagration would be initiated at the interface is that it was impossible to produce a perfectly smooth transition between the polymer and the pellet. The slight discontinuity would provide a site for two-dimensional convective heating which would further increase the interface temperature.

Since ignition, as determined by microscopic examination of the extinguished propellant surface, never occurred at the interface when the perchlorate pellet was upstream, it appears that for this test condition simple thermal ignition of the ammonium perchlorate pellet is the controlling process. For this test condition the interface was not raised to the thermal ignition temperature of the pellet and deflagration was not initiated. On the other hand, for tests in which the polymer was upstream, ammonium perchlorate decomposition products generated at the interface are swept over the face of the pellet where exothermic, catalyzed surface reactions occurred among these decomposition products supplying additional energy to help raise the temperature of the pellet surface to its thermal ignition temperature.

It should be noted that no evidence of ignition was observed when pellets of pure ammonium perchlorate were used in extended-phase propellants, even though a smooth interface did not exist between the pellet and the polymer. Also, it was noted that the kind of polymer used had no observable effect on the ignition characteristics of extended-phase propellants. Three types of polymers were used: (1) G-propellant binder composed of 85 per cent polybutadine-acrylic acid copolymer and 15 per cent Epon 828; (2) F-propellant binder had the same ratio of polymeric ingredients, but contained 10 per cent copper chromite catalyst, which is an amount equivalent to that used in the F-propellant composition; and (3) Krylon acrylic resin which was painted on the propellant surface.

As a supplementary study on ignition of extended-phase propellants, high-speed motion pictures were taken of propellant surfaces during ignition tests. Because of the low luminosity of the surface reactions for this kind of propellant, it was difficult to follow the ignition and deflagration processes. The best details were observed for a system composed of a half-cylinder of propellant B with F-propellant binder. This run was made with the polymer upstream. As expected, deflagration was initiated at the pellet-polymer interface and then spread rapidly over the remainder of the pellet surface. The reaction wave which moved across the surface extinguished and then reinitiated several times by what appeared to be a diffusion flame at the polymer-pellet interface.

The results of this study indicate that the thermal decomposition of ammonium perchlorate is the key reaction in the ignition process

and that the binder-fuel does not actively participate in the ignition process, and only after thermal ignition of the ammonium perchlorate occurs do reactions involving the polymer become important.

CHAPTER VIII

CONCLUSIONS

Through an analysis of the results on propellant ignition obtained in the research for this thesis and the information available from previous studies on propellant ignition, it is now possible to arrive at some rather firm conclusions about the ignition process for ammonium perchlorate-oxidized, composite propellants.

1. Ammonium perchlorate, composite propellants undergo ignition through a simple thermal process in which the temperature at the surface of the solid phase determines the ignition characteristics of the propellant. The slow process in ignition is the heating of the propellant surface to its thermal ignition temperature.

   Thermal Ignition Theory Predicts: Ignition of the propellant occurs when the solid, surface temperature reaches the level at which "boot-strapping" exothermic reactions supply heat flux at the surface of a level greater than that supplied externally. Furthermore, the ignition time for a given propellant, subjected to external heating, is a function only of the applied heat flux, $\bar{F}$, the initial propellant temperature, T_o, and the kinetics of the key ignition reaction, Equation (9). Thermal ignition theory says that $\ell n\ (t_i)$ is linear in $\ell n\ (\bar{F})$, and the slope of the line which represents ignition data on a

plot of $\ell n\ (\bar{F})$ versus $\ell n\ (t_i)^{1/2}$ is simply related to the activation energy of the key ignition reaction. This ignition process has been defined as simple thermal ignition in this work.

Experimental Data Show: Ignition data for cast propellants with a PBAA binder-fuel and catalyzed with 2 per cent copper chromite correlate with a single t_i, $\bar{F}$ relationship

$$t_i\ (\bar{F})^{1.84} = 28.94 \qquad (24)$$

(where t_i is in seconds and $\bar{F}$ has the units of cal/(cm)^2(sec); for an initial, uniform propellant temperature of about 300°K) for low radiant heat fluxes, $\bar{F}$ in the range of 1 to 13 cal/(cm)^2 (sec); and also with the same relationship at higher convective heat fluxes, $\bar{F}$ in the range of 70 to 160 cal/(cm)^2(sec), provided (1) the gas velocity across the propellant surface is greater than about 400 m/(sec) or (2) the surface is smooth (surface roughness less than about 5 microns). Similar t_i, $\bar{F}$ relationships with a (t_i) dependence on $\bar{F}$ with an exponent of -1.84 apply for uncatalyzed, cast propellant at low radiant heat fluxes, and for pressed propellant of carbon black, ammonium perchlorate, and copper chromite at low radiant fluxes and at higher convective fluxes for pressed propellants with smooth surfaces. A single t_i, $\bar{F}$ relationship correlates data for all of these propellants at low radiant heat fluxes and high convective heat fluxes if the parameters are made dimensionless as suggested by thermal

ignition theory to account for different thermophysical properties and different values for the pre-exponential factor, B, defined by Equation (7). Ignition data for cast propellant G (uncatalyzed) and propellant F (catalyzed with 2 per cent copper chromite), and pressed propellant CB (with 2 per cent copper chromite) are plotted in the form of a dimensionless heat flux, $\ell n\ (\bar{F}^*)$, versus a dimensionless ignition time, $\ell n\ (t_i^*)^{1/2}$, in Figure 61. Data used for construction of this graph are tabulated in Table 17.

2. The key ignition reaction in the simple thermal ignition process involves only the ammonium perchlorate; fuel ingredients play a secondary role.

   Experimental Data Show: Application of thermal ignition theory to data for cast propellants with or without copper chromite for tests in which the propellant ignites by a simple thermal ignition process, i.e., at low radiant heat fluxes or at high convective heat fluxes for the conditions described in connection with the first conclusion, gives an activation energy of 30 kcal/(mole). The activation energy for the catalyzed or uncatalyzed, low-temperature, thermal decomposition of ammonium perchlorate has been found from independent experiments to be about 30 kcal/(mole). Also, ignition data for propellants with either a polymer-fuel or a non-volatile fuel of carbon black give the same activation energy. The fact that ignition data for propellants with

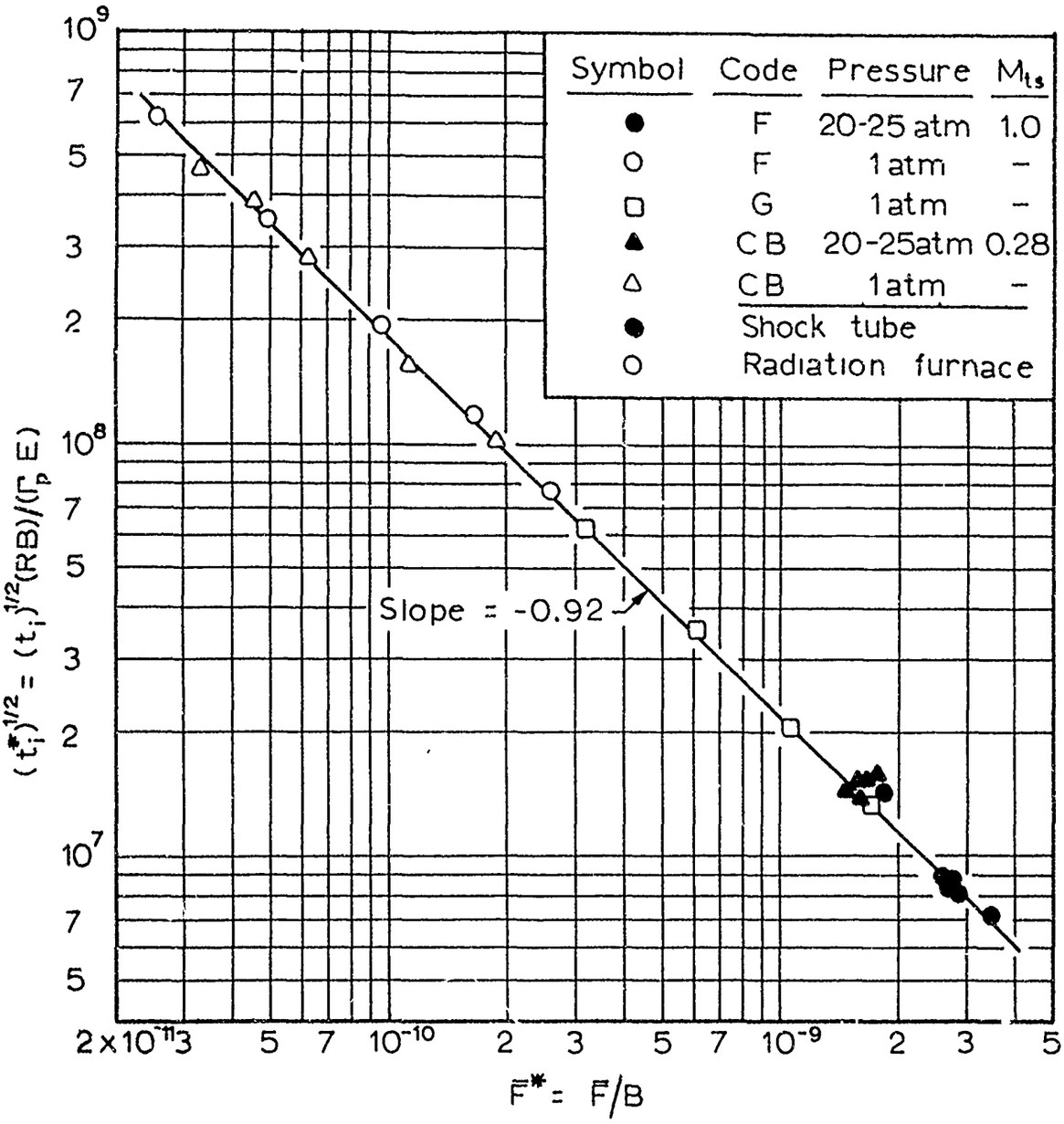

Figure 61

Ignition Data for Simple Thermal Ignition of Propellants F, G, and CB Plotted in Dimensionless Form as Suggested by Thermal Ignition Theory.

either a polymer-fuel or non-volatile, solid fuel correlate with a single t_i, $\bar{F}$ relationship if the parameters are put in dimensionless form is further support for this conclusion (see Figure 61).

3. The ignitability of propellants, which contain either copper chromite or iron oxide and have surface irregularities, is improved at low gas velocities by secondary ignition reactions at the surface which augment the externally applied heat flux from the hot, convective gases. A suitable environment for secondary ignition reactions, either gas-phase or heterogeneous-surface reactions, is established at the surface by two-dimensional heating of irregularities that produce localized hot spots on the surface. Reactive species are generated at these local areas of higher temperature and undergo further exothermic reactions at or near the surface. Environmental factors in convective heating experiments, such as (1) gas velocity across the propellant surface, (2) temperature of the convective gas, and (3) oxidizing species in the convective gas, affect only the secondary ignition reactions for propellants with rough surfaces and affect the over-all ignition process only to the extent that these secondary ignition reactions augment the heat flux supplied externally to the propellant surface.

   Experimental Data Show: When propellant surfaces are rough (irregularities greater than about 5 microns) ignition times increase at equivalent convective heat fluxes as the gas

velocity across the propellant surface is increased from low velocities, about 50 m/(sec), up to about 400 m/(sec). At higher gas velocities, irrespective of normal surface irregularities, ignition times are not affected by gas velocity and ignition times for propellants catalyzed with 2 per cent copper chromite are those defined by Equation (24) for simple thermal ignition. For propellants with smooth surfaces, ignition times are not altered by the velocity of the convective gas and ignition times are those expected for simple thermal ignition. The effect of a higher test-gas temperature at a given heat flux level is to reduce the ignition time for propellants with rough surfaces. Oxidizing species in the test gas affect only the ignition of propellants with rough surfaces. These observations suggest that: (1) at higher gas velocities reactive species generated by two-dimensional heating of surface irregularities are diluted and swept away by the fast-moving gas before they can react; (2) for propellants with smooth surfaces, the surface temperature of the propellant rises at a slower rate and the temperature distribution at the surface is more uniform, consequently no appreciable concentration of reactive species is produced at the surface; and (3) oxidizing species in the heating gas participate only in the secondary ignition process. Ignition studies on propellants with smooth surfaces with oxygen as the test gas have shown that heterogeneous attack

on the propellant surface by oxygen does not contribute importantly to the ignition process. When secondary ignition reactions contribute heat flux for heating the propellant surface, ignition data may still correlate by a simple t_i, $\bar{F}$ relationship, but the slope of the line that represents the data is no longer simply related to the activation energy of the key ignition reaction.

4. Additives used in propellants for enhancing the burning rate can affect the ignition process in two ways. Their contribution is dependent on the nature of the propellant surface and the kind of catalytic activity they exhibit. Additives can catalyze the decomposition of ammonium perchlorate which consequently alters the basic thermal ignition process, or they can catalyze both the decomposition of ammonium perchlorate and secondary ignition reactions, presumably at active sites on the surface. Copper chromite and ferric oxide affect both the simple thermal ignition and the secondary ignition process.

   Experimental Data Show: At low radiant heat fluxes, propellant F (with 2 per cent copper chromite) had shorter ignition times at equivalent heat fluxes than propellant G (without a catalyst). See Figure 4. The fact that catalyzed propellants with rough surfaces ignited in relatively short times in convective heating experiments, and propellant G did not ignite, indicates that ferric oxide and copper chromite also catalyze secondary ignition reactions.

CHAPTER IX

RECOMMENDATIONS FOR FURTHER RESEARCH

The following additional studies on propellant ignition are recommended:

1. A method should be developed for preparing very smooth surfaces on cast propellants containing large particles of ammonium perchlorate so that the effect of oxidizer particle size on the simple thermal ignition process can be more fully evaluated. This study could also provide information on the response of a heterogeneous propellant surface to high, externally applied heat fluxes. To obtain meaningful results, ammonium perchlorate particles must be exposed at the propellant surface.
2. The ignition of propellants with rough surfaces at low test-gas velocities, say 5 to 25 m/(sec), in both neutral and oxidizing gases should be investigated. Extremely low gas velocities could not be studied in the work for this thesis because of the test-period limitation in the shock-tube apparatus.
3. Ignition of propellants with rough surfaces at lower convective-gas temperatures, in the range of 600 to 700°K, should be studied to see if secondary ignition reactions are still important. This study could provide information on the nature of the secondary ignition process.

4. Further work is required to determine the effect of catalysts on the simple thermal ignition process. Uncatalyzed ammonium perchlorate propellants could not be ignited in the shock tube because of the test-period limitation. Uncatalyzed propellants should be thoroughly studied in convective heating experiments to provide data which can be compared to results obtained in radiant heating experiments and to those on catalyzed ammonium perchlorate propellants obtained in the research for this thesis. Both combustion and ammonium perchlorate decomposition catalysts should be evaluated further to study their effect on the ignition process. It would be of interest to obtain data on both cast and pressed propellants in these studies.

5. Ignition data are needed on the same propellant from both radiant and convective heating experiments at high heat fluxes for a wide range of test pressures. Initial studies should be performed on propellants containing carbon black or on propellant samples coated with a thin film of carbon black to ensure absorption of all radiant energy at the propellant surface.

6. To obtain more information on the nature of secondary ignition reactions associated with the ignition of propellants with rough surfaces, gas-phase combustion catalysts should be added in small concentrations to the test gas.

7. Measurements of propellant surface temperature during ignition experiments could reveal additional information about the ignition process. Measurements should be made on propellants with both rough and smooth surfaces.
8. The propellant ignition process should be photographed at low film speeds to see if luminous secondary ignition reactions are visible at the surface before a combustion flame appears. The shock tube would be a useful tool for this work because there would be no background radiation.
9. More realistic polymer-rich surfaces should be looked at, with an attempt to simulate the kind of polymer-rich surface that is formed when uncured propellant is cast around a mandrel. The distribution of oxidizer particles in the surface layers should be examined and the information used for calculating heat flux at the surface of ammonium perchlorate particles during ignition runs so that the experimental data can be evaluated with respect to thermal ignition theory.
10. An obvious extension of the work described in this thesis would be a study on the ignition of propellants containing high-energy, metal fuels.

LIST OF REFERENCES

1. Allen, H., Jr. and Pinns, M. L., "Relative ignitability of typical solid propellants with chlorine trifluoride," NASA TN D-1533 (1963).

2. Altman, D. and Grant, A. F., Jr., "Thermal theory of solid-propellant ignition by hot wires," Fourth Symposium (International) on Combustion (Williams and Wilkins Co., Baltimore, Md., 1953), pp. 158-161.

3. Anderson, R., Brown, R. S., and Shannon, L. J., "Ignition theory of solid propellants," AIAA Preprint No. 64-156 (January 1964).

4. Anderson, R., Brown, R. S., Thompson, G. T., and Ebeling, R. W., "Theory of hypergolic ignition of solid propellants," AIAA Preprint No. 63-514 (December 1963).

5. Arden, E. A., Powling, J., and Smith, W. A. W., "Observations on the burning of ammonium perchlorate," Combust. Flame, 6, 21-33 (1962).

6. Baer, A. D., "Ignition of composite rocket propellants," unpublished Ph.D. thesis, University of Utah, Department of Chemical Engineering (Salt Lake City, June 1959).

7. Baer, A. D., Personal communication, University of Utah, Salt Lake City, Utah (1964)

8. Baer, A. D., and Ryan, N. W., "Ignition of composite propellants by low radiant fluxes," AIAA J. 3, 884-889 (1965).

9. Baer, A. D., Ryan, N. W., and Salt, D. L., "Propellant ignition by high convective heat fluxes," Progress in Astronautics and Rocketry: Vol. 1. Solid Propellant Rocket Research, Edited by M. Summerfield (Academic Press, New York, 1960), pp. 653-672.

10. Bastress, E. K., Allan, D. S., and Richardson, D. L., "Solid propellant ignition studies, Arthur D. Little, Inc., Air Force Rocket Research Laboratories, Edwards AFB, Calif., Technical Documentary Report No. RPL-TDR-64-65, Final Report (October 1964), CONFIDENTIAL.

11. Beckstead, M. W., "Non-acoustic combustion instability of solid propellants," unpublished Ph.D. thesis, University of Utah, Department of Chemical Engineering (Salt Lake City, June 1965).

12. Bernstein, L., "Tabulated solutions of equilibrium gas properties behind the incident and reflected normal shock-wave in a shock tube: I. Nitrogen, II. Oxygen," Ministry of Aviation (Great Britain) Aeronautical Research Council Current Paper No. 626 (1963).

13. Beyer, R. B. and Fishman, N., "Solid propellant ignition studies with high flux radiant energy as a thermal source," Progress in Astronautics and Rocketry: Vol. I. Solid Propellant Research, Edited by M. Summerfield (Academic Press, New York, 1960), pp. 673-692.

14. Bircumshaw, L. L. and Newman, B. H., "The thermal decomposition of ammonium perchlorate: I. Introduction, experimental analysis of gaseous products, and thermal decomposition experiments," Proc. Roy. Soc. (London) Ser. A 227, 115-132 (1954).

15. Bircumshaw, L. L. and Newman, B. H., "The thermal decomposition of ammonium perchlorate: II. The kinetics of decomposition, the effect of particle size, and discussion of results," Proc. Roy. Soc. (London) Ser. A. 227, 228-241 (1954).

16. Boelter, L. M. K., Denison, H. G., Guibert, A. G., and Morrin, E. H., "An investigation of aircraft heaters: X. Measured and predicted performance of a fluted-type exhaust gas and air heat exchanger," NACA Wartime Report, ARR (WR W-16) (March 1943).

17. Boelter, L. M. K., Young, G., and Iverson, H. W., "An investigation of aircraft heaters: XXVII. Distribution of heat-transfer rate in the entrance section of a circular tube," NACA TN 1451 (July 1948).

18. Bogdan, L., "Thermal and electrical properties of thin-film resistance gages used for heat transfer measurements," AIAA J. 1, 2172-2173 (1963); also "High-temperature, thin-film resistance thermometers for heat transfer measurement," NASA CR-26 (1964).

19. Bohon, R. L., "Differential thermal analysis of explosives and propellants under controlled atmospheres," Anal. Chem. 33, 1451-1453 (1961).

20. Bradeley, J. N., Shock Waves in Chemistry and Physics (John Wiley and Sons, Inc., New York, 1962).

21. Cannon, W. A. and Welling, C. E., "Catalytic oxidation of automotive exhausts, laboratory evaluation of catalysts," Ind. Eng. Chem., Prod. Res. Develop. 1, 152-156 (1962).

22. Carslaw, H. S. and Jaeger, J. C., Conduction of Heat in Solids, 2nd Ed. (Oxford University Press, London, 1959).

23. Cheng, J., Personal communication, University of Utah, Salt Lake City, Utah (1964).

24. Churchill, S. W., Kruggel, R. W., and Brier, J. C., "Ignition of solid propellants by forced convection," Am. Inst. Chem. Eng. J. 2, 568-571 (1956).

25. Coates, R. L., "A quantitative experimental study of the oscillatory combustion of solid rocket propellants," unpublished Ph.D. thesis, University of Utah, Department of Chemical Engineering (Salt Lake City, August 1962).

26. Copper, J.A., "Experimental investigation of the equilibrium interface technique," Phys. Fluids 5, 844-849 (1962).

27. Cummings, G. A. McD., and Hall, A. R., "Perchloric acid flames: I. Premixed flames with methane and other fuels," Tenth Symposium (International) on Combustion (The Combustion Institute, Pittsburgh, 1965), pp. 1365-1372.

28. Davies, V. C. and Al-Arabi, M., "Heat transfer between tubes and a fluid flowing through them with varying degrees of turbulence due to entrance conditions," Inst. Mech. Eng. (London) 169, 993-1006 (1955).

29. Donaldson, A. B., "Flame extinction of solid propellants," unpublished Master's thesis, University of Utah, Department of Chemical Engineering (Salt Lake City, Utah, June 1965).

30. Dryden, H. L., "Transition from laminar to turbulent flow," High Speed Aerodynamics and Jet Propulsion: Vol. 5. Turbulent Flow and Heat Transfer, Edited by C. C. Lin (Princeton University Press, Princeton, 1959), pp. 3-74.

31. Dryden, H. L., Murnaghan, F. D., and Bateman, H., Hydrodynamics (Dover Publications, Inc., New York, 1956).

32. Evans, M. W., Beyer, R. B., and McCulley, L., "Initiation of deflagration waves at the surfaces of ammonium perchlorate-copper chromite-carbon pellets," J. Chem. Phys. 40, 2431-2438 (1964).

33. Francl, J. and Kingery, W. D., "Thermal conductivity: IV. Apparatus for determining thermal conductivity by a comparative method (Data for Pb, Al_2O_3, BeO, and MgO)," J. Am. Ceram. Soc. 37, 80-84 (1954).

34. Frazer, J. H. and Hicks, B. L., "Thermal theory of ignition of solid propellants," J. Phys. Colloid Chem. 54, 872-876 (1950).

35. Furukawa, G. T., Douglas, T. B., McCosky, R. E., and Ginnings, D. C., "Thermal properties of aluminum oxide from 0 to 1200°K," J. Res. Nat. Bur. S. 57, 67-82 (1956).

36. Galway, A. K. and Jacobs, P. W. M., "The thermal decomposition of ammonium perchlorate in the presence of manganese dioxide," Trans. Faraday Soc. 55, 1165-1172 (1959).

37. Galway, A. K. and Jacobs, P. W. M., "The thermal decomposition of ammonium perchlorate at low temperatures," Proc. Roy. Soc. (London) Ser. A 254, 455-469 (1960).

38. Galway, A. K. and Jacobs, P. W. M., "The thermal decomposition of ammonium perchlorate in the presence of carbon," Trans. Faraday Soc. 56, 581-590 (1960).

39. Gorring, R. L. and Churchill, S. W., "Thermal conductivity of heterogeneous materials," Chem. Eng. Progr. 57, 53-59 (July 1961).

40. Grant, E. H., Jr., Lancaster, R. W., Wenograd, J., and Summerfield, M., "A study of the ignition of solid propellants in a small rocket motor," AIAA Preprint No. 64-153 (January 1964).

41. Grant, E. H., Jr., Wenograd, J., and Summerfield, M., "Research on solid propellant ignitability and igniter characteristics," Aeronautical Engineering Report No. 662, Department of Aeronautical Engineering, Princeton University, Final Technical Report under Air Force Contract AF-AFOSR-62-91 (October 1963).

42. Hartunian, R. A. and Varwig, R. L., "On thin-film heat transfer measurements in shock tubes and shock tunnels," Phys. Fluids 5, 169-174 (1962).

43. Hermance, C E., Shinnar, R., Wenograd, J., and Summerfield, M., "Solid propellant ignition studies: ignition of the reaction field adjacent to the surface of a solid propellant," Aeronautical Engineering Report No. 674, Department of Aerospace and Mechanical Sciences, Princeton University, Final Technical Report under Air Force Grant AF-AFOSR-92-63 (December 1963).

44. Hermoni (Makovky), A. and Salmon, A., "The catalytic decomposition of ammonium perchlorate," Eighth Symposium (International) on Combustion (Williams and Wilkins Co., Baltimore, Md., 1962), pp. 656-662.

45. Hermoni (Makovky), A. and Salmon, A., "The catalytic decomposition of ammonium perchlorate in the gaseous phase," Israel J. Chem. 1, 313 (1963).

46. Hicks, B. L., "Theory of ignition considered as a thermal reaction," J. Chem. Phys. 22, 414-429 (1954).

47. Iverson, H. W., "Variation of the point unit thermal conductance on the entrance to tubes for a fluid flowing turbulently," unpublished Master's thesis, University of California (Berkeley, 1943). (Original thesis not examined, information abstracted from NACA TN 1451).

48. Jacobs, P. W. M. and Kureishy, A. R. T., "Thermal ignition in the system ammonium perchlorate-cuprous oxide," J. Chem. Soc., 556-561 (1962).

49. Jacobs, P. W. M. and Kureishy, A. R.T., "The effect of additives on the thermal decomposition of ammonium perchlorate," Eighth Symposium (International) on Combustion (Williams and Wilkins Co., Baltimore, Md., 1962), pp. 672-677.

50. Junkhan, G. H., "The effects of free-stream turbulence on heat transfer from a flat-plate with a pressure gradient," unpublished Ph.D. thesis, Department of Mechanical Engineering, Iowa State University of Science and Technology (Ames, 1964).

51. Keller, J. A., Baer, A. D., and Ryan, N. W., "The ignition of composite propellants by hot gases," Western States Section of the Combustion Institute Paper, WSS/CI Paper 64-27 (October 1964).

52. Keller, J. A. and Ryan, N. W., Measurement of heat flux from initiators for solid propellants," ARS J. 31, 1375-1379 (1961).

53. Kestin, J., Maeder, P. F., and Wang, H. E., "Influence of turbulence on transfer of heat from plates with and without a pressure gradient," Intern. J. Heat Mass Transfer 3, 133-154 (1961).

54. Kingery, W. D., "Thermal conductivity: XIV. Conductivity of multicomponent systems," J. Am. Ceram Soc. 42, 617-627 (1959).

55. Kling, R., Maman, A., and Brulard, J., "The kinetics of the ignition of composite solid propellants submitted to high heat fluxes," Rech. Aerosp. No. 103, 3-10 (1964).

56. Knuth, E. L., "Forced-convection heat transfers with time-dependent surface temperatures," AIAA J. 1, 1227-1229 (1963).

57. Kuratani, K., "Some studies on solid propellants: Part I. Kinetics of the thermal decomposition of ammonium perchlorate," Report No. 372, Aeronautical Research Institute, University of Tokyo (In English) (July 1962).

58. Lancaster, R. W. and Summerfield, M. "Experimental investigation of the ignition process of solid propellants in a practical motor configuration," Aeronautical Engineering Laboratory Report No. 548, Department of Aeronautical Engineering, Princeton University, Technical Report under Air Force Contract USAF-OSR AF 49(638)-960, AFOSR TN 836 (May 1961).

59. Latzko, H., "Heat transfer in a turbulent liquid or gas stream," NACA TM 1068 (1944). Trans. of Z. Angew. Math. Mech. (Germany) 1, 268-290 (1921).

60. Levy, J. B. and Friedman, R., "Further studies of pure ammonium perchlorate deflagration," Eighth Symposium (International) on Combustion (Williams and Wilkins Co., Baltimore, Md., 1962), pp. 663-672.

61. Lucks, C. F., Deem, H. W., and Wood, W. D., "Thermal properties of six glasses and two graphites," Bull. Am. Ceram. Soc. 39, 313-319 (1960).

62. Lucks, C. F., Matolich, J., and Van Velzor, J. A., "Experimental measurement of thermal conductivities, specific heats, and densities of metallic, transparent, and protective materials," Battelle Memorial Institute, U. S. Air Force Technical Report No. 6145 (Part III)(1954). (Original report not examined, information abstracted from J. Am. Ceram. Soc. 41, 461-463 (1958)).

63. Marrone, P. V. and Hartunian, R. A., "Thin-film thermometer measurements in partially ionized shock-tube flows," Phys. Fluids 2, 719-721 (1959)

64. Martinelli, R. C., Weinberg, E. B., Morrin, E. H., and Boelter, L. M. K., "An investigation of aircraft heaters: IV. Measured and predicted performance of longitudinally finned tubes," NACA Wartime Report, ARR(WR W-12) (October 1942).

65. McAlevy, R. F., III, "The ignition mechanism of composite solid propellants," unpublished Ph.D. thesis, Princeton University, Department of Aeronautical Engineering (Princeton, 1960).

66. McAlevy, R. F., III, Cowan, P. L., and Summerfield, M., "The mechanism of ignition of composite solid propellants by hot gases," Progress in Astronautics and Rocketry: Vol. 1. Solid Propellant Rocket Research. Edited by M. Summerfield (Academic Press, New York, 1960), pp. 623-652.

67. McCune, C. C., "Solid propellant ignition studies in a shock tube," unpublished Ph.D. thesis, University of Utah, Department of Chemical Engineering (Salt Lake City, August, 1961).

68. Mills, A. F., "Experimental investigation of turbulent heat transfer in the entrance region of a circular conduit," J. Mech. Eng. Sci. 4, 63-77 (1962).

69. Mitchell, R. C., "Flame spread on solid propellant," unpublished Ph.D. thesis, University of Utah, Department of Chemical Engineering (Salt Lake City, August 1963).

70. Mitchell, R. C. and Ryan, N. W., "Flame spread on solid propellant," AIAA Preprint No. 64-128 (January 1964).

71. Moore, J. and Sharp, D. E., "Note on the calculation of the effect of temperature on specific heat of glass," J. Am. Ceram. Soc. 41, 461-463 (1958).

72. Nanigian, J., Crookston, N. J., Jr., and Michelson, A., "Instantaneous heat transfer, pressure, and surface temperature characteristics of solid propellant igniters," U. S. Naval Propellant Plant Technical Memorandum Report No. 178 (April 1960).

73. Oberg. C. L., "Acoustic instability in propellant combustion," unpublished Ph.D. thesis, University of Utah, Department of Chemical Engineering (Salt Lake City, June 1965).

74. Palmer, H. B. and Knox, B. E., "Contact surface tailoring in a chemical shock tube," ARS J. 31, 826-828 (1961).

75. Plummer, W. A., Campbell, D. E., and Comstock, A. A., "Method of measurement of thermal diffusivity to 1000°C," J. Am. Ceram. Soc. 45, 310-316 (1962).

76. Prandtl, L. "The mechanics of viscous fluids," Aerodynamic Theory, Edited by G. W. F. Durand (Julius Springer, Berlin, 1935), Vol. 3, pp. 168-171. (Original article not examined, information abstracted from NACA TN 1451.)

77. Price, E. W., Bradley, H. H., Jr., Hightower, J. D., and Fleming, R. O., Jr., "Ignition of solid propellants," AIAA Preprint No. 64-120 (January 1964).

78. Roth, J. F. and Watchell, C. P., "Heat transfer and chemical kinetics in the ignition of solid propellants," Ind. Eng. Chem., Fundamentals 1, 62-67 (1962).

79. Rudinger, G., "Effect of boundary layer growth in a shock tube on shock reflection from a closed end," Phys. Fluids 4, 1463-1473 (1961).

80. Ryan, N. W., Baer, A. D., Keller, J. A., and Mitchell, R. C., "Ignition and combustion of solid propellants," Department of Chemical Engineering, University of Utah, Final Technical Report under Air Force Contract AF 49(638)-170, AFOSR 2225 (September 1961).

81. Ryan, N. W., Baer, A. D., Keller, J. A., and Mitchell, R. C., "Ignition and combustion of solid propellants," Department of Chemical Engineering, University of Utah, Technical Report under Air Force Grant 62-69, AFOSR 62-69 (September 1962).

82. Ryan, N. W., Baer, A. D., Keller, J. A., and Mitchell, R. C., "Ignition and combustion of solid propellants," Department of Chemical Engineering, University of Utah, Technical Report under Air Force Grant 40-63 AFOSR 40-63 (September 1963).

83. Ryan, N. W., Baer, A. D., and Keller, J. A., "Ignition and combustion of solid propellants," Department of Chemical Engineering, University of Utah, Technical Report under Air Force Grant 40-64, AFOSR 40-64 (September 1964).

84. Sharp, D. E. and Ginther, L. B., "Effect of composition and temperature on the specific heat of glass," J. Am. Ceram. Soc. 34 260-271 (1951).

85. Skinner, G. T., "Calibration of thin film gage backing materials," ARS J. 31, 671-672 (1961).

86. Solymosi, F. and Révész, L., "Catalysis of solid phase reactions, zinc oxide influenced thermal decomposition of ammonium perchlorate," Z. Anorg. Allgem. Chem. (In English) 322, 86-100 (1963).

87. Solymosi, F. and Révész, L., "Catalysis of reactions in the solid phase, thermal disintegration of ammonium perchlorate in the presence of ferric oxide," Foreign Technology Division, Air Force Systems Command, Document FTD-MT-63-244 (AD 605590). Trans. of Kinetika I. Kataliz (U.S.S.R.) 4, 88-96 (1963).

88. Strehlow, R. A. and Case, C. T., "Limitations of the reflected shock technique for studying fast chemical reactions," J. Chem. Phys. 35, 1506-1507 (1961).

89. Summerfield, M., Shinnar, R., Hermance, C. E., and Wenograd, J., "A critical review of recent research on the mechanism of ignition of solid propellants," Aeronautical Engineering Laboratory Report No. 661, Department of Aeronautical Engineering, Princeton University, Technical Report under Air Force Grant AF-AFOSR-92-63 (August 1963).

90. Thermophysical Properties Research Center, Data Book: Vol. 2. Nonmetallic Elements, Compounds, and Mixtures (Purdue University, Lafayette, Ind., December 1962), Table 2053.

91. Timmermans, J., Physico-Chemical Constants of Pure Organic Compounds (Elsevier Publishing Co., Inc., New York, 1950).

92. Vidal, R. J., "Model instrumentation techniques for heat transfer and force measurements in a hypersonic shock tunnel," Cornell Aeronautical Laboratory Report No. AD-917-A-1, WADC-TN-56-315, (AD 97238) (1956).

APPENDIX A

DESCRIPTION OF SHOCK-TUBE APPARATUS

For an ideal shock tube the process by which the gases are heated is illustrated by the x,t diagram in Figure 62. This diagram describes the gas-dynamic processes which follow the bursting of a diaphragm separating the low- and high-pressure gases in the shock tube. When the diaphragm bursts, the incident shock wave moves through the undisturbed gas in the driven end of the tube at a velocity which can be defined in terms of pressure ratio across the diaphragm and properties of the two gases. Meanwhile, the contact surface between the shock-heated gas and the cold, partially expanded driver gas follows the incident shock wave at the particle velocity of the gas. The incident shock wave is reflected at the closed end of the tube and moves back through the partially heated gas. The action of the reflected wave stagnates and again heats and compresses the gas in its path. It is this twice-heated gas behind the reflected shock wave that was used in these ignition studies. This corresponds to region 4 of the x,t diagram.

If shock tube conditions are carefully controlled, the movement of the contact surface between the hot and cold gases can be stabilized with respect to the shock tube. Under this condition the interface is said to be "matched" or tailored." The location of the stabilized contact surface in the driven end of the tube is dependent on the length of the driven end of the shock tube, strength of the incident shock wave, and properties of the driven gas. If the interface is matched,

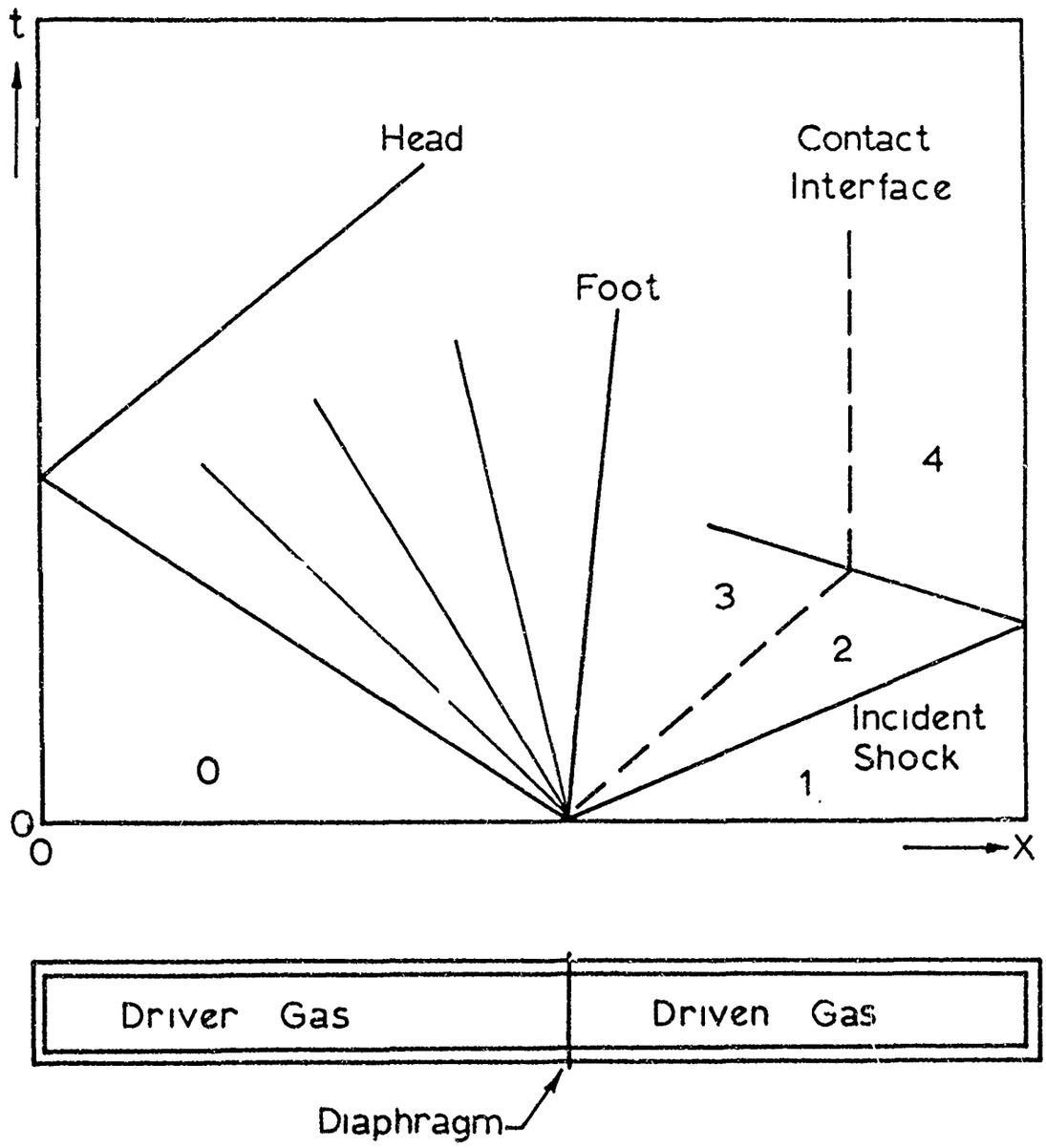

Figure 62

x,t Diagram of Wave Pattern in Shock Tube for Operation with "Matched" Interface

the reflected shock wave moves directly through the interface without interaction, thus providing a reservoir of relatively quiescent high-temperature gas.

When the diaphragm bursts and the incident shock moves into the driven end, the head of the isentropic rarefaction wave moves at the velocity of sound in the opposite direction through the high-pressure driver gas. The foot of the rarefaction wave will either follow the head of the wave or move in the opposite direction into the driven end at a much lower velocity. For a well-designed shock tube, it is the arrival of the reflected rarefaction wave at the test position that determines the length of time that shock-heated gases are available for test purposes.

ADAPTATION OF THE SHOCK TUBE FOR IGNITION STUDIES

The shock tube used in this work is the same one used by Baer [6, 9] for previous ignition studies on solid propellants. For this work the length of the driven section, the tube length from diaphragm position to entrance of the test section, was increased from 11.3 to 15.5 ft. and a new test section design was used. This shock tube has an inside diameter of 1 7/8 in., an outside diameter of 2 3/4 in., and a driver section with a length of 52.4 ft.

The driven section of the shock tube was modified at the end opposite the diaphragm position to accommodate the new test section. Figure 5 is a cutaway sketch of the driven end of the shock tube showing the position of the test section and Kistler, Model 601, quartz pressure pickup. The test section was inserted from the end

of the tube and held in position by a retaining flange. A more detailed sketch of the test section is given in Figure 6 showing the propellant sample holder, flow-control orifice plate, and quartz window.

The test section has a constant-area flow channel, 1.15-in. long by 0.500-in. wide by 0.250-in. high, with a bell-shaped entrance region. The bell-shaped entrance has a radius of curvature of 0.10 in. The center line of the window and propellant sample holder is 0.50 in. from the intersection of the bell-shaped entrance and the constant-area channel. The orifice plate is positioned on the downstream face of the test section with two small guide pins and held in place with two cap screws. A piece of vinyl or Teflon plastic tape served as the gasket between the orifice plate and the test section. Silicone grease was used between the quartz window and the test section to ensure a leak-proof seal. All other gas-tight seals were made with O-rings.

The orifice plates were made from 1.0-in. diameter steel disks with a thickness of 0.25 in. Three, critical-flow orifices with converging entrance sections were machined in each plate. Three orifices were used for flow control to give a more uniform flow pattern in the rectangular cross-section test channel. Each orifice plate was calibrated under critical flow conditions by the method described in Appendix G.

Figure 63 is a schematic representation of the shock tube pressurization system. The shock tube was designed for remote operation and the test cell was separated from the control room by a concrete wall containing a steel door. The shock tube was fabricated from several lengths of cold-drawn tubing. Each length was flanged and the seals between sections were made with O-rings.

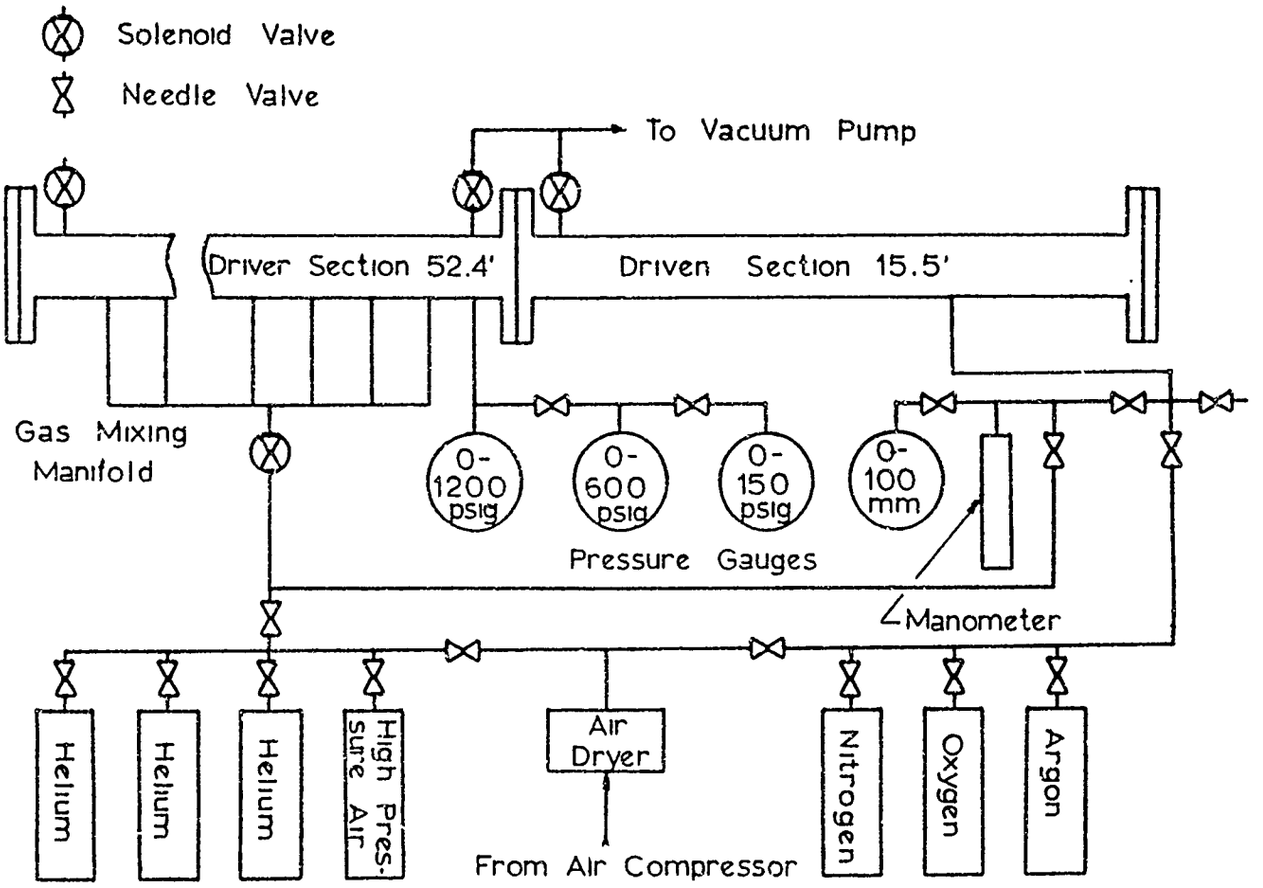

Figure 63

Pressurization System for Shock Tube.

FACTORS INVOLVED IN TEST SECTION DESIGN

Several factors were considered in the design of the test section used for ignition studies. First it was required that the flow channel have a rectangular cross-section. A flat wall facilitates the preparation of propellant samples and provides a uniform surface for observing ignition with high-speed photography. A second factor considered was the nature of the acoustic disturbance produced when the shock wave enters the test section. It is well known [20, 67] that the strength of the shock wave is increased upon entering a reduced cross-section channel. The reflection of this shock wave at the orifice plate produces a transient acoustic disturbance in the test section which decays rapidly in a short channel. The effect of channel length on the decay rate of this disturbance was studied by McCune [67]. A third consideration in the design of the test section was heat transfer to the wall. For hot gases entering a tube, convective heat transfer to the wall at the leading edge is much greater than it is several diameters downstream. Consequently, the test position was located very near the leading edge to take advantage of the higher heat transfer rate.

In terms of details of the test section design, critical tolerances were required on the test-section flow channel, heat flux gauges, and propellant sample holders to ensure reasonably flush mounting of heat flux gauges and propellant samples with test-section wall. The allowable tolerances on the length of heat flux gauges and propellant sample holders were $\pm$ 0.001 in. and $\pm$ 0.002 in., respectively. The average variation of the propellant surface from the flush mounted position was found to be about $\pm$ 30 microns, and that for the heat flux gauges about $\pm$ 15 microns. Although precautions were taken to ensure

flush mounting of propellant samples, it was found experimentally that ignition times for propellant samples mounted as much as 100 microns below the plane of the wall were in good agreement with those that were nearly flush with the wall.

DESCRIPTION OF SHOCK-TUBE INSTRUMENTS

The information which is needed from a shock tube run to characterize propellant ignition in terms of mean heat flux to the propellant surface is (1) the velocity of the incident shock wave, (2) pressure history in the shock tube near the test section, and (3) ignition time for the propellant. Other information needed for making calculations is obtained from initial shock-tube conditions and static measurements. Figure 64 shows the arrangement of the test instruments for an ignition run.

Thin-film resistance thermometers mounted flush with the shock-tube wall were used as shock sensors. The temperature rise of the shocked gases changes the resistance of the thin platinum film mounted on the flat surface of a pyrex cylinder. The temperature rise is detected as a change in emf across the platinum strip and the signal is amplified by a high-gain a-c amplifier. The amplified signal is used for starting or stopping a Berkeley, Model 7250 (10 microsecond), time-interval meter and for triggering the sweep of an oscilloscope. For the shock tube described by Figure 64, the first shock sensor was mounted 2.38 ft. from the diaphragm separating the high- and low-pressure sections of the tube. The signal from this sensor started both time-interval meters. A second and third sensor, 8.00 and 12.00 ft., respectively, downstream of the first were used for stopping the timers. The

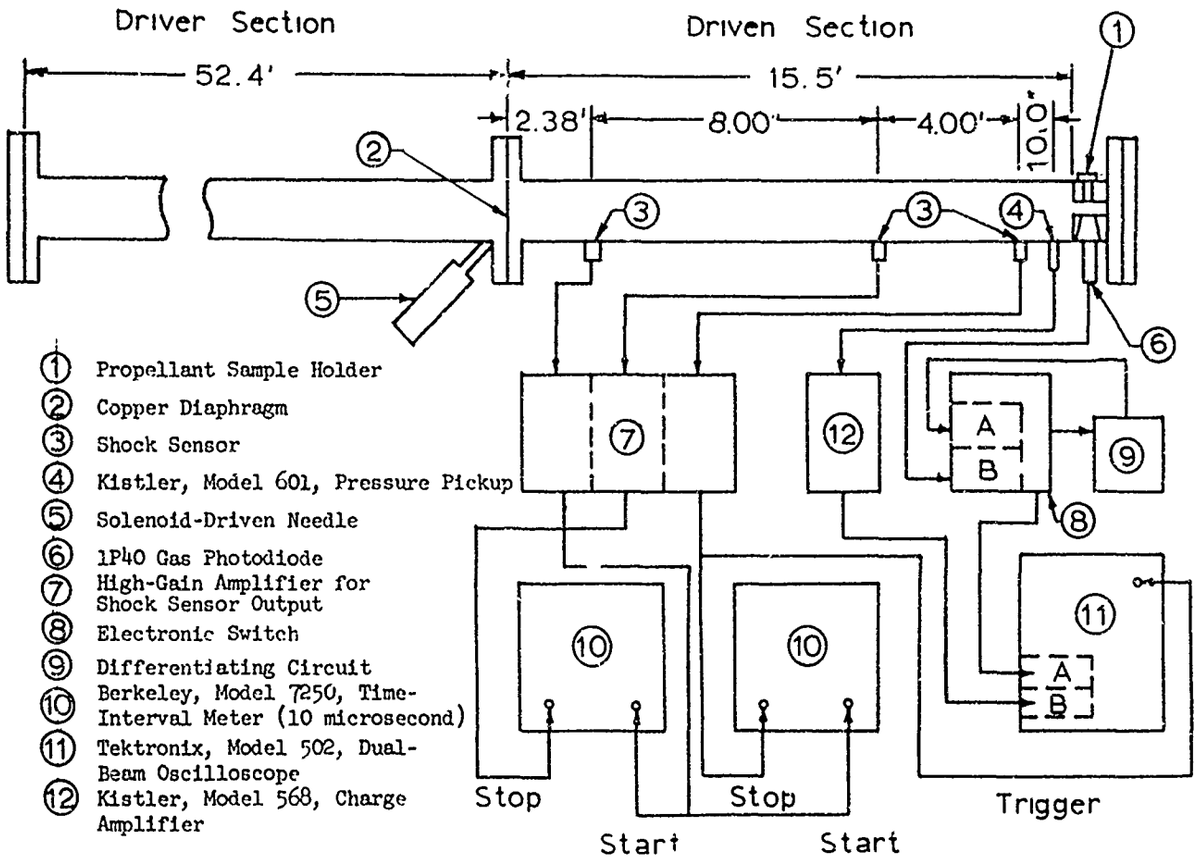

Figure 64

Wiring Diagram for Shock-Tube Instruments.

third sensor, only 13.6 in. from the test section also triggered the oscilloscope sweep. With this triggering scheme, shock-wave velocities were measured with a maximum error of ± 0.5 per cent. Further information on the manufacture and use of the resistance-thermometer shock sensor can be found in Reference 67.

For monitoring the pressure in the shock tube, a Kistler, Model 601, quartz pressure pickup in conjunction with a Model 568 charge amplifier, was used. The output signal from the charge amplifier was placed in one channel of a Tektronix, Model 502, dual-beam oscilloscope. The other oscilloscope channel was used for displaying the signal from a 1P40 gas photodiode used for ignition time measurements. The 1P40 photocell viewed the propellant surface through a window opposite the propellant sample position as shown in Figure 5. The 1P40 photocell has a response time of about 100 microseconds and has peak sensitivity to radiation in the infrared range at 8000 angstrom units. A direct signal from the photocell and the derivative of the signal were displayed on one beam of the oscilloscope. This was accomplished by passing the photocell signal through the A input of an electronic switch. The amplified output was differentiated by an RC circuit with a time constant of 100 microseconds. The differentiated signal was then returned to the B input of the electronic switch. Both of these signals, along with that from the pressure pickup, were displayed on the screen of the dual-beam oscilloscope (Tektronix 502) and recorded with a Polaroid Land camera. For many of the ignition runs, two dual-beam oscilloscopes were used with parallel circuits. One scope was

operated with a fast sweep rate for measuring ignition time and the second was used with a slower sweep rate for observing the behavior of the propellant burning after ignition.

For heat transfer measurements in the test section, the propellant sample holder was replaced with a heat flux gauge. For these runs only the temperature history of the heat flux gauge and pressure in the shock tube were monitored during runs. As for the igntion runs, signals from these sensors were displayed on the screen of a Model 502 oscilloscope and permanently recorded with a Polaroid camera.

APPENDIX B

EXPERIMENTAL PROCEDURE

To obtain the longest possible test period for the length of tube used, the shock tube was operated with a "matched" interface contact-surface in the driven section. This required careful control of initial shock-tube conditions.

In theory, it is possible to calculate from shock relations the required pressure ratio across the diaphragm and the compositions of the driver gas which will give the desired shock velocity in the driven gas selected. However, because of factors such as attenuation of the incident shock wave in the driven section, it is difficult to predict exactly the performance of a given shock tube without experimental characterization. In this work mixtures of helium and air were used as the driver gas. The driven gas was usually nitrogen; but air, oxygen, and argon were also used.

The normal procedure employed for making an ignition or heat transfer run in the shock tube was as follows:

1. The entire shock tube was flushed before each run with dry compressed air.
2. A copper diaphragm was then scribed and positioned between the driver and driven sections. At the same time the solenoid-driven diaphragm-bursting needle was repositioned.
3. A propellant sample was prepared and placed in the test section, and the end of the driven section was sealed to the atmosphere with a rubber stopper.

4. The driver section was partially pressurized.

5. The driven section was adjusted to the required pressure level. When gases other than air were used in the driven section, the driven section was evacuated to 10 mm absolute pressure and then refilled to atmospheric pressure. This operation was repeated three times for nitrogen, oxygen, and argon.

6. The pressure in the driver section was then slowly increased to the diaphragm burst pressure. (To ensure good mixing of driver gases, the gas entered the tube through 0.039-in. diameter holes drilled at 6-inch intervals in the tube wall.) Meanwhile, the triggering system for the oscilloscopes and time-interval meters was checked for proper functioning, and instruments were readied for recording data.

7. The diaphragm was burst and data were recorded.

When all systems were functioning properly, it was possible to complete a test in 20 minutes.

In addition to the normally followed procedure, special checks were made at regular intervals to ensure that all electronic instruments were operating properly. All electronic instruments were given an adequate warm-up period. The oscilloscopes were checked for vertical deflection against a calibrated signal each morning and one or two times during the day. At regular intervals the sweep rates of the oscilloscopes were compared with a crystal-controlled time calibrator. The time-interval meters were very reliable; however, elapsed time measurements were compared with signals from shock sensors by recording the signals

from the shock sensor via an oscilloscope and Polaroid camera. To ensure accuracy a signal from a time calibrator was superimposed on Polaroid recording of the shock sensor signals.

As mentioned previously, the Kistler, Model 601, pressure pickup and Model 568 charge amplifier were standardized against the dead-weight tester in millivolts output per psig.

For heat transfer tests it was necessary to adjust the heat flux gauge circuitry for ambient temperature changes during the day and then readjust vertical sensitivity of the oscilloscope to correspond to the heat flux gauge output. A description of the heat flux gauges is given in Appendix H.

The copper sheets used for diaphragm material were scribed by slowly moving a sharp-cornered machine tool across the sheet. The machine tool was mounted at a 45-degree angle, relative to the face of the copper sheet, on a slide which could be weighted to control the scribe depth in the copper sheet. It was found that relatively deep scribe marks were required to ensure consistent results and prevent fragmentation of the copper. With these precautions, diaphragms could be pressure burst within 5 psi of the desired pressure. For shock tube operation at 250 and 350 psig, a cold-rolled, annealed copper sheet 0.01-in. thick was used. Copper sheet with a thickness of 0.0075 in. was used for lower operating pressures.

The diaphragms were crimped around a plate with a square perforation and then positioned between the driver and driven sections of the shock tube. The perforated plate having diagonals of the same dimensions as the inside diameter of the tube was placed on the low-

pressure side of the diaphragm. The diaphragms were scribed so that the scribe marks matched the diagonals of the plate. The diaphragm and plate were held in position between two flanges, and during pressurization of the driver section the copper sheet expanded through the opening in the plate. The diaphragm was then ruptured by increasing the driver pressure a small amount or by striking it along a scribe mark with a solenoid-driven needle.

Both the driven and driver sections of the shock tube were cleaned frequently by pulling a damp cloth or one saturated with carbon tetrachloride through the tube with a nylon cord. The presence of a few dust particles in the driven gas did not interfere with photocell detection of ignition when nitrogen, air, or argon were used. However, with oxygen as the driven gas there was considerable deflection of the photocell signal produced by hot, incandescent dust particles immediately following the passage of the reflected shock wave. This contribution to the photocell signal lasted for only one or two milliseconds and did not preclude the determination of ignition time from oscilloscope recordings.

APPENDIX C

STUDIES FOR CHARACTERIZING SHOCK TUBE AND TEST SECTION

In order to assess quantitatively the rate of energy transfer to the propellant surface during ignition tests, it was first necessary to determine heat transfer to the test section wall in terms of shock parameters and flow rate of the convective gases. To provide this information, the following preliminary studies were conducted: (1) discharge coefficients were determined for flow-control orifices under critical flow conditions, (2) attenuation of the incident shock wave was measured so that properties of the shocked gases could be evaluated at the entrance to the test section, and (3) heat transfer to the test section wall at the sample position was measured for various shock-tube conditions.

CONTROL OF GAS VELOCITY THROUGH TEST SECTION

Heat transfer to the wall of the test section and therefore to the propellant surface under convective heating is controlled primarily by three variables: pressure, temperature, and velocity of the convective gases. The pressure and temperature of the convective gases are dependent on initial shock-tube conditions. However, in order to increase the versatility of the shock-tube apparatus and also to study the effect of gas velocity on propellant ignition, it was necessary to control the flow rate of the gas through the flow channel of the test section. For this purpose five different orifice plates were manufactured having flow areas ranging from 15 to 50 per cent of the area of

test-section flow channel. Each orifice plate had three, circular cross-section orifices with a converging entrance region. Three orifices were used, as shown by Figure 6, to improve the flow pattern in the test section.

Unless special precautions are taken in the design and manufacture of flow-control orifices, it is not possible to predict their flow characteristics with any degree of confidence. Furthermore, with three orifices close together in the plate some interference with gas flow would be expected. It was thus necessary to calibrate the orifice plates under conditions similar to those under which they would be used. A rarefaction tube was used for determining discharge coefficients for these orifices at pressures of 100 to 150 psig. A summary of results from this study is given by Table 18 and details of the experimental method employed are discussed in Appendix G.

ATTENUATION OF INCIDENT SHOCK WAVE

For calculating properties of the gases behind the reflected shock wave, it was necessary to know the strength of the incident shock wave as it reached the end of the tube. Because of viscous and heat transfer effects at the wall of the shock tube, the shock wave is attenuated as it moves through the driven section. The extent of this attenuation cannot be predicted exactly for a given shock tube, but can be easily measured.

Under normal shock-tube operation, measurement of the shock velocity was made by the arrangement shown in Figure 64. This provided a longer time interval for measurement when only two time-interval meters were available for use. To obtain data on attenuation, a

third time-interval meter was included and an additional shock sensor was placed in the shock-tube wall 4.00 ft. from the first. The circuitry was arranged so that each time-interval meter measured the average shock velocity over a 4.00-ft. section of the tube. From these data an average Mach number was obtained for positions 2.00, 6.00, and 10.00 ft. from the first shock sensor. The information from these measurements was put in the form shown by Figure 65, and the Mach number, M_E, at the end of the tube was determined by extrapolating these data to the end-wall, 13.13 ft. from the first shock detector. Converting the average values of Mach numbers over each station to local values and extrapolating the data via a quadratic equation gave, within experimental error, the same value for M_E as the extrapolation of average values. Each point on the graph of Figure 65 is an average of 15 to 40 individual measurements for different, initial shock-tube conditions. The maximum deviation of any single value from the average is less than 0.5 per cent. From these results it was possible to calculate M_E directly from the average Mach Number between stations 1 and 3, and 1 and 4. The Mach Number at the end of the tube for nitrogen, air, and argon driven gas can be represented by the following equations:

$$M_E = 0.933\ M_{13} \qquad \text{(C-1)}$$

$$M_E = 0.947\ M_{14} \qquad \text{(C-2)}$$

The subscripts refer to the positions of the shock sensors starting and stopping the timers.

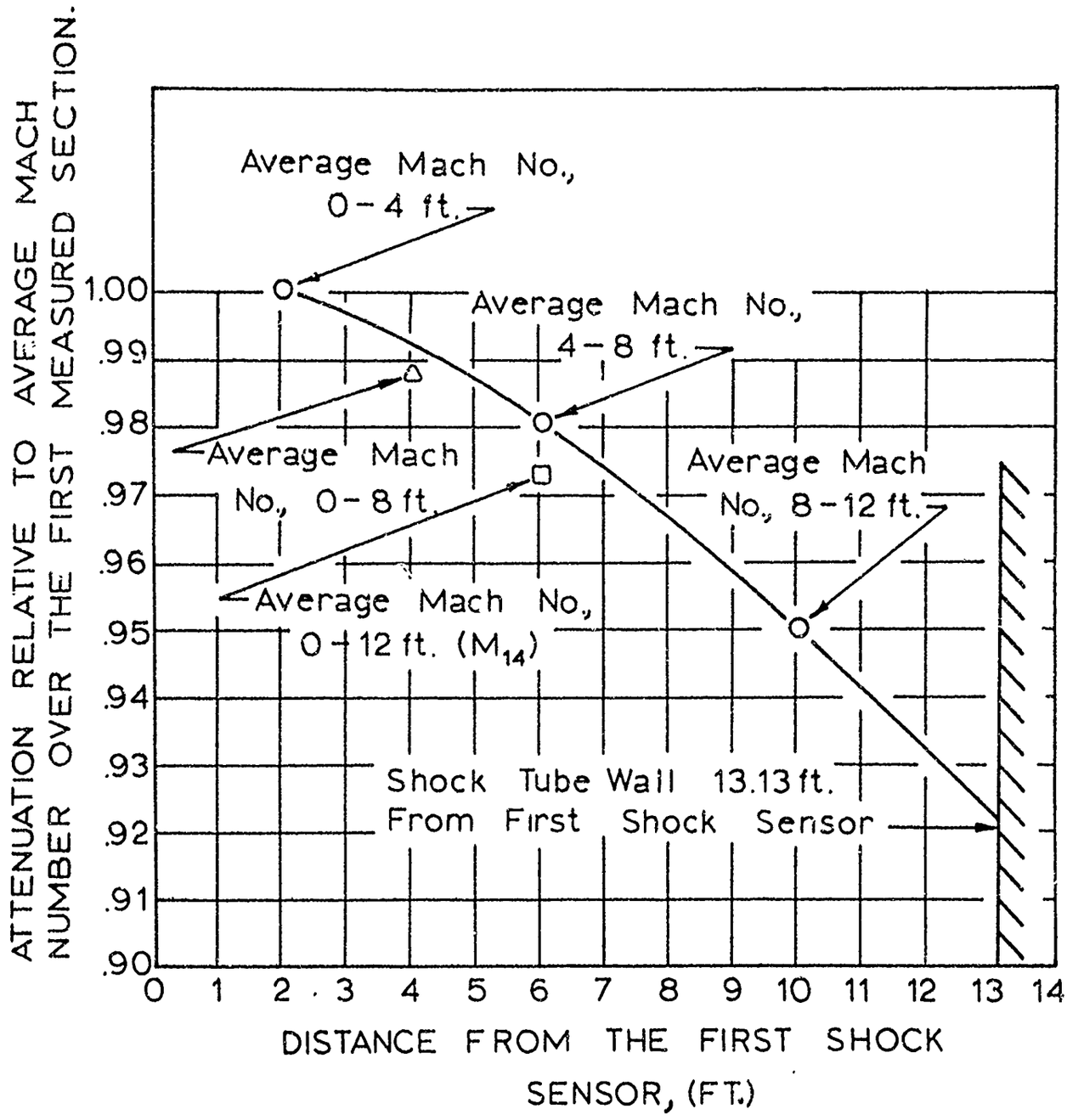

Figure 65

Attenuation of Incident Shock Wave in Air, Nirogen, or Argon.

It was found from this study that amount of attenuation of the incident shock wave was almost independent of Mach Number, driver gas pressure, and type of driven gas used.

HEAT TRANSFER TO WALL OF TEST SECTION

The heat transfer to the test-section wall at the test position was measured with heat flux gauges (thin-film platinum resistance thermometers bonded to a substrate of Pyrex 7740; Pyroceram 9608; or alumina, Alsimag 614. Liquid Bright Platinum, No. 05X, manufactured by the Hanovia Liquid Gold Division of Engelhard Industries, was used for preparing the resistance thermometers. The details of procedures used for manufacture and calibration of heat flux gauges are given in Appendix H. Figure 66 is a photograph of a heat flux gauge element and two assembled gauges. This type of heat flux gauge has a response time of a few microseconds [92] and faithfully records the temperature history at the surface of the substrate material. The experimentally measured temperature-time data were converted to heat flux at the gauge surface, or heat transfer coefficients were evaluated directly from temperature-time data through the application of unsteady-state heat transfer theory.

Nature of the Heat Transfer Problem

Heat transfer to the wall of the test-section flow channel can be compared to that for convective heat transfer to the wall in the entrance region of a tube. A reasonable assumption as to the nature of the gas flow in the entrance to the test section, for the experimental arrangement used in this work, is that the hot gases enter the

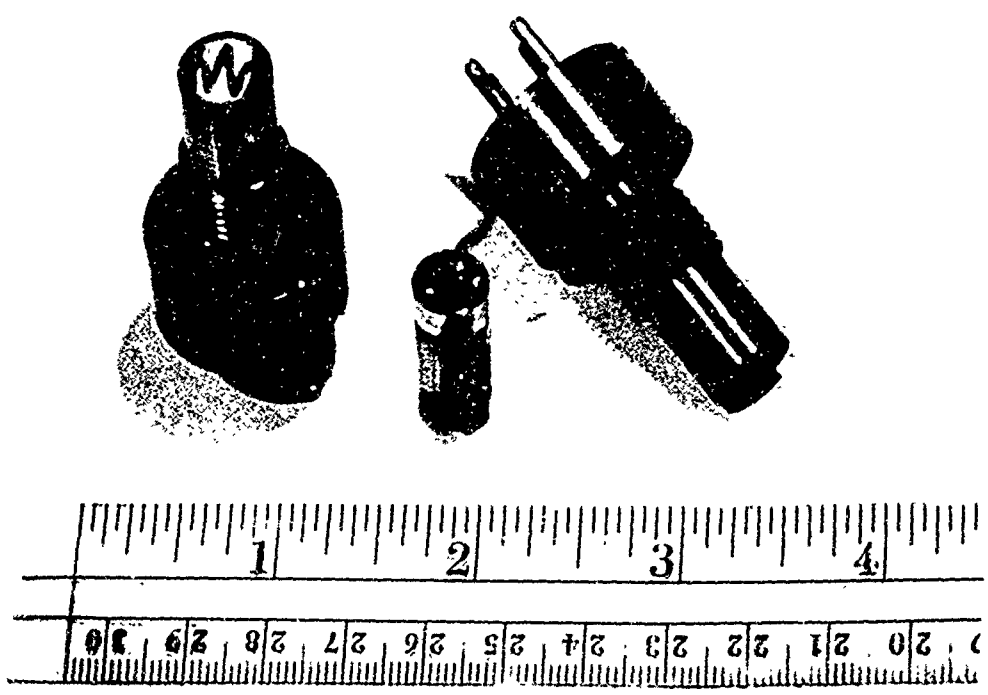

Figure 66

Photograph of Heat Flux Gauges. Assembled Gauges have Substrates of Alumina. Gauge Element in Foreground was Made of Pyrex 7740.

test section with a uniform velocity and temperature distribution, and that the boundary layer begins its development at the leading edge of the constant-area channel. For a bell-mouthed entrance the development of the boundary layer begins near the intersection of the bell-shaped entrance and the constant-area flow channel. For this flow condition, the heat transfer coefficient will be very large at the leading edge and will then decrease rapidly with distance downstream from the entrance region. At several tube diameters from the leading edge, the heat transfer coefficient takes on a constant value and no longer changes with distance. The form of the boundary layer at the wall in the entrance region is dependent on Reynolds number and the turbulence intensity in the free stream. The boundary layer at the wall can then be either a laminar, a turbulent, or a transition boundary layer, depending on the above factors. Since fluid flow and heat transfer to the wall in the entrance region are not well understood, it is not always possible to predict the heat transfer to the wall in this region without the aid of experimental data.

A number of analytical and experimental studies have been reported in the engineering literature for laminar and turbulent flow in entrance regions of tubes, but only cursory studies are reported for transition-region flow. Some of this earlier work that is related to the study conducted here is discussed in the following paragraphs.

Latzko [59] made the first theoretical analysis of turbulent heat transfer in the entrance region of a tube. The complex equations derived by Latzko for uniform velocity and temperature distribution at the inlet were simplified by Iverson [47] to the following form:

$$h_\ell = 0.0384\ G\ c\ \frac{1}{(Re_D)^{0.2214}}\ \left(\frac{D_H}{x}\right)^{0.1144} \qquad \text{(C-3)}$$

This equation applies for the entrance region where x/D_H is less than $(Re_D)^{0.25}$, where x is the distance from the leading edge. For this equation, fluid properties are evaluated at the local-mean, fluid temperature.

Martinelli [16, 64] approximated the heat transfer coefficient in the entrance region for turbulent flow by assuming that the flow in the entrance was similar to that along a flat plate until the boundary layer was fully developed. From this analysis, the local, turbulent heat transfer coefficient for heat transfer from high-temperature air in the entrance region for x/D_H ratios less 4.4 is:

$$h_\ell = 7.3 \times 10^{-4}\ \frac{(T_f)^{0.3}\ (G)^{0.8}}{(x)^{0.2}}\ [\text{Btu}/(\text{ft.})^2(\text{sec})(°\text{R})] \qquad \text{(C-4)}$$

Where G is the weight average mass flow rate, $lb/(ft.)^2(sec)$, and T_f is the film temperature, °R, and x is the distance from the leading edge, ft. The film temperature is defined as the average absolute temperature between the free stream and the wall. In this equation the combined temperature dependence for thermal conductivity, heat capacity, and viscosity of the air are accounted for by including the film temperature in the equation. Equation (C-3) can be simplified in a similar manner by considering the temperature dependence of the fluid properties.

Boelter, Young, and Iverson [17] studied experimentally steady-state heat transfer in the entrance region of a tube with different entrance configurations. They found for a bell-shaped entrance and turbulent flow with a uniform velocity and temperature distribution at the inlet that Equations (C-3) and (C-4) predicted within 10 per cent the heat transfer coefficient in the entrance region of the tube. To ensure the start of boundary layer development at the intersection between the bell-mouthed entrance and the uniform cross-section tube, a vent was placed at this intersection to bleed air from the boundary layer.

More recently, Mills [68] studied both laminar and turbulent flow with heat transfer in the inlet region of a tube downstream of a bell-mouthed entrance. Mills reported that for a condition of low free-stream turbulence, even for tube Reynolds numbers as high as 100,000, a laminar boundary layer formed at the inlet of the tube following a bell-mouthed entrance. This was followed by transition to a turbulent boundary layer at a critical Reynolds number of about 160,000, based on the distance from the leading edge. Even when free-stream turbulence was introduced by placing screens upstream of the heat transfer tube, a laminar boundary layer formed at the leading edge. Only when boundary layer trip-rings were placed at the leading edge was a completely turbulent boundary layer formed in the inlet region.

Except for heat transfer to rocket nozzles, where the cross-section changes with distance from the leading edge and extremely large Reynolds numbers are encountered, no thorough analysis has been made for unsteady-state convective heat transfer to inlet regions. Knuth [56]

has shown from theoretical considerations that for most applications unsteady-state, forced-convection heat transfer can be predicted to a good approximation by steady-state methods. This in part has been corroborated by the work of Baer [6] and McCune [67]. They found that experimental data for entrance-region heat transfer could be correlated by turbulent-flow heat transfer equations similar to Equations (C-3) and (C-4). The Iverson Equation (C-3) used by McCune predicted unsteady-state heat transfer coefficients within a few per cent of those obtained experimentally.

Measurement of Heat Transfer to the Test-Section Wall

From heat flux gauge measurements at the test-section wall, it was found that the heating process at the test position could be described in terms of transient heating of a semi-infinite solid through a constant, surface heat transfer coefficient. Temperature-time traces obtained from heat flux gauges showed, as was found by Baer [6] in earlier work, an initial, instantaneous temperature rise immediately behind the reflected shock which was related to the strength of the shock and to the pressure of the shock-heated gases. This temperature rise (ΔT_o) results from heat conduction from the stagnated, shock-heated gases.. This initial temperature jump due to conduction at the wall is immediately followed by forced convection from the hot gases flowing through the test section.

For transient heating of a semi-infinite body through a constant, surface heat transfer coefficient with an initial, uniform temperature (T_o), the temperature history for the surface is [Page 72, 22].

$$\frac{T_s - T_o}{T_g - T_o} = (1 - e^{N^2} \operatorname{erfc} N) \qquad \text{(C-5)}$$

$$N = \frac{h(t)^{1/2}}{\Gamma}$$

where T_o, T_s, and T_g are the initial gauge temperature, time-dependent surface temperature, and gas temperature, respectively.

For the case where a temperature jump occurs behind the reflected shock followed by convective heating of the wall, Baer [6] developed an equation similar to Equation (C-5) to define the heating process. For this analysis it was postulated that heat flux to the wall could be represented as the sum of two individual contributions: (1) heating of the wall from the boundary layer which is proportional to $(t)^{-1/2}$, and (2) heating across the boundary layer which is proportional to the difference between the gas temperature (T_g) and the surface temperature (T_s) of the heat flux gauge. The unsteady-state heat conduction equation with these restrictions is:

$$\rho c \frac{\partial T}{\partial t} = k \frac{\partial^2 T}{\partial x^2} \qquad \text{(C-6)}$$

$$\text{at } x = 0,\ F_s(0,t) = -k \frac{\partial T}{\partial x} = h(T_g - T_s) + \frac{k\Delta T_o}{(\Pi\alpha t)^{1/2}}$$

$$\text{at } t = 0,\ T(x) = T_o, \text{ all } x$$

$$\text{at } x = +\infty,\ T(t) = T_o, \text{ all } t$$

Where ΔT_o is the difference between the surface temperature behind the reflected shock (T_j) and the value T_o before the arrival of the shock

wave. Solution of the one-dimensional equation with the indicated boundary and initial conditions gives:

$$\frac{T_s - T_j}{T_g - T_j} = (1 - e^{N^2} \text{ erfc } N) \qquad \text{(C-7)}$$

This equation reduces to Equation (C-5) when $\Delta T_o = 0$.

Baer [6] found that the temperature-time traces obtained from heat flux gauges were closely represented by Equation (C-7) for the greater portion of the heating period. These observations were reaffirmed by the studies reported here.

In this work heat flux gauges with three different substrate materials, Pyrex 7740, Pyroceram 9608, and alumina (Alsimag 614) were used for heat transfer measurements. This was done in order to establish, as was expected, that heat transfer coefficients derived from tests with materials of different thermophysical properties were the same. These heat transfer coefficients could therefore be used for calculating heat transfer to propellant surface. Thermophysical properties of the heat flux gauges used and properties of the platinum resistance element on each are given in Table 19.

For heat transfer runs in the shock tube, the heat flux gauge was mounted in the test section with the gauge surface flush with the flow-channel wall. The gauge circuitry for temperature measurement is described in Appendix H. During heat transfer runs, signals from the heat flux gauge and the quartz pressure pickup were displayed on the screens of two Tektronix, Model 502, oscilloscopes and recorded with Polaroid Land cameras. For most of the tests a sweep rate of 0.5 msec/(cm) was used on one oscilloscope to expand the initial heating

transient, and a slower sweep rate, 5 msec/(cm), was used for obtaining pressure and heat transfer data for the entire test period. As indicated earlier, the shock wave that enters the test-section flow channel is stronger than the incident shock wave in the driven section of the shock tube. This shock produces an acoustic disturbance in the flow channel. The initial heating transient is more pronounced when a small flow-control orifice is used because of the larger, closed area for reflection. For all tests conducted, this initial heating transient produced by the acoustic disturbance which follows the reflected shock wave is almost completely damped within one millisecond. Figure 67 shows oscilloscope traces of pressure and temperature at the heat flux gauge surface for the first 0.6 milliseconds of a heat-transfer test. Both the heat flux gauge and the pressure transducer were mounted flush with the wall of the flow channel in the test section.

Figures 68 and 69 are temperature- and pressure-time traces for heat-transfer runs in the shock tube. The temperature-time trace shown by Figure 68 was obtained with a Pyrex heat flux gauge and the smallest critical-flow orifice used in this work. For this run (No. 35-31-2) the temperature-time relationship could be represented reasonably well for the time interval of 2 to 30 milliseconds by Equation (C-7). The latter time corresponds to the length of time required for the head of the rarefaction wave to arrive at the test section. This is shown by the rapid pressure drop on the oscilloscope trace (Figures 68 and 69). It was noted, as is shown by temperature-time trace of Figure 68, that small

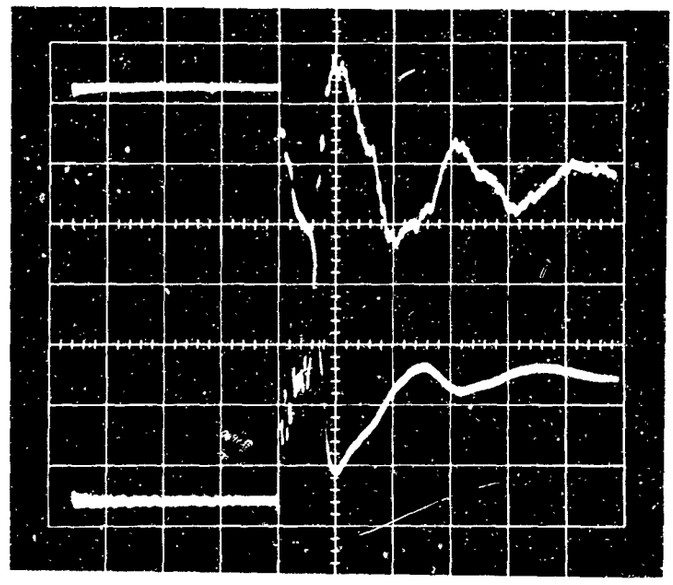

Figure 67

Oscillograph for Heat Transfer Run Showing the Initial Heating and Pressure Transients in the Test Section. Upper Left: Surface Temperature of Pyrex Heat Flux Gauge, 5°C/(div.). Lower Left: Pressure in Test Section, 20 psi/(div.). Time Base: 100 microseconds/(div.). Shock-Tube Conditions: P_o = 150 psig, M_E = 2.85, Flow-Control Orifice No. 3.

temperature fluctuations were usually present when the smallest flow-control orifice was used. The reason for these small temperature fluctuations is now not known, but could be caused by growth and decay of the laminar sublayer at low Reynolds numbers. The temperature-time trace of Figure 69 was obtained with the Pyrex heat flux gauge using the largest flow-control orifice. For this run (No. 35-31-7) the heat flux gauge surface temperature is represented by Equation (C-7) for the time interval of 1 to 13 milliseconds. After 13 milliseconds because of the large amount of processed gas which had passed through the test section, the cold, driver gas mixed with and cooled the shock-heated gases which greatly reduced the effective test period.

It is seen by comparing the two sets of data (Figures 68 and 69) that the initial heating transient is very weak for tests with the large flow-control orifice. The etched horizontal line on each figure defines the base line from which the heat flux gauge temperatures were measured and corresponds to the initial, uniform gauge temperature, T_o.

ANALYSIS OF RESULTS FROM HEAT TRANSFER STUDY

To obtain representative data for use in analyzing heat transfer to the propellant surface during ignition tests, measurements were made at the test-section wall for heat transfer from high-temperature air or argon. The test conditions employed in this heat transfer study were summarized earlier in Figure 7. For all tests the initial shock-tube conditions were adjusted to produce a "matched" interface behind the reflected shock. Under these

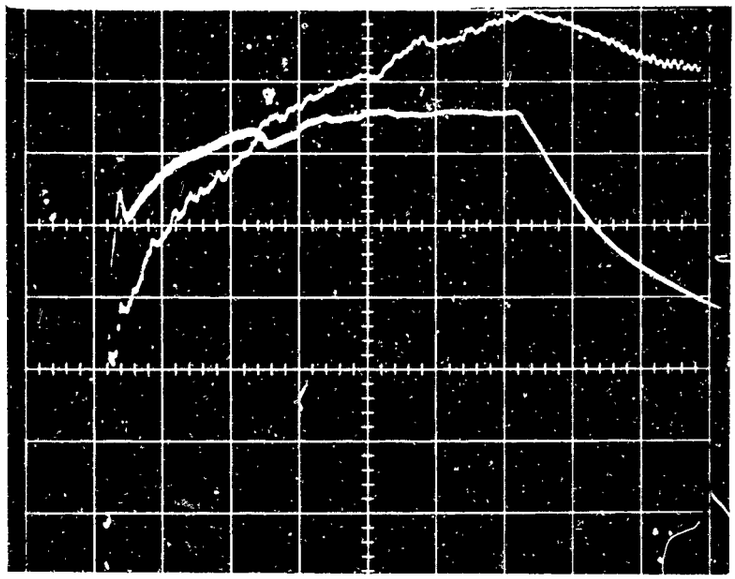

Figure 68

Oscillograph for Heat Transfer Run No. 35-31-2. Lower Trace: Pressure in Driven Section, 50 psi/(div.) Upper Trace: Surface Temperature of Pyrex Heat Flux Gauge, 25°C/(div.). Sweep Rate: 5 msec/(div.). Flow-Control Orifice No. 5, $P_o = 350$ psig, $M_E = 3.52$.

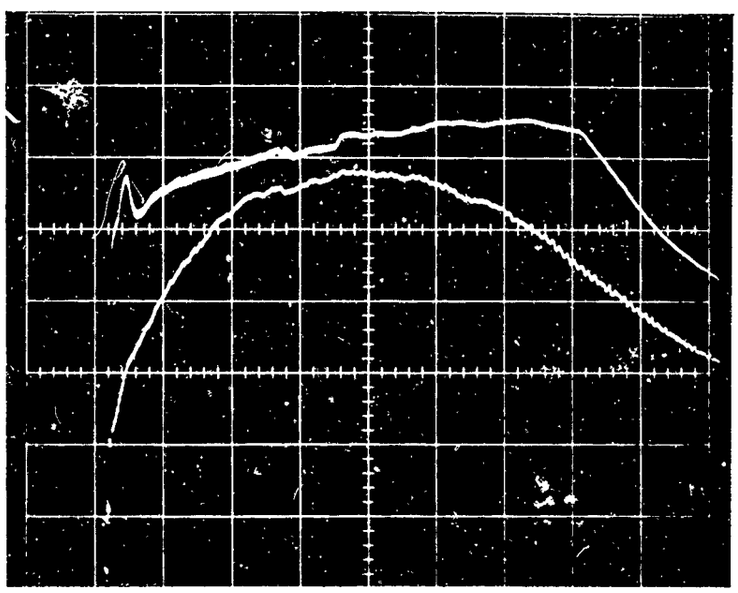

Figure 69

Oscillograph for Heat Transfer Run No. 35-31-7. Upper Trace: Pressure in Driven Section, 50 psi/(div.). Lower Trace: Surface Temperature of Pyrex Heat Flux Gauge, 50°C/(div.). Sweep Rate: 5 msec/(div.). Flow-Control Orifice No. 1, $P_o = 350$ psig, $M_E = 2.85$.

operating conditions, the maximum pressure rise (P_4') behind the reflected shock was usually with 85 to 95 per cent of the initial driver gas pressure (P_o). No attempt was made to measure gas temperatures behind the reflected shock wave. Gas temperatures were calculated using measured values of incident shock velocities. Data used for calculating temperatures behind the reflected shock are given in terms of incident Mach numbers for air, argon, and oxygen in Table 20.

The initial temperature rise (ΔT_o) at the test-section wall resulting from the passage of incident and reflected shocks was found to be a function of: (1) the Mach number of the incident shock wave, (2) the pressure behind reflected shock wave (P_4), (3) the thermophysical properties of the heat flux gauge substrate, and (4) the area of the flow-control orifice. Also, this initial temperature rise was different for air or argon. This would be expected since the thermal properties of the two gases are considerably different. Experimental, initial temperature rise (ΔT_o) data for all of the heat transfer tests are given in Table 21. These results are shown graphically for air as the driven gas in Figure 70 and for argon as the driven gas in Figure 71. For air, it was found that the initial temperature rise (ΔT_o) at the gauge surface could be represented by the following relationships:

For A_{or}/A_{ts} greater than 0.458:

$$\Delta T_o = 0°K \tag{C-8}$$

For A_{or}/A_{ts} less than 0.458:

$$\Delta T_o = 13.66\left(\frac{P_4}{P^*}\right)^{1/2}\left(\frac{\Gamma^*}{\Gamma}\right)\left(1 - \frac{A_{or}}{A^*}\right)(M_E - 1.20), \ [°K] \tag{C-9}$$

Where: P^* is a reference pressure having a value of 10 atm.

Γ^* is the thermal responsivity of the Pyrex heat flux gauge having a value of 0.0366 $cal/(cm)^2(sec)^{1/2}(°K)$.

A^* is the flow area of control orifice No. 1 having an area of 0.369 $(cm)^2$.

Although it would be difficult to derive Equation (C-9) from theoretical considerations alone, this equation is of the form that would be expected for the temperature rise at the wall immediately behind the reflected shock. Heat conduction from a high-temperature gas is dependent on the thermal responsivity of both the gas and the wall material. The thermal responsivity of the gas is proportional to $(P)^{1/2}$. The temperature rise at the wall is proportional to $1/\Gamma_w$. The strength of the reflected shock, and thus the gas temperature, is dependent on the closed area for reflection at the end of the test-section flow channel.

For flow-control orifice No. 1, which gave an area ratio of 0.458 (orifice flow area divided by cross sectional area of test-section flow channel), the initial temperature rise of the heat flux gauge substrate produced by conduction from hot gases was negligible relative to the rapid temperature rise at the wall from forced-convection heat transfer. This observation would be expected since the strength of the reflected shock in the flow channel was much weaker when a large flow-control orifice was used.

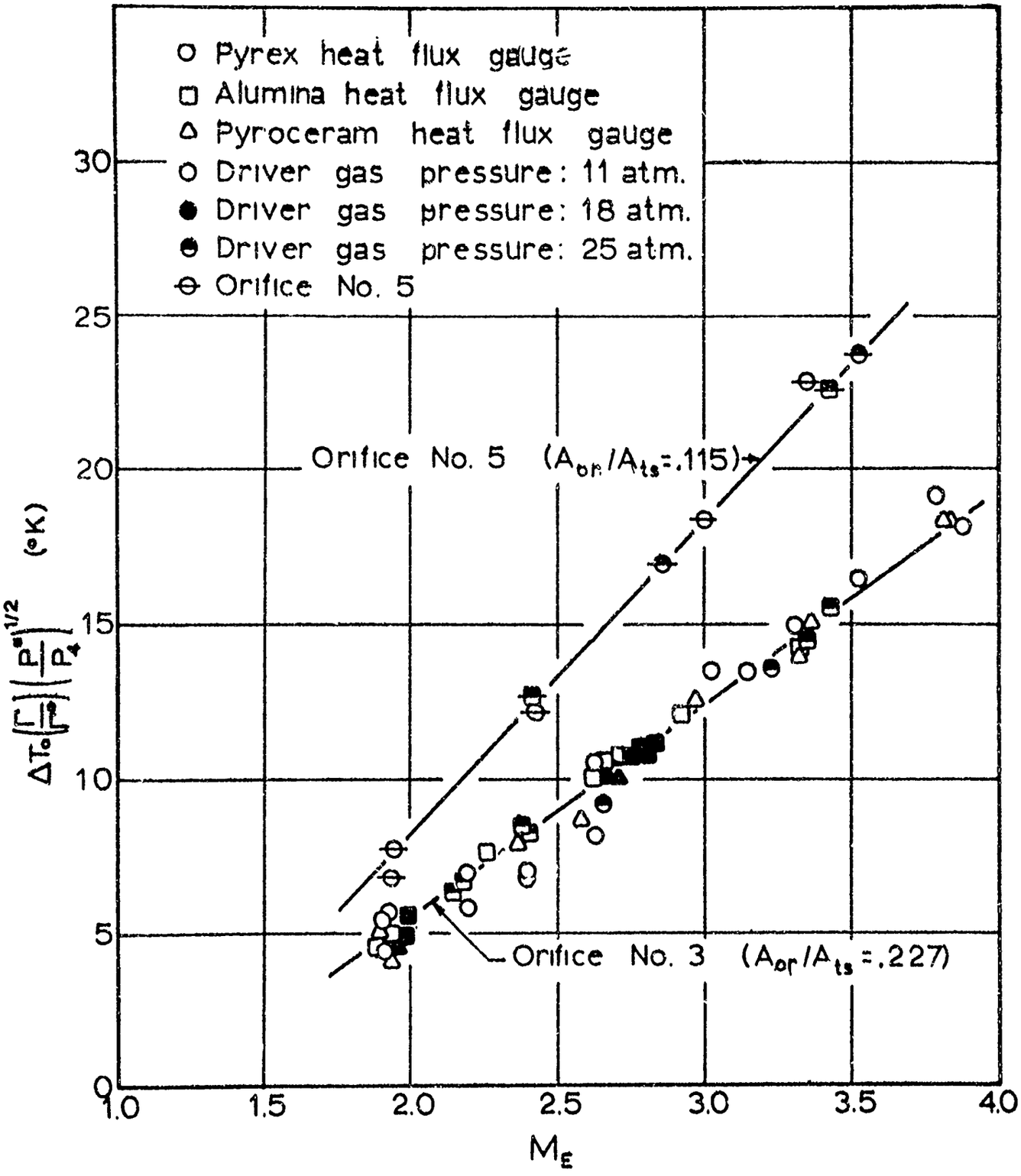

Figure 70

Initial, Instantaneous Temperature Rise Behind Reflected Shock Wave at the Test-Section Wall for Air.

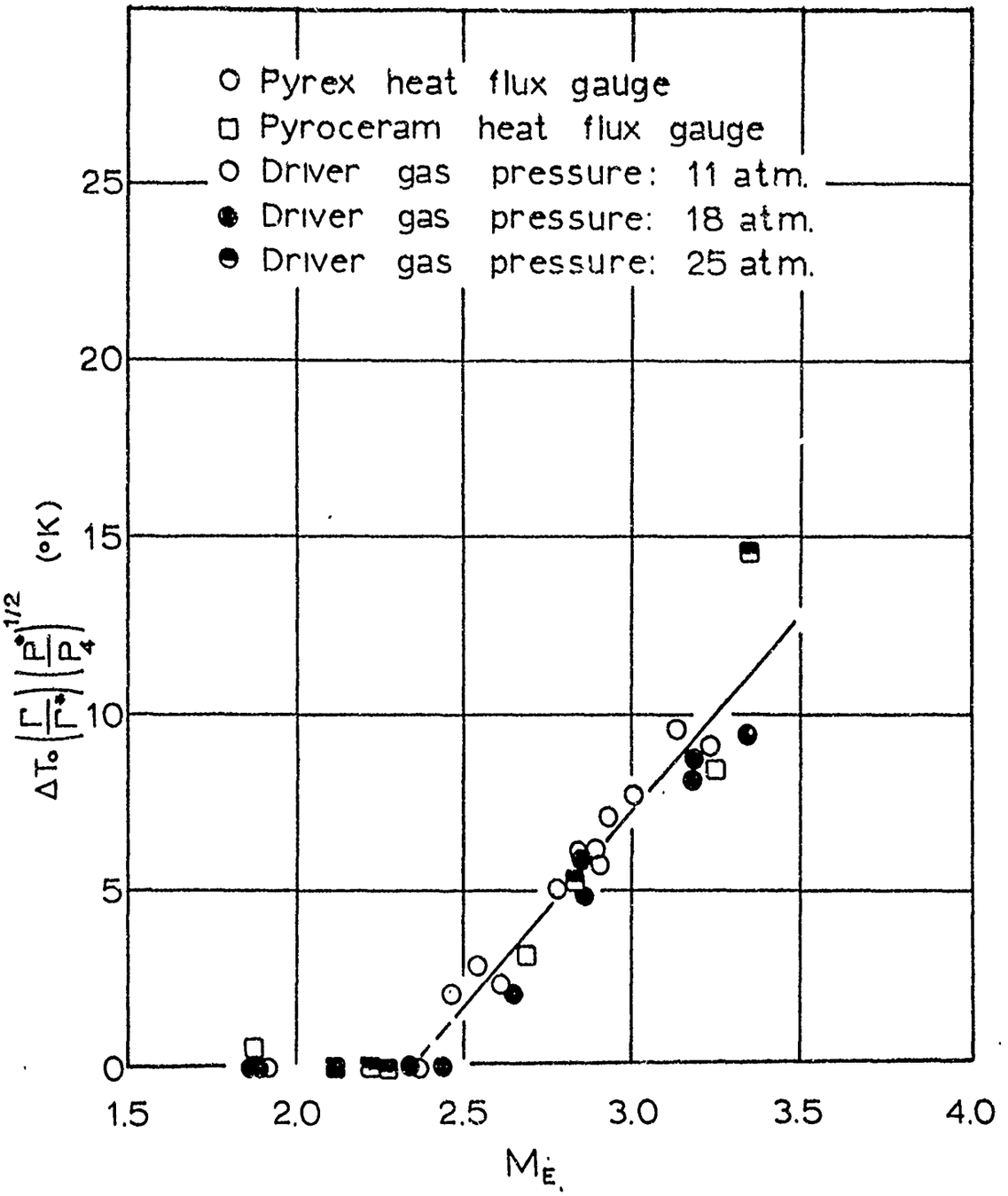

Figure 71

Initial, Instantaneous Temperature Rise Behind Reflected Shock Wave at the Test-Section Wall for Argon.

For argon as the driven gas and with the No. 3 flow-control orifice (area ratio of 0.227), the initial temperature rise could be approximated by:

For M_E less than 2.35:

$$\Delta T_o = 0°K \tag{C-10}$$

For M_E greater than 2.35:

$$\Delta T_o = 11.1 \left(\frac{P_4}{P^*}\right)^{1/2} \left(\frac{\Gamma^*}{\Gamma}\right) (M_E - 2.35), \ [°K] \tag{C-11}$$

With this information on initial temperature rise and calculated shocked-gas temperatures, local heat transfer coefficients were derived from temperature-time data by the method described in Appendix I. The temperature dependence of the thermophysical properties for heat flux gauges was taken into consideration for calculating heat-transfer coefficients from data obtained with Pyrex and alumina gauges (see Appendix I). Adequate data for thermal properties of Pyroceram 9608 were not available to compensate for temperature dependence of this material. Thermal diffusivity data on Pyroceram 9608 [75] indicate that thermal properties of this material are not a strong function of temperature.

Data for individual heat transfer runs with air or argon as the convective fluid are given in Table 22. In order to calculate heat transfer coefficients, it was necessary to determine the temperature of the gas behind the reflected shock for each run. Because of the problems associated with the measurement of temperatures behind

reflected shock waves, no direct measurements of gas temperatures were attempted but these were calculated from initial shock-tube conditions and measured incident shock-wave velocities. In general, measured gas temperatures behind reflected shocks are not in perfect agreement with those calculated from Rankine-Hugoniot relations and based on measured incident shock velocities. However, the agreement in most cases is sufficiently good so that calculated values can be used for shock-tube studies that do not involve chemical kinetics. In addition to the temperature uncertainty, inhomogeneities in the gas behind reflected shock waves caused by real-gas effects can give anomalous results for studies of chemical kinetics. Strehlow and Case [88], and Rudinger [79] have pointed out that the gas temperatures behind reflected shocks will increase with time because of the interaction of the reflected shock wave with the boundary layer. As a consequence, the true post-reflection gas temperature will be higher than that calculated from shock relations. This results because of the interaction of the reflected shock with the boundary layer and also with the contact surface for cases where the interface is not completely matched. These interactions produce weak compression shocks which further heat the gas behind the reflected shock.

For the shock tube tests conducted in this study, it was found that the pressure in the driven end of the tube increased with time after the reflected shock had passed the monitoring station. This post-reflection pressure rise, shown by Figures 68 and 69, continued for 15 to 20 milliseconds before leveling off. For reasons described in the previous paragraph and other real-gas effects, the temperature

of the gas behind the reflected shock also increases with time. Since these weak shock processes can be approximated by isentropic processes, it was suggested by Baer [6] and later by Copper [26] that the temperature rise of the gas behind the reflected shock could be calculated by assuming an isentropic compression from P_4 (pressure immediately behind the reflected shock) to P_4' (the maximum pressure observed for a given run). When this adjustment is made, the final gas temperature (T_4') is 5 to 10 per cent greater than the temperature immediately behind the reflected shock wave. This adjustment was applied to all gas temperatures in which air, oxygen, or nitrogen was used as the driven gas. This is a somewhat arbitrary gas temperature since the true gas temperature would vary with time for the first 15 to 20 milliseconds of each heat transfer test. It was shown, however, that when this gas temperature was used for calculating convective heat transfer to the different heat flux gauge substrate materials, excellent agreement among heat transfer coefficients was obtained. This indicates that the gas temperature calculated by this method is within a few per cent of the true gas temperature. Since compressibility effects were small for most of flow velocities encountered in this study, it was assumed that this gas temperature (T_4') was the same as the gas stagnation temperature (T_g) for all heat transfer calculations involving air, nitrogen, or oxygen; the recovery factor was assumed to be 1.0.

Experimental Data for Heat Transfer from High-Temperature Air

The results of the heat transfer study with air as the test gas are presented graphically in the form of G (mass flow rate in the test-section flow channel) versus $h/(T_f)^{0.3}$ in Figure 72. Data for individual runs are given in Table 22. Here the film temperature, T_f, is defined as the mean absolute temperature (°K) between the gas temperature (T_g) and the heat flux gauge surface temperature (T_s) 10 milliseconds after the start of heating. The local heat transfer coefficients at the wall test position are represented within 5 per cent by the following equation:

$$h = 1.70 \times 10^{-4} (T_f)^{0.3} (G)^{0.895} \; [\mathrm{cal}/(\mathrm{cm})^2(\mathrm{sec})(°\mathrm{K})] \qquad \text{(C-12)}$$

For T_f in °K and G in $g/(cm)^2(sec)$.

The thermal responsivity of the test-section wall, represented by the heat flux gauge substrate material, ranged from a value of 0.0366 $cal/(cm)^2(sec)^{1/2}(°K)$ for Pyrex to 0.208 $cal/(cm)^2(sec)^{1/2}(°K)$ for alumina. The fact that heat transfer coefficients for this wide range of thermophysical properties can be represented by a single relationship shows the method used for calculating gas temperature is a good approximation to the true gas temperature for gas flowing through the test section. Furthermore, it shows that the results from this correlation can be used directly to calculate heat transfer to the propellant surface.

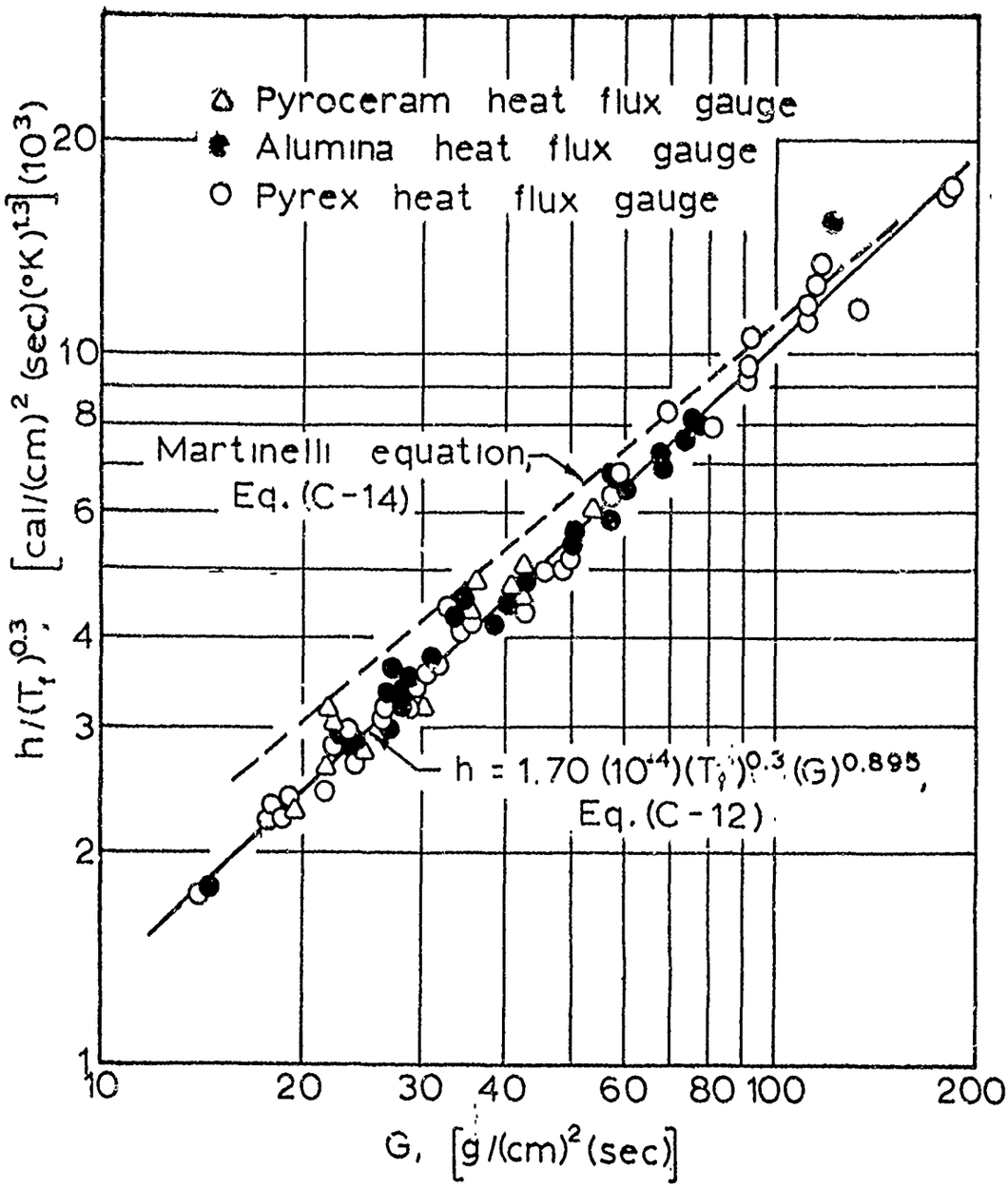

Figure 72

Heat Transfer Coefficients at the Test-Section Wall for High-Temperature Air, Correlated in Terms of Mass Flow Rate Through Flow Channel and Gas Film Temperature.

The Martinelli Equation, Equation (C-4), for heat transfer through a turbulent boundary layer has the following form in the cgs system of units:

$$h_\ell = 2.89 \times 10^{-4} \frac{(T_f)^{0.3} (G)^{0.8}}{(x)^{0.2}} \; [\text{cal}/(\text{cm})^2(\text{sec})(°\text{K})] \qquad \text{(C-13)}$$

Where T_f is in °K, x is in cm, and G has the units $g/(cm)^2 sec$. For x = 1.27 cm, the location of the test position from the leading edge, Equation (C-13) reduces to:

$$h = 2.75 \times 10^{-4} (T_f)^{0.3} (G)^{0.8} \; [\text{cal}/(\text{cm})^2(\text{sec})(°\text{K})] \qquad \text{(C-14)}$$

Equation (C-14) is shown by the dashed line on Figure 72 for comparison with the data obtained in this work.

In Figure 73 these same heat transfer data are presented in the form G versus $h/(T_g)^{0.3}$ as suggested by the Iverson Equation, Equation (C-3).

In this form the data are represented within 6 per cent by:

$$h = 1.435 \times 10^{-4} (T_g)^{0.3} (G)^{0.905} \; [\text{cal}/(\text{cm})^2(\text{sec})(°\text{K})] \qquad \text{(C-15)}$$

By comparing the results given in Figures 72 and 73, it is seen that the heat transfer coefficients obtained in this study are correlated slightly better when represented as a function of film temperature (T_f) rather than as a function of bulk, gas temperature (T_g). However, because of the difficulties encountered in defining a film temperature for use in unsteady-state heat transfer processes,

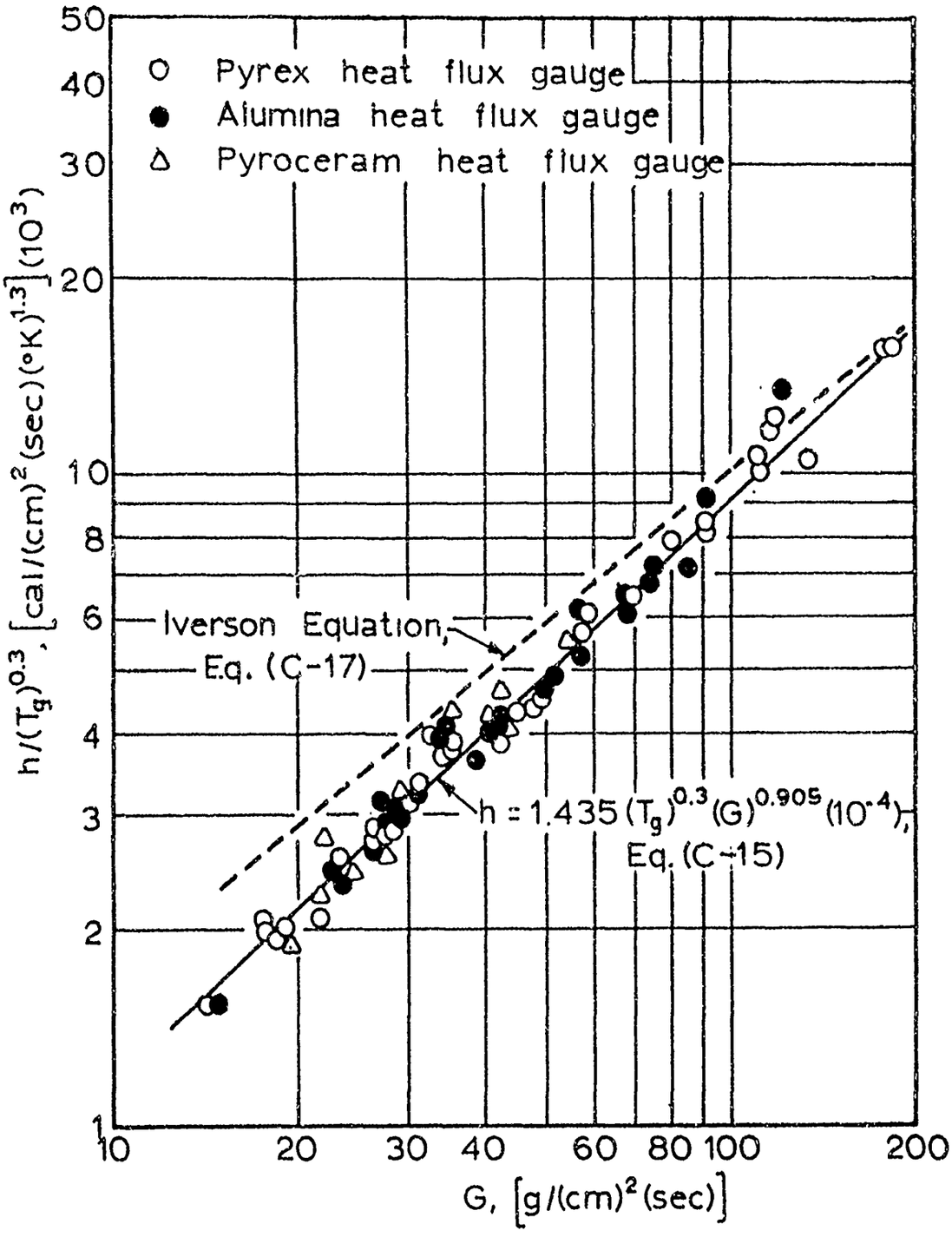

Figure 73

Heat Transfer Coefficients at the Test-Section Wall for High-Temperature Air, Correlated in Terms of Mass Flow Rate Through Flow Channel and Gas Stagnation Temperature.

all calculations for heat transfer to propellant surfaces were made using Equation (C-15) which represents the data for heat transfer coefficients as a function of the bulk, gas temperature.

The data for heat transfer coefficients given in Figure 73 are compared to the Iverson Equation as modified by Baer [6] for heat transfer through a turbulent boundary layer. The general form of this equation is:

$$h_\ell = 2.92 \times 10^{-4} (T_g)^{0.3} (G)^{0.78} (D_H/x)^{0.1144} \; [\mathrm{cal}/(\mathrm{cm})^2(\mathrm{sec})(^\circ\mathrm{K})] \quad \text{(C-16)}$$

Where T_g is in °K and G has the units $g/(cm)^2(sec)$. For the test position, where $x = 1.27$ cm, Equation (C-16) reduces to:

$$h = 2.79 \times 10^{-4} (T_g)^{0.3} (G)^{0.78} \; [\mathrm{cal}/(\mathrm{cm})^2(\mathrm{sec})(^\circ\mathrm{K})] \quad \text{(C-17)}$$

It is seen from this comparison that the data obtained from this heat transfer study, represented by either Equation (C-12) or (C-15), have a stronger dependence on G than that predicted for heat transfer through a turbulent boundary layer by the Martinelli and Iverson Equations, Equations (C-14) and (C-17), respectively.

For reasons which will be discussed in the following paragraphs, data for heat transfer coefficients obtained with the open test section (no flow-control orifice) for large Reynolds numbers (250,000 to 870,000) and high mass flow rates, greater than about 100 $g/(cm)^2$ sec, would not correlate with data obtained with smaller flow-control orifices by a single relationship if the actual mass flow rate, G, through the test section, based on a measured flow area of 0.777 $(cm)^2$,

were used. It was found, however, that if the mass flow rate were based on a defined flow area of 0.60 $(cm)^2$ for the open test section then heat transfer coefficients for all flow-control orifices could be correlated by a single relationship, either Equation (C-12) or (C-15). All calculations involving heat transfer to the propellant surface during ignition tests were based on this defined flow area of 0.60 $(cm)^2$ for the open test section so that a single correlation of heat transfer coefficients could be used for all calculations. The use of this single defined flow area for mass flow rate does not preclude accurate calculations of the heat transfer to a propellant surface since all heat transfer coefficients were based on experimental measurements.

The equations for entrance-region heat transfer developed by Martinelli and Iverson assume that flow in the entrance region is completely turbulent and that the turbulent boundary layer begins its development at the leading edge. In the experimental heat transfer study made by Boelter, et al. [17] with a bell-mouthed entrance, the intensity of the free-stream turbulence was apparently sufficiently large to ensure a turbulent boundary at the leading edge. Consequently, their results for inlet-region heat transfer were in reasonable agreement with equations for local heat transfer coefficients, Equations (C-3) and (C-4). However, they point out [page 9, 17] in referring to a publication by Prandtl [76] that "unless a turbulence promoter is used, a laminar boundary layer will usually precede the turbulent boundary layer". This would apparently be the condition that would exist for flow in the entrance region following bell-mouthed entrance with low intensity free-stream turbulence and a

uniform velocity and temperature profile at the inlet. They also point out that for a high tube Reynolds number and the above conditions, a transition from laminar to turbulent flow will occur downstream of the leading edge at a position which cannot be accurately predicted. This aspect of entrance-region flow is also discussed by Dryden, et al. [page 360, 31]. According to these authors, flow in the entrance region following a bell-mouthed inlet, depending on the Reynolds number, is either completely laminar or the boundary layer has both a laminar and turbulent part. However, for a blunt-end tube only a turbulent boundary layer exists in the inlet region that is produced by eddies that are initiated by the stream contraction. All of these observations are in substantial agreement with the experimental results on entrance-region heat transfer obtained by Mills [68].

In many respects heat transfer in the entrance of a tube with a bell-mouthed entrance is similar to that for heat transfer to a flat plate. Dryden [page 40, 30] suggests that the critical Reynolds number for transition from laminar to turbulent flow would be higher in the entrance of a tube than on a flat plate because of the negative pressure gradient in the entrance region of a tube. Again, as is the case for a flat plate, a high turbulence intensity in the free stream would reduce the critical Reynolds number for transition.

In a recent doctoral dissertation, Junkhan [50] reported a rather thorough investigation of the effect of free-stream turbulence and favorable negative pressure gradients on heat transfer from a flat plate. He found for a plate of zero incidence and zero pressure gradient that the effect of increased turbulence intensity was to

decrease the critical Reynolds number for transition from a laminar to a turbulent boundary layer on the flat plate. Under two other sets of test conditions, with more favorable pressure gradients and extremely high turbulent intensities ranging from about 3 to 8 per cent, it was no longer possible to detect from a logarithmic plot of Reynolds number versus Nusselt number a transition from laminar to turbulent flow. For high turbulence intensities and a negative pressure gradient at the wall, Junkhan concluded that the boundary layer for low Reynolds numbers no longer appears to be laminar, and that the boundary layer is quasi-laminar or is in transition. An interesting result of this work was that all of the experimental data for Reynolds numbers ranging from about 50,000 to 300,000 could be defined by a straight line on a plot of the logarithm of Reynolds number versus the logarithm of Nusselt number for a given pressure gradient. These results all fell within the region defined by equations for laminar boundary layer and turbulent boundary layer heat transfer. At lower Reynolds, around 50,000, the Nusselt numbers were in good agreement with Pohlhausen's equation for heat transfer from a flat plate with a laminar boundary layer and small temperature differences between the gas the the flat plate.

$$Nu_x = 0.295\ (Re_x)^{0.5} \qquad \text{(C-18)}$$

At higher Reynolds numbers, above a Reynolds number of about 300,000, the experimentally determined Nusselt numbers were in substantial agreement with those defined by von Karman's and Prandtl's equations, Equation (C-19) and (C-20), respectively, for heat transfer through a turbulent boundary layer.

$$Nu_x = 0.241\ (Re_x)^{0.8} \tag{C-19}$$

$$Nu_x = 0.236\ (Re_x)^{0.8} \tag{C-20}$$

The results reported by Junkhan are in substantial agreement with those reported by other investigators including recent results by Kestin, Maeder, and Wang [53]. However, none of these other investigators studied heat transfer from a flat plate over as large a range of pressure gradients and turbulence intensities as those reported by Junkhan.

In view of the foregoing discussion, it appears that the heat transfer data obtained from measurements at the test section wall in the work for this thesis are what should be expected for the test-section design used; that is, because of the high turbulence intensity in the free stream and favorable pressure gradient in the entrance to the test section, the local heat transfer coefficient should have a stronger dependence on mass flow rate than that predicted by turbulent-flow equations. Gas flow in the entrance region with a negative pressure gradient before the establishment of a fully developed boundary layer would be closely analogous to that for heat transfer to or from a flat plate under a negative pressure gradient. Although free-stream turbulence was not measured in this study, it would be expected to be of rather large intensity. In the shock tube turbulence is produced by interaction of the reflected shock with the boundary layer in the driven end of the shock tube and is produced also by the weak interaction of the reflected shock with the contact surface when perfect "matching" of the interface is not achieved. Also, turbulence is

introduced by the shock reflected from the orifice plate at the end of the flow channel. Under these flow conditions, the heat transfer coefficient would be expected to have a larger dependence on mass flow rate, G, than the 0.8 power dependence for heat transfer through a turbulent boundary that is predicted by Equations (C-3) and (C-4).

Another aspect of forced convection heat transfer that was encountered in this work, but does not appear to have been investigated experimentally, is heat transfer to a wall under transient conditions for the case where there is a discontinuity in thermal properties of the wall material. The discontinuity in thermal properties results because the test section, including the inlet region, is made from steel and the heat flux gauge substrates are made from glass or ceramics. Apparently the difference in thermal properties did not have a measurable effect on heat transfer, since heat transfer coefficients derived from temperature-time data for heat flux gauges made of different substrate materials could all be correlated within experimental error by one equation. It would be expected, however, that if the inlet to the test section were made of a different material having properties similar to that used for heat flux gauges, a higher heat transfer rate would have been measured at the test position. The reason for this, and it would apply only to the transient heating case, is that as the convective gas is passed over the steel inlet, the boundary layer is cooled more than if the gas were passed over a material with a smaller thermal responsivity. It should, therefore, be possible to increase the rate of heat transfer to the test position by using a different material for the bell-mouthed inlet.

In presenting experimental heat transfer data in the form suggested by Equations (C-13) and (C-16), the temperature dependence of h is indirectly related to its dependence on mass flow rate. This is true since the basic equation from which these equations were derived included terms for fluid properties and a Reynolds number. It can be readily shown by considering the effect of temperature on fluid properties when air is the heat transfer medium and flow is turbulent that h is proportional to $(T_g)^{0.3}$. However, for the case where h is proportional to $(Re)^{0.9}$, it is shown that h is approximately proportional to $(T_g)^{0.2}$. From the experimental data obtained from this study, it was not possible to determine experimentally the exact dependence of h on T_g, and a value of $(T_g)^{0.3}$ was used.

In addition to the heat transfer data presented by Figures 72 and 73, some exploratory tests were made for heat transfer to the test position under modified flow conditions. These results are given in Part I of Table 22. It was shown that when a sharp-edged orifice was used in the entrance to the test section in conjunction with a critical-flow orifice downstream, heat transfer coefficients could be increased as much as 300 per cent over those obtained with a smooth, bell-mouthed entrance. This observed effect of the sharp-edged inlet orifices on heat transfer to the wall of the entrance region of a tube is in general agreement with previous experimental work of Boelter, et al. [17], Davies and Al-Arabi [28], and Mills [68].

Experimental Data for Heat Transfer from High-Temperature Argon

As indicated earlier, heat transfer to the test section wall was also measured using argon as the convective gas. The primary interest in argon arises because higher gas temperatures can be obtained in a shock tube with a monatomic gas than with air or nitrogen for equivalent incident Mach numbers. This was of interest for studying propellant ignition in that propellants could be tested under higher gas temperatures without a reduction in the available test time. Heat transfer coefficients obtained with argon are presented as a function of mass flow rate through the test section by Figure 74. These data are tabulated in Part II of Table 22. Because of the high dependence of heat transfer coefficient on the Reynolds number for this test condition, h is a function only of G. It can be shown that for the case where h is directly proportional to the Reynolds number, the fluid properties of argon are dependent on temperature in such a way that the temperature effect on heat transfer coefficient is eliminated. The local heat transfer coefficients for argon can be represented within 4 per cent by:

$$h = 4.05 \times 10^{-4} (G)^{1.06} \; [\mathrm{cal}/(\mathrm{cm})^2(\mathrm{sec})(^\circ\mathrm{K})] \qquad \text{(C-21)}$$

Where G has the units $g/(cm)^2(sec)$.

Since h for argon was found to be proportional to $(G)^{1.06}$, a slight dependence of h on gas temperature would be expected; however, because of the scatter in the experimental data, the introduction of this temperature would not improve the correlation. The mass flow rates (G) and local heat transfer coefficients were evaluated at (T_4), the temperature of argon immediately behind the reflected shock, rather

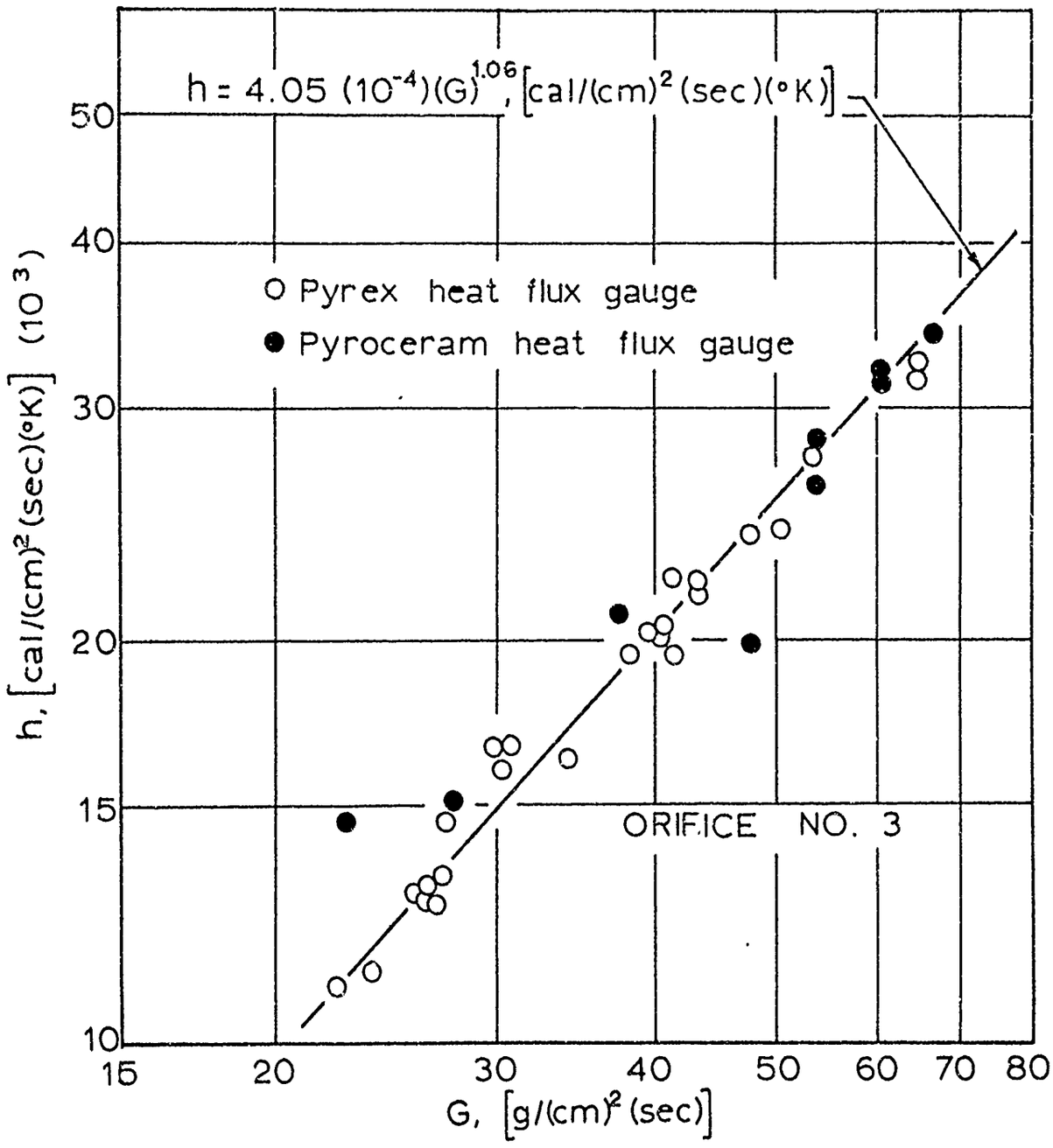

Figure 74

Heat Transfer Coefficients at the Test-Section Wall for High-Temperature Argon as a Function of Mass Flow Rate Through Flow Channel.

than at (T_4'), as for air. The use of T_4 as the gas temperature gave an improved correlation of these data and temperature-time data were still well represented by Equation (C-7). When T_4 was used as the gas temperature rather than T_4', the heat transfer data obtained with Pyrex and Pyroceram heat flux gauges coincided at high mass flow rates.

Since this heat transfer study using argon as the test gas was of an exploratory nature, tests were conducted with a single flow-control orifice. The results with argon, as did the results with air, show h to be a strong function of G, which indicates that the same type of flow conditions existed in the test section for both air and argon.

APPENDIX D

PROCEDURES USED FOR DETERMINING THERMOPHYSICAL PROPERTIES OF PROPELLANTS AND PROPELLANT INGREDIENTS[a]

The thermal responsivities for propellants and propellant ingredients needed for calculating the externally applied heat flux to the propellant surface during ignition tests were evaluated from either experimentally determined or published data for ρ, c, and k (or α). The procedures used for determining the individual thermophysical properties of propellants and ingredients are described below. Thermophysical properties of these materials are summarized in Table 4. Chemical compositions of the propellants and binders are given in Table 2.

DENSITY

The densities of propellants and binders were usually measured by water displacement. For some of the more rigid, cast propellants and pellets of pressed propellants, densities were obtained by direct measurements. It is expected that the densities are accurate to within $\pm$ 2 per cent of their actual values.

HEAT CAPACITY

The mean heat capacities of propellants and binder samples were determined between 95°C and room temperature, approximately 25°C, with a Dewar-flask calorimeter containing water. The calorimeter was

---

[a]The material presented in this appendix was adapted from that presented in Appendix A of Reference 81.

calibrated with copper bars of known heat capacity. Temperature changes of the water in the calorimeter were recorded to the nearest 0.01° C with a Beckman differential thermometer. The anticipated accuracy of heat capacity data is ±3 per cent. The measured values of heat capacity of the propellant and those calculated from the heat capacities of the individual ingredients differed by less than 3 per cent.

THERMAL DIFFUSIVITY

An unsteady-state method was used for obtaining experimental thermal diffusivity data on propellants, binders, and ammonium perchlorate. Solid cylinders of these materials were prepared with small-diameter thermocouples mounted in their geometric centers. The cylindrical samples were then quickly immersed in a liquid with a lower temperature than the sample. The temperature history at the center of the sample was recorded and used for calculating the thermal diffusivity of the material in the manner described below.

The samples of propellant and binder were solid cylinders 3.8 cm in diameter by about 10 cm in length. Propellant samples were coated with a thin film of silicone or acrylic resin to prevent dissolution fo the ammonium perchlorate at the propellant surface in the water used in the agitated bath. The ammonium perchlorate samples were made by cementing together pressed, cylindrical disks (99 per cent of theoretical density), 2.54 cm in diameter and 0.6 to 0.7 cm in thickness, to give cylindrical samples with a length of 4.0 to 4.5 cm. Carbon tetrachloride was used as the liquid for experiments on pure ammonium perchlorate samples.

The experimental temperature-time data were analyzed by the following method. It is found by plotting

$$\ln \frac{T_t - T_o}{T_b - T_o} \quad \text{versus} \quad t$$

that after a short, initial transient period the data plotted in this form are represented by a straight line. Where T_t, T_o, and T_b are the temperature at the center of the sample at time, t; initial uniform sample temperature; and temperature of the bath; respectively. During the period when the data plotted in this form are represented by a straight line, the following equation represents the unsteady-state heat transfer process, [page 228, 22]:

$$\frac{T_t - T_o}{T_b - T_o} = C_1 \quad \exp[-\alpha t(\lambda_1^2 + \beta_1^2)] \qquad \text{(D-1)}$$

Where α is the thermal diffusivity of the sample, and C_1 is a time-invariant constant. The constants λ and β are, respectively, the smallest roots of the equations:

$$\lambda\ell \tan \lambda\ell = \frac{h\ell}{k} \qquad \text{(D-2)}$$

and

$$a\beta \; J_1(a\beta) = \frac{ha}{k} \; J_o(a\beta) \qquad \text{(D-3)}$$

Where a is the radius of the cylinder, ℓ is the half-cylinder height, k is the solid thermal conductivity, and h is the surface heat transfer coefficient between the sample and the agitated bath. (The heat transfer coefficient is assumed to be constant over the sample surface.)

The surface heat transfer coefficient was determined by immersing a heated, solid cylinder of copper, 2.5 cm in diameter by 5 cm long, in the agitated liquid baths. For copper, the terms $h\ell/k$ and ha/k are so small that a limiting form of Equation (D-1) can be used which neglects the temperature gradient in the solid sample. In the water bath h was found to be 0.104 cal/(cm)^2(sec)(°K) and in the carbon tetrachloride bath h was found to be 0.025 cal/(cm)^2(sec)(°K). The sample position in the bath and degree of agitation were carefully controlled in all experiments to ensure that the experimentally determined values for h would apply for all thermal diffusivity tests.

In thermal diffusivity tests on propellants and binders, the terms, $h\ell/k$ and ha/k, were greater than 100, and the roots of Equation (D-1) are $\lambda_1 = 1.57$ and $\beta_1 = 2.40$. These values are essentially independent of h or k, and the thermal diffusivity (α) can be evaluated directly. For tests on propellants and binders, the initial, solid temperature was 95°C and the bath temperature was about 25°C.

For determination of thermal diffusivity of pressed ammonium perchlorate, the terms $h\ell/k$ and ha/k, had values in the range of 20 to 50, and λ_1 and β_1 were evaluated by a trial and error process from the experimental data. For tests on pressed ammonium perchlorate, the initial, solid temperature was in the range of 0° to 5°C, and the bath temperature was about 25°C. The error in thermal diffusivity measurementsis about $\pm$ 2 per cent.

THERMAL CONDUCTIVITY

The thermal conductivity of the various materials was calculated by the following equation:

$$k = \rho c \alpha \qquad \text{(D-4)}$$

The measured thermal conductivities for propellants were found to be within 3 per cent of values calculated from the thermal conductivities of individual ingredients by the Maxwell Equation as used by Gorring and Churchill [39]:

$$\frac{k}{k_1} = \frac{2 + \nu - 2\epsilon(1 - \nu)}{2 + \nu + \epsilon(1 - \nu)} \qquad \text{(D-5)}$$

Where: ν is the ratio of the thermal conductivities of the discontinuous phase to that of the continuous phase.

ϵ is the volume fraction of the discontinuous phase.

k_1 is the thermal conductivity of the continuous phase.

APPENDIX E

CALCULATIONS FOR IGNITION TEMPERATURE AND HEAT FLUX

The following discussion describes in considerable detail the method used for calculating the ignition temperature for linear heating, T_{si}^{L}, and the mean surface heat flux, $\overline{F}$, at the propellant surface during an ignition test in the shock tube.

SAMPLE CALCULATION

General Information for Ignition Run No. 212-24-2

1. The oscillograph for this run is shown in Figure 9b.
2. Propellant: F-9.
3. Thermal responsivity of propellant:

$$\Gamma_p = 0.0212 \text{ cal}/(\text{cm})^2(\text{sec})^{1/2}(°\text{K}).$$

4. Flow-control orifice: No. 3 [Area = $0.1832(\text{cm})^2$].
5. Atmospheric pressure: 25.25 in. Hg (12.4 psia).

Initial Shock-Tube Conditions

1. Shock-tube temperature, $T_1 = 20.0°C$.
2. Driven-section pressure, $P_1 = 10.0$ in. Hg (4.9 psia).
3. Driver-section pressure, $P_o = 350$ psig.
4. Driver gas composition, 6.2 and 93.8 volume per cent air and helium, respectively.

Data from Ignition Run

1. Average shock velocity between shock sensors 1 and 3,

$$M_{13} = 3.05$$

2. Initial pressure rise behind reflected shock wave,

$$P_4 = 235 \text{ psia } (16.0 \text{ atm.}).$$

3. Maximum pressure rise behind reflected shock wave,

$$P_4' = 341 \text{ psia } (23.2 \text{ atm.}).$$

4. Ignition time,

$$t_i = 13.8 \text{ msec.}$$

$$(t_i)^{1/2} = 3.72 \text{ (msec)}^{1/2} = 0.1176 \text{ (sec)}^{1/2}$$

Gas Properties at Entrance to Test Section

1. Mach number of the incident shock wave at end of driven section is calculated by Equation (C-1).

$$M_E = 3.05 \ (0.933) = 2.85$$

2. Temperature of the driven gas (nitrogen) immediately behind reflected shock wave is determined from a plot of T_4/T_1 versus Mach number for the data given in Table 20.

$$T_4 = 1202°K$$

3. The maximum temperature behind the reflected shock wave is calculated with the assumption that the processed gas behind the reflected shock wave undergoes an isentropic compression by weak shock processes from P_4 to P_4'. Using an average value for γ between T_4 and T_4',

$$T_4' = 1202 \left(\frac{23.2}{16.0}\right)^{(1.318 - 1.0)/(1.318)} = 1315°K.$$

Gas Properties at the Throat of Flow-Control Orifice

1. Temperature and pressure at the throat of the control orifice are calculated for critical-flow conditions at the throat. Using an average value for γ between T_4' and T_{or},

$$T_{or} = 1315\left(\frac{2}{1.320 + 1.0}\right) = 1134°K$$

$$P_{or} = 23.2\left(\frac{2}{1.320 + 1.0}\right)^{(1.320)/(1.320 - 1.0)} = 12.6 \text{ atm.}$$

2. Velocity of the gas at the throat of the orifice is the local velocity of sound and is calculated by:

$$(c_o)^2 = \frac{(\gamma_{or})(R)(T_{or})}{M}$$

$$(c_o)^2 = \frac{(1.327)(8.314 \times 10^7)(1134)}{28.016}$$

$$c_o = 6.68 \times 10^4 \text{ cm/(sec)}$$

3. The density of the gas at the throat of the orifice is calculated by the gas law.

$$\rho_{or} = 3.79 \times 10^{-3} \text{ g/(cm)}^3$$

4. Mass flow rate at the throat is the product of c_o and ρ_{or}.

$$G_{or} = (3.79 \times 10^{-3})(6.68 \times 10^4) = 253 \text{ g/(cm)}^2\text{(sec)}$$

Heat Transfer Coefficient

1. Mass flow rate through test-section flow channel is calculated with the continuity equation.

$$G = G_{or}\left(\frac{A_{or}}{A_{ts}}\right) = (253)(0.1832/0.8065) = 57.5\ g/(cm)^2(sec)$$

2. The heat transfer coefficient is calculated with Equation (16) or (C-15).

$$h = 1.435 \times 10^{-4}\ (1315)^{0.3}(57.5)^{0.905}$$

$$h = 4.84 \times 10^{-2}\ cal/(cm)^2(sec)(°K)$$

Ignition Temperature for Linear Heating

1. The initial, instantaneous temperature rise at the propellant surface produced by the passage of the shock waves is calculated with Equation (19) or (C-9).

$$\Delta T_o = 13.66\left(\frac{16.0}{10.0}\right)^{1/2}\left(\frac{0.0366}{0.0212}\right)\left(1.0 - \frac{0.1832}{0.369}\right)(2.85 - 1.20)$$

$$\Delta T_o = 24.8°K$$

2. T_j is calculated from Equation (15).

$$T_j = 293.2°K + 24.8°K = 318°K$$

3. The ignition temperature for linear heating, T_{si}^{L}, is calculated with Equation (14) or (C-7).

$$\frac{T_{si}^{L} - T_j}{T_g - T_j} = (1 - e^{N^2} \text{ erfc } N)$$

$$N = \frac{h(t_i)^{1/2}}{\Gamma_p} = \frac{(0.0484)}{(0.0212)} (0.1176) = 0.2685$$

$$T_{si}^{L} = 318 + (1315 - 318)(1.0 - e^{0.0721} \text{ erfc } 0.2685)$$

$$T_{si}^{L} = 560°K$$

$$\Delta T_{si}^{L} = (560°K - 293°K) = 267°K$$

Mean Surface Heat Flux, $\bar{F}$

1. The constant surface heat flux, $\bar{F}$, which will bring the propellant to its ignition temperature in time, t_i, is calculated with Equation (1).

$$\bar{F} = \left(\frac{0.0212}{2}\right)\left(\frac{1.7725}{0.1176}\right)(560 - 293)$$

$$\bar{F} = 42.7 \text{ cal/(cm)}^2\text{(sec)}$$

APPENDIX F

PROPELLANT SAMPLES

PREPARATION OF PROPELLANT SAMPLES

All of the propellant used for ignition studies was mixed in the propellant processing laboratory in the Department of Chemical Engineering. This facility has two laboratory-size, sigma-blade mixers manufactured by the Brabender Corporation. In the work described here 50 to 60 propellant sample holders were filled from one batch of propellant. Commercially available chemicals were used for all propellant compositions which were primarily ammonium perchlorate composite propellants with a fuel-binder of polybutadiene-acrylic acid copolymer cured with an epoxy curing agent (Epon 828).

The conventional mixing procedure used for processing propellant for this work was as follows:

1. The mixer was brought to a temperature of 60°C.
2. All ingredients were placed in the mixer. The ammonium perchlorate was added first, followed by all other solid ingredients. The liquid polymer was placed on top of the solid ingredients. The curing agent was added last.
3. The ingredients were held under a vacuum for 20 minutes before the mixer was started.
4. The ingredients were then mixed for 10 minutes under vacuum.
5. The mixer was stopped and the walls and blades were scraped with a spatula.
6. The mixer was then sealed and held under vacuum for 5 minutes before the mixing was resumed.

7. The final mixing period was 45 minutes under an absolute pressure of one inch Hg.

Freshly mixed propellant was immediately placed in the sample holders. In the preliminary phases of this study, propellant was cast directly into the cavity of the sample holders under vacuum to eliminate the entrapment of air. It was found later that the sample holders could be filled with a spatula under atmospheric conditions and that the entrapped air could be removed after the sample holders were filled. This was accomplished by placing the filled sample holders in a vacuum chamber, allowing the propellant to mushroom under pressure of internally trapped air, and then tamping the propellant with a Teflon-tipped rod. This operation was repeated until no further rising of the propellant occurred. These operations were all carried out under vacuum by placing the sample holders on a rotating jig and extending the tamping rod through an air-tight seal in the Plexiglass cover of the vacuum chamber. The last procedure facilitated preparation of samples for propellants which contained only a single particle size of ammonium perchlorate and were too viscous to cast directly into holders.

Since most of the ignition tests were conducted on freshly cut propellant surfaces, the sample holders were over-filled, and a fresh, smooth surface was carefully cut with a new, single-edge razor blade immediately before tests. Figure 75 is a photograph of sample holders filled with propellant. For tests in which smooth, polymer-rich surfaces were required, the sample surface was smoothed before curing by wiping the face of a slightly over-filled sample holder on a smooth Teflon sheet. This procedure removed all excess propellant and pushed the

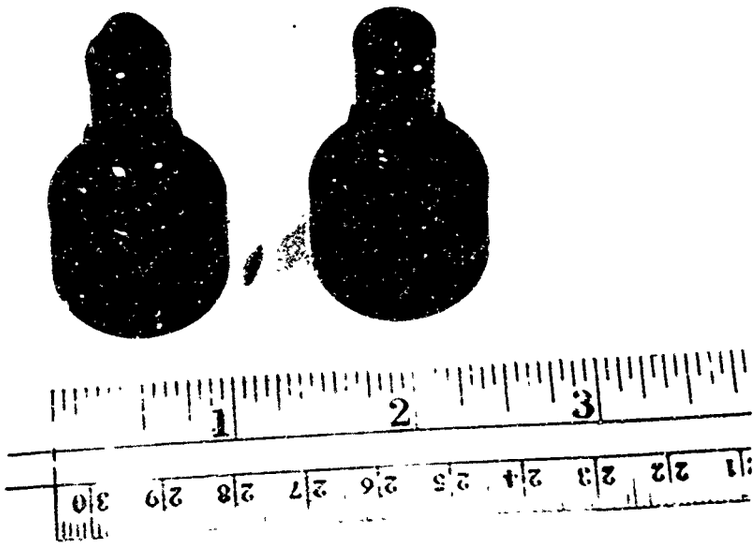

Figure 75

Photograph of Sample Holders Filled with Propellant. Left: As-Cast Propellant Sample. Right: Sample with Cut Surface.

large particles of ammonium perchlorate into the propellant matrix. A thin polymer coat always formed on the surfaces of these samples after they were placed in the curing oven.

Several of the propellants tested were processed entirely from solid ingredients, such as ammonium perchlorate, carbon black, and copper chromite. For preparing these pressed propellants, the ingredients were thoroughly blended and then the powder was pressed into a cylindrical pellet under a pressure of 100,000 psig. A small amount of moisture sprayed on the powder with an aspirator before processing greatly improved the structural integrity of the pellets. Pressed propellants were not oven dried, but were kept in a desiccator several days before being used in tests.

These pellets were then bonded into sample holders with an epoxy resin or an inorganic, copper-phosphoric acid cement. After the cements had hardened, the excess propellant that extended above the face of the sample holder was removed by sanding with a fine-grit silicon-carbide paper.

EFFECT ON IGNITION OF METHOD OF PREPARATION

A problem which always faces the experimental investigator of propellant ignition is that of sample preparation. In this work to obviate the problem, most of the propellant samples were prepared by casting propellant directly into sample holders. However, sometimes propellant to be tested is available only in slab form and samples must be cut and placed in sample holders. In this brief study, samples of F propellant were cut from a slab in the form of a solid cylinder using a cork borer or a leather punch and were then cemented into sample holders. Two different cements were used. Krylon brand

acrylic resin was used on a few samples, but because of its air drying properties, the polymer film would shrink and several coats were required to fill the void between sample and wall of the holder. A second adhesive used was an epoxy cement, Epox Cement No. 346, manufactured by the G. C. Electronics Co. This provided a good bond, but propellant surfaces had to be cut before the cement completely cured; otherwise the cement would break away from the edges of the propellant surface. Nevertheless, several propellant samples were prepared which could be tested. The results of these ignition tests on cemented samples are shown in Figure 76 and are compared with the results obtained with cast propellant samples. There is reasonable agreement between the two sets of data showing that it is possible to obtain useful experimental results from cemented samples.

Some of the problems that were anticipated, but did not arise in the work were: (1) that perchlorate particles would be loosened by cutting with the cork borer and thus allow hot gas from the passing shock wave to flow into the interstices between the particles and the binder which would promote early ignition, and (2) the surface of the organic cement having a lower thermal responsivity than the propellant would undergo a faster temperature rise and thus initiate ignition at the edges of the propellant surface. The fact that reasonable agreement was obtained using the two methods for sample preparation does not mean that some of these problems would not arise with a different propellant system.

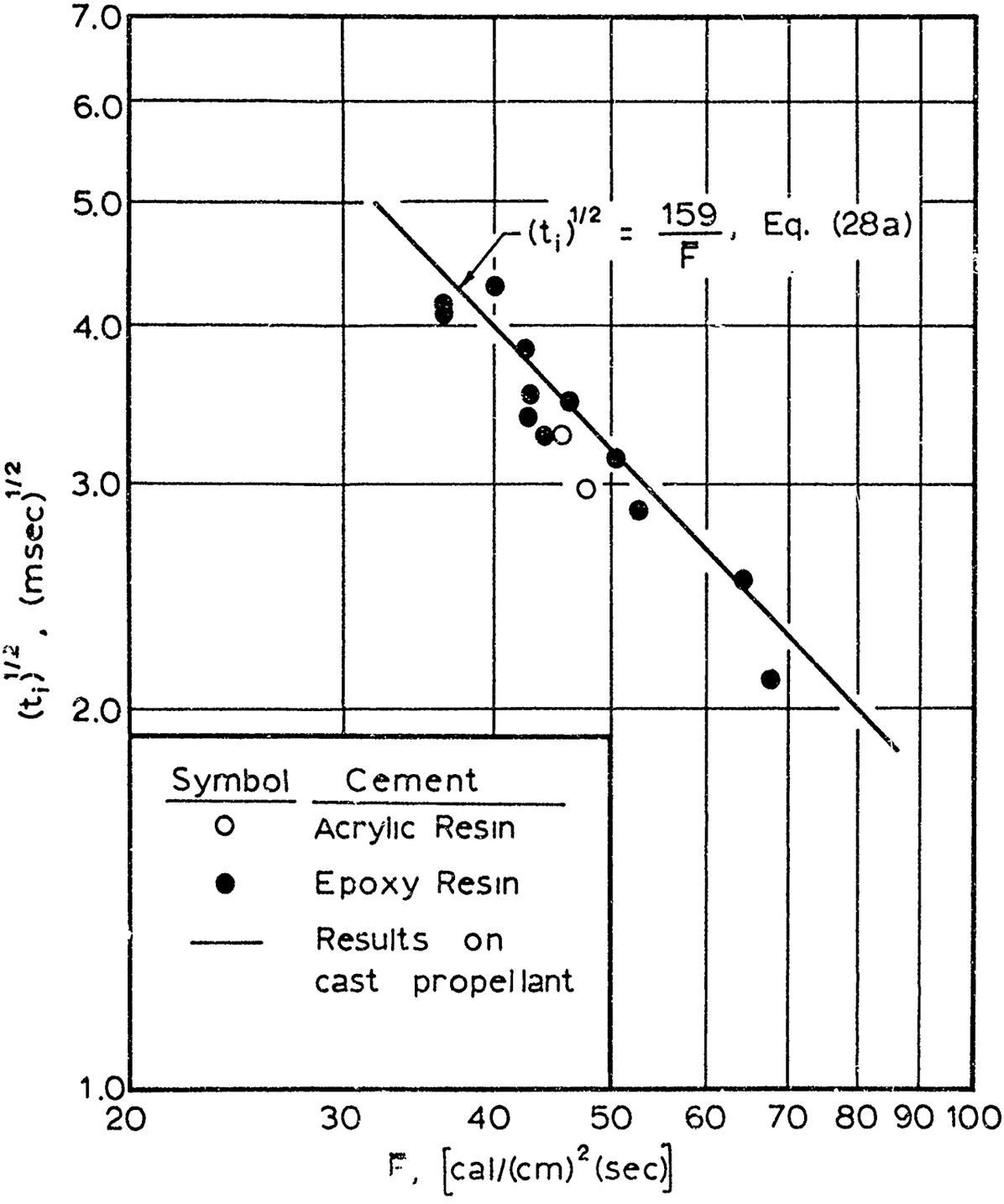

Figure 76

Ignition Data for F-Propellant in Nitrogen at a Test-Gas Velocity of Mach 0.13 for Propellant Samples Prepared by Different Methods.

If samples are to be cemented into sample holders, a non-shrinking cement having physical properties similar to those of the propellant would facilitate preparation of samples.

APPENDIX G

CALIBRATION OF FLOW-CONTROL ORIFICES

The orifices used for controlling the flow of the gas through the test section in ignition tests were calibrated with a rarefaction tube. From isentropic theory of rarefaction tube performance [69, 80], it can be shown that the effective area of a critical-flow orifice at the end of the rarefaction tube, A_{or}, through which the pressurized gas is discharged, following the instantaneous uncovering of the orifice, is related to other easily measured variables by the following equation:

$$\frac{A_{or}}{A_r} = (n - 1)\left(\frac{n}{n + 1}\right)^{n/2}\left(\frac{1 - \sigma_1}{\sigma_1}\right)\left[1 + (n - 1)\left(\frac{1 - \sigma_1}{\sigma_1}\right)^2\right]^{-n/2}$$

$$n = \frac{\gamma + 1}{\gamma - 1}$$

$$\sigma_1 = \left(\frac{P_1}{P_o}\right)^{1/1 + n}$$

Where: A_r is the area of the rarefaction tube.

P_o is the initial absolute pressure in the tube.

P_1 is the pressure in the tube immediately following the passage of the rarefaction wave (first plateau pressure).

γ is the ratio of specific heats for the test gas.

From Equation (G-1) it is seen that the only experimental data needed for determining the effective flow area of an orifice are readings of the initial temperature and pressure of the gas in the tube, and a total pressure drop across the rarefaction wave. P_1 must exceed ambient pressure enough to assure that sonic flow occurs at the orifice.

A Kistler, Model 401, quartz pressure pickup in conjunction with a Model 568 charge amplifier was used for measuring the pressure drop as the rarefaction wave passed the monitoring station in the tube wall. Several calibration runs were made on each orifice for an initial tube pressure of 100 psig. A few check runs were also made at initial tube pressures of 150 and 200 psig. The experimentally determined flow areas are compared with measured orifice areas in Table 18. With dry air as the test gas, experimentally determined flow areas from individual runs differed by less than two per cent from the average for all tests on a given orifice. As was expected, no effect of pressure on the discharge coefficient was found.

APPENDIX H

HEAT FLUX GAUGES

Heat flux gauges are versatile, sensitive, and fast-response temperature sensors. The heat flux gauges used in this work for measuring heat transfer to the wall of the test-section flow channel were made from small, solid cylinders of glass or ceramic materials. A thin platinum-film resistance thermometer was bonded to one flat face of the cylinder as shown in Figure 66. The platinum resistance thermometer measures the surface temperature of the gauge substrate as the gauge surface is exposed to external heating. This kind of sensor is most useful for heat transfer involving heat conduction or forced convection. Its greatest advantage over other temperature sensing devices is its fast response and high sensitivity. The response time for a heat flux gauge is of the order of a few microseconds, and the response time is dependent only on the thickness of the platinum film [92]. The sensitivity of the heat flux gauge can be varied depending on its application, but for this work a sensitivity of about one millivolt/^{o}C was used.

PREPARATION OF HEAT FLUX GAUGES

The heat flux gauges used in this work were made with substrates of Pyrex 7740, Pyroceram 9608, or alumina (Alsimag 614). One end face of cylinders of these materials was polished with 600-A grit, silicon-carbide paper and then degreased before the platinum paint (Liquid Bright Platinum, No. 05-X from the Hanovia Liquid Gold Division of Engelhard Industries, Inc.) was applied to the surface. A narrow strip, as illustrated in Figure 66, was painted across the face of the

gauge for the sensing element; and four leads were painted down the wall of the cylinders for making electrical connections. The freshly applied paint was allowed to dry at room temperature before the gauges were fired in a well-ventilated furnace. The Pyrex gauge element was fired for 30 minutes at 675°C. For ceramic gauges the temperature was increased to 800°C. Usually, one uniform coat (less than one-micron thick [92]) was sufficient to give the desired sensing element resistance of 50 to 500 ohms. About 10 coats of platinum paint were applied to walls of the cylinder. This provided a low resistance lead and also made an excellent base for attaching external leads to the gauge by soldering.

Heat-flux-gauge elements prepared in this manner were cemented into the holders with an epoxy resin. The resin provided a gas-tight seal and also served as an insulating material between the platinum leads and the wall of the holder.

DETERMINATION OF HEAT FLUX GAUGE PROPERTIES

Temperature Coefficient of Resistivity, β_0

The thin platinum film prepared from Liquid Bright Platinum, No. 05-X does not have the same electrical properties as pure platinum; and since these properties cannot be predicted, it was necessary to determine experimentally the resistance and the temperature coefficient of resistivity for each gauge. The experimental procedure used was to place the gauge in a glass tube and then immerse the assembly in a water bath. The film resistance versus temperature relationship was usually determined over the temperature range of 0 to 95°C. The film resistance was calculated from voltage measurements by comparing the voltage drop across

the gauge resistance element with that of a known resistance in the same series electrical circuit.

It was found that the experimental data for all the heat fluxes gauges in the temperature range of 0 to 95° C were well represented by an equation of the following form:

$$R_T = R_o (1 + \beta_o T) \qquad \text{(H-1)}$$

Where: R_o is the film resistance at 0° C.

T is the temperature in ° C.

β_o is the temperature coefficient of resistivity ohm/(ohm)(°C).

Experimentally determined values for the temperature coefficient of resistivity for heat flux gauges used in the research for this thesis are given in Table 19. Experimental data for a heat flux gauge with a substrate of Pyrex 7740 (Gauge No. 4) are plotted in the form of temperature versus film resistance in Figure 77.

Over the range of temperatures for which temperature-resistance data were obtained, the resistance of the platinum sensing element was found to be linear in temperature for all gauges. It is expected, however, based on data for pure platinum that the resistance of the sensing element would be a weaker function of temperature at temperatures above 100° C. Cheng [23] measured the sensing-element resistance as a function of temperature to 220° C on similar gauges, and found a slightly weaker dependence on temperature above about 110° C. This gave a resistance for the sensing element which was about one per cent lower at 200° C than that predicted from the linear dependence in the range of 0 to 100° C.

Bogdan [18] reported that the resistance of the platinum sensing element made with Liquid Bright Platinum No. 05-X for Pyrex heat flux

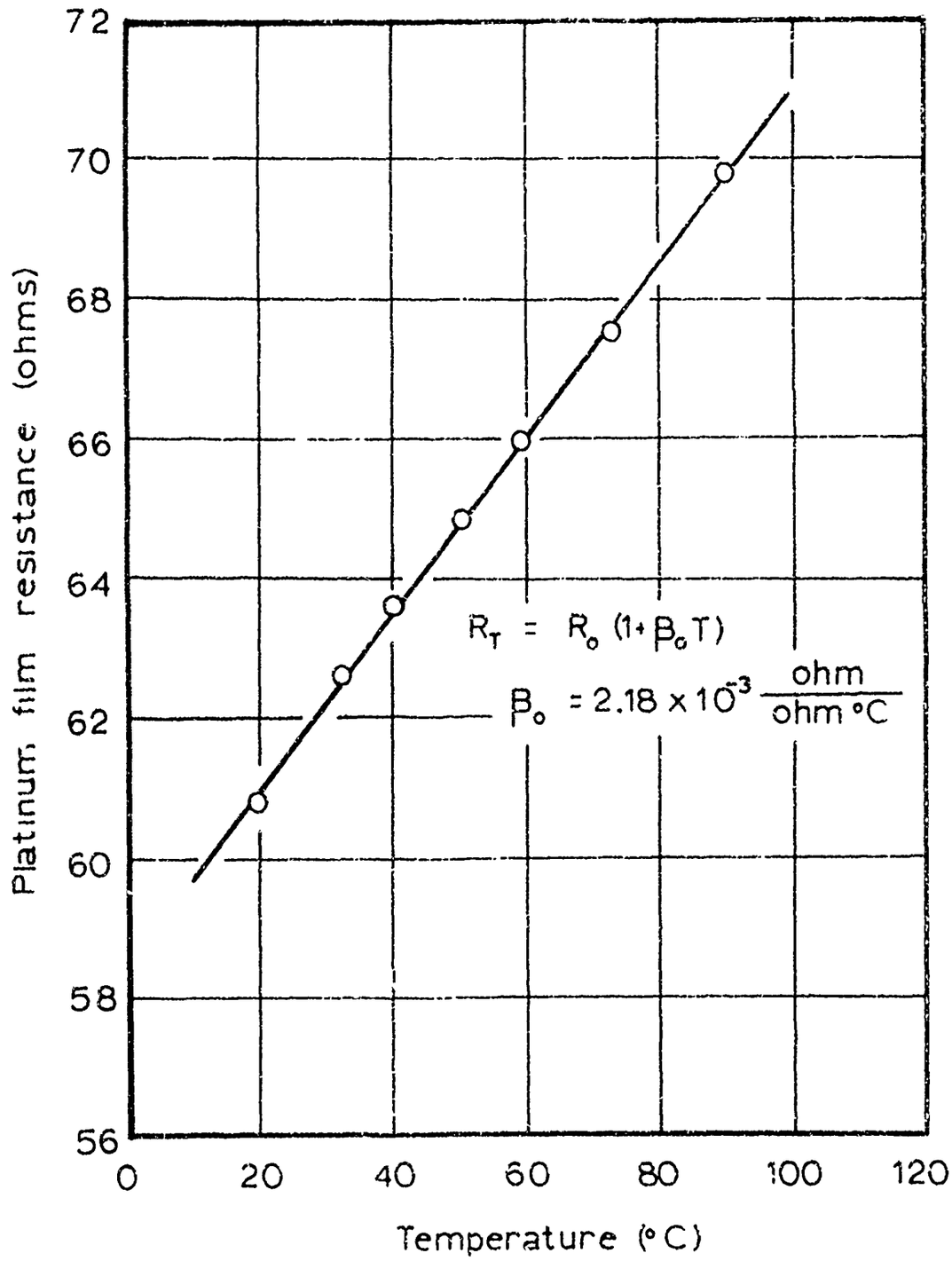

Figure 77

Temperature-Sensing Element Resistance Data for Pyrex 7740 Heat Flux Gauge (Gauge No. 4)

gauges can be represented by the following equation to 1000°F:

$$\left(\frac{dR}{dT}\right)_T \Big/ \left(\frac{dR}{dT}\right)_{70°F} = 1.018 - 2.59 \times 10^{-4}\ T \qquad \text{(H-2)}$$

Where: T is the ambient temperature in °F.

For heat flux gauge measurements reported in this work it was assumed, recognizing a small error would be introduced into derived values of heat flux to the test section wall, that the temperature coefficient of resistivity determined in the range of 0 to 90°C could be used over the range of 20°C to 300°C. For most of the heat transfer runs with Pyrex gauges, the gauge surface temperature did not exceed 200°C; and for the gauge made of alumina, the maximum surface temperature did not exceed 90°C, even at the highest heat transfer rates.

THERMAL RESPONSIVITY, Γ

The thermal responsivity of the gauge substrate is required for translating temperature-time data to heat flux at the gauge surface. In theory it should be possible to calculate the thermal responsivity of all materials used for gauge substrates from published data on thermal conductivity, density, and heat capacity.

It was found, however, that the thermal conductivity data for Pyrex 7740 reported in the literature by different investigators differed by as much as 20 per cent, and it was not possible to use published data for calculating the thermal responsivity of gauge materials. Consequently, it was necessary to determine independently the thermal responsivities for the gauges used in this work.

The method used for determining the room temperature thermal responsivities for gauges was to thrust an assembled gauge at room

temperature into a carbon tetrachloride bath at 0° C. The temperature change at the surface of the gauge as it was lowered into the bath was measured with the platinum resistance sensing element by the same methods used for obtaining temperature-time data from heat transfer runs in the shock tube. The gauge circuitry for temperature measurement is described in the following section. The instantaneous, temperature drop at the gauge surface as it entered the liquid was used for calculating thermal responsivity of the gauge material. For the case where two semi-infinite bodies of different uniform temperatures are instantaneously brought in contact with zero contact resistance. The equation which describes the interface temperature between the two bodies is discussed on page 88 of Reference 22, and reduces to the following form:

$$\frac{T_{ga} - T_i}{T_i - T_\ell} = \frac{\Gamma_\ell}{\Gamma_{ga}} \qquad \text{(H-3)}$$

Where T_{ga}, T_ℓ, and T_i are the initial uniform gauge temperature, initial uniform liquid temperature, and the temperature at the interface between the gauge and the liquid at the instant of contact, respectively. The mean thermal responsivity of carbon tetrachloride over the temperature range 0° C to T_i was calculated from what were believed to be the most reliable data for k, ρ and c. Data for k were taken from Reference 90, and data for ρ and c were taken from Reference 91.

The data on thermal responsivity at room temperature for the heat flux gauges used in this work are given in Table 19. The thermal responsivity for Pyrex 7740 of 0.0366 ± 0.0002 cal/(cm)^2(sec)$^{1/2}$ ($^{\circ}$K) is in excellent agreement with values reported by other

investigators. Baer [6], Bogdan [18], Hartunian and Varwig [42], and Skinner [85] report values for the thermal responsivity of Pyrex at room temperature of 0.0374, 0.0360, 0.0361, and 0.0363 cal/(cm)^2(sec)($^\circ$K), respectively. Except for the value reported by Baer, all the values quoted above were determined by a different experimental method than that used in this work. The other values were determined by observing the temperature rise at the gauge surface when a high-voltage electrical pulse was discharged through the platinum-resistance sensing element.

TEMPERATURE MEASUREMENT

The temperature history of the heat flux gauge surface during the time that the surface is exposed to external heating is measured by placing the gauge in a suitable electrical circuit so that the temperature change can be recorded as an emf drop across the platinum sensing element. The wiring diagram for measuring the temperature of the gauge surface is shown in Figure 78. The unique feature of the circuit illustrated in Figure 78 is that a temperature rise can be simulated for calibrating the vertical sensitivity of an oscilloscope by switching a predetermined resistance out of the series circuit.

It is seen by examination of the diagram in Figure 78, that the large current-control resistance in the circuit allows the resistance of the sensing element to change without producing an appreciable change in the circuit current. Consequently, for all practical applications the current in the circuit is constant and the change in resistance of the platinum film sensing element can be measured directly as a change in emf, the change in emf is linear with temperature if the temperature dependence of the platinum-sensing element can be

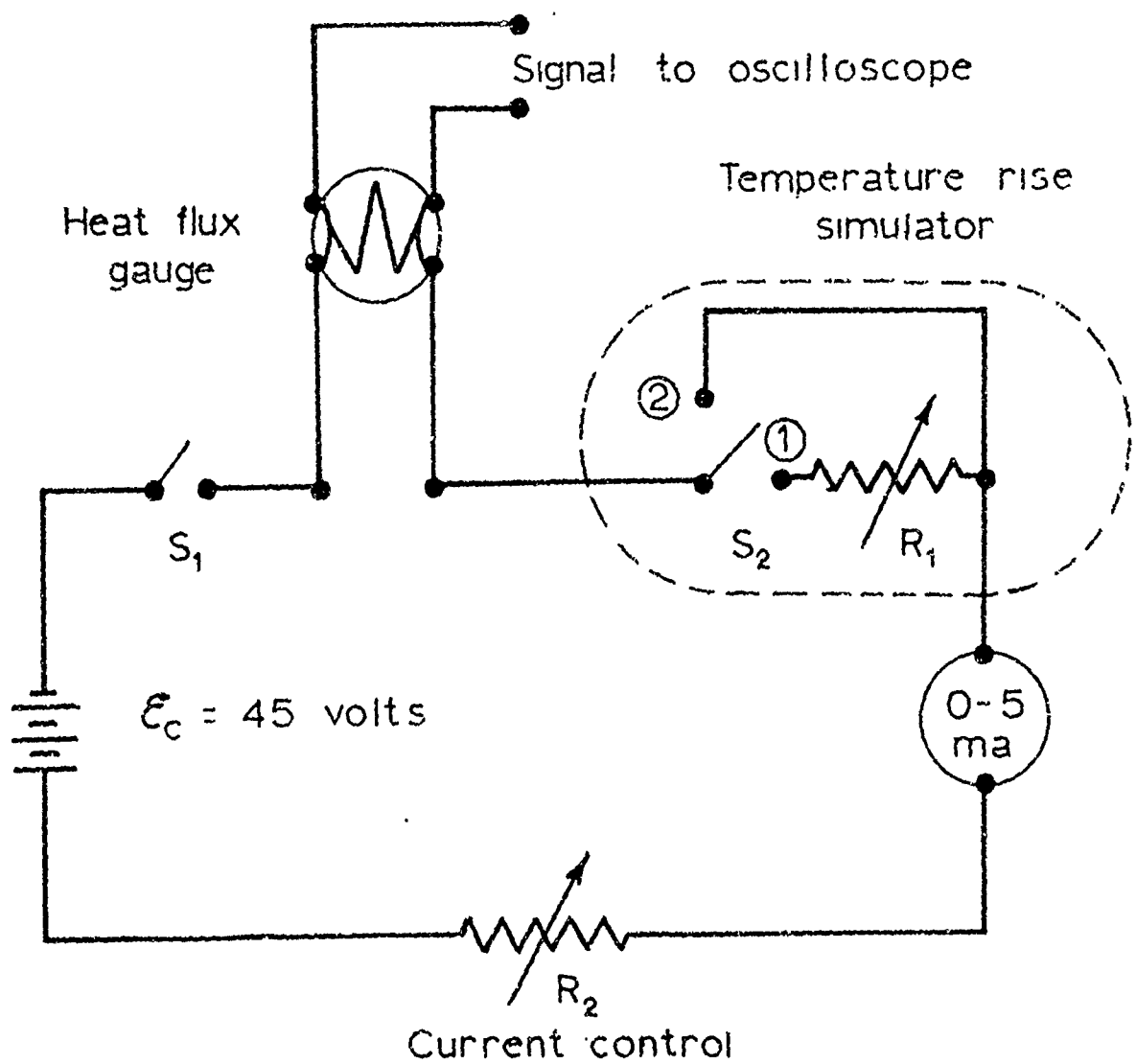

Figure 78

Wiring Diagram for Temperature Measurement with Heat Fluxes Gauges.

represented by Equation (H-1). To prevent heating of the gauge surface by energy dissipation in the sensing element, the circuit current was held below 5 milliamperes.

By an analysis of the circuit shown in Figure 78, it can be shown that the resistance, R_1, required for simulating a temperature rise ΔT is:

$$R_1 = \frac{R_c\ [\beta_o(\Delta T)]}{1 + \beta_o(T_1 + \Delta T)} \qquad \text{(H-4)}$$

Where T_1 is the initial, uniform gauge temperature and R_c is the total resistance in the circuit. It follows that when switch S_2 is in position 1, with S_1 closed, that the total emf drop, $\mathcal{E}_c$, across the circuit is:

$$\mathcal{E}_c = i_1\ (R_R + R_1 + R_g) = i_1\ (R_c) \qquad \text{(H-5)}$$

Where R_g is the gauge resistance, R_1 is the simulator resistance, and R_R represents all other resistances in the circuit. With switch S_2 in position 2, we have:

$$\mathcal{E}_c = i_2\ (R_R + R_g) = i_2\ (R_c - R_1) \qquad \text{(H-6)}$$

Since the gauge resistance remains unchanged, we have:

$$i_1 = e_{g_1}/R_g, \qquad i_2 = e_{g_2}/R_g \qquad \text{(H-7)}$$

Where the subscripts 1 and 2 represent the emf drop across gauge element for the different switch, S_2, positions. It follows that:

$$\frac{e_{g_1}(R_c)}{\mathcal{E}_c} = \frac{e_{g_2}(R_c - R_1)}{\mathcal{E}_c} \qquad \text{(H-8)}$$

Comparing this result with the emf changes that occur when the gauge surface temperature increases, we find since the current flow is essentially constant that:

$$i = e_{g_1}/R_{g_1} = e_{g_2}/R_{g_2} \qquad \text{(H-9)}$$

Here the subscripts 1 and 2 represent the gauge emf and gauge resistance for different temperatures.

Also:

$$R_{g_1} = R_o(1 + \beta_o T_1), \qquad R_{g_2} = R_o(1 + \beta_o T_2) \qquad \text{(H-10)}$$

Thus:

$$\frac{e_{g_1}}{e_{g_2}} = \frac{1 + \beta_o T_1}{1 + \beta_o T_2} \qquad \text{(H-11)}$$

It follows that the resistance R_1 needed to simulate a given temperature rise, ΔT, at the gauge surface by switching R_1 from the circuit is:

$$R_1 = \frac{R_c\ [\beta_o(\Delta T)]}{1 + \beta_o(T_1 + \Delta T)} \qquad \text{H-4)}$$

APPENDIX I

ANALYSIS OF DATA FROM HEAT FLUX GAUGE MEASUREMENTS

In the analysis of temperature-time data from heat flux gauge measurements, the conventional procedures were modified to include the temperature dependence of gauge thermophysical properties. The methods used for obtaining heat flux values at the gauge surface from T(t) data are described in this appendix.

CALCULATION OF HEAT FLUX FOR CONSTANT GAUGE PROPERTIES

The following discussion is transcribed with only minor modification from Reference 52.

From the theory of heat transfer to a semi-infinite body initially at uniform temperature and having thermophysical properties independent of temperature, one obtains the following equation:

$$F(t) = \frac{\Gamma}{(\Pi)^{1/2}} \frac{\partial}{\partial t} \int_0^t \frac{T(\lambda)}{(t - \lambda)^{1/2}} \, d\lambda \qquad \text{(I-1)}$$

Integration by parts followed by the indicated differentiation gives, provided T(0) = 0

$$\frac{(\Pi)^{1/2}}{\Gamma} F(t) = \int_0^t \frac{dT}{d\lambda} \frac{d\lambda}{(t - \lambda)^{1/2}} \qquad \text{(I-2)}$$

Equation (I-2) is the starting point of Nanigian [72] who developed an

equation for calculating heat flux-time relationships from data obtained from tests on propellant igniters. The procedure is to approximate the temperature trace by n straight-line segments bounded by $\lambda = 0, \ \theta_1, \theta_2, \ldots, \theta_n,$ where $\theta_n = t$ The slope of the ith segment is:

$$\left(\frac{dT}{d\lambda}\right)_i = \frac{T_i - T_{i-1}}{\theta_i - \theta_{i-1}} = m_i \qquad \text{(I-3)}$$

Equation (I-2) then becomes:

$$\frac{(\Pi)^{1/2}}{\Gamma} F(t) = \sum_{i=1}^{n} m_i \int_{\theta_{i-1}}^{\theta_i} \frac{d\lambda}{(t - \lambda)^{1/2}} =$$

$$2\sum_{i=1}^{n} m_i \left[(t - \theta_{i-1})^{1/2} - (t - \theta_i)^{1/2}\right] \qquad \text{(I-4)}$$

Equation (I-4) is the equation developed by Nanigian [72].

Heating of the surface after the passage of a shock wave or detonation wave at time zero is an interesting and sometimes important special case. As T(+0) is finite, Equation (I-2) is not applicable. Equation (I-1) is employed, assuming that T is constant at T_o to θ_1.

$$\frac{(\Pi)^{1/2}}{\Gamma} F(t) = T_o \frac{\partial}{\partial t} \int_0^{\theta_1} \frac{d\lambda}{(t - \lambda)^{1/2}} + \frac{\partial}{\partial t} \int_{\theta_1}^{t} \frac{T(\lambda)}{(t - \lambda)^{1/2}} d\lambda =$$

$$\left[\frac{T_o}{(t)^{1/2}} - \frac{T_o}{(t - \theta_1)^{1/2}}\right] + \left[\frac{T_o}{(t - \theta_1)^{1/2}} + \int_{\theta_1}^{t} \frac{dT}{d\lambda} \frac{d\lambda}{(t - \lambda)^{1/2}}\right] =$$

$$\frac{T_o}{(t)^{1/2}} + 2 \sum_{i=2}^{n} m_i \left[(t - \theta_{i-1})^{1/2} - (t - \theta_i)^{1/2}\right] \qquad \text{(I-5)}$$

Since there is no commitment as to the magnitude of θ_1, it can be made vanishingly small. The derivation can be modified to account for discontinuities in the temperature-time relationship at later times in the heating process.

Equations (I-4) and (I-5) were programmed for translating T(t) data to an F(t) relationship on the IBM 1620 and 7040 digital computers.

It was found that Equation (I-4) was not entirely suitable for translating temperature-time data for the case where T(t) approximated that for constant heat flux to the gauge surface. For the constant heat flux case, the calculated heat flux at the end of the initial time increment chosen was always higher than the actual value by about 10 per cent, even if the time interval taken was vanishingly small. The F(t) values calculated by Equation (I-4) would then approach a constant heat flux value asymptotically from a higher value as successive time intervals were taken. Baer [7] modified the numerical procedure for

integration of T(t) data for the first few time intervals when temperature-time data approximated that for the constant heat flux case.

The procedure was to calculate heat flux from T(t) data assuming the heat flux to be constant for the first few time intervals and then to calculate a correction term from the T(t) data to account for the deviation from the constant heat flux problem. The equation used to approximate the heat flux to the gauge surface for the first few increments was:

$$F(t) = \frac{\Gamma(\Pi)^{1/2}}{2} \left[\frac{T(t)}{(t)^{1/2}} + \frac{1}{\Pi(t)^{1/2}} \int_0^t \frac{(\lambda)^{1/2}\, T(t) - (t)^{1/2}\, T(\lambda)}{(t - \lambda)^{3/2}}\, d\lambda \right] \quad \text{(I-6)}$$

The analytical development of Equation (I-6) is described in Appendix B of Reference 6.

The numerical procedure for translating temperature-time data to heat flux at the gauge surface, as modified by Baer, was used for analyzing data in this study.

HEAT FLUX CALCULATIONS FOR TEMPERATURE-DEPENDENT GAUGE PROPERTIES

Recent experimental work by Skinner [85], Hartunian and Varwig [42], and Bogdan [18] on the temperature dependence of Γ for Pyrex heat flux gauges has shown that the variation of Γ with temperature must be included in the calculation for heat flux from heat flux gauge measurements. As a necessary part of the heat transfer study for this thesis, a method was developed for including the temperature dependence of Γ for heat flux gauges in F(t) calculations. It was found through numerical solution of the one-dimensional heat

conduction equation with consideration of the temperature-dependent gauge properties that measured temperature could be adjusted so that heat flux could be calculated by methods developed for calculation with constant gauge properties. It was found that the magnitude of the temperature adjustment was primarily dependent on the actual heat flux gauge surface temperature, and was only a weak function of the heat flux applied to the gauge surface, and was therefore essentially independent of time. As a consequence, it was possible to obtain a simple relationship for adjusting measured T(t) data.

A solution to the one-dimensional heat conduction equation

$$\rho c(T) \frac{\partial T}{\partial t} = \frac{\partial}{\partial x}\left[k(T) \frac{\partial T}{\partial x}\right] \qquad \text{(I-7)}$$

was obtained using the numerical method of Schmidt.
Where c(T) and k(T) were approximated by:

$$c_T = c_o (1 + a_o T) \qquad \text{(I-8)}$$

$$k_T = k_o (1 + b_o T) \qquad \text{(I-9)}$$

The results of the analysis on heat flux gauges made from Pyrex 7740 and alumina are described in the following sections. Published data on Pyroceram 9608 are not complete and it was not possible to include temperature-dependent thermal properties in calculations for this material. However, the thermal diffusivity data on Pyroceram 9608 reported by Plummer, et al. [75] indicate that the thermal conductivity of Pyroceram 9608 is a weak function of temperature.

Thermophysical Properties of Pyrex 7740

The $\Gamma(T)$ data for Pyrex 7740 reported by Hartunian and Varwig [42] and by Bogdan [18] are not consistent with $\Gamma(T)$ data derived from $k(T)$ and $c(T)$ data reported in the literature. The $\Gamma(T)$ data reported by Bogdan show a lower temperature dependence than those reported by Hartunian and Varwig, and are in better agreement with $\Gamma(T)$ derived from data on the individual thermal properties at temperatures below 100°C.

As a means of finding the temperature dependence of thermal conductivity, k, from the $\Gamma(T)$ data on Pyrex 7740 reported by Bogdan [18] that could be used in the numerical solution for Equation (I-7), a $k(T)$ relationship was derived from these data with the help of published data for $c(T)$ and density of Pyrex glass, 2.23 g/(cm)^3. The temperature-dependent values of specific heat were calculated using the Sharp-Ginther Equation for mean specific heat of glass [84]:

$$c_m = \frac{a(T) + c_o}{(1 + 0.00146\ T)} \qquad \text{(I-10)}$$

Where c_o is the true specific heat at 0°C and $\underline{a}$ is a constant that is characteristic of the glass composition. The specific heat of glass at temperature T is:

$$c_T = \frac{0.00146\ a\ (T)^2 + 2a(T) + c_o}{(1 + 0.00146\ T)^2} \qquad \text{(I-11)}$$

The constants for Pyrex were derived from the summary of results on Pyrex reported by Moore and Sharp [71] which were based on experimental

data of Lucks, et al. [62] for Pyrex 774. A value of 0.1695 cal/(g)(°C) was used for c_o, and $\underline{a}$ was found to have a value of 4.78×10^{-4} cal/(g)(°C) over the temperature range of 0 to 300°C.

The thermal conductivity data derived from the $\Gamma(T)$ data of Bogdan [18] using the values of heat capacity calculated with Equation (I-11) are given in Figure 79. These data are included in Figure 80 with the thermal conductivity data for Pyrex glass reported by other investigators.

To obtain a $k(T)$ approximation which could be used in the numerical solution of Equation (I-7), the temperature dependence for thermal conductivity of Pyrex 7740 was assumed to be a linear function, Equation (I-9). Since it was not possible to define precisely the temperature dependence for thermal conductivity from the data of Figure 80, two different values for the temperature dependence of thermal conductivity for Pyrex 7740 were used in calculations. For Case I, b_o in Equation (I-9) was taken to be 4.52×10^{-4}/°C which represents the temperature dependence for the $k(T)$ data derived from Bogdan's experimental $\Gamma(T)$ data at low temperatures (see Figure 81). For Case II, b_o was taken to be 9.29×10^{-4}/°C which is a reasonable approximation for the temperature dependence shown by the data of Plummer, et al. [75], Lucks, et al. [61], and Kingery [54].

Figure 79

Thermal Conductivity Data for Pyrex 7740
Derived from Thermal Responsivity Data

Temperature (°F)	Temperature (°C)	$\Gamma_T/\Gamma_{70°F}$ [a]	c [b] cal/(g)(°C)	k cal/(cm)(sec)(°C)
70	21.1	1.000	0.1788	3.247×10^{-3}
100	37.8	1.023	0.1856	3.274
150	65.6	1.057	0.1959	3.310
200	93.2	1.086	0.2051	3.337
300	148.9	1.132	0.2208	3.369
400	204.4	1.167	0.2338	3.382
500	260.0	1.191	0.2444	3.369
600	315.6	1.206	0.2534	3.332
700	371.1	1.220	0.2610	3.311

[a] Data from Figure 2, Reference 18.

$$\Gamma_{70°F} = 0.0737 \text{ Btu/(ft.)}^2\text{(sec)}^{1/2}(°F)$$
$$= 0.0360 \text{ cal/(cm)}^2\text{(sec)}^{1/2}(°K)$$

[b] Heat capacity calculated with Equation (I-11).

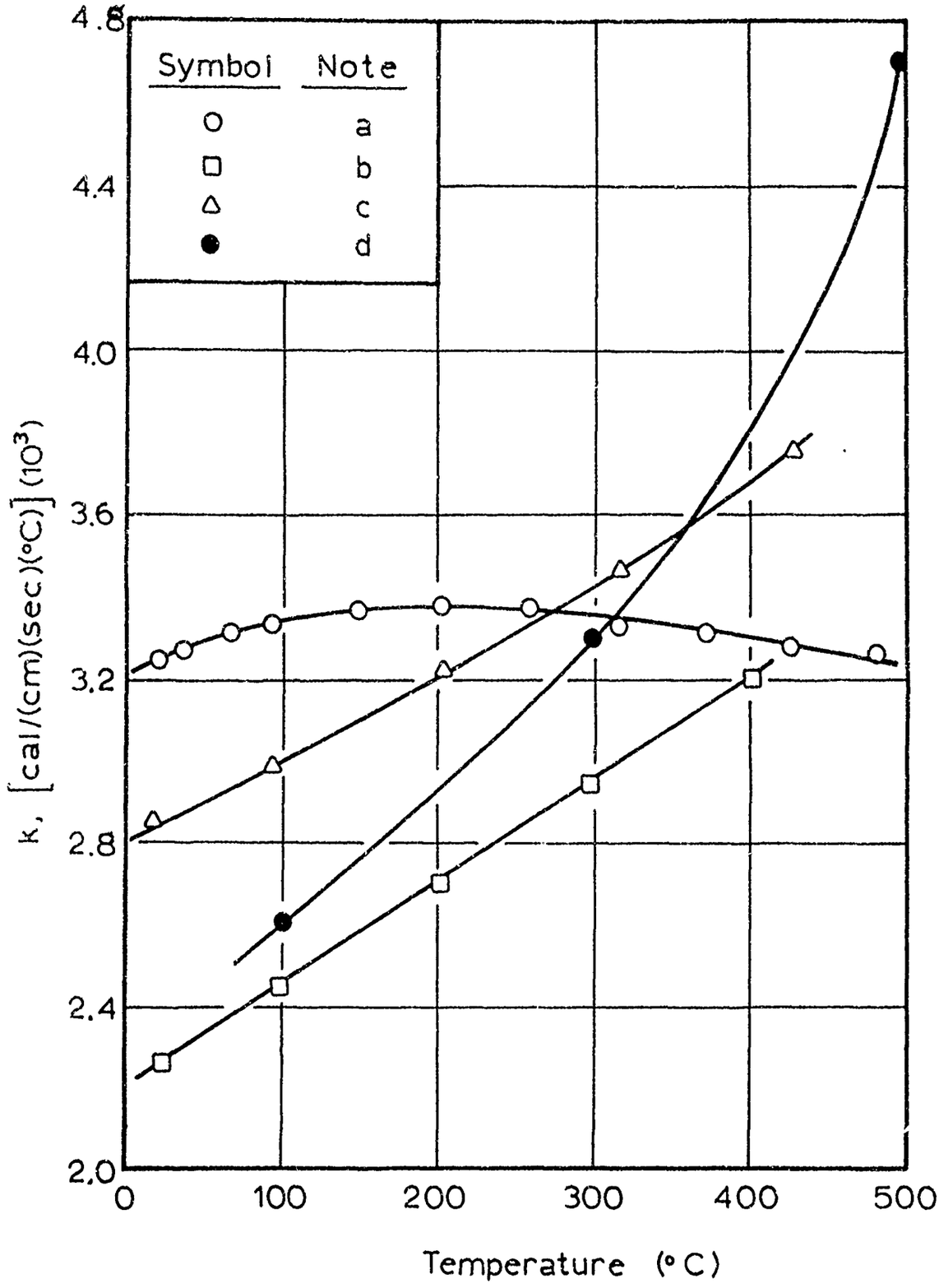

Figure 80

Thermal Conductivity Data for Pyrex Glass.
a. Bogdan [18].
b. Plummer, Campbell, and Woodstock [75].
c. Lucks, Deem, and Wood [61].
d. Kingery [54].

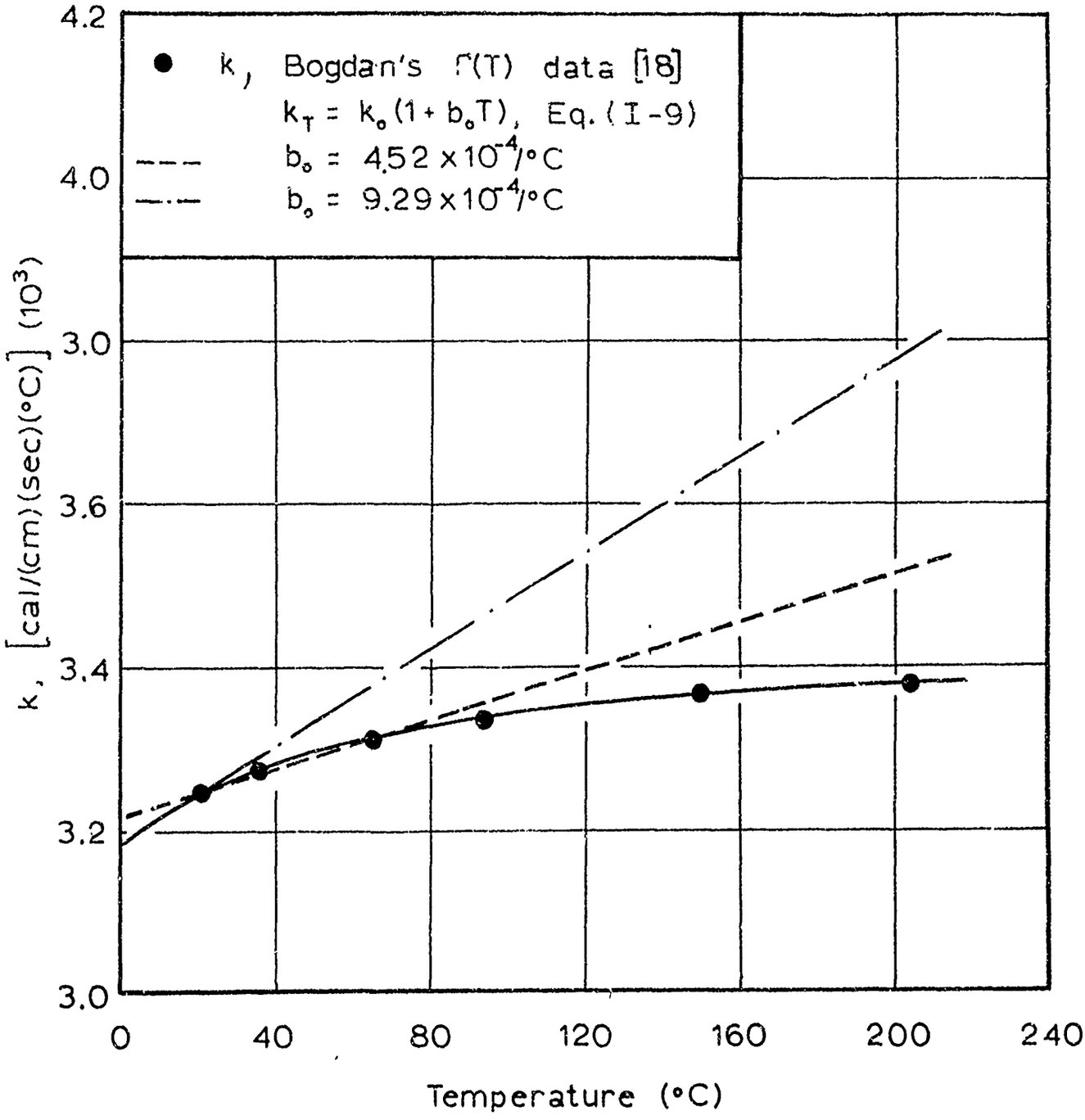

Figure 81

Assumed Temperature Dependence for Thermal Conductivity of Pyrex 7740.

The heat capacity data for Pyrex 7740 used in the numerical solution of Equation (I-7) were also approximated by a linear relationship. The c(T) data for Pyrex 7740 are probably accurate to within 2 per cent of their actual values, but the uncertainty in the k(T) data did not justify the use of a higher order equation for c(T) data. The temperature dependence of heat capacity for Pyrex glass is shown in Figure 82. The value for a_o in Equation (I-8), for the straight line in Figure 82, is $1.67 \times 10^{-3}/°C$. For reasons that will become apparent later, the straight line in Figure 82 intersects the c(T) curve at 26°C.

Thermophysical Properties of Alumina

The data for heat capacity of alumina (Alsimag 614) used in calculations were those reported for pure Al_2O_3 by Furukawa, et al. [35] (see Figure 83). The c(T) data for alumina were also approximated by a straight line, Equation (I-8). The value for a_o used for alumina was $2.25 \times 10^{-3}/°C$. Since no experimental data were available for the thermal conductivity of Alsimag 614, the k(T) data used for this material were based on a measured value of thermal responsivity at 28°C (see Table 19) and the temperature dependence of k for alumina derived from the data of Francl and Kingery [33]. The estimated values for the thermal conductivity of Alsimag 614 for the temperature range 28 to 200°C are given in Figure 83. The value for b_o in Equation (I-9) used in calculations was $-2.59 \times 10^{-3}/°C$.

The density of Alsimag 614 at room temperature was $3.74\ g/(cm)^3$.

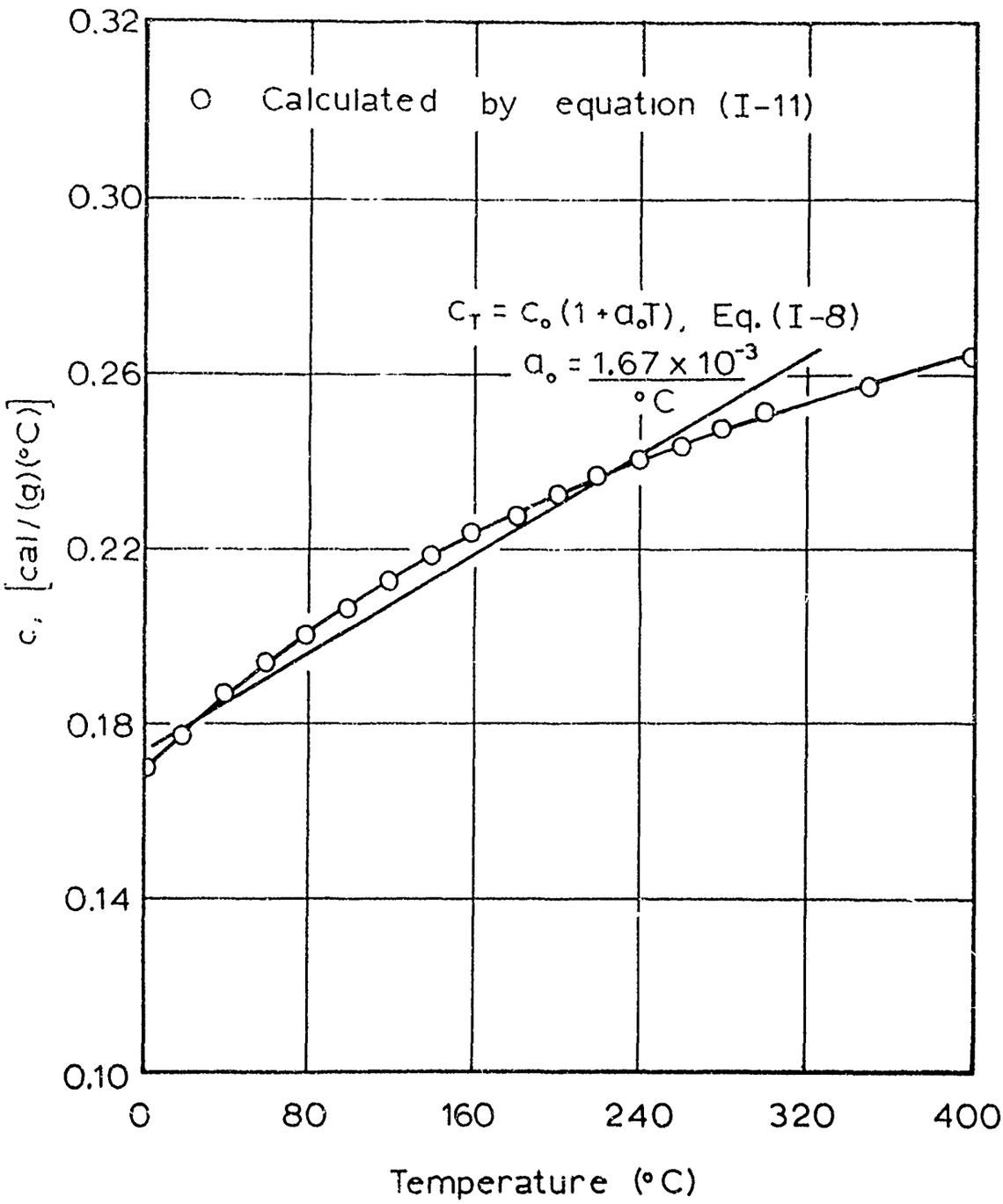

Figure 82

Temperature Dependence of Heat Capacity for Pyrex Glass

Figure 83

Thermal Conductivity and Heat Capacity for Alumina (Alsimag 614)

Heat Capacity[a]		Thermal Conductivity[b]	
Temperature (°C)	c cal/(g)(°C)	Temperature (°C)	k cal/(cm)(sec)(°C)
0	0.1715	28.0	6.22×10^{-2}
1.8	0.1726	50.0	5.84
6.8	0.1754	75.0	5.42
11.8	0.1782	100.0	5.04
21.8	0.1836	150.0	4.37
25.0	0.1852	175.0	4.08
36.8	0.1911	200.0	3.81
51.8	0.1980		
76.8	0.2083		
106.3	0.2192		
126.8	0.2254		
146.8	0.2310		
166.8	0.2360		

[a] Data for pure Al_2O_3 from Reference 35.

[b] Values based on experimentally determined thermal responsivity for Alsimag 614 at 28°C (see Table 19), and the temperature dependence of thermal conductivity based on experimental data for alumina reported by Francl and Kingery [33].

Calculations with Variable Gauge Properties

The calculated data derived from the numerical solution of Equation (I-7) for various assigned values of constant surface heat flux and temperature-dependent thermophysical properties for alumina and Pyrex 7740 showed that T(t) at the gauge surface was primarily a function of $\Gamma(T)$ of the gauge material and was a weak function of the applied heat flux. As a consequence it was possible to adjust the measured gauge surface temperatures so that the methods already described for translating T(t) data to heat flux at the gauge surface for constant gauge properties could be used.

The data for the thermophysical properties of Pyrex 7740 and alumina used in the numerical solution of Equation (I-7) are summarized in Figure 84. Calculated T(t) data at the gauge surface were obtained for Pyrex 7740 for surface heat fluxes of 10 and 50 $cal/(cm)^2(sec)$, and for alumina for surface heat fluxes of 10, 50, and 100 $cal/(cm)^2(sec)$.

Calculated T(t) data for the surface of Pyrex 7740 using the property values for Case I (Figure 84) are tabulated in Figure 85 for assigned constant surface heat fluxes of 10 and 50 $cal/(cm)^2(sec)$, and are compared with data for heating with constant gauge properties, Case III. The data of Figure 85 were plotted in the form T_{ga} versus $(T_{cp} - T_{ga})$. Where T_{ga} is the actual gauge surface temperature, °C, and T_{cp} is the temperature, °C, that the gauge surface would have reached at time, t, by the transient heating process if the gauge properties were independent of temperature (constant thermophysical properties). It was found, as mentioned

Figure 84

Data for Thermophysical Properties of Pyrex 7740 and Alumina Used for Calculations

	$(\rho c)_T$ [a]		k_T [b]	
	$(\rho c)_o$	a_o	k_o	b_o
Material	cal/(g)(°C)	$(°C)^{-1}$	cal/(cm)(sec)(°C)	$(°C)^{-1}$
Pyrex 7740[c]				
Case I:	0.403	0.00167	0.003325	0.000452
Case II:	0.403	0.00167	0.003325	0.000929
Case III:	0.403	0.0	0.003325	0.0
Alumina[d] (Alsimag 614)				
Case I:	0.699	0.00225	0.0583	-0.00259
Case II:	0.699	0.0	0.0583	0.0

[a] Data for (ρc) were approximated by:

$$(\rho c)_T = (\rho c)_o \, (1 + a_o \, T_{ga})$$

Where: T_{ga} is the temperature relative to the initial uniform gauge temperature, 28°C for alumina and 26°C for Pyrex 7740.

[b] Data for k were approximated by:

$$k_T = k_o \, (1 + b_o \, T_{ga})$$

[c] Thermal conductivity, k_o, at 26°C, based on $\Gamma(26°C)$ of 0.0353 $cal/(cm)^2(sec)^{1/2}(°K)$.

[d] Thermal conductivity, k_o, at 28°C, based on $\Gamma(28°C)$ of 0.202 $cal/(cm)^2(sec)^{1/2}(°K)$.

Figure 85

Calculated Surface Temperature-Time Data for Heating of a Semi-Infinite Body of Pyrex 7740 with Temperature-Dependent Thermophysical Properties

Time (msec)	Heat Flux: 50 cal/(cm)^2(sec) T_{cp} [a] (°C)	Heat Flux: 50 cal/(cm)^2(sec) T_{ga} [b] (°C)	Heat Flux: 10 cal/(cm)^2(sec) T_{cp} [a] (°C)	Heat Flux: 10 cal/(cm)^2(sec) T_{ga} [b] (°C)
0.5	36.1	35.8	7.3	7.3
1.0	50.8	49.9	10.2	10.2
2.0	71.7	69.6	14.4	14.3
3.0	87.7	84.6	17.6	17.4
4.0	101.2	97.0	20.3	20.1
5.0	113.9	107.9	22.6	22.4
10.0	159.9	149.7	32.0	31.5
15.0	195.8	180.8	39.2	38.5
20.0	226.1	206.5	45.2	44.3
25.0	252.7	228.7	50.6	49.4
30.0	276.9	245.8	55.4	54.0
35.0	299.0	266.4	59.8	58.2
40.0	319.7	282.9	63.9	62.2

[a] T_{cp} is the surface temperature at time, t, relative to the initial, uniform glass temperature (26°C) calculated assuming thermophysical properties are constant during the heating process (Case III).

[b] T_{ga} is the surface temperature at time, t, relative to the initial, uniform glass temperature (26°C) calculated assuming thermophysical properties are temperature-dependent (Case I).

earlier, that $(T_{cp} - T_{ga})$ was essentially independent of heat flux. It was thus possible to adjust all T(t) data from heat flux gauge measurements so that they could be used directly for obtaining heat flux at the gauge surface by the methods developed for constant gauge properties.

Calculated T(t) data at the surface for the two sets of temperature-dependent thermophysical properties for Pyrex could be represented by the following equations:

For Case I:

$$T_{cp} = T_{ga} + 4.59 \times 10^{-4} (T_{ga})^2 \qquad \text{(I-12)}$$

For Case II:

$$T_{cp} = T_{ga} + 6.15 \times 10^{-4} (T_{ga})^2 \qquad \text{(I-13)}$$

For alumina (Alsimag 614) the calculated T(t) data were represented by:

$$T_{cp} = T_{ga} - 4.1 \times 10^{-4} (T_{ga})^2 \qquad \text{(I-14)}$$

Where: T_{ga} is the measured gauge surface temperature (°C) relative to the initial, uniform gauge temperature; 26°C for Pyrex and 28°C for alumina.

T_{cp} is the surface temperature (°C) relative to the initial, uniform gauge temperature calculated, assuming gauge properties are constant.

Cheng [23] conducted experiments in a radiation furnace at constant heat fluxes for the purpose of determining how temperature-dependent gauge properties affected heat flux gauge measurements. Cheng prepared a Pyrex gauge for measurements by first coating the gauge surface, including the platinum sensing element, with silica; and then carefully depositing a thin layer of carbon from a benzene flame over the silica to ensure absorption of all radiant energy at the gauge surface. T(t) data from these measurements, when adjusted for temperature-dependent properties by Equation (I-12) and when the non-linearity of the temperature-resistance relationship for the platinum sensing element was included in calculations, gave a heat flux-time relationship that was nearly constant to 280°C. The maximum deviation of the data from the constant F(t) relationship was less than 2 per cent at 280°C, the derived F(t) relationship being in excellent agreement with that predicted for the black body temperature in the furnace.

CALCULATION OF HEAT TRANSFER COEFFICIENTS

Heat transfer coefficients were derived from T(t) data obtained with a heat flux gauge mounted in the test-section wall by two different methods. The first method involved the translation of T(t) data to an F(t) relationship from which an average heat transfer coefficient over the effective test period, t, was calculated by approximating the F(t) relationship by small straight line segments.

$$\bar{h} = \frac{1}{2t} \sum_{i=1}^{n} \left(\frac{F_i}{\Delta T_i} \quad \frac{F_{i-1}}{\Delta T_{i-1}} \right) (t_i - t_{i-1}) \qquad \text{(I-15)}$$

Where: $\Delta T_i = T_g - (T_{ga})_i$ at the end of the ith time interval.

T_g is the temperature of the convective gas (°K), and

T_{ga} is the gauge surface temperature (°K) at t_i.

This method for obtaining an average heat transfer coefficient could only be used on T(t) data for which there was not an instantaneous temperature rise at the wall following the passage of the reflected shock wave through the test section (see Figure 69).

The second method was to obtain the combination of instantaneous temperature rise behind the reflected shock wave, T_j, and the value for heat transfer coefficient, h, for Equation (14) or (C-7) that represented the experimental T(t) data for the effective test period, t. The equation used for this analysis was:

$$\frac{T_{cp} - T_j}{T_g - T_j} = (1 - e^{N^2} \operatorname{erfc} N) \qquad \text{(I-16)}$$

$$N = \frac{h(t)^{1/2}}{\Gamma}$$

The procedure was: (1) assume a value for T_j, (2) calculate a value for h, and (3) calculate a T(t) relationship by Equation (I-16) for comparing with experimental data. For this analysis it was necessary again to adjust the measured T(t) data for temperature-dependent thermophysical properties by Equation (I-12) for Pyrex 7740 gauges, and by Equation (I-14) for alumina gauges.

In Equation (I-16), T_{cp} is not the actual gauge temperature for heat transfer from the convective gas; however, for all T(t) data the temperature adjustment $(T_{cp} - T_{ga})$ was always less than 2 per cent of the total ΔT, $(T_g - T_{ga})$ for heat transfer. Where comparisons could be made for heat transfer coefficients obtained by the two methods, for example T(t) data obtained when the No. 1 flow-control orifice was used for controlling the flow of gas through the test section, values for heat transfer coefficients were within one or two per cent of each other. The heat transfer coefficients obtained from this analysis were correlated by the methods already described in Appendix C.

APPENDIX J

EFFECTIVE TEST TIME IN THE SHOCK-TUBE APPARATUS

Ideally, when the driven section of the shock tube is long, the length of time that shock-heated gas behind the reflected shock wave is available for test purposes is dependent only on the total length of the shock tube and the properties of the driver gas; the test period is terminated by the arrival of the head of the rarefaction wave at the test position. In this work because of the large amount of gas that was exhausted from the driven end through the test-section flow channel during tests with large flow-control orifices, the test period was shortened by the mixing of colder driver gas with the test gas as the supply of the latter was depleted.

The length of time available for tests with various flow-control orifices at the downstream end of the test-section flow channel is shown graphically in Figure 86 as a plot of Mach number of the incident shock wave at the entrance to the test section, M_E, versus the effective test period, t, in milliseconds. The data shown in Figure 86 were derived from the experimental T(t) data obtained in the heat transfer study. The effective test time is the time after start of heating that the experimental T(t) data deviated by 5 per cent from the curve defined by Equation (I-16) that best represents the experimental data. The straight lines in Figure 86 then represent the minimum test period in the shock tube for the various flow-control orifices.

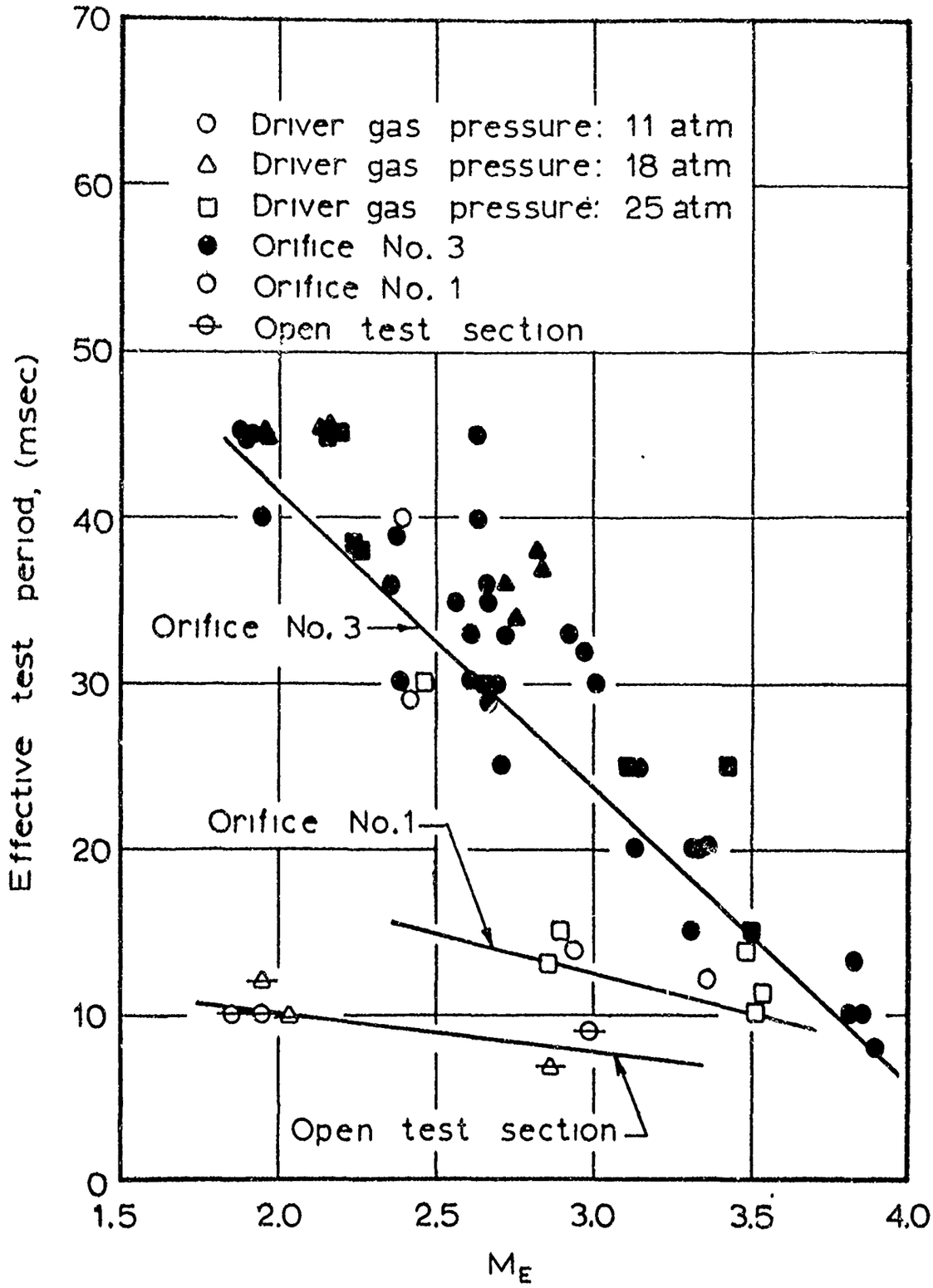

Figure 86

Effective Test Period in Shock-Tube Apparatus as Function of Mach Number of Incident Shock Wave for Different Flow-Control Orifices.

APPENDIX K

TABLES OF DATA

TABLE 1[a]

IGNITION DATA FOR CAST PROPELLANTS F[b] AND G[b] AND PRESSED PROPELLANT CB AT LOW RADIANT FLUXES. (INITIAL PROPELLANT TEMPERATURES: 28 ± 2°C)

Propellant	Furnace Temperature (°K)	Ignition Time, t_i (sec)	$(t_i)^{1/2}$ $(msec)^{1/2}$	Calculated Surface Heat Flux, $\bar{F}$ cal/(cm)^2(sec)
F	950	20.5	143.1	1.15
F	1110	6.92	83.2	2.15
F	1310	2.11	46.0	4.14
F	1508	0.76	27.6	7.22
F	1705	0.32	17.9	11.70
G	1110	9.30	96.4	2.08
G	1310	2.77	52.6	4.07
G	1508	0.97	31.2	7.14
G	1705	0.42	20.5	11.62
CB	1083	7.10	84.2	1.82
CB	1183	5.15	71.8	2.53
CB	1283	2.78	52.7	3.48
CB	1508	0.84	29.0	6.56
CB	1703	0.35	18.7	10.57

(a) These data were retabulated from Table VIII of Reference 82 and are shown graphically in References 8 and 82.

(b) Propellants F and G for this study were made using the standard composition and mixing procedure, but surfaces of test samples were coated with a thin film of carbon black (Philblack E) to eliminate surface reflectivity and ensure absorption of all radiant energy at the propellant surface.

TABLE 2

COMPOSITIONS OF PROPELLANT SYSTEMS

PART I: COMPOSITIONS OF CAST PROPELLANTS

Propellant Code	Ingredients (Weight Per Cent) PBAA Binder (a)	Catalyst	Ammonium Perchlorate	Ammonium Perchlorate Particle Size (b)
AA	23.0	2.0 Chromic Oxide (c)	37.5 37.5	15 micron (d) 85 micron (e)
AB	23.0	2.0 Cuprous Oxide (f)	37.5 37.5	15 micron (d) 85 micron (e)
AC	23.0	2.0 Cuprous Oxide (f) 1.0 Philblack E (g)	37.0 37.0	15 micron (d) 85 micron (e)
AD	23.0	2.0 Iron Oxide (h)	37.5 37.5	15 micron (d) 85 micron (e)
AE	22.3	5.5 Iron Oxide (h)	36.1 36.1	15 micron (d) 85 micron (e)
F	18.0	2.0 Copper Chromite (i)	40.0 40.0	75 micron (d) 200 micron (j)
F-M (k)	18.0	2.0 Copper Chromite (i)	40.0 40.0	15 micron (l) 200 micron (j)
G	18.0	None	41.0 41.0	15 micron (d) 200 micron (j)
GB	18.0	2.0 Sterling VR Carbon Black (m)	40.0 40.0	15 micron (l) 200 micron (j)

(continued)

TABLE 2 (continued)

PART I: COMPOSITIONS OF CAST PROPELLANTS

Propellant Code	Ingredients (Weight Per Cent) PBAA Binder (a)	Catalyst	Ammonium Perchlorate	Ammonium Perchlorate Particle Size (b)
J	18.0	2.0 Iron Oxide (h)	40.0 40.0	15 micron (d) 200 micron (j)
O	18.0	2.0 Copper Chromite(i)	60.0 20.0	15 micron (d) 200 micron (j)
P	23.0	2.0 Copper Chromite (i)	37.5 37.5	15 micron (d) 200 micron (j)
S	23.0	2.0 Copper Chromite (i)	75.0	85 micron (e)
U	23.0	2.0 Copper Chromite (i)	75.0	15 micron (l)
X	23.0	2.0 Iron Oxide (h)	75.0	70 micron (n)
Y	23.0	2.0 Zinc Oxide (f)	37.5 37.5	15 micron (d) 85 micron (e)
Z	23.0	2.0 Zinc Oxide (f) 1.0 Iron Oxide (h)	37.0 37.0	15 micron (d) 85 micron (e)

TABLE 2 (continued)

PART II: COMPOSITIONS OF PRESSED PROPELLANTS(p)

Propellant Code	Ingredients (Weight Per Cent) Fuel	Catalyst	Ammonium Perchlorate	Ammonium Perchlorate Particle Size (b)
A	None	None	100.0	15 micron (d)
B (q)	None	4.0 Copper Chromite (i)	48.0 48.0	15 micron (l) 200 micron (j)
CB-1 (r)	16.0 Philblack E (g)	2.0 Copper Chromite (i)	41.0 41.0	15 micron (l) 200 micron (j)
CB-2 (s)	16.0 Philblack E (g)	2.0 Copper Chromite (i)	41.0 41.0	15 micron (l) 200 micron (j)
D	18.0 Paraformaldehyde(t)	2.0 Copper Chromite (i)	40.0 40.0	15 micron (d) 85 micron (e)
E	4.5 Sterling VR Carbon Black (m)	2.5 Copper Chromite (i)	46.5 46.5	15 micron (d) 85 micron (e)

(a) The binder-fuel for these propellants was composed of 85.0 per cent of a liquid polybutadiene-acrylic acid copolymer cured with 15.0 per cent Epon 828. Propellants were cured seven days at 80°C.

(b) Ammonium perchlorate of the designated particle size means that 50 weight per cent of the particles have diameters less that the value indicated. For particle sizes greater than 35 microns, a screen analysis was used to determine particle diameters. For particles less than 15 microns in diameter, particle sizes were determined microscopically by first dispersing ammonium perchlorate in dry carbon tetrachloride with the aid of a wetting agent and then measuring diameters of 200 to 300 particles.

(c) Chrome oxide green, Technical Grade of Cr_2O_3.

(d) This 15-micron ammonium perchlorate was made by grinding a larger particle size ammonium perchlorate. Particle diameters ranged from less than one micron to greater that 25 microns. This ammonium perchlorate was obtained from Thiokol Chemical Corporation, Brigham City, Utah.

(e) This ammonium perchlorate was obtained from the American Potash and Chemical Corporation, and had a Tyler screen size of -150 + 200 mesh. Particle diameters ranged from 30 to 190 microns.

Table 2 (continued)

(f) J. T. Baker Chemical Company, Reagent Grade Chemical.

(g) A rubber-reinforcing carbon black obtained from Phillips Petroleum Company. Philblack E has a surface area of 142 square meters per gram.

(h) Pure red iron oxide, code R-1599, obtained from C. K. Williams and Company. Particle sizes ranged from less than one micron to ten microns in diameter, with 55.0 per cent of the particles having diameters of less than 0.25 microns.

(i) Copper Chromite Catalyst Cu-0202 P obtained from Harshaw Chemical Company and contains approximately 82 per cent CuO and 17 per cent Cr_2O_3. The weight-average particle diameter of the copper chromite is 3.7 microns [32].

(j) This ammonium perchlorate was obtained from the American Potash and Chemical Corporation and had a Tyler screen size of -48 + 100 mesh. Particle diameters ranged from 75 to 400 microns.

(k) This propellant differed from the regular F-propellant in that it contained 15-micron ammonium perchlorate obtained from the American Potash and Chemical Corporation in place of 15-micron ammonium perchlorate from Thiokol Chemical Corporation.

(l) This ammonium perchlorate was obtained from the American Potash and Chemical Corporation and was designated as 50 per cent less than 15 micron. Particle diameters ranged from less than one micron to greater than 25 microns. The particle size distribution was almost the same as that for the 15-micron material obtained from Thiokol Chemical Corporation.

(m) Sterling VR carbon black was obtained from the Cabot Corporation and has an average particle size of 51 millimicrons with a surface area of 25 square meters per gram [32].

(n) This ammonium perchlorate was obtained from the American Potash and Chemical Corporation and had a Tyler screen size of -200 + 325 mesh. Particle diameters ranged from 15 to 125 microns.

(p) All pressed propellants were formed under a pressure of 100,000 psig.

(q) Dry materials were thoroughly blended and then slightly moistened before being pressed into pellets.

(r) The Philblack E used in this propellant was fired at 1000°C for two hours in a loosely covered crucible to remove all volatile components. Philblack E, which is in the form of small spherical pellets, was ground and then dry blended with other ingredients.

Table 2 (continued)

(s) Composition was the same as that for Pressed Propellant CB-1, but for this propellant special care was taken to remove all heterogeneities by first thoroughly blending ingredients and then passing a dry blend of ingredients through a 270-mesh screen several times. Dry ingredients were moistened by spraying the surface with water. This method for preparing the ingredients gave a more uniform pellet of greater density than those from Propellant CB-1.

(t) Paraformaldehyde (purified) powder from J. T. Baker Chemical Company.

TABLE 3

IGNITION OF F-PROPELLANT IN NITROGEN

Run No.	Propellant Code	Flow Control Orifice	M_E	P_4 (atm)	P_4' (atm)	T_4' (°K)	U m/(sec)	G g/(cm)^2(sec)	h cal/(cm)^2(sec)(°K)	T_1 (°K)	ΔT_o (°K)	T_{si}^L (°K)	ΔT_{si}^L (°K)	t_i (msec)	$(t_i)^{1/2}$ (msec)$^{1/2}$	$\bar{F}$ cal/(cm)^2(sec)
								Part I. Propellant Samples with Cut Surfaces								
26-16-1	F-2	3	2.97	14.4	21.7	1389	99	52.3	45.2×10^{-3}	289	25	550	261	12.3	3.51	44.2
26-16-2	F-2	3	2.86	12.4	17.4	1306	96	43.3	37.4	291	22	531	240	18.0	4.25	33.6
26-16-3	F-2	3	2.86	12.7	17.4	1303	96	43.2	37.3	293	22	581	289	30.4 (a)	5.51	31.1
26-16-4	F-2	3	2.65	13.2	17.2	1158	91	45.6	37.8	293	20	542	249	30	--	27.0
26-16-5	F-2	3	2.81	11.9	17.4	1293	96	43.4	37.3	273	21	565	273	26.8	5.18	31.3
28-27-2	F-3	3	3.60	17.6	26.1	1898	115	53.3	50.5	300	38	550	250	3.2	1.79	82.9
28-27-3	F-3	3	3.48	16.5	25.0	1823	113	53.3	50.5	301	35	571	270	4.8	2.19	73.2
28-27-4	F-3	3	3.46	16.1	24.0	1806	113	50.4	47.3	301	34	580	279	5.8	2.41	68.8
28-27-5	F-3	3	3.40	14.4	20.6	1747	111	44.0	41.4	302	31	580	279	8.5	2.92	56.8
28-28-1	F-3	3	3.41	13.2	21.0	1787	112	44.2	41.9	301	30	575	274	7.5	2.74	59.4
28-28-2	F-3	3	3.48	14.4	23.5	1852	114	48.7	46.2	301	32	585	284	6.0	2.45	68.9
28-28-3	F-3	3	3.38	14.6	23.5	1780	112	49.7	46.4	301	32	549	248	4.7	2.17	67.9
28-29-1	F-3	3	3.39	14.0	21.6	1758	111	45.9	43.1	300	31	574	274	7.4	2.72	60.0
28-29-2	F-3	3	3.47	15.4	23.1	1807	113	48.4	45.6	300	33	585	285	6.6	2.57	65.8
28-29-3	F-3	3	2.81	16.1	23.1	1328	97	57.0	48.2	300	32	548	248	11.2	3.35	44.0
28-29-4	F-3	3	2.79	16.5	22.9	1298	96	57.2	48.0	300	24	573	273	16.0	4.0	40.5
28-29-5	F-3	3	2.81	17.3	23.2	1302	96	57.8	48.5	300	25	549	249	11.8	3.44	43.0
28-30-1	F-3	3	2.09	20.9	24.0	798	76	77.3	54.5	294	15	500	207	40 (b)	--	19.4
28-30-2	F-3	3	2.25	20.4	23.8	892	80	72.3	53.0	294	18	529	235	37 (b)	--	22.9
28-30-3	F-3	3	2.78	11.5	16.5	1274	95	41.5	35.7	294	20	557	263	28 (b)	--	29.5
28-31-1	F-3	3	3.40	11.1	17.1	1721	110	36.8	35.0	293	27	571	278	12.5	3.54	46.7
28-31-2	F-3	3	3.32	11.4	14.6	1607	106	32.6	30.8	294	32	562	268	18 (b)	--	37.5
28-31-3	F-3	3	3.36	11.7	17.0	1677	109	37.1	35.1	294	28	602	308	17.7	4.21	43.5
29-8-1	F-5	5	2.79	17.3	24.1	1285	48	30.7	27.2	298	37	549	268	36 (b)	--	24.8
29-8-2	F-5	5	3.47	15.4	23.3	1805	57	24.9	24.9	299	50	551	252	13.9	3.74	40.3
29-8-3	F-5	5	3.52	15.2	24.3	1874	58	25.4	25.7	300	50	550	250	11.3	3.36	44.1
29-8-4	F-5	5	2.84	16.7	24.3	1346	49	30.2	27.2	301	37	567	267	37.1(a)	6.10	26.0
29-8-5	F-5	5	2.88	16.5	24.2	1378	50	29.6	27.0	301	39	534	233	23.6	4.86	28.5
29-8-6	F-5	5	2.85	17.3	25.2	1344	49	30.5	27.5	301	38	517	216	19.9	4.46	28.8
29-8-7	F-5	5	2.83	16.7	23.7	1336	49	29.6	26.7	302	37	557	255	35 (b)	--	25.6
29-8-8	F-5	5	3.07	16.8	24.1	1506	52	28.2	26.5	302	43	526	224	15.9	3.99	33.3
29-8-9	F-5	5	3.07	17.4	23.9	1492	52	28.1	26.3	302	44	565	263	26.0	5.10	30.6

(continued)

TABLE 3 (Continued)

Run No.	Propellant Code	Flow Control Orifice	M_E	P_4 (atm)	P_4' (atm)	T_4' (°K)	U $\frac{m}{(sec)}$	G $\frac{g}{(cm)^2(sec)}$	b $\frac{cal}{(cm)^2(sec)(°K)}$	T_1 (°K)	ΔT_o (°K)	T_{si}^L (°K)	ΔT_{si}^L (°K)	t_i (msec)	$(t_i)^{1/2}$ $(msec)^{1/2}$	$\bar{\dot{q}}$ $\frac{cal}{(cm)^2(sec)}$
								Part I: Propellant Samples with Cut Surfaces (Continued)								
29-9-1	F-5	5	3.11	17.1	23.6	1485	52	27.9	26.1×10^{-3}	295	44	542	247	22.2	4.70	31.2
29-9-2	F-5	5	2.97	11.6	17.1	1408	50	20.8	19.7	295	33	507	212	33 (b)	--	21.9
29-9-4	F-5	5	3.30	11.0	17.1	1664	55	19.1	19.1	295	39	530	235	26.8	5.18	27.0
29-9-5	F-5	5	3.37	11.6	17.1	1689	55	18.8	19.0	295	41	541	247	29 (b)	--	27.2
29-9-6	F-5	5	3.37	11.6	17.1	1681	55	18.4	18.6	295	41	536	241	29 (b)	--	26.6
29-9-7	F-5	5	3.35	10.3	16.4	1709	55	18.0	18.3	295	38	535	240	29 (b)	--	26.5
29-9-8	F-5	5	3.44	16.7	23.4	1735	56	25.5	25.2	296	51	555	259	16.1	4.01	38.4
29-9-9	F-5	5	3.42	17.2	23.4	1705	55	25.7	25.3	296	51	538	242	13.8	3.72	38.7
29-9-10	F-5	5	3.45	16.0	23.4	1758	56	25.3	25.1	296	50	572	276	18.8	4.34	37.8
29-11-1	F-5	5	3.43	15.6	23.9	1766	56	25.7	25.6	296	49	572	276	18.0	4.25	38.6
29-11-2	F-5	5	3.45	15.3	23.8	1786	56	25.5	25.4	297	49	575	278	18.0	4.25	38.9
29-11-3	F-5	5	3.47	15.7	23.7	1791	56	25.3	25.3	298	49	567	269	16.5	4.06	39.5
29-11-4	F-5	5	3.46	15.9	23.9	1790	56	25.6	25.5	298	50	559	261	14.8	3.86	40.3
29-11-5	F-5	5	3.45	15.2	24.0	1707	57	25.5	25.5	299	49	604	305	22.5	4.75	38.2
29-11-6	F-5	5	3.09	17.3	24.1	1508	52	28.2	26.5	301	44	542	241	19.2	4.38	32.6
29-11-7	F-5	5	3.06	17.2	24.1	1484	52	28.4	26.5	301	43	524	223	16.2	4.03	32.8
29-11-8	F-5	5	3.09	16.5	24.1	1523	52	28.1	26.4	301	43	525	224	15.4	3.93	33.9
29-12-1	F-5	5	2.83	17.1	24.2	1313	49	30.4	27.2	297	38	552	255	35 (b)	--	25.8
29-12-2	F-5	5	2.85	17.6	25.0	1331	49	31.2	27.9	298	39	545	247	28.8	5.37	27.4
29-12-3	F-5	5	2.84	16.3	24.0	1338	49	29.9	33.5	298	37	535	237	27.3	5.23	26.9
29-12-4	F-5	5	2.87	16.9	25.5	1367	50	31.4	28.4	298	38	572	274	34.4	5.86	27.7
29-12-5	F-5	4	2.85	16.7	23.9	1345	64	38.4	33.8	300	34	543	243	19.0	4.36	33.1
29-12-6	F-5	4	2.88	18.1	25.7	1359	64	41.0	36.0	300	36	538	238	15.0	3.89	36.5
29-13-1	F-5	4	2.80	16.0	24.1	1326	63	39.0	34.2	300	32	559	259	23.7	4.88	31.6
29-13-2	F-5	4	3.44	16.7	23.8	1773	73	33.2	32.2	301	46	539	238	7.7	2.78	50.9
29-13-3	F-5	4	3.46	14.9	23.4	1826	74	32.1	31.5	301	44	548	247	8.4	2.90	50.6
29-13-4	F-5	4	2.67	17.4	25.1	1235	61	42.2	35.9	301	31	526	225	18.5	4.31	31.1
29-13-5	F-5	4	2.63	16.6	24.2	1209	61	41.2	34.9	301	29	536	235	24.2	4.92	28.4
29-14-2	F-5	4	3.35	10.5	16.5	1727	72	23.3	23.2	298	35	565	267	24.0(a)	4.91	32.4
29-14-3	F-5	4	3.39	10.4	17.1	1766	73	23.8	23.8	298	35	577	279	24 (b)	--	33.8
29-14-4	F-5	3	3.40	16.0	22.9	1746	111	48.8	45.5	301	33	581	280	7.0	2.65	62.7
29-14-5	F-5	3	3.44	16.0	23.0	1775	112	48.7	45.6	302	33	592	290	7.3	2.70	63.8
29-14-6	F-5	3	2.85	16.2	23.3	1351	98	56.9	48.3	302	25	544	242	9.9	3.15	45.7
29-14-7	F-5	3	2.83	16.7	23.2	1330	97	57.2	48.3	302	25	565	263	13.0	3.61	43.3
29-14-8	F-5	3	2.83	16.7	22.9	1324	97	56.6	47.8	302	25	562	260	13.1	3.62	42.7
29-14-9	F-5	3	2.44	17.6	23.8	1070	87	65.7	51.4	301	20	563	262	26.1	5.11	30.5
29-19-1(c)	F-5	3	2.83	17.0	24.2	1327	97	59.6	50.1	300	25	553	253	10.9	3.30	45.5
29-19-2(c)	F-5	3	2.87	17.4	24.2	1352	98	59.0	50.0	301	26	541	240	9.9	2.99	47.8

(continued)

TABLE 3 (Continued)

Run No.	Propellant Code	Flow Control Orifice	M_E	P_4 (atm)	P_4' (atm)	T_4' (°K)	U $\frac{m}{(sec)}$	G $\frac{g}{(cm)^2(sec)}$	h $\frac{cal}{(cm)^2(sec)(°K)}$	T_1 (°K)	ΔT_o (°K)	T^L_{si} (°K)	ΔT^L_{si} (°K)	t_i (msec)	$(t_i)^{1/2}$ $(msec)^{1/2}$	$\bar{F}$ $\frac{cal}{(cm)^2(sec)}$
Part I: Propellant Samples with Cut Surfaces (Continued)																
29-25-1	F-6	3	2.44	16.9	23.7	1069	87	65.6	51.3×10^{-3}	299	19	582	283	33 (b)	--	29.3
29-25-2	F-6	3	2.82	16.9	23.2	1307	96	57.7	48.5	299	25	550	251	12.0	3.46	43.1
29-25-3	F-6	3	3.42	14.6	23.0	1796	112	48.4	45.5	299	32	585	286	6.9	2.63	64.7
29-25-4	F-6	3	3.08	17.0	23.3	1488	102	54.2	47.6	300	29	558	258	8.6	2.94	52.4
29-25-5	F-6	3	2.65	17.3	24.2	1212	93	62.5	50.9	299	23	566	267	17.0	4.13	38.4
29-25-6	F-6	3	2.64	16.7	23.3	1202	92	60.6	49.4	299	22	567	268	18.9	4.35	36.6
29-25-7	F-6	3	2.44	16.4	23.8	1080	88	65.4	51.3	299	19	586	287	33 (b)	--	29.7
210-3-1	F-6	2	3.41	15.2	23.3	1751	165	73.2	65.6	296	17	641	345	6.4	2.54	51.0
210-3-2	F-6	2	3.40	15.1	23.0	1736	164	72.5	64.9	296	19	626	330	6.0	2.46	80.1
210-3-3	F-6	2	2.84	16.6	22.4	1321	144	85.0	69.1	297	13	591	295	9.6	3.10	56.5
210-3-4	F-6	2	2.84	16.2	23.5	1332	144	84.9	69.2	297	13	604	307	10.4	3.23	56.5
210-3-5	F-6	2	2.41	16.9	23.6	1048	128	96.8	72.5	297	10	574	278	17.8	4.22	39.1
210-3-6	F-6	2	2.45	17.9	23.7	1057	129	96.7	72.6	297	11	637	341	32 (b)	--	35.5
210-4-1	F-6	2	2.46	16.9	23.7	1065	129	96.3	72.5	294	10	637	343	32 (b)	--	36.0
210-4-2	F-6	2	2.64	16.7	23.7	1179	136	91.0	71.0	294	12	596	302	14.7	3.84	46.9
210-4-3	F-6	2	2.62	16.7	23.6	1173	136	91.3	71.1	295	12	607	312	16.5	4.07	45.6
210-4-4	F-6	1	3.44	15.2	23.3	1780	231	99.4	87.0	297	0	662	365	4.4	2.10	103.3
210-4-5	F-6	1	3.46	14.9	23.3	1804	233	98.7	86.8	297	0	650	353	3.9	1.98	106.1
210-4-6	F-6	1	3.46	14.8	23.3	1812	233	98.5	86.2	298	0	652	354	3.9	1.98	106.5
210-4-7	F-6	1	2.84	16.7	23.5	1323	200	116.8	92.1	298	0	666	368	10.9	3.30	66.3
210-4-8	F-6	1	2.84	16.4	23.8	1332	200	118.0	93.2	298	0	641	343	8.5	2.92	70.0
210-4-9	F-6	1	2.84	16.5	23.5	1325	201	116.7	92.1	298	0	643	345	9.0	3.0	68.3
210-6-1	F-6	1	2.62	16.7	23.7	1147	187	126.9	95.2	288	0	647	359	16.0(a)	4.00	53.3
210-6-2	F-6	1	2.63	15.9	23.5	1166	188	125.1	94.4	288	0	657	369	16.6(a)	4.08	53.8
210-6-3	F-6	1	3.06	15.9	23.4	1445	209	111.2	90.5	291	0	663	372	8.3	2.88	76.7
210-6-4	F-6	1	2.91	16.9	23.4	1355	201	115.0	91.5	291	0	659	368	9.9	3.15	69.5
210-6-5(d)	F-6	3	2.83	15.9	23.5	1300	96	58.5	49.0	291	25	535	243	10.8	3.29	44.0
210-6-6(d)	F-6	3	2.80	16.3	23.5	1279	95	59.0	49.2	292	24	581	290	18.5	4.30	40.0
210-6-7(d)	F-6	3	2.82	16.4	23.5	1296	96	58.6	49.1	293	25	547	255	12.4	3.53	43.0
210-9-1(d)	F-6	3	2.60	16.3	23.5	1167	91	62.1	50.1	294	21	545	251	16.8	4.10	36.3
210-9-2(d)	F-6	3	2.63	16.7	23.3	1174	91	61.4	49.6	295	22	547	253	17.0	4.14	36.4
210-9-3(d)	F-6	3	2.81	17.6	23.5	1280	95	59.0	49.2	295	25	540	245	11.5	3.40	42.9
210-9-4(d)	F-6	3	2.84	16.5	23.5	1312	96	58.2	48.9	296	25	568	273	14.5	3.82	42.6
210-9-5(d)	F-6	3	3.07	16.7	23.5	1465	102	55.0	48.0	296	28	566	270	10.0	3.16	50.8
210-9-6(d)	F-6	3	2.94	16.7	23.5	1376	99	56.8	48.6	296	27	567	271	12.2	3.50	46.1
210-9-7(d)	F-6	3	3.08	16.7	23.5	1485	102	54.6	47.9	297	29	552	255	8.2	2.87	52.8

(continued)

TABLE 3 (Continued)

Run No.	Propellant Code	Flow Control Orifice	M_E	P_4 (atm)	P_4' (atm)	T_4' (°K)	U $\frac{m}{(sec)}$	G $\frac{g}{(cm)^2(sec)}$	h $\frac{cal}{(cm)^2(sec)(°K)}$	T_1 (°K)	ΔT_o (°K)	T^L_{si} (°K)	ΔT^L_{si} (°K)	t_i (msec)	$(t_i)^{1/2}$ $(msec)^{1/2}$	$\bar{F}$ $\frac{cal}{(cm)^2(sec)}$
Part I: Propellant Samples with Cut Surfaces (Continued)																
210-9-8(d)	F-6	3	3.43	15.9	23.3	1749	111	49.8	46.3×10^{-3}	296	33	535	239	4.4	2.10	67.8
210-9-9(d)	F-6	3	3.40	15.2	23.3	1738	110	50.0	46.4	296	32	567	271	6.3	2.52	64.2
212-24-1	F-9	3	2.82	16.3	22.8	1350	98	55.7	47.4	293	25	585	292	16.9	4.11	42.2
212-24-2	F-9	3	2.85	16.0	23.2	1315	96	57.5	48.4	293	25	560	267	13.8	3.72	42.7
212-24-3	F-9	3	3.07	15.0	23.1	1495	103	53.6	47.2	294	27	571	277	10.4	3.38	50.9
212-24-4	F-9	2	2.86	16.0	23.3	1327	144	84.4	68.7	293	13	676	383	20 (b)	--	50.8
212-24-5	F-9	2	2.87	16.8	24.8	1338	144	89.4	72.6	294	13	619	325	10.8	3.44	58.7
212-24-6	F-9	2	2.85	15.4	22.9	1333	144	82.7	67.5	294	13	603	309	11.0	3.46	55.3
212-26-1	F-9	2	2.80	16.1	23.5	1286	142	86.5	69.6	292	13	626	335	14.7	3.84	51.8
212-26-2	F-9	2	2.84	16.5	23.5	1300	142	86.0	69.5	292	13	628	336	14.4	3.80	52.7
212-26-3	F-9	2	3.11	17.6	25.4	1482	152	86.8	72.9	292	16	624	332	7.9	2.82	70.2
212-27-1	F-9	2	3.09	17.6	24.[illegible]	1454	150	85.4	71.4	290	16	605	315	7.6	2.76	67.9
212-27-2	F-9	2	3.06	16.6	23.5	1436	150	81.9	68.5	291	15	612	321	9.1	3.02	63.3
212-28-1	F-9	2	3.35	14.5	23.4	1704	162	74.5	66.1	292	15	622	330	6.1	2.48	79.5
212-28-2	F-9	2	3.38	15.2	23.6	1710	163	75.0	66.6	294	16	625	332	6.0	2.46	80.4
212-28-3	F-9	2	2.59	16.9	23.9	1153	134	93.2	72.0	294	12	620	326	19.5	4.42	43.8
212-28-4	F-9	2	2.63	18.0	24.3	1162	135	94.4	73.1	294	12	617	323	17.8	4.22	45.4
212-28-5	F-9	2	2.60	17.4	24.3	1156	135	94.6	73.1	294	12	593	299	14.5	3.81	46.7
31-2-1	F-9	1	2.81	16.0	23.1	1294	198	116.5	91.3	293	0	628	335	9.1	3.02	66.1
31-2-2	F-9	1	3.09	16.2	23.4	1475	211	110.0	90.2	293	0	644	351	6.7	2.59	80.5
31-2-3	F-9	1	3.04	16.3	23.1	1441	209	109.8	89.3	294	0	665	371	8.6	2.94	75.1
31-2-4	F-9	1	3.06	15.7	23.1	1479	212	108.3	88.9	295	0	654	359	7.3	2.70	79.0
31-2-5	F-9	1	2.61	16.7	23.7	1175	189	125.7	95.0	295	0	650	355	14.4	3.80	55.5
31-2-6	F-9	1	2.83	18.2	24.2	1286	198	122.0	95.0	296	0	682	386	13 (b)	--	63.6
31-2-7	F-9	1	2.62	16.2	23.5	1175	189	124.2	94.0	295	0	673	378	17.9	4.24	53.1
31-2-8	F-9	1	2.61	16.7	23.5	1168	189	124.6	94.1	296	0	652	356	15.2	3.90	54.2
31-2-9	F-9	1	2.83	16.3	23.5	1318	200	117.4	92.4	296	0	644	349	9.3	3.06	67.9
31-2-10	F-9	1	3.08	15.8	23.3	1491	212	108.8	89.5	296	0	657	361	7.1	2.67	80.5
43-19-1	F-30M	None	3.10	14.6	22.1	1511	715	166.9	132.4	294	0	705	411	4.4(e)	2.10	116.4
43-19-2	F-30M	None	3.24	14.3	21.6	1622	740	156.9	127.9	296	0	706	410	3.7(e)	1.93	126.6
43-19-3	F-30M	None	2.74	15.4	21.5	1249	650	179.2	133.4	295	0	719	424	10.0(e)	3.16	79.6
43-19-4	F-30M	5	3.23	14.7	21.8	1602	53	24.8	24.0	296	43	524	229	16.9	4.11	24.0
43-19-5	F-30M	5	3.06	14.7	21.1	1471	51	25.0	25.6	296	40	552	256	32 (b)	--	26.9
43-19-6	F-30M	5	3.50	13.1	21.2	1845	57	22.4	22.8	296	47	601	305	27 (b)	--	34.9

(continued)

TABLE 3 (Continued)

Run No.	Propellant Code	Flow Control Orifice	r_E	P_4 (atm)	P_4' (atm)	T_4' (°K)	U $\frac{m}{(sec)}$	G $\frac{g}{(cm)^2(sec)}$	h $\frac{cal}{(cm)^2(sec)(°K)}$	T_1 (°K)	ΔT_c (°K)	T_{si}^L (°K)	ΔT_{si}^L (°K)	t_i (msec)	$(t_i)^{1/2}$ $(msec)^{1/2}$	$\bar{F}$ $\frac{cal}{(cm)^2(sec)}$
								Part I: Propellant Samples with Cut Surfaces (Continued)								
43-19-7	F-30M	4	3.47	13.7	21.7	1809	74	29.9	29.5×10^{-3}	297	42	498	202	5.7	2.40	50.2
43-19-8	F-30M	4	3.25	14.6	21.6	1623	70	31.5	30.0	297	39	504	207	8.3	2.89	42.7
42-19-9	F-30M	4	3.07	14.8	21.4	1428	67	32.8	30.2	297	36	497	200	10.0	3.16	37.6
43-19-10	F-30M	4	2.80	15.0	22.0	1310	63	36.0	31.6	297	31	516	219	18.1	4.26	30.6
43-20-1	F-30M	4	2.98	13.7	22.1	1439	66	34.3	31.2	293	33	520	227	14.8	3.86	35.0
43-20-2	F-30M	4	2.64	16.5	22.8	1178	60	39.3	33.2	294	29	532	239	30.0	5.49	25.9
43-20-3	F-30M	1	2.75	14.8	21.6	1266	196	110.1	86.2	294	0	555	261	5.6	2.37	65.4
43-20-5	F-30M	1	3.47	9.3	15.8	1835	235	66.2	60.8	296	0	589	293	4.8	2.19	79.3
43-20-6	F-30M	1	2.75	10.3	15.2	1275	197	77.0	62.5	297	0	553	256	10.0	3.16	48.1
43-20-7	F-30M	1	3.29	5.9	9.5	1685	225	41.8	39.1	297	0	555	258	11 (b)	--	46.2
43-20-8	F-30M	1	2.50	11.2	16.1	1110	184	87.9	67.6	297	0	588	291	20.0(a)	4.48	38.7
44-14-1	F-30M	3	2.79	15.7	21.2	1262	95	53.8	45.0	293	24	527	234	12.8	3.58	38.8
44-14-2	F-30M	3	3.37	14.6	21.2	1682	109	46.3	42.8	294	31	547	253	6.8	2.61	57.7
44-14-3	F-30M	3	3.22	14.6	20.7	1570	105	46.7	42.3	294	29	530	236	7.2	2.68	52.2
44-14-4	F-30M	3	3.20	14.4	21.2	1566	105	47.9	43.2	295	28	518	223	6.0	2.46	54.0
44-14-5	F-30M	3	2.80	15.2	21.6	1294	96	54.1	45.6	296	25	532	337	12.0	3.46	40.6
44-15-1	F-30M	1	2.78	14.7	21.1	1278	197	106.8	84.1	294	0	611	317	9.6	3.10	60.8
44-15-2	F-30M	1	3.27	14.4	21.2	1617	221	94.8	81.0	295	0	602	307	4.4	2.10	87.0
44-14-6	F-38M	3	2.82	14.7	21.4	1311	96	53.0	45.0	296	23	544	248	13.4	3.66	40.2
44-14-7	F-38M	3	3.30	14.6	22.0	1640	107	46.3	42.5	296	30	533	237	6.3	2.52	56.1
44-15-3	F-38M	1	3.19	15.0	20.8	1547	216	95.2	80.2	295	0	584	288	4.4	2.10	81.6
44-15-4	F-38M	1	2.82	14.8	21.6	1317	200	107.6	85.4	297	0	597	300	7.3	2.71	66.1
44-15-5	F-38M	1	2.72	14.8	20.3	1238	194	104.8	81.9	298	0	585	288	8.8	2.97	57.6
44-15-6	F-38M	1	2.86	10.5	16.3	1377	204	79.6	65.9	298	0	609	311	11.6	3.42	54.2
44-17-1	F-38M	1	2.83	10.6	16.1	1321	200	80.0	65.3	294	0	542	348	18.3	4.28	48.3
44-21-1	F-38M	1	3.05	11.0	15.9	1435	208	75.9	63.9	290	0	590	300	9.6	3.10	57.5
44-21-2	F-38M	1	3.05	11.0	16.4	1444	209	77.9	65.6	291	0	593	302	9.1	3.02	59.5
44-21-3	F-38M	1	3.62	9.4	15.7	1922	240	64.3	60.1	291	0	637	347	6.4	2.53	81.2
44-21-4	F-38M	3	3.50	9.3	16.1	1834	113	33.6	32.9	292	26	538	246	8.7	2.96	49.5
44-21-5	F-38M	3	3.03	11.0	16.1	1438	101	38.0	34.2	292	23	550	258	19.1	4.38	35.0

(continued)

TABLE 3 (Continued)

Run No.	Propellant Code	Flow Control Orifice	M_E	P_4 (atm)	P_4' (atm)	T_4' (°K)	U $\frac{m}{(sec)}$	G $\frac{g}{(cm)^2(sec)}$	h $\frac{cal}{(cm)^2(sec)(°K)}$	T_1 (°K)	ΔT_o (°K)	T^L_{si} (°K)	ΔT^L_{si} (°K)	t_i (msec)	$(t_i)^{1/2}$ $(msec)^{1/2}$	$\bar{P}$ $\frac{cal}{(cm)^2(sec)}$
								Part I. Propellant Samples with Cut Surfaces (Continued)								
49-8-1	F-32	3	2.84	16.7	22.7	1310	96	56.4	47.5×10^{-3}	297	25	543	247	11.7	3.42	42.8
49-8-2	F-32	3	2.47	16.1	22.5	1081	88	61.6	48.6	297	19	523	226	16.2	4.03	33.3
49-8-3	F-32	3	3.52	13.8	22.7	1865	114	46.9	44.7	298	32	552	255	4.7	2.17	69.7
49-8-4	F-32	3	3.68	12.2	21.8	2030	119	43.1	42.5	298	32	563	266	4.6	2.15	73.5
49-15-1	F-32	3	3.25	13.5	21.9	1660	108	48.1	44.2	297	28	555	258	7.2	2.69	57.1
49-15-2	F-32	3	2.86	15.0	22.7	1354	98	55.3	47.2	297	24	554	257	12.1	3.48	43.9
49-15-3	F-32	None	3.31	13.8	20.6	1640	751	147.5	122.1	297	0	713	415	3.8(e)	1.95	126.4
49-15-4	F-32	None	3.61	13.1	20.8	1926	804	138.4	120.2	297	0	725	428	2.7(e)	1.65	154.0
49-15-5	F-32	None	3.09	13.9	21.3	1525	718	160.0	127.8	297	0	688	391	4.0(e)	2.00	115.9
								Part II. Propellant Samples with Polymer-Rich Surfaces								
29-29-1	F-6	3	3.35	15.5	23.3	1670	108	50.9	46.6	292	31	610	318	10.7	3.28	57.8(f)
										292	44	704	412	10.7	3.28	53.9(g)
29-29-2	F-6	3	3.45	14.4	23.2	1778	112	49.1	46.0	292	32	614	322	9.4	3.07	62.4(f)
										292	44	710	418	9.4	3.07	58.5(g)
29-29-4	F-6	3	2.83	16.7	23.5	1293	96	58.7	49.1	293	25	568	275	15.4	3.94	41.6(f)
										293	35	644	351	15.4	3.94	38.3(g)
29-29-5	F-6	3	2.83	16.5	23.7	1299	96	59.0	49.4	293	25	597	304	19.8	4.45	40.5(f)
										293	34	677	384	19.8	4.45	37.0(g)
29-29-6	F-6	3	2.80	16.2	23.5	1286	95	59.0	49.2	293	24	559	266	14.3	3.79	41.8(f)
										293	34	634	341	14.3	3.79	38.6(g)
29-29-7	F-6	3	3.05	16.6	22.8	1428	100	54.1	47.0	293	28	585	292	13.9	3.73	46.5(f)
										293	39	667	374	13.9	3.73	43.0(g)
29-29-8	F-6	3	3.02	16.3	23.1	1420	100	55.1	47.7	293	28	561	267	10.9	3.30	48.1(f)
										293	38	638	345	10.9	3.30	44.8(g)

(a) An indication of localized ignition at time indicated.
(b) Propellant sample did not ignite. Value for ignition time is that for the minimum test period at specified shock tube conditions.
(c) Sample prepared by cementing solid cylinder of propellant in sample holder with Krylon acrylic resin.
(d) Sample prepared by cementing solid cylinder of propellant in sample holder with G. C. Electronics Co. Epox Cement (No. 346).
(e) Sample ignited at time indicated, but was later extinguished by cold driver gas entering test section.
(f) Mean heat flux and ignition temperature based on propellant thermophysical properties.
(g) Mean heat flux and ignition temperature based on polymer thermophysical properties.

TABLE 4

THERMOPHYSICAL PROPERTIES OF PROPELLANTS AND PROPELLANT INGREDIENTS (a)

Propellant or Ingredients	Test Temp. (°C)	Heat Capacity c cal/(g)(°K)	Density (b) ρ g/(cm)^3	Thermal Diffusivity, α (cm)^2/(sec)	Thermal Conductivity, k cal/(cm)(sec)(°K)	Thermal Responsivity, Γ (kρc)$^{1/2}$ cal/(cm)^2(sec)$^{1/2}$(°K)
				Part I: Ingredients		
Ammonium perchlorate (c)	20	0.256 (d)	1.95 (e)	2.22×10^{-3}	1.108×10^{-3}	2.35×10^{-2}
	60	0.275 (d)	-	-	-	2.44 (f)
	25	-	1.97 (g)	-	1.12 (g)	-
Copper chromite	60	0.147 (h)	-	-	-	-
F-propellant Binder (i)	60	0.424	1.11	1.055	0.471	1.53
	20	-	1.11	1.002	-	-
G-Propellant Binder (j)	60	0.465	0.956	0.982	0.437	1.39
	20	-	0.956	0.982	-	-
Iron Oxide	60	0.168 (h)	-	-	-	-
				Part II: Cast Propellants		
AA	60	-	-	-	-	2.03 (k)
AB	60	-	-	-	-	2.03 (k)
AC	60	-	-	-	-	2.03 (k)
AD	60	0.316 (l)	1.58	-	-	2.03 (k)
AE	60	0.311 (l)	1.60	-	-	2.02 (k)
F	60	0.316	1.63	1.700	0.876	2.12
	20	-	1.63	1.731	-	-
G	60	0.311	1.60	1.710	0.851	2.06
	20	-	1.60	1.730	-	-

(continued)

TABLE 4 (Continued)

Propellant or Ingredients	Test Temp. (°C)	Heat Capacity c cal/(g)(°K)	Density (b) ρ g/(cm)^3	Thermal Diffusivity, α (cm)^2/(sec)	Thermal Conductivity, k (cal/(cm)(sec)(°K)	Thermal Responsivity, Γ $(k\rho c)^{1/2}$ cal/(cm)^2(sec)$^{1/2}$(°K)
			Part II. Cast Propellants (Continued)			
GB(m)	60	0.311	1.60	1.710×10^{-3}	0.851×10^{-3}	2.06×10^{-2}
J	60	0.307 (l)	1.63	-	-	2.06 (n)
	120	0.334	1.63	-	-	2.24 (p)
O (q)	60	0.316	1.63	1.700	0.876	2.12
P	60	0.316 (l)	1.58	1.65 (k)	-	2.03 (k)
S	60	0.316 (l)	1.58	1.65 (k)	-	2.03 (k)
U	60	0.316 (l)	1.58	1.65 (k)	-	2.03 (k)
V (r)	60	-	1.53	1.603	-	-
W (r)	60	-	1.52	1.610	-	-
X	60	-	-	-	-	2.03 (k)
Y	60	-	-	-	-	2.03 (k)
			Part III: Pressed Propellants			
A	20	0.256	1.95	2.22×10^{-3}	1.108×10^{-3}	2.35×10^{-2}
B	60	-	-	-	-	2.35 (s)
CB-1	60	0.260	1.65	2.40	-	2.10
CB-2	60	0.260	1.77	2.40	-	2.25
D	60	-	-	-	-	2.10 (s)
E	60	-	-	-	-	2.30 (s)

Table 4 (Continued)

(a) Unless otherwise indicated, all data for thermophysical properties were obtained by the methods described in Appendix D.

(b) All density values are for a temperature of 20°C.

(c) Data were obtained on pressed cylinders of ammonium perchlorate.

(d) These data were interpolated from JANAF Thermochemical Data on ammonium perchlorate which were calculated and compiled by the Thermal Laboratory of Dow Chemical Company, September, 1961.

(e) Density values were taken from the Handbook of Chemistry and Physics, 43rd Edition.. Pressed samples of ammonium perchlorate had densities which ranged from 97 to 98 per cent of this value.

(f) This value was calculated with the assumption that density and thermal conductivity remained constant at their 20°C values.

(g) These values were taken from Reference [32].

(h) These values were estimated from heat capacity data given by Lange's Handbook of Chemistry.

(i) F-propellant binder had the following ingredients: 18.0 parts of polymer (85.0 per cent PBAA and 15.0 per cent Epon 828) and 2.0 parts of copper chromite catalyst by weight.

(j) G-propellant binder had the same polymer composition as F-propellant binder, but did not contain copper chromite.

(k) These values were not determined experimentally, but were estimated from experimental data on propellants F, V, and W.

(l) Heat capacity for these propellants was estimated by summing the values for individual ingredients.

(m) Thermal properties of GB-propellant were assumed to be the same as those for G-propellant.

(n) This value was calculated with the assumption that the thermal conductivity of J-propellant was the same as that for F-propellant.

(p) Thermal responsivity was calculated with a mean value of heat capacity for ammonium perchlorate between 300 and 540°K. The heat capacity values at 60°C were used for all other ingredients. The thermal conductivity of the propellant at 60°C was also used in this calculation.

Table 4 (Continued)

(q) Thermal properties of O-propellant were assumed to be the same as those for F-propellant.

(r) These propellants were made specifically to determine the effect of ammonium perchlorate particle size and concentration of ammonium perchlorate on thermal diffusivity. Both propellants contained the following ingredients by weight: 70 per cent ammonium perchlorate, 28 per cent PBAA binder, and 2 per cent copper chromite. The particle size of the ammonium perchlorate was 15 micron in V-propellant and 200 micron in W-propellant.

(s) This value was estimated from experimental data on pressed propellants A and CB.

TABLE 5

IGNITION DATA FOR F-PROPELLANT IN ARGON

(Propellant Samples with Cut Surfaces)

Run No.	Propellant Code	Flow Control Orifice	M_E	P_4 (atm)	P_4' (atm)	T_4 (a) (°K)	U $\frac{m}{(sec)}$	G $\frac{g}{(cm)^2(sec)}$	h $\frac{cal}{(cm)^2(sec)(°K)}$	T_1 (°K)	ΔT_o (°K)	T^L_{si} (°K)	ΔT^L_{si} (°K)	t_i (msec)	$(t_i)^{1/2}$ $(msec)^{1/2}$	$\bar{F}$ $\frac{cal}{(cm)^2(sec)}$
49-8-5	F-32	3	3.43	14.6	21.3	2745	127	47.3	24.0×10^{-3}	298	27	455	173	2.5	1.58	65.0
49-8-6	F-32	3	2.77	14.6	21.5	1855	104	57.9	29.8	299	11	505	206	8.0	2.83	43.0
49-8-7	F-32	3	2.69	13.9	21.5	1765	101	59.3	30.6	299	8	546	247	12.2	3.50	40.3
49-8-8	F-32	3	2.36	12.7	20.6	1380	89	64.1	33.2	300	0	526	227	16.2	4.03	33.5
49-8-9	F-32	3	1.95	13.8	21.9	975	75	81.3	42.6	300	0	488	188	25.2	5.03	22.2
49-8-10	F-32	3	1.80	14.2	21.7	840	70	86.9	45.5	300	0	456	156	24.5	4.96	18.7
49-8-11	F-32	3	2.99	13.5	21.4	2130	111	54.0	27.7	300	17	504	203	5.8	2.41	50.1
49-8-12	F-32	1	3.12	13.3	20.9	2310	233	101.6	53.0	300	0	585	285	3.2	1.79	94.3
49-8-13	F-32	1	2.73	14.0	21.2	1795	204	116.1	61.0	300	0	563	263	4.1	2.03	78.0
49-8-14	F-32	1	2.54	13.9	20.8	1570	192	123.1	65.3	299	0	561	262	5.2	2.28	69.4
49-8-15	F-32	-	2.40	12.9	20.9	1405	181	123.0	65.5	299	0	621	322	8.6	2.94	65.1
49-12-1	F-32	1	2.61	14.6	21.4	1635	200	125.7	67.0	296	0	581	285	5.2	2.28	74.2
49-12-2	F-32	1	2.39	10.6	21.6	1400	181	135.0	72.5	297	0	608	311	9.2	3.04	61.6
49-14-3	F-32	3	3.13	12.7	20.1	2295	115	48.9	25.0	297	17	525	228	7.3	2.71	51.1
49-14-4	F-32	3	2.52	13.5	22.0	1540	94	65.2	33.8	297	5	511	213	11.7	3.42	36.9
49-14-5 (b)	F-32	3	2.00	13.0	20.0	1015	-	-	-	-	-	-	-	-	-	-
49-14-6	F-32	3	2.18	12.2	19.7	1190	83	65.6	34.2	298	0	596	198	22.0	4.70	25.1

(a) For argon the gas temperature used was that immediately behind the reflected shock, T_4, and was not adjusted for the post-reflection rise. Test section gas velocity, U, and mass flow rate, G, are also based on this value of gas temperature.

(b) Propellant sample did not ignite.

TABLE 6

IGNITION DATA FOR F-PROPELLANT IN AIR

Run No.	Propellant Code	Flow Control Orifice	M_E	P_4 (atm)	P_4' (atm)	T_4' (°K)	U $\frac{m}{(sec)}$	G $\frac{g}{(cm)^2(sec)}$	h $\frac{cal}{(cm)^2(sec)(°K)}$	T_1 (°K)	ΔT_o (°K)	T^L_{si} (°K)	ΔT^L_{si} (°K)	t_i (msec)	$(t_i)^{1/2}$ $(msec)^{1/2}$	$\bar{F}$ $\frac{cal}{(cm)^2(sec)}$
							Part I. Propellant Samples with Cut Surfaces									
26-13-1	F-2	3	2.85	16.6	24.3	1354	96	60.3	51.0×10^{-3}	301	25	543	242	8.8	2.97	48.6
26-13-2	F-2	3	2.79	15.2	22.3	1312	95	56.3	47.5	301	23	551	250	12.4	3.52	42.1
26-13-3	F-2	3	2.86	16.5	24.2	1360	96	59.8	50.7	301	25	511	210	6.0	2.45	51.1
26-13-5	F-2	3	2.83	11.7	17.3	1343	96	43.1	37.5	301	21	550	249	18.5	4.30	34.3
26-14-1	F-2	3	2.81	17.1	24.0	1300	94	60.9	50.8	297	25	533	236	9.3	3.05	45.9
26-14-2	F-2	3	2.32	17.1	24.2	998	83	70.3	53.5	298	17	572	274	36 (a)	-	26.9
26-14-3	F-2	3	3.45	15.6	23.7	1789	110	50.8	47.5	299	33	552	253	4.6	2.14	70.2
26-14-4	F-2	3	3.46	15.2	23.3	1809	111	49.8	46.8	300	33	528	228	3.5	1.87	72.4
26-14-5	F-2	3	2.91	17.8	24.0	1362	96	59.3	50.3	300	27	517	217	6.5	2.55	50.7
26-14-6	F-2	3	2.85	11.7	17.7	1365	97	43.7	38.2	300	21	492	192	8.5	2.92	39.0
26-14-7	F-2	3	2.84	11.5	17.7	1365	97	43.7	38.2	300	21	528	228	13.5	3.68	36.9
26-14-8	F-2	3	2.83	11.8	17.4	1341	96	43.3	37.7	300	21	533	233	15.5	3.94	37.7
26-15-1	F-2	3	2.73	12.7	17.4	1235	92	45.4	38.3	295	20	517	222	17.1	4.14	31.9
26-15-2	F-2	3	2.72	11.8	17.4	1251	93	45.1	38.2	295	20	525	230	18.2	4.26	32.0
26-15-3(b)	F-2	3	2.90	11.8	17.4	1364	97	43.1	37.7	296	22	477	181	7.4	2.72	39.5
43-20-4	F-30M	1	2.78	15.4	21.9	1281	194	112.7	88.3	296	0	577	282	6.3	2.52	66.7
49-14-9	F-32	3	3.28	13.7	19.9	1646	106	44.5	41.1	299	29	256	555	8.3	2.88	52.7
49-14-10	F-32	3	2.80	14.5	20.8	1304	94	52.7	44.6	300	23	229	528	11.3	3.36	40.4
49-14-11	F-32	3	2.89	14.6	21.4	1379	97	52.7	45.4	299	23	219	518	8.0	2.84	45.9
							Part II. Propellant Samples with Polymer-Rich Surfaces									
26-13-4	F-2	3	2.88	16.6	24.2	1377	97	59.4	50.6	301	26	537	236	7.8	2.80	50.1(e)
										301	36	607	306	7.8	2.80	46.9(d)
26-15-4	F-2	3	2.97	13.6	19.5	1408	98	47.5	41.6	301	25	570	269	15.5	3.94	40.5(c)
										301	34	647	346	15.5	3.94	37.7(d)
26-15-5	F-2	3	2.84	11.6	17.3	1353	95	43.2	37.6	296	21	568	272	24.0	4.90	33.0(c)
										296	29	645	349	24.0	4.90	30.5(d)
26-15-6	F-2	3	2.89	11.7	17.4	1315	95	43.9	37.9	296	21	561	265	23.0(e)	4.80	32.9(c)
										296	29	636	340	23.0(e)	4.80	30.4(d)

(a) Propellant sample did not ignite; value for ignition time is that for the minimum test period at specified shock tube conditions.
(b) Cut surface was roughened by scraping with a razor blade.
(c) Mean heat flux and ignition temperature based on propellant thermophysical properties.
(d) Mean heat flux and ignition temperature based on polymer thermophysical properties.
(e) An indication of localized ignition at time indicated.

TABLE 7

IGNITION DATA FOR PROPELLANTS O AND P IN NITROGEN

Run No.	Propellant Code	Flow Control Orifice	M_E	P_4 (atm)	P_4' (atm)	T_4' (°K)	U m/(sec)	G g/(cm)^2(sec)	h cal/(cm)^2(sec)(°K)	T_1 (°K)	ΔT_o (°K)	T^L_{si} (°K)	ΔT^L_{si} (°K)	(t_i) (msec)	$(t_i)^{1/2}$ (msec)$^{1/2}$	$\bar{F}$ cal/(cm)^2(sec)
				Part I. Propellant Samples with Cut Surfaces												
31-18-1	O-1	3	2.79	15.3	22.7	1287	95	56.8	47.6 x 10^{-3}	296	23	560	264	15.2	3.90	40.3
31-18-3	O-1	3	2.85	17.4	22.7	1303	96	56.4	47.5	297	25	559	262	14.1	3.78	41.5
31-18-4	O-1	3	3.00	15.9	22.5	1424	100	53.4	46.4	297	27	558	261	10.8	3.29	47.1
31-18-5	O-1	3	3.47	14.4	22.7	1811	113	47.7	45.0	297	32	558	261	5.4	2.32	66.8
31-18-6	O-1	3	3.50	14.8	23.0	1828	113	48.0	45.4	297	33	567	270	5.6	2.37	67.9
31-18-7	O-1	3	3.07	16.1	23.1	1482	102	53.7	47.2	297	32	543	246	7.8	2.80	52.4
31-21-1	O-1	3	3.42	14.7	22.7	1721	110	48.8	45.2	289	32	578	289	8.0	2.84	60.7
31-21-6	O-1	1	3.48	14.6	22.0	1780	232	93.6	82.4	294	0	657	363	4.8	2.20	98.3
31-21-7	O-1	1	3.48	13.7	22.3	1812	233	94.2	83.3	295	0	645	351	4.1	2.03	102.8
31-21-8	O-1	1	3.17	16.1	22.1	1525	215	102.2	85.2	295	0	626	331	5.8	2.41	81.7
31-22-1	O-1	1	3.10	15.9	22.9	1474	211	107.5	88.3	292	0	643	351	7.0	2.65	78.9
31-22-2	O-1	1	2.83	15.3	22.5	1302	199	113.0	89.0	292	0	645	353	10.8	3.29	63.9
31-22-3	O-1	1	2.83	16.3	22.7	1300	199	114.1	89.7	293	0	628	335	9.2	3.04	65.5
31-22-4	O-1	1	2.63	16.1	22.9	1173	189	121.1	91.8	294	0	650	356	15.6	3.96	53.5
32-16-1	P-1	3	3.47	14.3	21.9	1793	112	46.2	43.6	296	34	552	256	5.1	2.26	6[illegible]
32-16-2	P-1	3	3.47	13.8	22.9	1826	113	47.7	45.1	297	36	578	281	5.8	2.41	66.5
32-16-3	P-1	3	3.47	15.2	22.9	1788	112	48.3	45.3	297	34	572	275	5.7	2.39	65.6
32-18-1	P-1	3	3.08	15.2	22.5	1490	102	52.3	46.1	295	29	569	274	9.7	3.12	50.0
32-18-2	P-1	3	3.08	15.7	23.0	1489	102	53.4	47.0	296	29	573	277	9.7	3.12	50.7
32-18-3	P-1	3	2.83	14.8	23.1	1347	98	56.6	48.1	296	25	579	283	14.0	3.74	43.0
32-18-4(a)	P-1	3	2.83	15.8	23.0	1323	97	56.8	48.0	296	25	552	255	11.2	3.35	43.4
32-18-5(a)	P-1	3	2.83	15.3	22.7	1330	97	55.8	47.3	296	25	561	264	12.5	3.44	42.5
32-18-9(b)	P-1	1	3.45	14.4	22.0	1779	231	94.0	82.7	296	0	652	356	4.2	2.06	98.8
32-18-10(b)	P-1	1	3.43	14.8	22.3	1757	230	95.5	83.6	296	0	646	350	4.1	2.0[illegible]	98.3
32-18-11(b)	P-1	1	3.07	14.8	22.1	1494	213	103.3	85.5	296	0	666	370	7.6	2.76	76.3
32-18-12(b)	P-1	1	3.07	15.8	22.2	1475	211	104.3	85.9	297	0	665	369	7.8	2.80	75.1
32-18-13(b)	P-1	1	2.84	15.6	22.5	1328	201	111.5	88.4	297	0	657	360	10.0	3.16	64.8
32-20-1(b)	P-1	1	2.84	15.9	22.2	1307	199	111.1	87.7	294	0	647	353	10.1	3.18	63.2
32-20-2	P-1	1	2.62	16.1	22.1	1180	190	116.8	89.0	296	0	644	348	14 (c)	-	52.9
32-20-3(b)	P-1	1	3.46	14.4	22.0	1795	232	93.2	82.3	297	0	662	365	4.4	2.10	98.9
32-20-5	P-1	3	3.48	14.4	22.0	1805	112	46.3	43.8	298	34	578	281	6.3	2.52	63.6
32-20-6	P-1	3	3.08	15.4	22.8	1504	103	52.7	46.6	298	29	572	274	9.3	3.06	51.0
32-20-7	P-1	3	2.82	16.1	22.3	1308	96	55.5	46.8	298	26	567	268	14.1	3.76	40.7

(continued)

TABLE 7 (Continued)

Run No.	Propellant Code	Flow Control Orifice	M_E	P_4 (atm)	P_4' (atm)	T_4' (°K)	$\frac{U}{m}$ (sec)	$\frac{G}{g}$ $(cm)^2(sec)$	$\frac{h}{cal}$ $(cm)^2(sec)(°K)$	T_1 (°K)	ΔT_o (°K)	T_{si}^L (°K)	ΔT_{si}^L (°K)	(t_i) (msec)	$(t_i)^{1/2}$ $(msec)^{1/2}$	$\frac{\bar{F}}{cal}$ $(cm)^2(sec)$
							Part I. Propellant Samples with Cut Surfaces (Continued)									
32-20-8(a)	P-1	2	3.48	13.7	22.0	1828	168	67.4	61.7×10^{-3}	298	18	596	297	4.0	2.00	84.6
32-20-9(a)	P-1	2	2.97	16.7	22.5	1400	148	79.2	65.9	298	15	602	304	8.6	2.94	59.0
32-20-10(a)	P-1	2	2.83	15.5	22.1	1330	144	80.1	65.6	298	14	599	300	10.1	3.18	53.7
32-20-11(a)	P-1	2	2.86	15.9	22.3	1340	145	80.3	65.8	299	14	573	274	7.6	2.76	56.6
32-20-12(a)	P-1	2	3.05	15.2	22.1	1476	152	75.8	64.4	299	15	598	300	7.3	2.70	63.1
32-20-13(a)	P-1	2	3.11	15.7	22.3	1509	153	75.7	64.7	298	16	580	282	5.7	2.39	67.1
							Part II. Propellant Samples with Polymer-Rich Surfaces									
32-18-6	P-1	3	2.83	15.8	22.9	1317	97	56.8	47.9	297	25	642	345	27 (c)	-	37.8
32-18-7	P-1	3	3.07	15.3	22.5	1492	103	52.3	46.1	297	28	641	344	18.3	4.29	45.7
32-18-8	P-1	3	3.45	14.2	22.5	1794	112	47.5	44.7	297	33	694	398	15.8	3.98	56.9

(a) Small amount of hot nitrogen leaked by orifice gasket; as a consequence, values for ignition temperature and surface heat flux are only approximate.
(b) Sample ignited at the time indicated, but was later extinguished by colder driver gas entering the test section.
(c) Propellant sample did not ignite. Value for ignition time is that for the minimum test period for specified shock tube conditions.

TABLE 8

IGNITION DATA FOR S-PROPELLANT IN NITROGEN

Run No.	Propellant Code	Flow Control Orifice	M_E	P_4 (atm)	P_4' (atm)	T_4' (°K)	$\frac{U_m}{(sec)}$	$\frac{G_g}{(cm)^2(sec)}$	$\frac{h_{cal}}{(cm)^2(sec)(°K)}$	T_1 (°K)	ΔT_o (°K)	T^L_{si} (°K)	ΔT^L_{si} (°K)	t_i (msec)	$(t_i)^{1/2}$ $(msec)^{1/2}$	$\bar{F}_{cal}$ $(cm)^2(sec)$
Part I. Propellant Samples with Cut Surfaces																
33-21-1	S-1	3	3.27	15.0	23.0	1649	108	50.6	46.2×10^{-3}	298	31	594	297	8.7	2.96	57.2
33-21-2	S-1	3	2.82	15.0	22.5	1334	97	55.4	47.0	298	24	575	277	14.3	3.78	41.6
33-21-3	S-1	3	2.82	15.5	22.7	1324	97	56.1	47.5	298	25	583	285	15.6	3.96	41.1
33-21-4	S-1	3	3.09	15.0	22.5	1515	103	51.7	45.9	299	28	580	281	10.1	3.18	50.3
33-21-5	S-1	3	3.49	13.9	22.3	1847	114	46.2	44.0	299	34	623	324	8.6	2.94	62.8
33-21-6	S-1	3	3.47	13.8	22.2	1833	113	46.2	43.9	300	33	588	288	6.5	2.55	64.3
33-21-7	S-1	3	3.10	14.6	22.5	1540	104	51.4	45.9	300	28	611	312	12.8	3.58	49.6
34-30-1	S-2	3	2.85	15.7	22.3	1332	97	54.8	46.5	298	25	599	301	18.5	4.30	39.8
34-30-2(a)	S-2	3	2.78	14.5	19.5	1265	95	49.2	41.6	297	23	604	307	29.7	5.45	32.1
34-30-3	S-2	3	2.85	15.9	22.2	1315	96	55.0	46.5	296	26	578	282	16.0	4.00	40.1
35-1-1	S-2	3	2.82	16.0	22.9	1306	96	56.9	47.8	296	25	608	313	20.8	4.56	39.0
35-1-2	S-2	3	2.83	16.0	22.9	1317	97	56.6	47.8	297	25	586	290	16.3	4.05	40.8
35-1-3	S-2	3	3.08	15.9	22.6	1487	102	52.5	46.3	298	30	589	292	11.2	3.35	48.8
35-2-1	S-2	3	3.09	15.8	22.7	1490	102	52.7	46.5	297	29	601	303	12.7	3.57	48.5
35-2-2	S-2	3	3.10	15.8	22.9	1503	103	52.8	46.7	297	30	591	294	11.2	3.35	50.0
35-2-3	S-2	3	3.48	14.5	22.5	1811	113	47.1	44.5	298	25	588	290	6.6	2.58	64.3
35-2-4	S-2	3	3.48	14.4	22.2	1811	113	46.5	44.0	298	34	598	300	7.4	2.72	62.8
35-2-5	S-2	3	3.35	14.4	22.6	1726	110	48.6	45.1	298	35	594	296	7.9	2.82	59.9
35-4-7(b)	S-2	1	3.43	13.5	22.0	1793	232	93.6	82.6	297	0	675	378	4.8	2.19	98.1
35-4-8(b)	S-2	1	3.50	14.5	22.6	1830	235	94.9	84.1	297	0	656	358	3.8	1.95	104.6
35-4-9(b)	S-2	1	3.25	14.7	22.1	1638	222	98.4	84.1	298	0	652	354	5.2	2.28	88.4
35-4-10(b)	S-2	1	3.09	15.8	22.9	1506	213	106.3	88.0	298	0	656	357	6.4	2.54	80.4
35-6-4(b)	S-2	1	2.83	16.4	22.5	1316	200	112.4	88.8	299	0	684	386	12.6	3.56	61.9
35-6-5(b)	S-2	1	2.98	15.3	22.4	1429	208	107.0	87.1	299	0	672	373	8.8	2.97	71.6
Part II. Propellant Samples with Polymer-Rich Surfaces																
35-2-6	S-2	3	3.15	15.4	21.6	1537	104	49.4	44.2	298	30	662	364	21 (c)	-	45.1
35-2-7	S-2	3	3.47	14.5	22.9	1819	113	47.8	45.2	298	34	667	369	12.0	3.46	60.5
35-3-1	S-2	3	3.49	13.7	22.5	1835	113	46.9	44.5	296	33	643	349	10.2	3.20	61.7
35-3-2	S-2	3	3.44	14.8	22.5	1771	111	47.6	44.6	297	34	638	341	10.8	3.29	59.1
35-3-3	S-2	3	3.33	15.3	22.7	1691	109	49.4	45.5	298	33	674	376	15.8	3.98	53.8
35-3-4	S-2	3	3.27	15.7	22.3	1621	107	49.4	45.0	298	32	684	386	20.0	4.48	49.1
35-3-5	S-2	3	3.08	15.7	22.7	1494	103	52.7	46.5	298	29	667	370	22 (c)	-	44.8

(continued)

TABLE 8 (Continued)

Run No.	Propellant Code	Flow Control Orifice	M_E	P_4 (atm)	P_4' (atm)	T_4' (°K)	U $\frac{m}{sec}$	G $\frac{g}{(cm)^2(sec)}$	h $\frac{cal}{(cm)^2(sec)(°K)}$	T_1 (°K)	ΔT_o (°K)	T_{si}^L (°K)	ΔT_{si}^L (°K)	t_i (msec)	$(t_i)^{1/2}$ $(msec)^{1/2}$	$\bar{F}$ $\frac{cal}{(cm)^2(sec)}$
Part II. Propellant Samples with Polymer-Rich Surfaces (continued)																
35-6-1(a)	S-2	1	3.47	14.4	22.1	1790	232	93.9	82.8 x 10^{-3}	295	0	772	476	8.8	2.97	91.3
35-6-2(a)	S-2	1	3.47	13.4	21.8	1816	234	92.1	81.7	296	0	847	551	13.0	3.61	86.9
35-6-3(b)	S-2	1	3.09	16.0	21.5	1478	211	101.0	83.5	298	0	748	450	14.5	3.81	67.2
35-7-1(b)	S-2	1	3.25	14.6	22.3	1625	221	99.7	84.9	296	0	774	479	11.8	3.44	72.0
35-7-2(b)	S-2	1	2.84	15.7	21.8	1313	200	108.8	86.2	296	0	706	410	16.1	4.02	58.2
Part III. Propellant with Polymer-Rich Surfaces (Thickness of Polymer Film Reduced by Dissolving with Benzene)[d]																
35-4-1	S-2	3	3.45	14.4	22.7	1772	112	48.0	45.0	293	33	683	390	15.2	3.92	56.9
35-4-2	S-2	3	3.43	14.4	21.6	1740	111	46.2	43.2	294	33	658	364	14.4	3.80	54.1
35-4-3	S-2	3	3.22	15.0	21.7	1577	105	48.9	44.2	294	31	629	335	15.2	3.90	48.9
35-4-4	S-2	3	3.09	15.9	22.9	1488	102	53.1	46.8	295	30	636	341	17.4	4.17	46.5
35-4-5	S-2	3	2.97	15.2	22.9	1415	100	54.5	47.2	295	27	636	341	20.5	4.54	42.8
35-4-6	S-2	3	2.82	16.1	22.2	1293	96	55.5	46.6	296	26	615	320	24.2	4.94	37.0

(a) An indication of localized ignition at the time indicated.
(b) Sample ignited at time indicated, but was later extinguished by cold driver gas entering test section.
(c) Sample did not ignite. Value for ignition time is that for the minimum test period at specified shock tube conditions.
(d) Thickness of polymer-rich surface was reduced shortly after samples were placed in curing oven by painting with benzene and then removing the liquid layer.

TABLE 9

IGNITION DATA FOR U-PROPELLANT IN NITROGEN

Run No.	Propellant Code	Flow Control Orifice	M_E	P_4 (atm)	P_4' (atm)	T_4' (°K)	U $\frac{m}{(sec)}$	G $\frac{g}{(cm)^2(sec)}$	h $\frac{cal}{(cm)^2(sec)(°K)}$	T_1 (°K)	ΔT_o (°K)	T^L_{si} (°K)	ΔT^L_{si} (°K)	t_i (msec)	$(t_i)^{1/2}$ $(msec)^{1/2}$	$\bar{F}$ $\frac{cal}{(cm)^2(sec)}$
Part I. Propellant Samples with Cut Surfaces																
37-30-3	U-1	3	2.82	15.0	22.8	1358	98	55.5	47.4×10^{-3}	304	24	657	353	27 (a)	-	38.7
37-30-4	U-1	3	3.20	15.6	22.0	1570	105	49.8	44.8	304	31	678	374	20.8	4.56	46.6
37-30-5	U-1	3	3.36	13.4	22.2	1794	112	46.7	44.1	305	31	692	387	15.5	3.94	56.0
37-30-6	U-1	3	3.05	15.3	22.2	1513	103	51.1	45.4	305	28	677	372	23 (a)	-	44.1
37-30-7	U-1	1	3.04	14.9	22.0	1509	214	102.4	85.1	305	0	668	363	7.2	2.68	77.0
37-31-1	U-1	1	3.44	13.8	21.6	1813	234	91.3	81.0	301	0	722	421	6.4	2.53	94.6
38-23-1	U-2	3	2.85	15.2	22.4	1345	97	54.8	46.7	299	25	635	336	24.5	4.96	38.6
38-23-2	U-2	3	3.07	15.2	22.6	1504	103	52.2	46.2	300	28	670	370	22 (a)	-	44.8
38-23-3	U-2	3	3.42	13.9	22.3	1804	112	46.7	44.1	300	33	706	406	17 (a)	-	56.0
38-26-1	U-2	1	3.43	12.9	21.2	1801	233	89.6	79.5	298	0	733	436	7.4	2.72	91.1
38-26-2	U-2	1	3.49	13.7	22.0	1844	235	92.2	82.2	299	0	753	455	7.2	2.69	96.3
38-26-3	U-2	1	3.21	14.5	21.8	1593	219	98.6	83.6	302	0	670	368	6.4	2.53	82.7
38-26-4	U-2	1	3.09	15.2	22.7	1528	215	104.6	87.0	301	0	688	388	7.8	2.80	79.0
38-26-5	U-2	1	2.82	15.8	22.8	1328	201	113.2	89.6	300	0	697	397	13 (a)	-	62.6
38-26-6	U-2	1	2.84	15.5	22.7	1348	202	112.0	89.2	300	0	640	340	8.0	2.84	68.4
38-27-1	U-2	1	2.85	15.5	22.2	1338	201	109.7	87.3	299	0	693	394	13 (a)	-	62.2
38-29-8	U-2	2	3.07	15.2	20.6	1495	152	70.2	60.3	304	15	697	393	17 (a)	-	54.2
38-29-9	U-2	2	3.26	13.7	20.8	1677	161	66.6	59.5	304	16	635	331	7.5	2.74	68.8
47-25-1	U-4	1	3.41	14.4	21.4	1766	231	91.7	80.7	301	0	732	432	7.5	2.74	89.6
47-25-2	U-4	1	3.29	15.0	21.6	1667	224	95.4	82.2	301	0	676	375	6.0	2.46	87.1
47-25-3	U-4	1	3.11	15.0	21.9	1532	215	101.0	84.4	302	0	729	427	10.8	3.29	74.0
47-25-4(b)	U-4	None	3.32	14.5	21.2	1700	756	150.6	125.0	302	0	741	439	3.7	1.93	129.9
47-25-5(b)	U-4	None	3.12	14.9	21.7	1545	722	161.9	129.7	302	0	792	490	6.6	2.58	108.5
47-25-6(b)	U-4	None	3.54	13.8	20.6	1883	796	138.7	119.6	303	0	753	453	3.1	1.76	145.3
47-25-7	U-4	3	3.54	13.8	21.4	1732	116	43.6	42.1	305	34	668	363	11.6	3.41	60.7
47-25-8	U-4	3	3.28	14.6	21.2	1683	109	46.3	42.8	305	31	684	379	18.9	4.46	49.6
47-25-9	U-4	3	3.72	13.5	21.6	2067	120	42.2	41.9	305	36	707	402	12 (a)	-	66.0
53-13-1	U-5	1	3.42	13.3	19.8	1715	227	86.0	75.5	291	0	706	415	8.3	2.88	81.8
53-13-2	U-5	1	3.39	14.3	20.4	1688	226	89.1	77.6	293	0	737	444	10 (a)	-	79.9
53-13-3	U-5	1	3.24	14.7	20.5	1588	219	92.6	78.9	296	0	725	429	10.9	3.30	74.0
53-13-4	U-5	1	3.34	14.5	21.2	1705	227	92.5	80.5	296	0	677	381	6.0	2.45	88.1

(continued)

TABLE 9 (Continued)

Run No.	Propellant Code	Flow Control Orifice	M_E	P_4 (atm)	P_4' (atm)	T_4' (°K)	U m/(sec)	G g/(cm)^2(sec)	h cal/(cm)^2(sec)(°K)	T_1 (°K)	ΔT_o (°K)	T^L_{si} (°K)	ΔT^L_{si} (°K)	t_i (msec)	$(t_i)^{1/2}$ (msec)$^{1/2}$	$\bar{F}$ cal/(cm)^2(sec)
Part I. Propellant Samples with Cut Surfaces (continued)																
53-13-5	U-5	1	3.48	14.0	20.9	1793	232	88.7	78.6 x 10^{-3}	296	0	777	481	10 (a)	-	86.5
53-13-6	U-5	1	3.59	13.9	21.2	1883	238	87.6	78.9	296	0	726	430	6.3	2.51	98.4
53-13-7	U-5	1	3.51	13.8	22.3	1851	236	97.5	82.8	297	0	737	440	6.4	2.53	98.9
53-13-12	U-5	None	3.47	13.9	20.6	1774	773	143.1	120.9	296	0	863	567	7 (a)	-	121.8
53-15-1(b)	U-5	None	3.44	14.6	21.2	1736	765	148.5	124.2	294	0	792	498	4.9	2.21	128.0
53-15-2(b)	U-5	None	3.24	14.9	20.6	1581	731	152.0	123.3	295	0	777	482	6.3	2.51	109.2
53-15-3	U-5	None	3.15	15.2	20.5	1517	716	154.2	123.4	297	0	771	474	7 (a)	-	102.0
53-16-14	U-5	3	3.21	15.2	22.2	1589	106	49.8	45.0	298	31	675	376	20 (a)	-	47.9
53-16-15	U-5	1	3.61	13.8	22.3	1937	241	91.0	82.4	298	0	731	433	5.4	2.32	105.9
53-16-16	U-5	1	3.34	15.2	21.9	1679	225	96.3	83.1	298	0	733	435	8.5	2.92	84.9
Part II. Propellant Samples with Polymer-Rich Surfaces																
37-31-4	U-1	1	3.45	14.4	22.0	1814	234	92.7	82.2	303	0	728	425	6.4	2.53	85.6
37-31-5	U-1	1	3.05	14.8	21.8	1505	213	101.6	84.4	303	0	719	416	10.7	3.28	72.4
37-31-6	U-1	1	2.82	15.0	22.3	1352	202	109.8	87.7	303	0	658	355	9.3	3.06	66.2
37-31-7(c)	U-1	1	2.59	16.0	22.0	1182	190	116.4	88.7	303	0	663	359	15.8	3.98	51.4
38-29-1	U-2	3	2.54	16.4	22.4	1124	89	60.2	48.2	298	21	586	287	28.8	5.38	30.4
38-29-2	U-2	3	2.82	15.2	21.3	1311	86	52.9	44.8	299	24	573	275	16.4	4.05	38.6
38-29-3	U-2	3	3.08	15.3	22.0	1498	103	51.0	45.2	299	29	612	313	14.5	3.82	46.8
38-29-4	U-2	3	3.26	15.2	21.4	1627	107	47.5	43.4	300	31	604	304	11.0	3.32	52.1
38-29-5	U-2	3	3.47	13.7	21.0	1817	113	44.0	41.9	300	33	576	276	6.5	2.55	61.5
28-29-6	U-2	1	3.22	14.3	20.4	1611	220	91.6	78.5	301	0	715	414	9.6	3.10	76.0
38-29-7	U-2	1	2.82	14.3	21.1	1345	202	104.0	83.4	303	0	673	371	11.8	3.44	61.9
Part III. Propellant Samples with Polymer-Rich Surfaces (Surfaces Salted with 15-Micron Ammonium Perchlorate Before Curing)																
37-31-2	U-1	1	3.05	15.5	22.4	1495	213	104.5	86.4	302	0	713	411	9.8	3.14	73.6
37-31-3(d)	U-1	1	3.15	16.1	23.3	1572	218	105.8	88.7	302	0	630	328	4.4	2.10	88.9
38-23-4	U-2	3	3.52	13.5	22.0	1886	115	45.2	43.4	300	33	612	312	7.5	2.74	64.8
38-23-5	U-2	3	3.28	15.1	22.0	1658	108	48.4	44.4	301	32	575	274	7.5	2.74	56.9
38-23-6	U-2	3	2.85	15.3	22.1	1349	98	54.1	46.2	301	26	570	269	13.3	3.66	42.0
38-23-7	U-2	3	2.53	15.4	21.4	1135	90	57.2	46.1	301	22	533	232	16.6	4.08	32.4
38-27-2	U-2	1	3.46	13.7	21.6	1817	234	90.9	80.8	300	0	603	303	2.8	1.67	102.9
38-27-3	U-2	1	3.07	14.6	21.3	1500	213	99.2	82.5	300	0	631	331	6.0	2.46	76.7
38-27-4	U-2	1	2.80	14.4	21.8	1329	201	108.1	86.0	301	0	654	353	10.1	3.18	63.2
38-27-5	U-2	1	2.61	15.4	22.4	1205	191	116.9	89.7	301	0	648	347	12.8	3.59	55.2

(continued)

TABLE 9 (Continued)

Run No.	Propellant Code	Flow Control Orifice	M_E	P_4 (atm)	P_4' (atm)	T_4' (°K)	U_m (m/sec)	G_g (g/(cm)^2(sec))	h (cal/(cm)^2(sec)(°K))	T_1 (°K)	ΔT_o (°K)	T^L_{si} (°K)	ΔT^L_{si} (°K)	t_i (msec)	$(t_i)^{1/2}$ (msec)$^{1/2}$	$\bar{F}$ (cal/(cm)^2(sec))
Part IV. Propellant Samples with Polymer-Rich Surfaces (Surfaces Salted with 15-Micron Ammonium Perchlorate 3 Hours After Start of Cure)																
38-27-6	U-2	1	2.79	15.0	21.9	1320	200	109.1	86.7×10^{-3}	301	0	599	298	6.4	2.54	67.0
38-27-7	U-2	1	3.48	13.6	21.6	1847	236	90.1	80.5	301	0	622	321	3.1	1.76	103.7
38-27-8	U-2	1	3.14	15.2	22.0	1549	216	100.7	84.5	301	0	627	326	5.0	2.24	83.0
38-28-1	U-2	1	2.63	16.2	22.0	1193	191	115.4	88.3	303	0	592	290	8.2	2.87	57.6
38-28-2	U-2	1	2.61	15.4	21.7	1195	191	113.9	87.3	303	0	593	290	8.4	2.90	57.0
38-28-3	U-2	3	2.83	15.7	22.3	1337	97	54.8	46.6	302	25	532	230	8.7	2.95	44.3
38-28-4	U-2	3	3.11	15.2	22.0	1531	104	50.5	45.0	301	29	538	237	6.4	2.53	53.2
38-28-5	U-2	3	3.29	15.2	21.4	1651	108	47.0	43.2	301	32	543	243	5.8	2.42	57.3
38-28-6	U-2	3	2.61	15.9	21.9	1187	92	57.3	46.8	301	22	508	208	10.0	3.16	37.4

(a) Propellant sample did not ignite. Value for ignition time is that for the minimum test period at specified shock tube conditions.
(b) Sample ignited at the time indicated, but was later extinguished by cold driver gas entering the test section.
(c) An indication of localized ignition at the time indicated.
(d) This sample was specially prepared by spraying a 10 per cent water solution of ammonium perchlorate on the polymer-rich surface to produce crystals of ammonium perchlorate on the surface.

TABLE 10

STRAND BURNING RATE DATA FOR PROPELLANTS AT 20°C

Propellant Code	Burning Rate, [cm/(sec)] at 1.0 atm.	at 10.0 atm	Constants for Burning Rate Equation (a) a	n	Pressure Range (atm)
F	-	0.793	0.3207	0.393	6.8 - 58.0
F-M (b)	0.289	1.040	0.2886	0.579	1.0 - 7.8
			0.3917	0.424	7.8 - 34.0
G (b)	0.143	0.520	0.1431	0.560	1.0 - 20.4
J	0.332	0.773	0.3322	0.366	6.8 - 57.8
U (b)	0.347	1.235	0.3465	0.552	1.0 - 20.4

(a) Burning rate dependence on pressure is represented by:

$$r_p = a(P)^n$$

Where: r_p is the burning rate in cm/(sec) and P is the pressure in atm.

(b) Experimental data for these propellants are tabulated in Table 19 of Reference 11.

TABLE 11

IGNITION DATA FOR U-PROPELLANT IN ARGON AND OXYGEN

(Propellant Samples with Cut Surfaces)

Run No	Propellant Code	Flow Control Orifice	M_E	P_4 (atm)	P_4' (atm)	T_4' (°K)	$\frac{U}{m}$ (sec)	$\frac{G}{g}$ $(cm)^2(sec)$	$\frac{h}{cal}$ $(cm)^2(sec)(°K)$	T_1 (°K)	ΔT_o (°K)	T^L_{si} (°K)	ΔT^L_{si} (°K)	t_i (msec)	$(t_i)^{1/2}$ $(msec)^{1/2}$	$\frac{\bar{F}}{cal}$ $(cm)^2(sec)$
Part I. Ignition in Argon																
49-12-3	U-4	1	3.10	12.9	20.7	2269(a)	231	101.4	53.0×10^{-3}	299	0	713	414	7.4	2.72	87.3
49-12-4	U-4	1	2.58	13.9	21.2	1624(a)	196	123.2	65.5	300	0	699	399	12.0	3.47	62.4
49-12-5	U-4	1	3.28	16.1	20.9	2533(a)	244	97.0	50.5	300	0	676	376	4.8	2.19	97.8
49-14-1	U-4	3	2.99	13.3	19.9	2102(a)	110	50.2	25.7	296	15	664	368	27.1	5.21	40.3
49-14-2	U-4	3	3.27	15.3	20.5	2490(a)	120	47.7	24.2	296	23	654	358	17.2	4.15	47.0
49-14-7(b)	U-4	3	2.50	16.3	20.4	1528(a)	-	-	-	-	-	-	-	-	-	-
49-14-8	U-4	3	3.32	15.1	19.9	2580(a)	122	45.7	23.0	300	24	621	322	14.0	3.75	49.9
Part II. Ignition in Oxygen																
53-15-4(c)	U-5	None	3.16	16.1	20.9	1439	653	172.8	134.7	296	0	756	459	6.5	2.55	102.5
53-15-5(c)	U-5	None	3.36	15.0	19.7	1593	686	154.8	125.7	296	0	836	539	8.3	2.88	106.5
53-15-6(c)	U-5	None	3.15	15.9	20.9	1443	654	172.6	134.6	297	0	700	403	4.4	2.10	109.3
53-15-7	U-5	None	3.52	14.5	19.8	1733	715	148.7	124.3	298	0	858	560	7 (d)	-	120.5
53-15-8	U-5	None	3.52	15.0	20.0	1721	712	150.7	125.6	298	0	857	560	7 (d)	-	120.4
53-15-9(c)	U-5	None	3.38	16.0	20.5	1608	689	159.9	129.8	298	0	787	489	5.6	2.37	117.4
53-15-10(c)	U-5	None	3.62	14.9	19.9	1795	727	147.0	124.3	297	0	787	490	4.2	2.05	136.0
53-15-11	U-5	1	3.16	16.1	20.2	1430	195	103.2	84.3	296	0	704	408	12 (d)	-	67.1
53-15-12	U-5	1	3.32	16.0	20.6	1563	203	100.5	84.5	298	0	681	384	7.4	2.72	80.3
53-16-1	U-5	1	3.14	15.9	21.6	1446	196	109.5	89.2	296	0	609	313	5.0	2.24	79.7
53-16-2	U-5	1	3.22	16.3	22.7	1515	200	112.3	92.6	296	0	749	453	10.9	3.30	78.0
53-16-3	U-5	1	3.60	14.0	20.5	1820	219	92.2	81.8	298	0	801	504	10 (d)	-	90.6
53-16-4	U-5	1	3.41	16.4	21.3	1627	207	101.6	86.4	298	0	679	382	6.1	2.47	87.9
53-16-5	U-5	3	3.62	15.5	21.8	1819	106	48.8	46.0	298	37	685	387	13 (d)	-	61.1
53-16-5	U-5	3	3.20	17.9	22.1	1493	96	54.8	48.2	298	33	667	369	20 (d)	-	46.9
53-16-7	U-5	1	3.20	15.7	21.3	1517	200	105.4	87.5	296	0	696	400	18.5	2.92	78.0
53-18-1	U-5	None	3.18	16.3	21.0	1425	650	174.9	135.7	293	0	762	468	7 (d)	-	100.7
53-18-2(c)	U-5	None	3.46	15.0	20.4	1660	700	156.8	128.7	294	0	777	484	4.9	2.21	124.3
53-18-3(c)	U-5	None	3.33	14.8	20.8	1581	684	163.5	131.7	293	0	776	482	5.5	2.34	117.0
53-18-4	U-5	1	3.67	15.2	23.2	1854	221	103.2	91.2	294	0	766	472	6.2	2.49	107.9
53-18-5	U-5	1	3.44	16.9	22.3	1638	208	106.2	90.1	294	0	761	467	9.5	3.08	96.2

Table 11 (Continued)

(a) For argon the gas temperature used was that immediately behind the reflected shock, and was not adjusted for the post-reflection rise. Test section gas velocity, U, and mass flow rate, G, are also based on this value of gas temperature.

(b) Propellant sample did not ignite.

(c) Sample ignited at the time indicated, but was later extinguished by cold driver gas entering the test section.

(d) Propellant sample did not ignite. Value for ignition time is that for the minimum test period at specified shock tube conditions.

TABLE 12

IGNITION DATA FOR J-PROPELLANT IN NITROGEN[a]

(Propellant Samples with Cut Surfaces)

Run No.	Propellant Code	Flow Control Orifice	M_E	P_4 (atm)	P_4' (atm)	T_4' (°K)	U $\frac{m}{(sec)}$	G $\frac{g}{(cm)^2(sec)}$	h $\frac{cal}{(cm)^2(sec)(°K)}$	T_1 (°K)	ΔT_o (°K)	T^L_{si} (°K)	ΔT^L_{si} (°K)	t_i (msec)	$(t_i)^{1/2}$ $(msec)^{1/2}$	$\bar{F}$ $\frac{cal}{(cm)^2(sec)}$
44-27-1	J-2	3	2.79	15.0	20.5	1269	95	51.7	43.5×10^{-3}	295	24	555	261	17.2	4.15	36.3
											22	539	244			36.9
44-27-2	J-2	3	2.78	14.7	20.2	1265	95	51.1	43.0	296	23	570	274	20.6	4.55	34.9
											21	553	257			35.5
44-27-3	J-2	3	3.45	13.8	20.3	1761	111	43.2	40.9	296	32	561	265	6.9	2.63	58.2
											29	542	246			58.8
44-27-4	J-2	3	3.29	13.9	21.2	1646	108	46.6	42.9	294	30	581	288	9.6	3.10	53.4
											28	562	267			54.1
44-27-5	J-2	3	2.64	15.4	22.4	1190	92	58.5	47.7	294	22	582	286	24.1	4.91	33.8
											20	564	270			34.5
44-27-6	J-2	3	3.08	14.8	22.1	1487	102	51.4	45.4	294	28	581	287	11.9	3.45	48.0
											26	562	268			48.8
44-27-7(b)	J-2	1	3.49	13.3	22.0	1837	235	92.1	82.0	296	0	697	401	5.4	2.33	99.6
												671	375			101.4
44-27-8(b)	J-2	1	3.26	14.0	21.7	1647	223	96.3	82.6	297	0	687	390	7.0	2.65	85.1
												663	366			86.9
44-27-9(b)	J-2	1	3.09	14.0	21.2	1513	214	98.1	81.9	297	0	654	357	7.4	2.72	75.7
												632	335			77.2
44-27-10(b)	J-2	1	2.84	15.2	21.6	1322	200	107.7	85.6	297	0	638	341	9.6	3.10	63.6
												618	321			5.1
44-27-11(b)	J-2	1	2.63	15.4	21.7	1188	190	114.2	87.4	297	0	678	381	19.2	4.39	50.1
												658	361			51.7
44-27-12	J-2	5	3.51	13.3	21.5	1855	57	22.6	23.0	297	49	524	228	10.7	3.28	40.2
											45	508	211			40.5
44-27-13	J-2	5	3.31	15.2	20.8	1632	54	23.4	22.9	297	47	529	232	16.6	4.08	32.9
											43	512	216			33.2
44-27-14	J-2	5	3.10	14.7	21.4	1504	52	25.1	23.8	297	42	514	217	17.1	4.14	30.3
											38	498	202			30.6
44-27-15	J-2	5	2.87	15.2	21.5	1338	49	26.8	24.4	296	37	512	216	24.1	4.91	25.4
											34	498	201			25.7
44-27-16	J-2	5	2.63	15.6	21.9	1184	46	29.1	25.3	296	32	518	222	38 (c)	-	20.8
44-30-1	J-2	5	3.46	13.3	21.2	1805	57	22.5	22.8	296	49	526	230	12.3	3.51	37.9
44-30-2	J-2	5	2.79	15.9	21.4	1271	48	27.3	24.5	296	36	531	234	36 (c)	-	22.5
44-30-3	J-2	5	3.07	15.8	22.0	1475	51	26.1	24.5	297	43	538	241	22.9	4.79	29.1
44-30-4	J-2	5	3.14	15.2	22.6	1543	53	26.1	24.9	297	42	582	285	31 (c)	-	29.6
44-30-5	J-2	3	3.48	13.3	21.4	1819	113	44.7	42.5	296	32	575	279	6.7	2.59	62.2
44-30-6	J-2	3	2.84	16.9	22.0	1313	96	54.7	46.2	295	25	578	283	16.9	4.11	39.7
44-30-7	J-2	3	3.38	11.8	15.9	1673	108	34.7	32.9	295	29	582	288	15.8	3.98	41.8

(continued)

TABLE 12 (Continued)

Run No.	Propellant Code	Flow Control Orifice	M_E	P_4 (atm)	P_4' (atm)	T_4' (°K)	$\frac{U}{m}$ (sec)	$\frac{G}{g}$ $(cm)^2(sec)$	$\frac{h}{cal}$ $(cm)^2(sec)(°K)$	T_1 (°K)	ΔT_o (°K)	T^L_{si} (°K)	ΔT^L_{si} (°K)	t_i (msec)	$(t_i)^{1/2}$ $(msec)^{1/2}$	$\frac{\bar{F}}{cal}$ $(cm)^2(sec)$
44-30-8(b)	J-2	1	3.51	13.2	20.6	1830	235	86.6	77.4×10^{-3}	295	0	640	345	4.2	2.05	97.2
44-30-9(b)	J-2	1	3.28	14.6	21.5	1634	222	95.8	82.0	295	0	649	353	5.6	2.37	86.2
44-30-10(b)	J-2	1	2.80	14.8	21.2	1289	198	107.1	84.5	295	0	691	396	16.6	4.08	56.1
44-30-11(b)	J-2	1	3.05	10.5	16.1	1482	212	75.3	64.1	295	0	640	345	11.8	3.44	57.9

(a) For ignition runs where two sets of results are given, the first set was based on thermophysical properties of the propellant at 60°C (Γ_p = 0.0206 cal/$(cm)^2$ $(sec)^{1/2}$(°K)). The second set was based on a Γ_p of 0.0224 cal/$(cm)^2(sec)^{1/2}$(°K) that included a mean value for the heat capacity of ammonium perchlorate between 300° and 540°K.

(b) Propellant sample ignited at the time indicated, but was later extinguished by cold driver gas entering the test section.

(c) Propellant sample did not ignite. Value for ignition time is that for the minimum test period at the specified shock tube conditions.

TABLE 13

IGNITION DATA FOR PROPELLANTS AD AND AE

(Propellant Samples with Cut Surfaces)

Run No.	Propellant Code	Flow Control Orifice	M_E	P_4 (atm)	P_4' (atm)	T_4' (°K)	U_m (sec)	G_g $\frac{}{(cm)^2(sec)}$	h $\frac{cal}{(cm)^2(sec)(°K)}$	T_1 (°K)	ΔT_0 (°K)	T_{si}^L (°K)	ΔT_{si}^L (°K)	t_i (msec)	$(t_i)^{1/2}$ $(msec)^{1/2}$	$\bar{F}$ $\frac{cal}{(cm)^2(sec)}$
								Part I. Ignition in Nitrogen								
46-3-8	AD-1	3	3.48	13.2	21.9	1842	114	45.5	43.4×10^{-3}	298	32	645	346	10.7	3.28	60.2
46-3-9	AD-1	3	3.51	14.0	21.6	1842	114	44.8	42.8	298	34	655	357	11.8	3.44	59.1
46-3-10	AD-1	3	2.83	15.4	22.3	1331	97	54.8	46.5	299	26	584	286	16.0	4.00	40.7
46-3-11	AD-1	3	3.10	15.2	22.0	1513	103	50.8	45.3	299	29	600	301	12.6	3.56	48.2
46-15-1	AD-1	3	3.52	13.7	21.4	1830	113	44.6	42.4	295	34	621	327	9.6	3.10	60.0
46-15-2	AD-1	3	3.92	12.2	21.2	2203	124	40.0	40.7	295	37	667	372	8.5	2.92	72.6
46-15-3	AD-1	3	3.09	15.0	21.4	1482	102	49.9	44.1	295	29	583	288	12.4	3.52	46.5
46-15-4	AD-1	3	2.83	15.1	21.8	1313	96	54.0	45.7	295	25	586	290	18.1	4.26	38.8
46-15-10	AD-1	5	3.57	14.5	22.0	1877	58	23.0	23.5	297	53	626	328	26 (b)	-	36.6
46-15-11	AD-1	1	3.59	13.8	22.0	1907	239	90.6	81.7	297	0	701	403	4.8	2.09	104.7
46-15-12	AD-1	1	3.13	15.0	21.4	1557	217	97.6	82.2	297	0	658	361	6.7	2.69	79.3
45-28-1	AE-1(a)	1	2.80	14.8	21.7	1278	197	110.0	86.3	291	0	671	380	13.3	3.72	57.9
45-28-2	AE-1(a)	1	3.25	15.0	22.3	1592	219	100.5	85.0	292	0	662	370	6.1	2.47	84.8
45-28-3	AE-1(a)	3	3.46	14.5	22.0	1757	111	46.3	43.9	292	34	597	305	8.3	2.88	59.9
45-28-4	AE-1(a)	3	3.09	15.1	22.5	1483	102	52.4	46.2	292	29	588	296	12.0	3.47	48.4
45-28-5	AE-1(a)	3	2.83	15.3	21.9	1299	96	54.6	46.1	293	25	552	259	13.2	3.64	40.4
45-29-6	AE-1(a)	3	2.57	15.4	22.6	1205	92	58.6	48.0	293	23	572	281	20.1	4.50	35.4
46-3-1	AE-1	3	3.46	13.1	21.8	1812	113	49.0	43.2	295	32	635	340	10.7	3.28	59.1
46-3-2	AE-1	3	3.25	14.4	22.0	1628	107	48.7	44.4	295	31	595	300	10.0	3.16	53.7
46-3-3	AE-1	3	3.08	15.4	22.3	1483	102	51.8	45.7	295	29	605	310	14.0	3.75	46.9
46-3-4	AE-1	3	2.87	15.7	23.2	1352	98	56.7	48.2	296	26	587	291	14.6	3.82	43.1
46-3-5	AE-1	3	2.64	16.1	22.9	1199	92	59.6	48.7	297	23	618	321	30 (b)	-	33.2
46-3-6	AE-1	3	3.48	13.5	21.5	1822	113	44.9	42.7	297	33	616	319	9.0	3.0	60.2
46-3-7	AE-1	3	3.86	12.5	21.8	2179	123	41.6	42.0	298	37	654	356	7.3	2.7	74.6
46-15-5	AE-1	3	2.83	15.0	21.2	1313	96	52.5	44.6	296	25	625	329	27 (b)	-	35.8
46-15-6	AE-1	3	3.10	14.3	21.8	1521	104	50.2	44.7	296	29	611	314	14.1	3.76	44.7
46-15-7	AE-1	5	3.09	14.9	22.8	1517	52	25.4	24.1	297	43	571	275	30 (b)	-	28.4
46-15-8	AE-1	5	3.56	13.3	21.3	1880	58	22.1	22.7	297	50	617	320	26 (b)	-	35.6
46-15-9	AE-1	5	3.60	13.8	21.3	1905	58	22.1	22.7	297	52	623	326	26 (b)	-	36.2

(continued)

TABLE 13 (Continued)

Run No	Propellant Code	Flow Control Orifice	M_R	P_4 (atm)	P_4' (atm)	T_4' (°K)	U $\frac{m}{sec}$	G $\frac{g}{(cm)^2(sec)}$	h $\frac{cal}{(cm)^2(sec)(°K)}$	T_1 (°K)	ΔT_o (°K)	T^L_{si} (°K)	ΔT^L_{si} (°K)	t_i (msec)	$(t_i)^{1/2}$ $(msec)^{1/2}$	$\bar{F}$ $\frac{cal}{(cm)^2(sec)}$
							Part I. Ignition in Nitrogen (continued)									
46-15-13	AE-1	1	3.08	14.6	21.2	1490	212	99.3	82.4×10^{-3}	297	0	666	369	8.1	2.85	73.3
46-15-14	AE-1	1	2.88	15.2	22.1	1360	203	108.4	86.9	298	0	672	374	10.5	3.24	65.4
46-16-1	AE-1	1	3.25	14.6	21.4	1606	220	96.4	82.0	294	0	660	366	6.2	2.49	83.1
46-16-2	AE-1	1	3.53	13.8	20.7	1817	234	87.2	77.8	294	0	650	356	4.4	2.10	96.0
46-16-3	AE-1	1	3.99	12.5	20.8	2242	259	78.3	75.2	295	0	745	451	4.6	2.15	119.0
46-16-8	AE-1	1	3.57	13.8	21.3	1874	237	88.3	79.4	296	0	661	365	4.1	2.03	101.9
46-16-9	AE-1	None	3.31	14.7	20.6	1638	743	148.7	122.2	296	0	722	426	4.0	2.00	121.1
							Part II. Ignition in Argon									
46-16-11	AD-1	3	3.42	15.4	21.7	2695(d)	123	47.7	24.3	296	26	568	272	7.6	2.76	58.4
46-16-12	AD-1	3	2.92	14.3	21.4	2013(d)	108	55.5	28.5	296	14	564	268	11.4	3.38	45.0
46-17-1	AD-1	3	2.76	14.8	22.6	1782(d)	101	62.1	32.0	292	10	580	284	15.2	3.90	41.6
46-17-2	AD-1	3	2.34	13.3	22.0	1314(d)	86	70.4	36.5	292	0	520	228	21.0	4.59	30.6
46-17-3(a)	AD-1	3	1.96	14.3	22.0	964(d)	-	-	-	292	-	-	-	-	-	
46-17-4	AD-1	3	2.56	13.3	22.2	1558(d)	95	65.3	33.5	292	5	539	247	14.9	3.86	36.4
46-17-5	AD-1	3	3.06	13.5	21.0	2159(d)	112	52.6	26.8	292	17	559	267	10.6	3.26	46.7
							Part III. Ignition in Oxygen									
53-16-8	AD-1	3	3.20	16.1	20.6	1497	96	51.0	45.2	296	32	466	170	2.7	1.64	58.9
53-16-9	AD-1	1	3.15	15.7	20.5	1438	195	104.3	85.2	296	0	597	301	5.0	2.24	76.4
53-16-10	AE-1	1	2.93	16.5	19.8	1270	184	107.6	84.5	297	0	612	316	8.8	2.97	60.2
53-16-11	AE-1	1	3.27	15.2	19.9	1528	201	98.0	82.1	297	0	532	234	2.4	1.55	85.7
53-16-12	AE-1	3	2.74	14.7	19.6	1187	86	54.8	44.9	297	24	526	228	13.6	3.69	35.0
53-16-13	AE-1	3	2.88	14.2	18.6	1272	89	50.1	42.3	298	25	450	152	4.0	2.0	43.0

(a) Propellant cured for 12 hours at 80°C.
(b) Propellant sample did not ignite. Value for ignition time is that for the minimum test period at the specified shock tube conditions.
(c) Propellant sample ignited at the time indicated, but was later extinguished by cold driver gas entering the test section.
(d) For argon the gas temperature used was that immediately behind the reflected shock, and was not adjusted for the post-reflection rise.

TABLE 14

IGNITION DATA FOR PROPELLANTS IN CATALYST STUDY

(Propellant Samples with Cut Surfaces)

Run No.	Propellant Code	Flow Control Orifice	M_E	P_4 (atm)	P_4' (atm)	T_4' (°K)	U $\frac{m}{(sec)}$	G $\frac{g}{(cm)^2(sec)}$	h $\frac{cal}{(cm)^2(sec)(°K)}$	T_1 (°K)	ΔT_o (°K)	T^L_{si} (°K)	ΔT^L_{si} (°K)	t_i (msec)	$(t_i)^{1/2}$ $(msec)^{1/2}$	$\bar{F}$ $\frac{cal}{(cm)^2(sec)}$
31-11-1	G-3	3	3.43	14.3	21.6	1727	110	46.4	43.2×10^{-3}	290	32	660	371	16 (a)	-	53.5
31-11-2	G-3	3	3.43	14.0	21.2	1724	110	45.5	42.5	290	32	656	365	16 (a)	-	52.7
31-11-3	G-3	3	3.44	13.4	20.9	1751	111	44.6	41.9	292	32	659	367	16 (a)	-	53.0
31-11-4	G-3	1	3.44	14.4	22.3	1747	229	97.0	84.7	292	0	780	488	11 (a)	-	89.1
53-13-8	G-22	1	3.34	14.4	22.3	1698	226	97.5	84.3	295	0	780	485	11 (a)	-	84.4
53-13-10	G-22	None	3.27	13.9	20.5	1632	742	148.5	121.9	296	0	806	510	7 (a)	-	111.3
53-13-9	GB-2	1	3.48	14.0	21.2	1796	232	89.8	79.5	295	0	776	481	10 (a)	-	87.8
53-13-11	GB-2	None	3.48	14.2	20.7	1779	774	143.3	121.2	296	0	860	564	7 (a)	-	123.0
45-12-1	X-1	3	3.49	15.1	21.4	1769	111	45.3	42.7	294	35	586	292	7.7	2.78	59.9
45-12-2	X-1	3	3.29	14.4	21.5	1647	108	47.4	43.5	295	31	641	346	15.0	3.88	50.9
45-12-3	X-1	3	3.06	14.0	20.9	1471	102	48.8	43.2	294	28	644	350	23 (a)	-	41.5
45-12-4	X-1	3	3.26	14.0	21.5	1602	106	48.1	43.7	295	31	599	304	11.3	3.36	51.4
45-12-5	X-1	3	3.13	13.7	21.6	1543	104	49.2	44.1	295	28	610	315	14.1	3.76	47.8
45-12-6(c)	X-1	1	3.44	14.0	20.6	1746	229	88.7	78.1	295	0	687	392	6.4	2.54	88.2
45-12-7(c)	X-1	1	3.28	15.4	21.6	1611	221	96.8	82.5	295	0	673	378	6.7	2.59	93.0
45-12-8	X-1	1	2.81	14.4	21.1	1307	199	105.6	83.8	296	0	669	373	13 (a)	-	58.8
45-12-9	X-1	1	3.09	14.7	21.5	1498	213	100.2	83.3	296	0	725	429	12 (a)	-	70.5
45-22-1	Y-1	3	3.23	14.0	21.9	1622	107	48.7	44.3	297	30	671	374	19 (a)	-	48.8
45-22-2	Y-1	3	3.45	13.1	21.2	1803	112	44.6	42.3	297	32	682	385	16 (a)	-	54.8
45-22-8	Y-1	1	3.48	13.1	20.7	1838	235	86.7	77.6	300	0	753	453	8.1(b)	2.85	90.5
46-16-4	Y-1	1	4.06	12.0	21.0	2322	263	77.9	75.6	295	0	835	539	7.2(a)	2.68	114.3
45-22-3	Z-1	3	3.49	13.6	21.3	1817	113	44.6	42.4	297	33	693	396	16.7	4.05	55.1
45-22-4	Z-1	3	3.29	13.7	20.6	1654	108	45.3	41.8	297	30	662	364	19 (a)	-	50.3
45-22-9(c)	Z-1	1	3.47	12.8	20.8	1835	235	87.0	77.9	300	0	753	453	8.1	2.85	90.6
46-16-5(c)	Z-1	1	4.08	13.1	21.3	2318	263	79.0	76.5	295	0	737	443	3.9	1.98	127.5
46-16-10	Z-1	3	3.93	12.7	19.9	2176	123	38.0	38.7	296	38	659	363	9.1	3.02	48.4
45-22-5	AA-1	3	3.37	12.7	20.2	1727	110	43.4	40.8	298	31	662	364	17 (a)	-	50.3
45-22-10	AA-1	1	3.53	13.1	21.3	1884	238	88.1	79.4	300	0	744	444	6.8(b)	2.61	96.8
45-28-7	AA-1	5	3.49	14.0	22.2	1807	57	23.6	23.8	293	50	614	321	27 (a)	-	35.2
46-16-6	AA-1	1	3.98	13.0	20.6	2220	258	78.2	74.9	295	0	783	488	5.9(b)	2.43	114.3
45-22-6	AB-1	3	3.40	12.5	19.3	1761	111	41.1	39.0	298	30	658	360	17 (a)	-	49.7
45-22-11(c)	AB-1	1	3.44	13.2	21.0	1805	233	88.9	79.0	300	0	703	403	6.1	2.48	92.9
45-28-8	AB-1	5	3.61	13.2	21.8	1915	51	25.0	23.6	293	51	624	331	26 (a)	-	36.9
46-16-7	AB-1	1	3.98	12.3	20.8	2248	259	78.5	75.4	296	0	788	492	5.2 (b)	2.28	122.7
45-22-7	AC-1	3	3.51	13.1	21.0	1858	114	43.3	41.6	299	33	717	419	18.9	4.35	54.8
45-22-12(c)	AC-1	1	3.48	13.3	21.0	1839	235	88.1	78.8	300	0	719	419	6.4	2.53	94.3

Table 14 (Continued)

(a) Propellant did not ignite. Value for ignition time is that for the minimum test period at specified shock tube conditions.

(b) No sustained burning, but a strong photocell signal was observed at the time indicated.

(c) Ignition occurred at the time indicated, but was later extinguished by cold driver gas entering the test section.

TABLE 15

IGNITION DATA FOR PRESSED PROPELLANTS[a]

Run No.	Propellant Code	Flow Control Orifice	M_E	P_4 (atm)	P_4' (atm)	T_4' (°K)	$\frac{U}{m}$ (sec)	$\frac{G}{g}$ $(cm)^2(sec)$	$\frac{h}{cal}$ $(cm)^2(sec)(°K)$	T_1 (°K)	ΔT_o (°K)	T^L_{si} (°K)	ΔT^L_{si} (°K)	t_i (msec)	$(t_i)^{1/2}$ $(msec)^{1/2}$	$\frac{F}{cal}$ $(cm)^2(sec)$
Part I. Ignition in Nitrogen																
41-10-1(b)	B	3	3.43	13.8	21.4	1755	111	45.5	42.8×10^{-3}	294	28	639	344	17 (c)	-	54.3
41-10-2	B	3	3.42	13.8	21.4	1757	111	45.5	42.7	295	28	640	345	17 (c)	-	54.8
41-6-1	CB-1	3	3.25	14.8	22.2	1614	107	49.4	44.9	295	30	630	335	14.7	3.84	51.2
41-6-2	CB-1	3	3.51	14.3	22.1	1824	113	46.2	43.8	295	33	561	266	5.7	2.39	65.6
41-6-3	CB-1	3	3.44	14.9	21.8	1749	111	46.6	43.6	296	33	576	280	7.4	2.72	60.5
41-6-4	CB-1	3	2.86	15.2	22.1	1344	97	54.2	46.2	296	25	549	253	12.0	3.47	42.9
41-7-1	CB-1	3	2.71	15.0	22.2	1236	94	56.8	47.0	293	22	572	280	20.6	4.55	36.3
41-7-2	CB-1	3	2.80	15.0	22.1	1296	96	55.2	46.5	294	24	552	258	14.2	3.77	40.3
41-7-3(d)	CB-1	3	2.99	14.8	22.2	1424	100	52.7	45.9	294	26	553	259	10.6	3.26	46.8
41-10-3	CB-1	3	3.21	13.8	21.2	1594	106	47.6	43.2	295	28	670	375	22.9	4.79	46.1
41-10-4	CB-1	3	2.83	14.9	21.5	1310	96	53.4	45.2	295	24	534	239	11.7	3.42	41.1
41-21-5	CB-1	3	3.28	14.5	22.0	1646	108	48.5	44.5	295	30	584	289	9.5	3.09	55.2
41-21-6	CB-1	1	2.85	15.4	22.3	1328	201	110.5	87.7	296	0	630	334	3.8	2.97	46.3
41-21-7	CB-1	1	2.64	15.5	22.3	1194	191	117.2	89.6	295	0	681	385	19.3	4.40	51.6
41-21-8	CB-1	1	2.95	15.7	22.7	1398	206	109.5	88.4	296	0	607	312	6.0	2.45	74.9
44-24-1	CB-2	3	2.84	15.9	22.2	1306	96	55.2	46.5	291	22	487	196	7.6	2.76	44.9
44-24-2	CB-2	3	2.84	15.7	22.0	1289	96	55.0	46.3	291	23	597	306	27 (c)	-	46.3
44-24-3	CB-2	3	3.30	15.2	20.8	1602	106	46.4	42.3	292	29	468	176	3.5	1.87	59.2
44-24-4	CB-2	3	3.17	13.1	18.2	1517	103	41.8	37.9	293	25	588	295	21 (c)	-	0.6
44-24-5	CB-2	3	3.47	11.8	19.9	1812	113	41.8	39.9	293	27	543	250	7.1	2.67	59.1
45-1-1	CB-2	1	3.54	13.8	22.0	1860	236	91.8	82.0	295	0	753	459	8.9	2.97	97.5
45-1-2	CB-2	1	3.30	14.6	22.0	1651	223	97.4	83.5	295	0	691	396	8.4	2.90	86.1
45-1-3	CB-2	1	3.10	15.0	21.8	1496	213	101.6	84.2	295	0	697	402	12 (c)	-	73.1
45-1-4	CB-2	1	3.32	14.2	20.8	1673	225	95.8	82.6	295	0	701	406	9.8	2.97	84.3
45-1-5	CB-2	3	3.49	13.5	22.1	1835	113	46.0	43.8	295	30	658	364	15 (c)	-	59.2
45-1-6	CB-2	2	3.50	13.1	21.4	1835	168	65.6	60.3	295	16	721	426	13 (c)	-	74.4
45-9-6	CB-2	1	3.27	14.2	20.6	1557	217	94.2	79.6	295	0	661	366	9.1	3.02	76.5
44-21-6(d)	D	3	3.10	15.1	21.3	1479	102	49.6	43.9	293	28	576	282	12.8	3.59	46.4
44-22-1(e)	D	3	2.75	14.8	20.8	1245	94	53.1	44.3	292	23	563	271	20.6	4.64	35.1
44-22-2(e)	D	3	3.31	14.1	20.7	1640	107	45.7	42.0	293	30	598	305	12.3	3.36	51.1
44-23-1(e)	D	3	3.27	13.5	20.8	1634	107	46.1	42.3	294	29	655	361	19.8	4.45	47.8
44-23-2(e)	D	3	3.46	13.5	20.7	1777	112	43.8	41.4	295	31	676	382	18.2	4.27	52.7
44-23-3(e)	D	3	3.27	13.9	20.6	1622	107	45.6	41.8	295	29	593	298	11.2	3.35	0.7

(continued)

TABLE 15 (Continued

Run No.	Propellant Code	Flow Control Orifice	M_E	P_4 (atm)	P_4 (atm)	T_4 (°K)	U $\frac{m}{sec}$	G $\frac{g}{(cm)^2(sec)}$	h $\frac{cal}{(cm)^2(sec)(°K)}$	T_1 (°K)	ΔT_o (°K)	T^L_{s1} (°K)	ΔT^L_{s1} (°K)	t_i (msec)	$(t_i)^{1/2}$ $(msec)^{1/2}$	$\bar{P}$ $\frac{cal}{(cm)^2(sec)}$
							Part I. Ignition in Nitrogen (continued)									
44-23-4(e)	D	4	3.27	14.2	20.8	1621	70	30.2	28.9 x 10^{-3}	295	40	540	245	14.0	3.74	38.6
44-23-5(e)	D	4	3.48	13.2	20.8	1808	74	28.6	28.3	296	42	634	338	25 (c)	-	39.8
44-21-7(d)	E	3	2.98	15.2	20.8	1387	99	50.2	43.5	294	24	596	302	24 (c)	-	39.8
44-21-8(d)	E	3	3.44	13.2	20.8	1758	111	44.2	41.6	293	29	596	303	12.2	3.50	55.9
44-22-3(d)	E	3	3.39	13.8	20.2	1715	110	43.6	40.8	294	28	622	328	17 (c)	-	51.3
44-22-4	E	3	3.50	13.7	21.3	1806	113	44.7	42.4	295	29	573	279	8.7	2.96	60.9
44-22-5	E	1	3.44	12.4	19.9	1778	231	85.0	75.5	295	0	717	422	10 (c)	-	35.9
44-22-6	E	1	3.31	15.1	20.6	1632	222	91.9	79.0	296	0	703	407	11 (c)	-	79.1
							Part II. Ignition in Oxygen									
45-9-1(h)	CB-2	3	3.27	15.9	19.3	1488	96	47.8	42.5	295	29	601	305	19 (c)		44.2
45-9-2(h)	CB-2	3	3.70	13.8	19.4	1876	107	42.7	41.1	295	33	536	241	5.2	2.30	66.0
45-9-3(h)	CB-2	1	3.38	14.2	19.8	1621	207	94.7	81.0	296	0	661	366	7.7	2.78	93.1
45-9-4(h)	CB-2	1	3.36	14.0	19.7	1617	207	94.2	80.5	295	0	651	356	7.3	2.71	93.0
45-8-1	E	3	2.98	12.4	16.3	1328	91	42.8	37.2	296	22	550	254	24 (c)		33.4
45-8-2	E	3	2.87	14.8	20.5	1277	89	55.1	46.1	297	22	588	292	26 (c)	-	36.8
45-8-3	E	3	3.35	15.8	18.9	1548	98	46.0	41.6	297	29	599	303	18 (c)	-	46.1
45-9-5(g)	E	1	3.39	14.4	20.3	1636	208	96.8	82.9	295	0	690	394	9.3	3.02	84.3

(a) Pellets, unless otherwise indicated, were cemented into sample holders with G C. Electronics Epox Cement No. 346, and surfaces were finished with 600-A grit size silicon carbide paper.
(b) Although photocell signal was very weak, examination of extinguished sample showed that deflagration started at a flaw in the surface at the pellet-epoxy resin interface and at an agglomerate of copper chromite.
(c) Pellet did not ignite. Value for ignition time is that for the minimum test period at specified shock tube conditions.
(d) Pellet was pressed into sample holder. No potting agent was used.

(e) Pellet surface was finished with 500-A grit-size silicon carbide paper.

(f) Pellet surface was finished with 320-A grit-size silicon carbide paper.

(g) Pellet ignited but was later extinguished by cold driver gases.

(h) For these runs with oxygen as the test gas, pellets were potted in sample holder with Fleck's red copper cement.

TABLE 16

IGNITION DATA FOR EXTENDED-PHASE PROPELLANTS IN NITROGEN

Run No.	Flow Control Orifice	M_E	P_4' (atm)	T_4' (°K)	U m/(sec)	G g/(cm)^2(sec)	h cal/(cm)^2(sec)(°K)	T_1 (°k)	ΔT_o (°K)	ΔT^L_{si} (°K)	t_i (msec)	$\bar{F}$ cal/(cm)^2(sec)
Part I. Propellant Samples Composed of Pressed Propellant A and F-Propellant Binder												
31-21-2(a)	3	3.45	22.5	1745	111	48.1	[illegible] 9 x 10^{-3}	292	30	350	16 (b)	57.2(c)
									46	484	16 (b)	51.9(d)
(Sample was oriented in test section so that hot gas passed over the ammonium perchlorate pellet first. Sample did not ignite, but numerous small surface cracks appeared in the pellet.)												
31-21-3(a)	1	3.46	22.3	1734	229	96.1	83.7	294	0	438	10 (b)	90.4(c)
									0	588	10 (b)	79.6(d)
(Same test arrangement as that for Run 31-21-2. Sample did not ignite, but a number of surface cracks appeared).												
31-21-4(a)	1	3.46	22.0	1748	229	94.5	82.7	294	0	438	10 (b)	90.4(c)
									0	588	10 (b)	79.7(d)
(Hot gas passed over polymer first. Sample did not ignite, but surface cracks formed in pellet).												
31-21-5(a)	1	3.48	21.8	1764	230	93.5	82.1	294	0	441	10 (b)	90.9(c)
									0	592	10 (b)	80.2(d)
(Hot gas passed parallel to polymer-ammonium perchlorate interface. Sample did not ignite, but some small cracks developed at the surface of pellet and some charring of polymer occurred.)												
32-20-4(e)	3	3.48	22.0	1787	112	46.5	43.8	298	30	352	16 (b)	57.5(c)
									46	488	16 (b)	52.3(d)
(Hot gas passed parallel to the polymer-ammonium perchlorate interface. Sample did not ignite, but small cracks formed at surface of pellet)												

(continued)

TABLE 16 (Continued)

Run No.	Flow Control Orifice	M_E	P_4' (atm)	T_4' (°K)	U_m (sec)	G $\frac{g}{(cm)^2(sec)}$	h $\frac{cal}{(cm)^2(sec)(°K)}$	T_1 (°K)	ΔT_o (°K)	ΔT^L_{si} (°K)	t_i (msec)	$\bar{F}$ $\frac{cal}{(cm)^2(sec)}$
Part II. Propellant Samples Composed of Pressed Propellant B and F-Propellant Binder												
41-20-1(a)	3	3.30	22.7	1672	108	49.7	45.6×10^{-3}	294	27 42	356 489	19 (b) 19 (b)	53.5(c) 48.1(d)
(Hot gas passed over pellet first. No indication of ignition.)												
41-20-2(a)	3	3.46	22.0	1798	112	46.2	43.7	295	29 44	352 489	16 (b) 16 (b)	57.7(c) 52.4(c)
(Hot gas passed over pellet first. No indication of ignition.)												
41-20-3(a)	3	3.52	22.5	1862	114	46.5	44.4	295	29 45	251 361	5.8 5.8	68.4(c) 64.2(d)
(Hot gas passed over polymer first. A fairly strong photocell signal was observed at 5.8 milliseconds, and was followed by a number of weaker fluctuations. Examination of recovered sample after test showed that steady deflagration of the perchlorate sample had occurred, but was extinguished by the termination of the test period.)												
41-20-4(a)	3	3.50	21.8	1825	113	45.5	43.2	295	29 45	355 494	16.0 16.0	58.2(c) 52.9(d)
(Hot gas passed parallel to binder pellet interface. There was a fairly strong photocell signal at 16 milliseconds. Examination of sample after test showed that deflagration started at a flaw in the pellet at the interface between pellet and epoxy resin potting agent and spread across the pellet surface. Sample was extinguished at the end of test period.)												
41-21-1(a)	3	3.49	22.0	1787	112	46.4	43.7	293	30 45	329 461	13.5 13.5	58.8(c) 53.7(d)
(Hot gas passed over pellet first. Strong photocell deflection at 13.5 milliseconds. Examination of sample after test showed deflagration started at a flaw in the pellet surface near the pellet-epoxy resin potting agent and spread across pellet surface. Hot combustion gases from deflagrating pellet charred the polymer surface downstream. Sample was extinguished at end of test period.)												

(continued)

TABLE 16 (Continued)

Run No.	Flow Control Orifice	M_E	P_4' (atm)	T_4' (°K)	U m/(sec)	G g/(cm)^2(sec)	h cal/(cm)^2(sec)(°K)	T_1 (°K)	ΔT_o (°K)	ΔT^L_{si} (°K)	t_i (msec)	$\bar{F}$ cal/(cm)^2(sec)
						Part II (continued)						
41-21-2(a)	3	3.52	22.0	1837	113	45.9	43.7×10^{-3}	294	29	352	15 (b)	59.7(c)
									45	491	15 (b)	54.3(d)
	(Hot gas passed over pellet first. No indication of ignition.)											
41-21-3(a)	3	3.47	21.9	1797	112	46.1	43.6	295	29	351	16 (b)	57.6(c)
									44	488	16 (b)	52.3(d)
	(Hot gas passed over pellet first. Only a slight fluctuation in photocell signal. Examination of recovered sample did not show any evidence of ignition.)											
41-21-4(a)	3	3.48	22.0	1811	113	46.2	43.7	295	29	250	6.4	64.9(c)
									44	358	6.4	60.7(d)
	(Same sample that was used for Run 41-21-3, but rotated in test section so hot gas passed over polymer first. A fairly strong photocell deflection occurred at 6.4 milliseconds. Examination of recovered sample showed deflagration started at polymer-pellet interface and spread across entire pellet surface.)											
41-25-3(f)	3	3.11	22.3	1510	103	51.5	45.6	296	27	332	22 (b)	46.5(c)
									39	454	22 (b)	41.5(d)
	(No evidence of ignition was observed).											
41-25-4(f)	3	3.32	22.3	1688	109	48.4	44.6	296	27	347	18 (b)	53.6(c)
									41	479	18 (b)	48.4(d)
	(Only a few small fluctuations were observed on photocell signal. Examination of recovered sample showed that deflagration of the pellet was initiated on the downstream edge of polymer buttons.)											
41-25-5(g)	3	3.12	22.5	1532	104	51.4	45.8	296	25	338	21.9	47.3(c)
									38	462	21.9	42.3(d)
	(Strong photocell signal at 21.9 milliseconds. Deflagration started at trailing edge of upstream button of polymer and propagated past the two downstream buttons and then was extinguished by cold gases entering the test section. There was considerable undermining of upstream button of polymer.)											

(continued)

(continued)

TABLE 16 (Continued)

Run No.	Flow Control Orifice	M_E	P_4' (atm)	T_4' (°K)	U m/sec	G g/(cm)^2(sec)	h cal/(cm)^2(sec)(°K)	T_1 (°K)	ΔT_o (°K)	ΔT_{si}^L (°K)	t_i (msec)	$\bar{F}$ cal/(cm)^2(sec)
						Part II (continued)						
43-5-4(h)	3	3.08	21.5	1472	102	50.2	44.3×10^{-3}	294	25	315	22 (b)	44.1(c)
	(No evidence of ignition was observed.)											
43-5-5(h)	3	3.23	21.6	1594	106	48.4	44.0	294	27	333	20 (b)	48.9(c)
	(Same sample that was used for Run 43-5-4. No evidence of ignition was observed.)											
43-5-6(h)	3	3.43	21.6	1764	111	46.0	43.2	294	26	290	10.4	59(c)
	(Same sample that was used for Run 43-5-5. Fairly strong photocell signal at 10.4 milliseconds. Examination of extinguished sample showed deflagration started at trailing edge of a small speck of polymer on the face of the pellet.)											
43-6-1(i)	3	3.46	21.6	1785	112	45.7	43.1	292	28	346	16 (b)	56.7(c)
	(Hot gas passed over polymer first. No evidence of ignition was observed.)											
43-6-7(i)	2	3.52	22.2	1831	168	68.0	62.2	293	15	387	10.3	79.1(c)
	(Same sample that was used for Run 43-6-1. Examination of extinguished sample showed deflagration started at two locations at the pellet-polymer interface. Hot gas passed over polymer first.)											
43-6-3(i)	2	3.49	21.7	1806	167	67.0	61.1	294	15	410	13.0	74.6(c)
	(Hot gas passed over polymer first. Examination of extinguished sample showed deflagration initiated at a small crack in the pellet.)											
						Part III. Propellant Samples Composed of Pressed Propellant B and G-Propellant Binder						
41-25-1(f)	3	3.51	21.6	1836	113	45.0	42.9	294	29	295	9.8	61.8(c)
									48	450	9.8	56.0(d)
	(Entire surface of pellet ignited. Examination of extinguished sample showed considerable charring of all polymer. Surface regression was greatest at the trailing edges of polymer buttons. Some polymer was removed at trailing edge where greatest regression of pellet was observed.)											

(continued)

TABLE 16 (Continued)

Run No.	Flow Control Orifice	M_E	P_4' (atm)	T_4' (°K)	U m/(sec)	G g/(cm)^2(sec)	h cal/(cm)^2(sec)(°K)	T_1 (°K)	ΔT_o (°K)	ΔT^L_{si} (°K)	t_i (msec)	$\bar{F}$ cal/(cm)^2(sec)
						Part III (continued)						
41-25-2(f)	3	3.31	22.2	1655	108	48.3	44.3×10^{-3}	295	28 47	338 501	18.1 18.1	52.2(c) 45.8(d)
	(Deflagration process was the same as that observed for Run 41-25-1).											
	Part IV. Propellant Samples Composed of Pressed Propellant B and Acrylic Resin											
43-5-1(i)	3	3.07	21.9	1476	102	51.1	45.1	293	24	320	22 (b)	44.8(c)
	(Hot gas passed over polymer first. Examination of extinguished sample showed deflagration started at crack in pellet surface.											
43-5-2(h)	3	3.11	21.7	1496	103	50.3	44.6	294	25	323	22 (b)	44.6(c)
	(No evidence of ignition was observed.)											
43-5-3(h)	3	3.48	21.8	1472	112	46.1	43.5	294	29	350	16 (b)	57.3(c)
	(Same sample that was used for Run 43-5-2. No evidence of ignition was observed.)											

Table 16 (Continued)

(a) Sample composed of a half-cylinder of pressed ammonium perchlorate bonded in sample holder with an epoxy-type cement (G. C. Electronics Epox Cement No. 346). The remainder of the cylindrical volume of the sample holder was filled with propellant binder and cured for 7 days at 80°C.

(b) Sample did not ignite. Value for ignition time is that for the minimum test period at specified shock tube conditions.

(c) Heat flux and surface temperature calculated using thermophysical properties of ammonium perchlorate pellet.

(d) Heat flux and surface temperature calculated using thermophysical properties of rubber binder.

(e) Sample prepared by cutting V-shaped notch at the diameter in the face of ammonium perchlorate pellet and filling with propellant binder.

(f) Sample prepared by placing three small buttons of uncured binder at different locations on the polished face of the pellet and then curing for 7 days at 80°C.

(g) Sample prepared by drilling three small holes in the face of a mounted pellet of ammonium perchlorate and carefully filling the holes with uncured binder and then curing for 7 days at 80°C.

(h) Sample prepared by painting a small circular area near center of pellet face with thin coat of polymer.

(i) Sample prepared by painting one-half of pellet face with thin coat of polymer.

TABLE 17

IGNITION DATA IN DIMENSIONLESS FORM FOR SIMPLE THERMAL IGNITION OF CAST PROPELLANTS F AND G, AND PRESSED PROPELLANT CB[a]

PART I: KINETIC AND THERMAL RESPONSIVITY DATA

Propellant	E_a/R (°K)	Pre-Exponential Factor, B cal/(cm)^2(sec)	Γ_p cal/(cm)^2(sec)$^{1/2}$(°K)
F	15,500	4.45×10^{10}	0.0212
G	15,500	0.67×10^{10}	0.0206
CB	15,500	5.60×10^{10}	0.0210

PART II: IGNITION AT LOW RADIANT HEAT FLUXES IN AIR

Propellant	t_i (sec)	$(t_i^*)^{1/2}$(b)	$\bar{F}$ cal/(cm)^2(sec)	$\bar{F}^*$ (c)
F	20.50	61.3×10^{-7}	1.15	2.58×10^{-11}
F	6.92	35.6	2.15	4.83
F	2.11	19.6	4.14	9.30
F	0.76	11.8	7.22	16.20
F	0.32	7.66	11.70	26.30
G	9.30	6.40	2.08	31.00
G	2.77	3.48	4.07	60.70
G	0.97	2.07	7.14	106.50
G	0.42	1.36	11.62	173.40
CB	7.10	45.80	1.82	3.25
CB	5.15	39.10	2.53	4.52
CB	2.78	28.70	3.48	6.22
CB	0.84	15.80	6.56	11.70
CB	0.35	10.20	10.57	18.90

TABLE 17 (Continued)

PART III: IGNITION AT HIGH CONVECTIVE FLUXES IN NITROGEN

Run No.	Propellant	M_{ts}	t_i (sec)	$(t_i^*)^{1/2}$ (b)	$\bar{F}$ cal/(cm)^2(sec)	$\bar{F}^*$ (c)
43-19-1	F-30M	1.0	4.4×10^{-3}	8.99×10^{6}	116.4	2.62×10^{-9}
43-19-2	F-30M	1.0	3.7	8.26	126.6	2.84
43-19-3	F-30M	1.0	10.0	13.50	79.6	1.79
49-15-3	F-32	1.0	3.8	8.35	126.4	2.84
49-15-4	F-32	1.0	2.7	7.07	154.0	3.46
49-15-5	F-32	1.0	4.0	8.56	115.9	2.60
45-1-1	CB-2	0.28	8.8	16.20	97.5	1.74
45-1-2	CB-2	0.28	8.4	15.80	86.1	1.54
45-1-4	CB-2	0.28	8.8	16.20	86.3	1.54
45-9-6	CB-2	0.28	9.1	16.40	76.5	1.37
45-9-3 (d)	CB-2	0.28	7.7	15.10	83.1	1.48
45-9-4 (d)	CB-2	0.28	7.3	14.70	83.1	1.48

(a) Data for an initial, uniform propellant temperature of about 300°K.

(b) $$(t_i^*) = t_i \frac{(RB)^2}{(\Gamma_p E)} \qquad (12)$$

(c) $$\bar{F}^* = \bar{F}/B \qquad (13)$$

(d) Ignited in oxygen.

TABLE 18

DATA FOR FLOW-CONTROL ORIFICES

Orifice Number	Measured Area $(cm)^2$	Orifice Discharge Coefficient, C_D	Flow Area, A_{or} $(cm)^2$	Flow Area, A_{or} $(in.)^2$	Area Ratio (A_{or}/A_{ts})[a]
None[b]	0.8065	0.964	0.777[c]	0.1205	0.964
1	(d)	-	0.3690	0.0572	0.458
2	0.2866	0.940	0.2693	0.04174	0.334
3	0.2071	0.885	0.1832	0.02840	0.227
4	0.1479	0.813	0.1203	0.01865	0.149
5	0.1013	0.918	0.0930	0.01441	0.115

(a) Flow area of orifice divided by area of test-section flow channel.

(b) Flow channel of test section controlled flow of gas from shock tube.

(c) For reasons discussed on page 287, all calculations involving mass flow rate, such as heat transfer to the test section wall, for the open test section were based on a defined flow area of 0.60 $(cm)^2$.

(d) Area could not be measured precisely because the thin, metal walls separating the three, circular cross-section orifices in the plate were removed to enlarge the flow area.

TABLE 19

PROPERTIES OF HEAT FLUX GAUGES

Gauge Property	Gauge No. 1	Gauge No. 3	Gauge No. 4
Substrate Material	Alumina[a] (Alsimag 614)	Pyroceram 9608[b]	Pyrex 7740[b]
Thermal Responsivity[c], $(k\rho c)^{1/2}$, $[cal/(cm)^2(sec)^{1/2}(°K)]$	0.208 ± 0.005 at 28°C	0.0449 ± 0.0006 at 26°C	0.0366 ± 0.0002 at 26°C
$[Btu/(ft)^2(sec)^{1/2}(°R)]$	26.5	5.52	4.50
No. of Determinations	4	5	5
Temperature Coefficient of Resistance for Platinum film[c] $[ohm/(ohm)(°K)]$	2.54×10^{-3}	2.54×10^{-3}	2.18×10^{-3}
Effective temperature range (°C)	0 - 100	0 - 100	0 - 100

(a) Dense alumina containing 96 per cent Al_2O_3 with MgO and SiO_2. Manufactured by American Lava Corporation, Chattanooga 5, Tenn.

(b) Manufactured by Corning Glass Works, Corning, New York.

(c) Determined experimentally by method described in Appendix H.

TABLE 20

GAS TEMPERATURES BEHIND REFLECTED SHOCK WAVES
IN AIR, ARGON, AND OXYGEN

Incident Shock Mach Number (M_1)	Driven Gas Temperature Ratio (T_4/T_1)		
	Air[a]	Argon[b]	Oxygen[c]
1.6	1.80	2.30	1.80
1.8	2.12	2.82	2.08
2.0	2.45	3.41	2.40
2.2	2.82	4.05	2.72
2.4	3.21	4.74	3.07
2.6	3.61	5.49	3.44
2.8	4.01	6.30	3.83
3.0	4.42	7.14	4.24
3.2	4.87	8.06	4.68
3.4	5.33	9.05	5.14
3.6	5.82	10.12	5.62
3.8	6.32	11.21	6.14
4.0	6.85	-	6.66

(a) Values from Reference 6.

(b) Values from Reference 74.

(c) Values from Reference 12.

TABLE 21

SUMMARY OF INITIAL TEMPERATURE RISE DATA FOR HEAT FLUX GAUGES

PART I: WITH AIR THE TEST GAS

Run No.	M_E	P_o (atm)	P_4 (atm)	ΔT_o (°K)	$\Delta T_o \cdot (\Gamma/\Gamma^*)(P^*/P_4)^{\frac{1}{2}}$ (°K)
		Orifice No. 5, Pyrex Heat Flux Gauge			
35-31-1	2.85	24.7	16.2	21.5	16.9
35-31-2	3.52	24.7	14.4	28.5	23.7
37-20-5	1.93	11.1	8.0	6.2	6.9
37-20-6	1.94	11.1	8.2	7.0	7.7
37-20-7	2.42	10.9	7.4	10.5	12.2
37-20-9	2.98	10.9	6.7	15.0	18.4
37-20-10	3.34	10.6	6.0	17.0	22.8
		Orifice No. 5, Alumina Heat Flux Gauge			
39-22-4	3.42	23.3	13.4	4.6	22.6
39-22-6	2.41	24.0	7.4	1.8	12.5
		Orifice No. 3, Pyrex Heat Flux Gauge			
35-31-3	3.52	24.7	14.6	20.0	16.5
35-31-4	3.21	24.5	15.9	17.0	13.5
35-31-5	2.65	24.7	16.9	12.0	9.2
37-18-3	1.91	11.1	7.9	5.0	5.6
37-18-4	2.18	11.1	7.4	6.0	7.0
37-18-5	1.90	11.1	8.0	4.5	5.4
37-18-6	1.91	11.1	7.8	4.0	4.5
37-18-7	1.92	11.1	7.9	4.0	4.5
37-18-8	2.18	11.1	7.4	5.0	5.8
37-18-9	2.39	11.1	7.5	6.0	6.9
37-18-10	2.39	11.1	7.4	6.0	7.0
37-18-11	2.62	11.1	7.3	7.0	8.2
37-18-12	2.62	11.1	7.4	9.0	10.5
37-18-13	3.01	11.1	6.7	11.0	13.5
37-18-14	3.13	11.1	6.6	11.0	13.5
37-19-4	1.91	11.1	7.8	4.5	5.1
37-19-5	3.30	11.1	6.4	12.0	15.0
37-19-6	3.79	11.1	5.4	14.0	19.1
37-19-7	3.88	11.1	5.1	13.0	18.2

(continued)

TABLE 21 (Continued)

PART I: WITH AIR THE TEST GAS

Run No.	M_E	P_o (atm)	P_4 (atm)	ΔT_o (^oK)	$\Delta T_o(\Gamma/\Gamma^*)(P^*/P_4)^{\frac{1}{2}}$ (^oK)
		Orifice No. 3, Pyroceram Heat Flux Gauge			
37-26-1	1.90	11.1	8.0	3.7	5.0
37-26-5	1.93	11.1	7.9	3.1	4.3
37-26-6	2.36	11.1	7.3	5.5	8.0
37-26-7	2.97	11.1	7.0	8.5	12.5
37-26-8	3.36	11.1	7.0	10.0	15.0
37-26-9	3.84	11.1	5.4	11.0	18.4
37-26-10	3.82	11.1	5.4	11.0	18.4
18-5-1	2.57	11.1	7.3	6.0	8.6
18-5-2	3.32	11.1	6.2	9.0	14.0
18-5-3	1.95	17.9	12.4	4.1	4.5
18-5-5	2.67	17.9	11.6	8.7	10.0
18-5-6	2.68	17.9	12.5	9.0	10.0
18-7-1	2.70	17.9	11.6	8.7	10.0
		Orifice No. 3, Alumina Heat Flux Gauge			
18-7-2	1.95	11.1	8.4	0.8	5.0
18-7-3	1.89	11.1	7.4	0.7	4.6
18-7-4	2.63	11.1	7.6	1.6	10.4
19-5-1	2.66	11.1	7.5	1.6	10.5
19-5-2	2.62	11.1	8.0	1.6	10.2
19-5-3	2.66	10.7	7.8	1.6	10.3
19-5-4	2.71	11.1	8.2	1.7	10.7
19-5-5	2.91	11.1	6.5	1.7	12.0
19-5-6	3.31	11.1	6.4	2.0	14.2
19-5-7	1.96	17.9	12.9	1.0	5.0
19-5-8	1.99	17.9	12.6	1.1	5.6
19-5-9	2.72	16.8	10.3	1.9	10.7
19-6-1	2.82	17.5	10.8	2.0	11.0
19-6-2	2.77	16.8	11.1	2.0	10.8
19-6-3	2.17	24.7	18.8	1.6	6.7
19-6-4	2.15	24.7	18.4	1.5	6.3
19-6-5	3.34	23.3	15.7	3.2	14.5
19-6-6	2.25	24.7	19.7	1.9	7.7
19-18-2	2.37	24.7	17.6	1.9	8.2
19-18-3	2.37	24.7	16.7	1.8	7.9
19-18-4	3.42	24.7	14.7	3.3	15.5
19-18-5	2.80	17.9	11.4	2.0	10.7

TABLE 21 (Continued)

PART II: WITH ARGON THE TEST GAS

Run No.	M_E	P_o (atm)	P_4 (atm)	ΔT_o (^oK)	$\Delta T_o(\Gamma/\Gamma^*)(P^*/P_4)^{\frac{1}{2}}$ (^oK)
		Orifice No. 3, Pyrex Heat Flux Gauge			
19-8-1	1.89	11.1	6.60	0	0
19-8-2	1.90	11.1	6.80	0	0
19-8-3	1.86	11.1	6.53	0	0
19-8-4	2.35	11.1	4.76	0	0
19-8-5	2.33	11.1	5.99	0	0
19-9-1	2.48	11.1	5.85	1.5	2.0
19-9-2	2.55	11.1	5.58	2.0	2.7
19-9-3	2.79	11.1	6.33	4.0	5.0
19-12-1	2.90	11.1	6.53	5.0	6.2
19-12-2	2.86	11.1	6.94	5.0	6.0
19-12-3	2.95	11.1	7.35	6.0	7.0
19-12-4	2.90	11.1	7.21	5.0	5.9
19-12-5	3.03	11.1	8.23	7.0	7.7
19-12-6	3.15	11.1	7.01	8.0	9.6
19-12-7	3.24	11.1	7.55	8.0	9.2
19-12-8	1.88	17.9	10.70	0	0
19-12-9	1.86	17.9	11.00	0	0
19-13-1	2.33	17.9	9.80	0	0
19-13-2	2.45	17.9	9.25	0	0
19-13-3	2.66	17.9	9.87	2.0	2.0
19-13-5	2.85	17.9	10.40	6.0	5.9
19-13-6	2.87	17.9	10.50	5.0	4.9
19-13-7	3.19	19.9	12.00	9.0	8.2
19-13-8	3.20	17.9	13.60	10.0	8.6
19-13-9	3.35	17.9	11.30	10.0	9.4
		Orifice No. 3, Pyroceram Heat Flux Gauge			
38-6-2	1.87	10.7	6.06	0	0
38-6-3	2.69	10.9	5.58	2.0	3.3
38-6-4	3.24	11.1	7.08	6.0	8.7
38-6-5	2.12	17.9	8.85	0	0
38-6-6	2.26	21.3	10.80	0	0
38-6-7	2.83	22.6	13.60	5.0	5.3
38-7-1	2.23	21.3	10.30	0	0
38-7-2	2.35	23.5	12.20	0	0
38-7-3	3.35	24.2	15.70	15.0	14.7

TABLE 22

SUMMARY OF HEAT TRANSFER RESULTS

PART I: HEAT TRANSFER FROM HIGH-TEMPERATURE AIR

Run No.	M_E	T_o (°K)	T_4 (°K)	T_4' (°K)	P_4 (atm)	P_4' (atm)	T_s (a) (°C)	T_f (b) (°K)	G $\frac{g}{(cm)^2(sec)}$	Re_x	h $\frac{cal}{(cm)^2(sec)(°K)}$	$h/(T_4')^{0.3}$ $\frac{cal}{(cm)^2(sec)(°K)^{1.3}}$	$h/(T_f)^{0.3}$ $\frac{cal}{(cm)^2(sec)(°K)^{1.3}}$	Time (c) Interval (msec)
								Orifice No. 5, Pyrex Heat Flux Gauge						
35-31-1	2.85	300	1230	1335	16.2	22.5	88.0	860	28.5	7.36×10^4	24.5×10^{-3}	2.83×10^{-3}	3.22×10^{-3}	1-35
35-31-2	3.52	300	1690	1850	14.4	21.7	129.0	1140	23.2	4.98	23.8	2.49	2.88	2-30
37-20-5	1.93	302	705	760	8.0	10.5	25.4	545	17.9	6.48	14.7	2.00	2.21	1-47
37-20-6	1.94	302	715	760	8.2	10.6	28.0	545	17.9	6.48	15.2	2.08	2.29	1-47
37-20-7	2.42	303	985	1065	7.4	10.1	38.5	700	14.3	4.19	12.4	1.53	1.74	1-37
37-20-9(d)	2.98	303	1325	1455	6.7	9.9	68.5	915	12.0	2.94	14.7	1.65	1.90	1-32
37-20-10(d)	3.34	304	1580	1750	6.0	9.5	77.0	1065	10.4	2.30	14.6	1.55	1.80	1-29
								Orifice No. 5, Alumina Heat Flux Gauge						
39-22-4	3.42	293	1575	1735	13.4	20.3	22.7	1025	22.5	5.00	23.2	2.48	2.91	1-33
39-22-6	2.41	293	950	1030	7.4	10.1	6.4	665	14.7	4.39	12.5	1.56	1.78	1-41
310-15-1(e)	2.62	293	1070	1155	16.5	22.7	13.0	730	31.0	8.67	26.8	3.22	3.70	1-39
310-15-2(e)	3.51	293	1645	1820	13.8	21.7	24.0	1070	23.4	5.05	22.7	2.39	2.81	1-30
								Orifice No. 3, Pyrex Heat Flux Gauge						
35-31-3	3.52	300	1690	1840	14.6	21.4	180.0	1160	45.3	9.72	41.2	4.32	4.96	1-15
35-31-4	3.21	300	1470	1580	15.9	21.8	152.0	1015	49.8	11.6	41.2	4.52	5.16	1-25
35-31-5	2.65	300	1115	1190	16.9	22.1	123.0	805	58.7	16.2	50.9	6.09	6.85	1-30
37-18-3	1.91	300	695	745	7.9	10.3	39.9	545	35.1	12.8	27.8	3.82	4.20	1-45
37-18-4	2.18	300	835	905	7.4	10.1	48.7	630	30.8	9.98	24.5	3.18	3.54	1-45
37-18-5	1.90	301	690	740	8.0	10.3	39.3	540	35.2	12.9	28.3	3.91	4.30	1-45
37-18-6	1.91	302	695	735	7.8	9.7	39.0	540	33.2	12.2	28.6	3.94	4.34	1-45
37-18-7	1.92	303	700	740	7.9	9.7	40.0	540	33.1	12.1	28.9	3.98	4.39	1-45
37-18-8	2.18	303	840	910	7.4	10.2	47.0	630	31.2	10.1	25.3	3.35	3.67	1-44
37-18-9	2.39	303	970	1050	7.5	10.3	55.8	705	29.1	8.66	24.1	2.99	3.37	1-32
37-18-10	2.39	304	970	1050	7.4	10.2	55.0	705	28.9	8.60	23.0	2.85	3.22	1-39
37-18-11	2.62	304	1110	1200	7.3	10.1	66.0	785	26.6	7.31	23.4	2.79	3.16	3-30
37-18-12	2.62	304	1110	1200	7.4	10.1	71.1	790	26.6	7.31	23.9	2.85	3.23	1-33
37-18-13	3.01	304	1350	1485	6.7	10.0	80.0	935	23.6	5.72	20.9	2.34	2.68	1-30
37-18-14	3.13	303	1430	1565	6.6	9.7	87.0	975	22.2	5.22	22.1	2.44	2.81	1-20
37-19-4	1.91	304	700	755	7.8	10.3	37.5	550	34.8	12.6	26.9	3.69	4.06	5-45
37-19-5	3.30	304	1550	1710	6.4	9.9	89.0	1055	21.7	4.86	19.0	2.10	2.43	1-25
37-19-6	3.79	304	1910	2180	5.4	9.9	114.0	1300	19.1	3.73	20.3	2.02	2.36	1-10
37-19-7	3.88	304	1980	2280	5.1	9.9	111.0	1350	18.6	3.54	19.9	1.95	2.28	1-8

(continued)

TABLE 22 (Continued)

Run No.	M_E	T_o (°K)	T_4 (°K)	T_4' (°K)	P_4 (atm)	P_4' (atm)	T_s (a) (°C)	T_r (b) (°K)	$\frac{G}{g}$ $(cm)^2(sec)$	Re_x	$\frac{h}{cal}$ $(cm)^2(sec)(°K)$	$\frac{h/(T_4')^{0.3}}{cal}$ $(cm)^2(sec)(°K)^{1.3}$	$\frac{h/(T_r)^{0.3}}{cal}$ $(cm)^2(sec)(°K)^{1.3}$	Time (c) Interval (msec)
Orifice No. 3, Pyroceram Heat Flux Gauge														
37-26-1	1.90	300	670	715	8.0	10.2	34.2	525	35.3	13.3×10^4	31.0×10^{-3}	4.30×10^{-3}	4.73×10^{-3}	1-45
37-26-5	1.93	301	700	755	7.9	10.5	33.8	545	35.4	12.8	28.4	3.89	4.30	1-45
37-26-6	2.36	301	945	1035	7.3	10.3	45.5	690	29.6	8.85	22.8	2.84	3.21	1-36
37-26-7	2.97	303	1320	1475	7.0	10.1	72.5	925	24.1	5.86	21.7	2.43	2.80	1-32
37-26-8	3.36	303	1590	1750	7.0	9.8	85.0	1070	21.3	4.71	21.5	2.28	2.64	1-20
37-26-9	3.84	303	1940	2220	5.4	10.1	99.0	1305	19.3	3.73	19.8	1.96	2.30	1-10
37-26-10	3.82	303	1930	2200	5.4	9.9	98.0	1300	19.1	3.70	19.7	1.96	2.29	2-13
18-5-1	2.57	301	1070	1160	7.3	10.1	49.5	755	27.1	7.56	21.9	2.65	3.01	1-35
18-5-2	3.32	302	1540	1720	6.2	9.9	95.2	1060	21.8	4.86	25.5	2.73	3.16	1-20
18-5-3	1.95	304	720	780	12.4	16.3	47.7	565	54.2	19.3	40.6	5.52	6.07	1-40
18-5-5	2.67	305	1150	1250	11.6	15.9	86.0	820	41.3	11.1	35.1	4.14	4.69	1-30
18-5-6	2.68	305	1160	1240	12.5	16.4	85.5	815	42.6	11.5	34.9	4.12	4.68	1-29
18-7-1	2.70	300	1140	1240	11.6	16.4	94.5	820	42.6	11.5	39.2	4.62	5.23	1-30
Orifice No. 3, Alumina Heat Flux Gauge														
18-7-2	1.95	304	720	760	8.4	10.3	8.0	535	34.5	12.5	30.1	4.11	4.57	1-25
18-7-3	1.89	304	690	740	7.4	9.8	7.4	530	33.3	12.3	28.6	3.94	4.35	1-45
18-7-4	2.63	304	1115	1200	7.6	10.3	13.0	760	27.2	7.48	24.3	2.90	3.32	1-45
19-5-1	2.66	292	1090	1170	7.5	9.9	14.0	740	27.0	7.50	26.4	3.17	3.64	1-35
19-5-2	2.62	294	1080	1160	8.0	10.7	12.6	730	28.8	8.04	25.6	3.08	3.54	7-40
19-5-3	2.66	294	1100	1180	7.8	10.5	13.2	745	28.0	7.75	24.4	2.92	3.35	10-36
19-5-4	2.71	294	1130	1200	8.2	10.7	13.8	755	28.2	7.74	24.9	2.97	3.42	1-25
19-5-5	2.91	299	1270	1420	6.5	10.8	15.7	865	26.2	6.52	23.4	2.65	3.08	3-33
19-5-6	3.31	300	1540	1700	6.4	10.9	19.2	1010	24.0	5.39	22.4	2.41	2.82	1-15
19-5-7	1.96	300	720	775	12.9	17.1	12.6	545	56.9	20.2	45.0	6.12	6.81	1-45
19-5-8	1.99	300	730	795	12.6	17.1	11.5	555	56.2	19.7	39.2	5.29	5.88	1-15
19-5-9	2.72	300	1155	1265	10.3	14.9	18.6	790	38.3	10.2	30.8	3.62	4.16	1-36
19-6-1	2.82	298	1205	1345	10.8	15.8	21.6	830	41.9	10.8	35.0	4.03	4.66	5-38
19-6-2	2.77	300	1185	1295	11.1	16.0	20.1	810	40.6	10.7	33.6	3.91	4.50	4-34
19-6-3	2.17	300	830	885	18.8	24.2	19.0	605	74.8	24.5	55.4	7.24	8.12	1-45
19-6-4	2.15	300	820	880	18.4	24.3	18.6	600	75.5	24.9	55.0	7.20	8.08	1-45
19-6-5	3.34	300	1555	1690	15.7	22.7	37.5	1015	50.1	11.3	44.8	4.82	5.62	1-20
19-6-6	2.25	300	875	925	19.7	24.4	19.9	620	73.8	23.6	53.4	6.88	7.75	1-38
19-18-2	2.37	289	915	980	17.6	23.1	19.9	645	68.0	21.0	47.9	6.07	6.88	1-15
19-18-3	2.37	289	910	990	16.7	23.0	21.1	650	67.3	20.6	51.3	6.47	7.34	1-20
19-18-4	3.42	290	1550	1715	14.7	22.8	37.0	1020	50.0	11.2	43.4	4.65	5.43	1-25
19-18-5	2.80	288	1160	1255	11.4	16.4	21.0	790	42.1	11.2	35.8	4.20	4.84	1-37

(continued)

TABLE 22 (Continued)

Run No.	M_E	T_o (°K)	T_4 (°K)	T_4' (°K)	P_4 (atm)	P_4' (atm)	T_s (a) (°C)	T_f (b) (°K)	$\frac{G}{g}$ $\frac{}{(cm)^2(sec)}$	Re_x	$\frac{h}{cal}{(cm)^2(sec)(°K)}$	$\frac{h}{(T_4')^{0.3}}$ $\frac{cal}{(cm)^2(sec)(°K)^{1.3}}$	$\frac{h}{(T_f)^{0.3}}$ $\frac{cal}{(cm)^2(sec)(°K)^{1.3}}$	Time (c) Interval (msec)
Orifice No. 1, Pyrex Heat Flux Gauge														
35-31-6	3.52	300	1685	1820	15.1	21.2	265.0	1190	90.6	19.6×10^4	30.2×10^{-3}	8.44×10^{-3}	9.51×10^{-3}	1-10
35-31-7	2.85	300	1230	1340	15.4	22.0	219.0	930	110.4	23.6	92.1	10.63	11.84	1-13
35-31-8	2.82	299	1245	1350	16.0	22.2	211.0	930	111.1	28.5	87.0	10.01	11.18	1-15
35-31-9	3.53	299	1690	1850	14.3	21.4	278.0	1215	91.0	19.5	76.2	8.19	9.27	1-11
37-19-3	3.36	303	1590	1775	6.1	9.9	142.0	1110	42.3	9.97	36.7	3.89	4.48	1-12
37-20-2	2.94	300	1290	1430	6.5	10.0	118.5	925	48.6	12.1	38.9	4.40	5.01	1-14
37-20-3	2.45	300	980	1060	7.4	10.1	94.6	725	57.6	17.0	46.1	5.70	6.40	1-29
37-20-4	1.94	301	705	760	7.8	10.1	67.9	565	68.5	24.7	56.2	7.69	8.40	1-47
Orifice No. 1, Alumina Heat Flux Gauge														
39-22-1	2.47	292	975	1050	15.4	21.4	43.9	700	121.4	35.7	110.0	13.66	15.45	1-30
39-22-2	3.49	291	1615	1755	14.4	20.8	68.3	1060	90.8	20.0	86.6	9.21	10.72	1-14
39-22-3	2.39	293	935	1030	6.9	10.1	18.2	670	58.1	17.4	45.9	5.72	6.51	1-40
No Orifice (Open Test Section), Pyrex Heat Flux Gauge														
19-20-2	2.86	286	1180	1305	10.8	16.1	186.0	890	133.6	45.1	89.5	10.40	11.65	1-7
19-20-3	2.04	286	730	755	14.2	16.3	119.0	580	179.7	84.5	114.6	15.68	16.99	5-10
19-20-4	1.95	287	675	730	13.1	16.1	115.0	565	180.9	86.8	114.0	15.76	17.04	1-12
19-20-6	1.85	288	635	675	8.0	10.1	79.5	520	118.4	59.7	87.9	12.45	13.46	1-10
19-20-7	1.94	288	675	725	7.9	10.2	85.0	550	114.9	55.3	85.3	11.83	12.83	1-10
19-20-8	2.97	288	1255	1380	8.5	9.9	160.5	915	79.9	26.2	61.6	7.05	7.94	1-9
Orifice No. 3, Rectangular Orifice Upstream, (f) Pyrex Heat Flux Gauge														
19-21-3	1.91	289	665	725	7.8	10.5	69.5	540	36.3	-	60.7	8.12	9.16	1-45
19-21-4	1.91	295	680	735	7.9	10.6	72.0	550	36.2	-	62.6	8.62	9.40	1-45
Orifice No. 5, Rectangular Orifice Upstream, (f) Pyrex Heat Flux Gauge														
19-21-5	1.91	295	680	735	7.8	10.5	54.0	545	18.1	-	45.2		5.82	1-45
No Orifice (Open Test Section Downstream), Rectangular Orifice Upstream, (f) Pyrex Heat Flux Gauge														
19-[illegible] (g)	1.91	288	660	710	8.2	10.5	-	-	52.8	-	46.2	6.44	-	-
19-[illegible]-2 (g)	1.92	288	670	710	8.3	10.4	49.0	525	52.1	-	40.0	5.58	6.11	1-20
19-21-6 (g)	1.96	296	710	760	12.5	16.3	62.0	560	78.8	-	43.3	5.91	6.49	1-30

(continued)

TABLE 22 (Continued)

PART II. HEAT TRANSFER FROM HIGH-TEMPERATURE ARGON

Run No.	M_E	T_o (°K)	T_4 (°K)	P_4 (atm)	P_4' (atm)	$G^{(h)}$ $\frac{g}{(cm)^2(sec)}$	$Re_x^{(h)}$	$h^{(h)}$ $\frac{cal}{(cm)^2(sec)(°K)}$	Time Interval[c] (msec)
					Orifice No. 3, Pyrex Heat Flux Gauge				
19-8-1	1.89	296	915	6.60	10.6	40.4	10.4×10^4	20.1×10^{-3}	5-40
19-8-2	1.90	296	920	6.81	10.7	40.8	10.4	21.0	5-40
19-8-3	1.86	296	890	6.53	10.7	41.6	10.9	19.5	1-40
19-8-4	2.35	296	1355	4.76	9.53	30.0	5.94	16.6	1-30
19-8-5	2.33	295	1330	5.99	10.8	34.2	6.86	16.3	1-30
19-9-1	2.48	294	1470	5.85	10.2	30.9	5.81	16.6	1-35
19-9-2	2.55	295	1560	5.58	10.3	30.2	5.47	15.5	1-35
19-9-3	2.79	295	1845	6.33	10.0	27.1	4.40	13.3	1-23
19-12-1	2.90	293	1965	6.53	10.4	27.3	4.26	14.6	1-20
19-12-2	2.86	298	1950	6.94	10.0	26.3	4.12	13.1	1-17
19-12-3	2.95	298	2060	7.35	10.3	26.3	3.98	12.8	1-23
19-12-4	2.90	297	1995	7.21	10.3	26.8	4.14	12.7	1-25
19-12-5	3.03	297	2165	8.23	10.3	25.7	3.76	12.9	1-20
19-12-6	3.15	296	2320	7.01	9.3	22.4	3.14	11.0	2-20
19-12-7	3.24	296	2445	7.55	10.3	23.9	3.24	11.3	2-20
19-12-8	1.88	295	895	10.7	16.5	64.3	16.7	31.6	3-25
19-12-9	1.86	295	885	11.0	16.5	64.6	16.9	32.7	3-30
19-13-1	2.33	296	1330	9.80	16.7	53.2	10.7	27.5	5-30
19-13-2	2.45	296	1450	9.25	16.5	50.4	9.58	24.4	5-35
19-13-3	2.66	296	1690	9.87	16.6	47.9	7.73	24.1	1-30
19-13-5	2.85	296	1925	10.4	16.4	43.4	6.86	21.6	1-25
19-13-6	2.87	295	1945	10.5	16.3	43.3	6.81	22.2	1-27
19-13-7	3.19	295	2360	12.0	16.5	39.6	5.48	20.3	1-25
19-13-8	3.20	295	2380	13.6	17.0	41.2	5.68	22.4	1-25
19-13-9	3.35	295	2565	11.3	16.7	38.1	4.97	19.5	1-25
					Orifice No. 3, Pyroceram Heat Flux Gauge				
38-6-2	1.87	303	915	6.06	9.80	37.6	9.65	21.0	1-40
38-6-3	2.69	303	1770	5.58	9.94	27.6	4.61	15.2	1-35
38-6-4	3.24	304	2495	7.06	9.80	22.7	3.03	14.7	1-25
38-6-5	2.12	304	1150	8.85	15.8	53.8	11.9	28.4	4-40
38-6-6	2.26	304	1290	10.80	18.7	60.5	12.4	31.7	3-25
38-6-7	2.83	304	1950	13.6	20.3	53.4	8.37	26.2	1-25
38-7-1	2.23	301	1245	10.3	18.2	60.5	12.7	31.3	3-25
38-7-2	2.35	301	1370	12.2	21.3	66.6	13.1	34.1	1-20
38-7-3[i]	3.35	301	2640	15.7	21.3	47.6	6.13	19.9	1-25

Table 22 (Continued)

(a) Heat Flux Gauge Surface Temperature at 10 milliseconds after start of heating.

(b) Film temperature evaluated at the arithmetic mean of absolute gas temperature and absolute heat flux gauge surface temperature after 10 milliseconds of heating.

(c) Time interval over which temperature history can be represented within 5 per cent by Equation (14) for heating of a semi-infinite solid through constant heat transfer coefficient.

(d) For these runs a small amount of hot gas leaked by the orifice gasket.

(e) For these runs a fine screen was placed at entrance of test section as a turbulence promoter.

(f) The rectangular orifice used in the entrance to the test section was a critical flow orifice with minimum dimensions of 0.254 by 1.219 cm. These were trial runs to investigate the effect of entrance conditions on heat transfer to the test section wall.

(g) All data, except temperature-time data, for heat flux gauge were estimated for these runs.

(h) Mass velocity, Reynolds number, and heat transfer coefficient calculated assuming gas temperature to be that behind reflected shock with no contribution from isentropic temperature rise behind reflected shock.

(i) For this run with an extremely high gas temperature it appears that some shorting of the gauge occurred from ionization of argon. (See Reference 63.)

APPENDIX L

NOMENCLATURE

Symbol	Definition	Units
A_{or}	Flow area of flow-control orifice at downstream end of test section	$(cm)^2$
A_{ts}	Area of test-section flow channel	$(cm)^2$
A^*	Area of flow-control orifice No. 1 used in Equations (19) and (C-9)	$(cm)^2$
B	Product of frequency factor, Z, and energy released at the propellant surface per unit area, Q_s (see p. 26)	$cal/(cm)^2(sec)$
C_i	Coefficient in Equation (27)	-
c	Heat capacity	cal/(g)(°K)
D_H	Hydraulic diameter of flow channel, four times the cross-sectional area divided by the wetted perimeter of the channel	cm
E_a	Activation energy for key ignition reaction	cal/(mole)
E_i	Ignition energy defined by Equation (11)	$cal/(cm)^2$
F	Heat Flux	$cal/(cm)^2(sec)$
F_s	Surface heat flux	$cal/(cm)^2(sec)$
$\bar{F}$, $\bar{F}_s$	Mean surface heat flux, defined on p. 18	$cal/(cm)^2(sec)$
$\bar{F}^*$	Dimensionless heat flux, defined by Equation (12)	-
F_T	Total heat flux at the propellant surface	$cal/(cm)^2(sec)$
G	Mass flow rate of test gas through flow channel	$g/(cm)^2(sec)$
h	Convective heat transfer coefficient	$cal/(cm)^2(sec)(°K)$
k	Thermal conductivity	cal/(cm)(sec)(°K)

Symbol	Definition	Units
K	Constant, defined by Equation (3)	dimensionless
M_E	Mach number of incident shock wave at entrance to test section	dimensionless
M_{ts}	Mach number of test-gas flowing through test-section flow channel	dimensionless
N	$N = \frac{h(t)}{\Gamma}$	dimensionless
n	Exponent in Equation (27)	-
P	Pressure	atm
P_o	Initial driver-gas pressure in shock tube	atm
P_1	Initial driven-gas pressure in shock tube	atm
P_4	Pressure immediately behind reflected shock wave	atm
P_4'	Maximum pressure rise behind reflected shock wave	atm
P^*	Reference pressure (10 atm) used in Equations (19) and (C-9)	atm
Q_s	Energy released at the propellant surface by key ignition reaction	$cal/(cm)^2(sec)$
Q_v	Heat of reaction per unit volume of propellant	$cal/(cm)^3$
R	Gas constant: 1.987 8.314×10^7	cal/(mole)(°K) ergs/(mole)(°K)
Re_x	Reynolds number of fluid stream, based on distance from leading edge	dimensionless
S	Slope of line that represents ignition data plotted in the form $\ln(\bar{F})$ versus $\ln(t_i)^{1/2}$	-
t	Time	sec, msec
t_i	Ignition time	sec, msec
$(t_i)^*$	Dimensionless ignition time, defined by Equation (12)	-

Symbol	Definition	Units
T_o	Initial uniform temperature of solid	°K
ΔT_o	Initial, instantaneous temperature rise at the test-section wall following the passage of the reflected shock wave through test section, defined by Equations (19) and (20)	°K
T_1	Initial temperature of the gas in driven section of the shock tube; also represents the initial uniform temperature of the propellant sample and heat flux gauge	°K
T_4	Temperature immediately behind reflected shock wave	°K
T_4'	Maximum temperature rise behind reflected shock wave	°K
T_f	Film temperature for heat transfer from hot gas $T_f = \frac{T_g + T_s}{2}$	°K
T_g	Stagnation temperature of convective gas	°K
T_j	Total temperature at test-section wall following passage of reflected shock wave, defined by Equation (15)	°K
T_s	Surface temperature	°K
T_{si}	Surface temperature of the propellant at ignition	°K
T_{si}^L	Ignition temperature for linear heating	°K
ΔT_{si}^L	Change in temperature of the propellant surface during linear heating $\Delta T_{si}^L = T_{si}^L - T_o$	°K
T_{si}^T	Thermal ignition temperature	°K
U	Mean gas velocity through test section	m/sec
x	Distance into solid measured from the surface	(cm)

Symbol	Definition	Units
α	Thermal diffusivity	$(cm)^2/sec$
Γ	Thermal responsivity, the square root of the product of thermal conductivity, density, and heat capacity	$cal/(cm)^2(sec)^{1/2}(°K)$
Γ_w	Thermal responsivity of the wall material	$cal/(cm)^2(sec)^{1/2}(°K)$
Γ_p	Thermal responsivity of the propellant	$cal/(cm)^2(sec)^{1/2}(°K)$
Γ^*	Reference thermal responsivity, see Equations (19) and (21)	$cal/(cm)^2(sec)^{1/2}(°K)$
Π	Numerical constant (3.14159...)	dimensionless
ρ	Density	$g/(cm)^3$

Security Classification

DOCUMENT CONTROL DATA - R&D

(Security classification of title, body of abstract and indexing annotation must be entered when the overall report is classified)

1. ORIGINATING ACTIVITY *(Corporate author)* University of Utah 1400 East 2nd South Salt Lake City, Utah 84112	2a. REPORT SECURITY CLASSIFICATION UNCLASSIFIED 2b GROUP

3. REPORT TITLE
IGNITION OF AMMONIUM PERCHLORATE-BASED PROPELLANTS BY CONVECTIVE HEATING

4. DESCRIPTIVE NOTES *(Type of report and inclusive dates)*
Scientific Interim

5. AUTHOR(S) *(Last name, first name, initial)*
John A. Keller
Alva D. Baer
Norman W. Ryan

6. REPORT DATE	7a. TOTAL NO. OF PAGES	7b. NO. OF REFS
August 1, 1966	423	92

8a. CONTRACT OR GRANT NO. AF-AFOSR-40-64 b. PROJECT NO. 9711-01 c. 61445014 d. 681308	9a. ORIGINATOR'S REPORT NUMBER(S) 9b. OTHER REPORT NO(S) *(Any other numbers that may be assigned this report)*

10. AVAILABILITY/LIMITATION NOTICES

1. Distribution of this document is unlimited

11. SUPPLEMENTARY NOTES	12. SPONSORING MILITARY ACTIVITY AF Office of Scientific Research (SREP) 1400 Wilson Boulevard Arlington, Virginia 22209

13. ABSTRACT

A study was made of the ignition of ammonium perchlorate-based propellants by convective heat fluxes of 20 to 160 cal/ $(cm)^2$ (sec) in a shock-tube apparatus. The results of this research showed that ammonium-perchlorate propellants ignite by a thermal process in which the slow step in the sequence of events which lead to steady deflagration of the propellant is raising the surface to its ignition temperature. The results also suggest that the key chemical process in ignition is the thermal decomposition of ammonium perchlorate; reactions involving fuel ingredients become important immediately following that reaction. Deviations from behavior predicted by simple thermal theory were found for propellants with rough surfaces, but not for those with smooth surfaces.

DD FORM 1 JAN 64 1473

Security Classification

Security Classification

14 KEY WORDS	LINK A ROLE	LINK A WT	LINK B ROLE	LINK B WT	LINK C ROLE	LINK C WT
Propellant Ignition						
Composite Propellants						
Ammonium Perchlorate						
Ignition						
Convective Heating						
Heat Transfer						
Shock Tube						

INSTRUCTIONS

1. ORIGINATING ACTIVITY: Enter the name and address of the contractor, subcontractor, grantee, Department of Defense activity or other organization *(corporate author)* issuing the report.

2a. REPORT SECURITY CLASSIFICATION: Enter the overall security classification of the report. Indicate whether "Restricted Data" is included. Marking is to be in accordance with appropriate security regulations.

2b. GROUP: Automatic downgrading is specified in DoD Directive 5200.10 and Armed Forces Industrial Manual. Enter the group number. Also, when applicable, show that optional markings have been used for Group 3 and Group 4 as authorized.

3. REPORT TITLE: Enter the complete report title in all capital letters. Titles in all cases should be unclassified. If a meaningful title cannot be selected without classification, show title classification in all capitals in parenthesis immediately following the title.

4. DESCRIPTIVE NOTES: If appropriate, enter the type of report, e.g., interim, progress, summary, annual, or final. Give the inclusive dates when a specific reporting period is covered.

5. AUTHOR(S): Enter the name(s) of author(s) as shown on or in the report. Enter last name, first name, middle initial. If military, show rank and branch of service. The name of the principal author is an absolute minimum requirement.

6. REPORT DATE: Enter the date of the report as day, month, year; or month, year. If more than one date appears on the report, use date of publication.

7a. TOTAL NUMBER OF PAGES: The total page count should follow normal pagination procedures, i.e., enter the number of pages containing information.

7b. NUMBER OF REFERENCES: Enter the total number of references cited in the report.

8a. CONTRACT OR GRANT NUMBER: If appropriate, enter the applicable number of the contract or grant under which the report was written.

8b, 8c, & 8d. PROJECT NUMBER: Enter the appropriate military department identification, such as project number, subproject number, system numbers, task number, etc.

9a. ORIGINATOR'S REPORT NUMBER(S): Enter the official report number by which the document will be identified and controlled by the originating activity. This number must be unique to this report.

9b. OTHER REPORT NUMBER(S): If the report has been assigned any other report numbers *(either by the originator or by the sponsor)*, also enter this number(s).

10. AVAILABILITY/LIMITATION NOTICES: Enter any limitations on further dissemination of the report, other than those imposed by security classification, using standard statements such as:

(1) "Qualified requesters may obtain copies of this report from DDC."

(2) "Foreign announcement and dissemination of this report by DDC is not authorized."

(3) "U. S. Government agencies may obtain copies of this report directly from DDC. Other qualified DDC users shall request through _____."

(4) "U. S. military agencies may obtain copies of this report directly from DDC. Other qualified users shall request through _____."

(5) "All distribution of this report is controlled. Qualified DDC users shall request through _____."

If the report has been furnished to the Office of Technical Services, Department of Commerce, for sale to the public, indicate this fact and enter the price, if known.

11. SUPPLEMENTARY NOTES: Use for additional explanatory notes.

12. SPONSORING MILITARY ACTIVITY: Enter the name of the departmental project office or laboratory sponsoring *(paying for)* the research and development. Include address.

13. ABSTRACT: Enter an abstract giving a brief and factual summary of the document indicative of the report, even though it may also appear elsewhere in the body of the technical report. If additional space is required, a continuation sheet shall be attached.

It is highly desirable that the abstract of classified reports be unclassified. Each paragraph of the abstract shall end with an indication of the military security classification of the information in the paragraph, represented as *(TS)*, *(S)*, *(C)*, or *(U)*.

There is no limitation on the length of the abstract. However, the suggested length is from 150 to 225 words.

14. KEY WORDS: Key words are technically meaningful terms or short phrases that characterize a report and may be used as index entries for cataloging the report. Key words must be selected so that no security classification is required. Identifiers, such as equipment model designation, trade name, military project code name, geographic location, may be used as key words but will be followed by an indication of technical context. The assignment of links, rules, and weights is optional.